SLAG DETACHABILITY FROM SUBMERGED ARC WELDS.

by

ADEßISI OLADIMEJI OLADIPUPO

S.M., MASSACHUSETTS INSTITUTE OF TECHNOLOGY

(1984)

B.Sc., UNIVERSITY OF IFE, ILE-IFE NIGERIA

(1980)

SUBMITTED TO THE DEPARTMENT OF

MATERIALS SCIENCE & ENGINEERING IN PARTIAL

FULFILMENT OF THE REQUIREMENT FOR THE

DEGREE OF

DOCTOR OF SCIENCE

at the

MASSACHUSETTS INSTITUTE OF TECHNOLOGY

FEBRUARY 1987

SIGNATURE OF AUTHOR_____

Department of Materials Science & Engineering
January, 9 1987.

CERTIFIED BY_____

Professor Thomas W Eagar
Thesis Supervisor

ACCEPTED BY_____

Professor Samuel M. Allen, Chairman
Departmental Committee on Graduate Students
Department of Materials Science & Engineering

SLAG DETACHABILITY FROM

SUBMERGED ARC WELDS.

by

ADEBISI OLADIMEJI OLADIPUPO

Submitted to the Department of Materials Science & Engineering
on January 9, 1987 in partial fulfilment of the
requirements for the Degree of Doctor of Science in
Materials Engineering.

ABSTRACT

Over fifty percent (50%) of the total steel weld metal is deposited by one of the flux-shielded processes. Slag adherence to the weld metal surface is one of the major factors controlling the usefulness of these processes. Slag attachment to the weld metal, especially in a multipass welding, can severely degrade the weld metal properties. Hence, any improvement in the welding flux technology that eases slag detachability will be applicable to both a wide range of industries and a wide range of welding processes. Some fluxes provide slags of poor detachability with certain electrodes and/or base metal while the same fluxes provide slags of easy detachability with other electrode-base metal combinations. On the other hand, changing of the process parameters (e.g. cooling rate) alone has been observed to affect detachability. In the cases of adherent slags, what are the mechanisms of adherence? In order to understand the mechanics of this adherence and identify the major factors affecting detachability, the physiochemical properties of the flux, electrode and base plates were studied.

Chromium, and chromium oxide were found to affect the detachability of welding slags. Several welds were made with stainless steel electrodes (26.27 wt%Cr), chromium oxide-rich flux and some deposited with mild steel electrodes (no chromium) on chromium-containing base metals. Examination of the weld metal surfaces, after the slag had been detached, by scanning electron microscopy showed the presence of faceted slag particles of high melting temperature which formed during slag-metal reaction and attached in the solidifying weld metal. X-ray diffraction analyses showed these particles to be chromium spinels (iron chromate, magnesium-aluminum-chromate). These particles have a melting temperature in excess of 1600^{0}C. On the other hand, titanium oxide's detrimental effect on slag detachability was due to the formation of high melting temperature (> 1900^{0}C) perovskites (calcium titanate) that also attach to the solidifying weld metal. The irregular interfaces formed by these solid reaction products then provide regions into which the molten slag solidifies and mechanically interlocks resulting in poor slag detachability.

The effects of base metal composition and the surface condition of the base metal were also studied and found to affect the detachability of slag

both physically and chemically. When changing from steel base metal to a nickel-based alloy, detachability worsened significantly. This effect was related to the presence of chromium in the nickel-based alloy (16 wt% Cr) compared with the steel base metal (1.35 wt% Cr) which results in a chemical effect because of the formation of chromium spinels as reaction products as noted above. However, when comparing different steel base metals with little or no chromium the difference in slag detachability was attributed to the base metals' thermal contraction characteristics. The experimental observations on detachability and the results of dilatometric measurements confirmed that the use of absolute values of the coefficients of thermal expansion of slag and base metal to determine which flux composition will provide easy detachability can be erroneous. The mean integrated differential thermal contraction of the slag-metal systems were evaluated from the softening temperature of the slag to 30 ^{0}C. A comparison of the detachability of slags from welds made on mild steel (1010 steel) base metal and HY80 base metal (quenched and tempered martensitic steel) showed that the integrated differential thermal contraction per unit length was smaller with mild steel base metal than with HY80 base metal and that the slags of corresponding welds were more difficult to detach in the case of the mild steel base metal. This correlation of integrated differential thermal contraction per unit length with detachability was found to be valid only in the cases of slags with microcrack-free structures. Furthermore, the cooling rate of the slag-metal system has an effect on the detachability. The higher the cooling rate, the poorer the detachability.

The surface condition of the base metal, that is whether descaled or scaled, was found to affect the detachability of the slag. Scaled base metal provided slags that were more difficult to detach than the slags from a thoroughly descaled base metal under the same conditions of welding. This deleterious effect was attributed to the formation of a chemical bond when the molten slag dissolves the scale and forms a glass. Also, the presence of scale will increase the oxidizing potential of the slag making it easier to oxidize deleterious elements like chromium in the base metal (even when the base metal is low in chromium).

The general findings of this work show that chemical effects due to slag-metal reactions are more important than physical effects of differential thermal expansion. However, in the absence of chemical effects the differential thermal contraction (expansion) is a more useful indicator of ease of detachability than the absolute value of the coefficient of thermal expansion of the slag or weld metal. Also, the correlation of differential thermal contraction with detachability of slag has to be done with the knowledge of the structure of the slags in question. Finally, the chemical composition of the base metal and its surface condition are also important factors that affect the degree of slag detachability.

Thesis Supervisor: Dr. Thomas W. Eagar

Title: Associate Professor of Materials Engineering

TABLE OF CONTENTS

LIST OF TABLES

LIST OF FIGURES

ACKNOWLEDGEMENTS

My sincere and warmest gratitude goes to Professor T. W. Eagar who believed in and guided me throughout my academic career at M.I.T. His aptitude for fundamental research into industrial problems and propensity for work were constant sources of inspiration for me and I believe others too.

I hereby thank my colleagues of the Materials Joining Laboratory for their constant advice and companionship; especially Dr. C. Sorenson for his invaluable assistance with the computer hardware and software. I thank Mr. David Lange of the Harvard University Geology department for his technical assistance. I also thank Ms. Veronica Ayeni for her moral support when I needed it most.

This acknowledgement will be grossly incomplete without the mention of the generous financial support provided by the National Science Foundation under contract No. 8502411-DMR.

CHAPTER ONE

INTRODUCTION

The importance of welding flux technology becomes evident when one considers that well over 50% of all steel weld metal is deposited by one of the flux shielded processes, including shielded metal arc, submerged arc, flux-cored arc and electroslag processes. Hence any improvement in welding flux technology is applicable to both a wide range of industries and a wide range of welding processes. For instance, there has been an increase in the use of heavy steel plates to build large structures like supertankers, submarines, pressure vessels, aircraft carriers etc., which necessitates the use of a highly efficient welding process. Since the mid 1960's a novel welding process: Narrow Gap Welding has been developed to improve the efficiency of welding these heavy plates. Originally, the Gas Metal Arc Welding (GMAW) process was used; however this process can produce many defects in the weld metal unless it is carefully controlled. A more desirable process is narrow gap submerged arc welding which is gradually replacing narrow gap gas metal arc welding. Submerged arc welding solves many of the problems but has an inherent problem of its own: slag detachabilty. Thus, one can see how understanding and being able to control the detachability of slag will be of great commercial interest. On the other hand, the properties of a submerged arc welded steel plate are dependent on a miriad of welding parameters which are interrelated. Flux composition is one of the most important of these variables.

For any given flux composition, there are many important functions

which the flux must perform. It must control the weld metal composition as well as provide arc stability - a function known to be assisted by the presence of alkali metal ions. Yet another function is to provide atmospheric protection for the molten metal - a function known to be controlled by the viscosity of the molten slag. Finally, the slag must be easily removed; it must be detachable. Unfortunately, detachability is an elusive property of a flux and only the most qualitative information is known about factors influencing the ease of slag removal.

Although slag detachability seems to be a mundane problem, it is of basic commercial interest. It is the requirement of slag detachability which, in commercial flux development, controls further study of the properties of a potential new flux. Most new flux compositions are developed empirically. Once made, the trial flux is used in an actual weldment. If the slag does not readily detach, the composition is generally considered unsuitable for commercial use, no matter how good the mechanical properties of the weld metal that are obtained. This is because a flux manufacturer cannot market a flux that requires more labor to remove than to deposit. By applying the principles of chemical equilibrium developed in his thesis, Chai (1) has reduced the average development time of a new commercial flux from ten man-years to one man-year. Most of the current development time for new fluxes is spent on trial and error fine adjustment of flux composition that will provide "operability". Operability is a subjective term which is strongly influenced by "detachability". If a fundamental basis for detachability could be determined, the development time for new fluxes would be reduced even further and fluxes could be tailored to specific new steels to provide the best overall properties.

A literature survey on past work done on slag detachability showed no consensus on the mechanisms of slag-metal bonding even in cases where similar observations had been made. Davis and Bailey (2) in their study of the physical and chemical properties of welding fluxes, alluded to the problem of slag detachability and how these properties can affect the degree of slag detachability. They suggested that a very sluggish slag may not be displaced by the molten weld while a very fluid slag will run to the side and front of the arc and overlap with the molten weld causing slag entrapment. The mechanism of this possible overlapping is not clear. Welding fluxes are designed to have a lower bulk density than the weld metal so as to protect the weld metal from atmospheric contaminants. In many cases, researchers have speculated without apparent foundation when trying to explain slag detachability. One such example was found in the work of Patchett and Renwick (3) on carbonate, alumina, basic and acidic fluxes. They found good slag detachability with acidic fluxes and attributed this to a phase change occuring during cooling which created a significant difference in thermal contraction characteristics. However, no measurement of these contraction characteristics was made. Podgaetskii (4) suggested that the "locking" of slag in defects at the weld metal surface, such as undercutting, partial penetration etc, is due to the differences in thermal expansions of slag and weld metal. This inference is not very clear. Is it being suggested that differential thermal expansion causes the slag to "lock" in geometrical defects? Or that differential thermal expansion itself causes geometrical defects to form on the weld metal surface? Whatever effects differential thermal expansion may cause, its magnitude is expected to be very important. Nonetheless, there are examples in determining slag detachability where the thermal mismatch is large, and the

slag is difficult to detach while when the thermal mismatch is small the slag detaches rather easily. However, it is very possible that geometrical defects will aid mechanical retention of the slag at the weld metal surface but the mechanism by which differential thermal expansion causes geometrical defects and/or causes the slag to "lock" in these defects is not clear.

Just as work has been done on the effects of the physical properties of welding flux on slag detachability, so also has work been done on the effects of the chemical properties of the flux. The effects of chromium, titanium, vanadium and their oxides on slag detachability have been investigated more than any other constituents of the weld metal and flux compositions. This is because of the good mechanical properties conferred on the weld metal by these elements. For instance, chromium provides corrosion inhibition while titanium deoxidizes and refines the weld metal. Yakobashvili (5) investigated the effects of Cr and V on the interfacial tensions between slag and weld metal and related his measurements to slag adhesion. He concluded that Cr and V lower the interfacial tensions between slag and weld, thereby increasing the work of adhesion which implies worsening detachability of slag. Rabkin et al. (6,7) in depositing weld metal with electrodes containing 9 wt.%Cr and 9.7 wt.%V observed poor detachability of the slags. They attributed this to the formation of spinels of a wustite lattice at the interface which reduced the interfacial tension between the slag and metal and the asymmetry (in the slag and metal structures) at the slag-metal interface. This explanation is not very convincing as no report of work done at identifying the type of spinels and their lattice parameters or surface tensions, was made.

The interaction between the many different factors that may affect slag detachability makes its fundamental understanding more challenging. For instance, Hazlett (8) in his investigation of the effect of light coatings on the surface tension of iron found that ferrous oxide produced a large reduction in the surface tension of iron. He explained this as due to the increased oxygen at the interface. Fluxes of high oxygen potential can cause arc instability with attendant undercutting. The filling of these undercuts by the coating mix may result in stronger adherence. Hence, one may hypothesize that the effect of surface tension on slag detachability is a factor that will depend on other factors like the oxidizing potential of the flux. From this brief review, we ask the following questions: What are the main factors affecting slag detachability? How do these factors determine the detachability of slags? This thesis is an attempt to answer these questions and suggest reasons for the difficulty in reaching a consensus in the literature on the mechanisms of slag-to-metal bonding.

This thesis is organized into three parts. The first part discusses the welding procedure, welding materials used and the method for assessing the degree of slag detachability. It will be noted that even though the method might be semi-quantitative, it is reproducible and better than other methods which have been used to quantify slag adherence (9). The second part discusses the effects of chemical composition of the flux, welding electrode and base metal on slag detachability. Though the physical interaction between slag and metal precedes their chemical interaction, physical bonding by weak van der Waals forces will be insignificant in the presence of chemical bonding. Hence, the thesis work has centered on chemical effects. The third part discusses the effect of differential

thermal expansion on slag detachability. Also, thermal and stress analyses showed the effects of the softening point of the slag, the slag (flux) thickness and differential thermal contraction per unit length on the magnitudes of the residual stresses in the slag-metal system. These three separate parts are then tied together in a chapter containing the general conclusions of this work.

CHAPTER TWO

CHEMICAL FACTORS AFFECTING SLAG DETACHABILITY

ABSTRACT

Submerged arc welding was used to study the mechanisms of slag-metal bonding in flux-shielded welding processes. Three different base metals, six different commercial fluxes, four welding electrodes and four laboratory-prepared fluxes were used. A semi-quantitative scheme for assessing the degree of slag detachability which is very simple and reproducible was established. Among the three base metals used, HY80 had the easiest detachability, Inconel 600 the worst and mild steel (1010 steel) was intermediate for comparable slag samples. These differences in detachability can be explained by both physical and chemical bonding effects.

Chromium and titanium are detrimental to slag detachability due to the formation of spinels and perovskites in the slag phase which interlock with the weld metal surface. The formation of the chromium spinel also depends on the oxidizing potential of the flux. For scaled base metal, dissolution of the scale by molten slag results in chemical bonding and very tightly adherent slags. It was also observed that calcium fluoride had a detrimental effect on slag detachability by its influence on slag viscosity and melting temperature.

1. INTRODUCTION AND PREVIOUS WORK

The numerous advantages of using submerged arc welding (e.g. good fusion, good weld metal properties, high deposition rate etc) over some other welding processes made it the choice of this research. In order to compare the degree of slag detachability of different welding fluxes, one must establish and use a scheme to assess the detachability of their slags. Many attempts have been made by researchers to quantify slag detachability. Yakobashvili (9) used Dupré's equation (eqn 1) to quantify slag adhesion (W):

$$W = \sigma_m + \sigma_s - \sigma_{sm} \qquad (1)$$

where W is the work of adhesion, σ_m, σ_s and σ_{sm} are the surface tensions and interfacial tensions of the weld metal and slag.

The various surface tensions were measured at 1550^0C by a weight loss technique (10). This technique involves melting the end of sample rods of the slag and weld metal into graphite crucibles and weighing the molten droplet. The surface tension (σ) is then determined from the following equations:

$$\sigma = mg/r * F \qquad (2)$$

where F is a coefficient depending on radius (r) of the rod and volume (V) of the melted droplet.

$$F = 1/[2\pi f(r/V^{1/3})] \qquad (3)$$

where f is a function whose values have been taken from the work of V.D. Hawkins as tabulated in reference (11).

To find the interfacial tension between slag and metal, an end of the metal rod is dipped in molten slag and the melted droplet's weight is determined

from the volume displacement and the interfacial tension calculated from equations (2) and (3). Using equations (1) through (3), Yakobashvili found that for $W < 900$ dynes/cm, the slag was easily detached while for $W > 900$ dynes/cm it was difficult to detach. It is obvious that the measuring technique is only applicable at the melting points of the metal and slag. Also, it is inappropriate to apply equation (1), an equilibrium equation, to bonding, a non-equilibrium process which occurs at low temperatures. Only at high temperatures where surface and bulk diffusion compensate for interfacial distortions can the use of equation (1) be justified. The Dupré equation is only valid for a planar interface without intermediate phases that could create discontinuous gaps at the interface. This condition of a planar interface is not always the case in welding due to the geometrical defects resulting from arc instability, gas evolution, and/or formation of intermetallic compounds. Furthermore, the equation does not incorporate a term for strain energy due to the mismatch in coefficients of thermal expansion of the slag and the weld metal. This strain energy term would be necessary in a quantitative analysis of the bonding between the slag and the weld metal as it reduces the strength of the bond. Experimental evidence for the incorrectness of using surface tension measurements to quantify slag detachability was found in the work of S.A. Shono (12). The adhesion of two slag systems A and B were determined from the Young's equation:

$$\gamma_m = \gamma_{ms} + \gamma_s \cos\theta \qquad (4)$$

where γ_m, γ_s and γ_{ms} are the surface tensions and interfacial tension of the metal and slag and θ is the contact angle between the molten slag and the metal substrate.

The marginal angle of contact (θ) was determined by the applied droplet

method. The adhesion values found for the slag systems A and B are 560 mJ/m^2 and 520 mJ/m^2 respectively. But in spite of the higher adhesion value of slag A, it was more easily detachable than slag B. A more accurate approach was taken by Vornovtskii et al. (13) and Pokhodnya et al. (14) to quantify slag detachability. A pendulum of known weight, length, and angle of deflection was allowed to hit the back of the weld deposit that had been clamped in a jaw. The energy expended in removing the slag from a 1 cm^2 area of the weld was evaluated and was used as the criterion for assessing the difficulty of slag detachability. This method clearly excludes the study of slags that may readily detach as they might detach from the weld during the clamping process. Even for slags that do not readily detach, it was found in this study that some left a tightly adherent thin film of oxide on the weld metal after the bulk slag had been chipped off. The method of Vornovtskii and Pokhodnya is not clear on how to rate such slags. For a complete understanding of the mechanisms of slag-metal bonding, it is necessary to include both readily detachable slags and slags that are difficult to detach. Given the above considerations, a simple, reproducible and comprehensive technique for assessing the degree of slag detachability was established and used in this study.

The importance of chemical composition of a flux, welding electrode and/or base metal on the resulting weld metal properties cannot be overemphasized. In addition to controlling the mechanical properties, the compositions also control the detachability of slags. Chemical reactions at the slag-metal interface can result in the formation of compounds that may improve or worsen slag detachability. Several investigators (14-21) have found intermediate phases at the slag-metal and ceramic-metal boundaries and

have attributed these to bonding between the materials. Yakobashvili (5) and Rabkin et al (6,7) attributed the detrimental effects of chromium and vanadium on detachability to the effects of these elements on the surface tension of the metal (σ_m), the surface tension of the slag (σ_s) and the interfacial tension between the slag and the metal (σ_{sm}); however, basing the effects of chromium and vanadium on slag detachability solely on their effects on the various surface tensions is not adequate. Given the model which they used to evaluate adhesion, the resultant adhesion from the chromium effect should change only slightly when chromium and vanadium are alloyed with the weld metal. If the addition of chromium to the weld metal increases its surface tension as they suggest, the loss of chromium to the slag should decrease the weld metal surface tension and hence improve slag detachability. Thus, the magnitude of change in the interfacial tension will be dependent on transport of chromium across the slag-metal interface.

In their work on the effect of titanium on slag detachability, Pokhodnya (15) and Bobrikov (22) suggested that the existence of a suboxide of titanium at the slag-metal interface was responsible for the observed slag adherence. They claimed that this occured due to the oxide layer having a similar crystal lattice parameter with the weld metal which allowed epitaxial growth on the weld. In another effort, Pokhodnya (14) claimed that titanium oxide in the slag improved detachability by halting the interaction of the interlayer formed with the molten slag. It was suggested that titanium oxide dissolved the interlayer. Kohno et al. (23) in their development of new fluxes of improved weld metal toughness for HSLA steels, found that the slag system of TiO_2-CaO-CaF_2-Al_2O_3 had poor detachability due the presence of high amounts of high melting perovskite ($CaTiO_3$) at the

slag-metal interface. Okuda and Kumagai (24) in their study of slag adhesion in submerged arc welding, concluded that slag adherred only to the HAZ of the weld metal and not the weld metal surface and that the base metal and weld metal chemical compositions do not affect slag detachability.

From the brief introduction above, it is evident that the literature on slag detachability is varied in explaining the chemical effects of slag detachability. There is no consistent opinion on the factors affecting slag detachability; and when there is, the mechanisms of their influence are not well understood. The selection of factors examined in this study was based on the existing lack of consensus in the literature.

2. EXPERIMENTAL PROCEDURES

(A). WELDING

A schematic of the welding process is shown in figure 1. Submerged arc welds (SAW) were made with a Linde VI-800 CV/DC power supply using a UCC-8 controller, and Linde EH-10 wire feeder head. The welding travel speed was controlled by a Union Carbide "J" governor which had been previously calibrated for time-distance measurements. The welding parameters (current, voltage, travel speed, electrode stickout, electrode diameter, and preheat temperature) used in this study were maintained constant and are shown in Table 1. A guide rail was made to maintain the flux level during welding. The rail was filled with flux to just cover the electrode and then levelled off to one inch depth.

Bead-on plate weld deposits were made on three different base metals: namely, HY-80, mild steel (1010 steel), and Inconel 600 under scaled and descaled conditions. Also, artificial base metals were made from the welding electrodes for the study of the effect of cooling rate on slag detachability. Six-inch lengths of an electrode wire were spliced and bound together with pieces of the same electrode. The bundled electrode was then laid in the groove of a water-cooled copper trough and a weld was made (25) The compositions of the welding electrodes; AX-90, Linde 36, Linde 40, and 309L, and the compositions of the base metals used are shown in Table 2. Table 3 shows the compositions of the welding fluxes used. The four laboratory-prepared fluxes were made to study the effects of chromium oxide, titanium oxide and calcium fluoride on slag detachability. Linde 80, and

Linde 60 commercial fluxes, were alloyed with 20 wt.% Cr_2O_3 [Flux Cr80], 20 wt.% TiO_2 [Fluxes Ti80, and Ti60] and 20 wt.% CaF_2 [Flux CF60]. Both bonded (Cr80) and prefused (Ti80, Ti60, CF60) fluxes were made. All of the fluxes used in this study were pre-dried in an oven before use and not recycled after use.

Various analytical tools including the scanning electron microscope, electron microprobe analyzer, x-ray photoelectron spectrometer, and x-ray diffractometer were used to characterize the slag-metal interface and to measure composition of elements in both slag and weld metal samples. Samples for the SEM and XPS analysis were used as received after having been cleaned ultrasonically. The samples for the electron microprobe analysis were cold-mounted, ground flat and polished smooth on a diamond wheel to 0.25 micron grit. All samples except those for XPS analysis were carbon-coated.

(B). FLUX PREPARATION

(I) Bonded

Linde 80 flux and chromic oxide powder were mixed in a ratio of 4:1 by weight respectively. The mixture was then blended dry in a V-blender at 0.5 Hz for thirty minutes. Sodium silicate was used as the flux binder. The bonded flux which was pelletized and dried at a low temperature was then crushed and sized to 30 mesh.

(II) Prefused

As above, Linde 80 flux and titania powder were mixed in a ratio of 4:1 by weight and blended dry. The mixture was then melted in an induction furnace using a graphite crucible and the flux held molten for thirty minutes. The molten flux was then poured onto a chill plate. The glassy product was abraded to remove adhering graphite, crushed and then screened to 30 mesh.

The weld metal deposits and their corresponding slags were coded as [electrode-base metal-flux] for ease in identifying samples. For instance, a weld made with AX-90 electrode on a descaled HY-80 base metal using Lincoln 880 flux is coded as AX-HY-880. When the weld metal is deposited on a scaled base metal, an S is attached to the base metal designation e.g. AX-HYS-880.

(C). DEGREE OF SLAG DETACHABILITY ASSESSMENT

A semi-quantitative scheme was devised to assess the degree of slag detachability. About five minutes was allowed after a weld was made before the restraints on the base metal were removed. The welding head was then pushed out of the way and the guide rail removed carefully; not to disturb the slag. The base metal was first tilted along the weld length to see if the slag would come off with the unspent flux. If not, the back of the base metal was then struck with a hammer one or two times and the slag detachability was again observed by tilting the plate to an angle greater than 30 degrees. If the slag still adhered, then its sides were chiseled

until it detached from the weld metal surface.

During the above-mentioned assessment, the cleanliness of the weld metal surface and its heat affected zone (HAZ) were noted. The state of the slag after detachment was also observed; that is whether it came off as one lump or in several pieces. Using a scale of 1 - 10, a numerical strength was assigned to the slag detachability as shown in Table 4. The higher the number, the worse the slag detachability. A description of each assessment is given in Appendix 1.

(D) ANALYTICAL TOOLS

(I) Scanning Electron Microscopy (SEM)

A model AMR 1000A Scanning Electron Microscope with an attached X-ray spectrometer was used to observe the surfaces of slag and weld metal as received. The resolution of this instrument which depends on the conduction and cleanliness of the sample and on the operator technique is about 70 Å when using a tungsten filament. A 20 KV accelerating voltage was used to provide good resolution without damaging the surface structures. For identification of these structures, Energy Dispersive X-ray Analysis (EDAX) and X-ray elemental mapping were performed.

(II) Electron Microprobe Analysis (EMPA)

A CAMECA 3-spectrometer 8-crystal electron microprobe analyzer was used to measure the composition of the individual phases in the slag

microstructure and qualitatively determine what these were. This practice was necessitated by the difficulty inherent in measuring elemental bulk composition in a heterogeneous slag system. The appropriate accelerating voltage for each anlysis was chosen to be 1.5 - 2 times the excitation potential of the highest atomic number element suspected to be contained in the sample. Hence, at least a 20 KV accelerating potential was used for all samples.

(III) X-Ray Powder Diffraction (XRD)

For a positive identification of the different second phases in the slag, X-ray diffraction analysis was performed using a General Electric Diano diffractometer. Slag samples were ground to 325 mesh size in order to minimize low-angle absorption of the incident X-ray beam. The powdered sample was mixed with an organic solvent till it was free-flowing and then spread on a glass slide to cover its width and dried. The diffraction parameters used are shown in appendix 2. CuKα radiation was used except when the slag contained a high percent of manganese oxide and iron oxide (from scaled base plate study) in which case it was replaced with CrKα radiation. This was necessary to reduce the background fluorescence that might otherwise have occured with the CuKα radiation.

The sample was scanned from the low angle to the high angle and the diffraction peaks were recorded as a function of two-theta ($2\theta^{0}$) degrees on a strip chart recorder. The peaks were then analyzed and the different phases identified using the ASTM Powder Diffraction Files.

(IV) X-Ray Photoelectron Spectroscopy (ESCA)

The surfaces of the weld metal specimens and control samples were examined with a Physical Electronics 548 X-ray photoelectron spectrometer equipped with a MgKα X-ray source and a cylindrical mirror analyzer. The pass energy of the electron energy analyzer was initially set at 100 eV for a general elemental survey of both a control sample and the weld sample surfaces from 0-1000 eV. The control samples were made by cold-pressing 1/2 inch diameter pellets of the oxide powder at 51 ksi pressure. The peak positions of elements of interest were then more accurately determined by running a multiplex analysis, after one minute sputtering, at a pass energy of 25 eV which provided a high signal to noise ratio. The signal was optimized by maximizing the peak of Auger reflected electrons. The spectrometer was used to determine the phases that might be present on the weld metal surfaces by indicating the chemical states of the constituent elements of the phases. The data were input to a computer and analyzed with MACS V6D Surface Analysis software. This analysis was used to supplement those of the SEM and XRD.

3. RESULTS AND DISCUSSION

The results of the slag detachability assessment are given in Table 4. It shows that for comparable samples, detachability is best with HY80 base metal, worst for Inconel 600 and mild steel is intermediate. Also, detachability from a scaled base metal surface is worse than from a descaled base metal surface. Appendix 3 shows the compositions of the weld metal and slag samples. The scheme used to appraise slag detachability was objective up to the scale of 4 as no subjective application of force was involved. Even when an impact force is applied, for instance at scale number greater than four, the scheme will still provide a comparative study as long as the investigator is consistent in the choice of tools used. Furthermore, the scheme considers the possibility of slag adherence not only to the weld metal but also to its heat affected zone (HAZ) and the adherence of flakes even after the bulk slag had been detached.

(A) EFFECT OF CHROMIUM AND ITS OXIDE

Chromium in the flux, electrode and/or base metal was found to be detrimental to slag detachability. Table 5 shows a summary of the degree of slag detachability for the slag systems investigated with chromium effect. Most of the samples with chromium effects were made using 309L (26.27 wt% Cr) welding electrode. Careful inspection of Table 5 shows that it does not matter whether the chromium is contained in the base metal, the electrode or the flux; it is detrimental to slag detachability in any case. Examination by XPS and SEM of the peeled weld metal surface and/or slag interface of samples reported in Table 5 showed the presence of chromium spinels and

suboxide as confirmed by X-ray diffraction analysis of their corresponding slags (Table 6). Figures 2-4 show pairs of macrographs of weld metal surfaces with and without chromium in which macrographs (b) show the effect of chromium to produce adherent slags on the weld metal and/or HAZ. Figures 5-7 are electron micrographs showing the structure of some slags. In figure 5, the chromium content of the spinel (labelled A in the photogragh) was measured using an Electron Microprobe Analyzer (EMPA). In figures 6 and 7 one can see the effect of adding chromium to the weld metal and chromium oxide to the flux as chromium spinels are formed as additional phases to the metallic precipitates in the polished slag samples. As shown in figure 8, it was found that as the chromium oxide content of the spinel and slag increased, the slag detachability worsened (going from 2.5 to 9.0). Figure 9 also shows the detrimental effect of welding with stainless steel electrodes.

Diffusion profiles of chromium in the weld metal were measured for slag samples AX-HY-Cr8, 309-HY-60, and AX-IN-60 and are shown in figures 10-12. Figure 10 shows a higher chromium content at the interface than in the bulk while figures 11 and 12 show a lower concentration of chromium at the interface. Figure 10 can be explained with a series of chemical reactions:

$$2(Cr_2O_3) + 2\underline{Si} = 4\underline{Cr} + 3(SiO_2) \qquad (5)$$

$$(Cr_2O_3) + \underline{Mn} = 2\underline{Cr} + 3(MnO) \qquad (6)$$

The flux (Cr80) used for sample AX-HY-Cr8 (figure 10) is rich in chromium oxide. Silicon and manganese in the weld will reduce the chromium oxide according to equations (5) and (6) thus transferring chromium into the weld. Hence, the concentration of chromium at the slag-metal interface will be higher than in the bulk of the weld metal. On the other hand, the lower

chromium concentration at the slag-metal interface of figures 11 and 12 can be explained with the following reaction equations:

$$\underline{Fe} + 2\underline{Cr} + 4\underline{O} = (FeO.Cr_2O_3) \quad (7)$$

$$\underline{Cr} + \underline{O} = (CrO) \quad (8)$$

$$2\underline{Cr} + 4FeO = 3\underline{Fe} + (FeO.Cr_2O_3) \quad (9)$$

The flux used for welding samples 309-HY-60 (figure 11) and AX-IN-60 (figure 12) has no chromium oxide while the chromium contents of the welding electrode or base metal are high as shown in Table 2. The above observations on the distribution of chromium in the weld metal was also observed by Mitra (25) in his work on slag-metal reactions during submerged arc welding of low alloy and stainless steels. Chromium in the weld and base metal is oxidized into the slag as suboxide and spinels according to equations 7-9; hence it is depleted at the slag-metal boundary. The formation of spinels and solid products at the slag-metal interface can be related to the detachability of slags by considering the work done by Riboud and Lucas (26) on the influence of mass transfer upon surface phenomenon in iron and steelmaking. They found that spontaneous emulsification (dispersion of metallic precipitates into the slag) occured during the reduction of the slag by the metal. Most importantly, it was found that the interfacial tension rapidly decreased during the slag-metal reaction giving a flat droplet. The formation of solid reaction products (like chromite) at the interface and their slow dissolution by the slag could passivate the reaction at its peak thereby confining the slag droplet to its flat form. This phenomenon, in addition to the irregular interface formed by the reaction products, would aid the bonding of slag to the weld metal surface. The formation of an irregular interface is schematically shown below and confirmed to be the case experimentally.

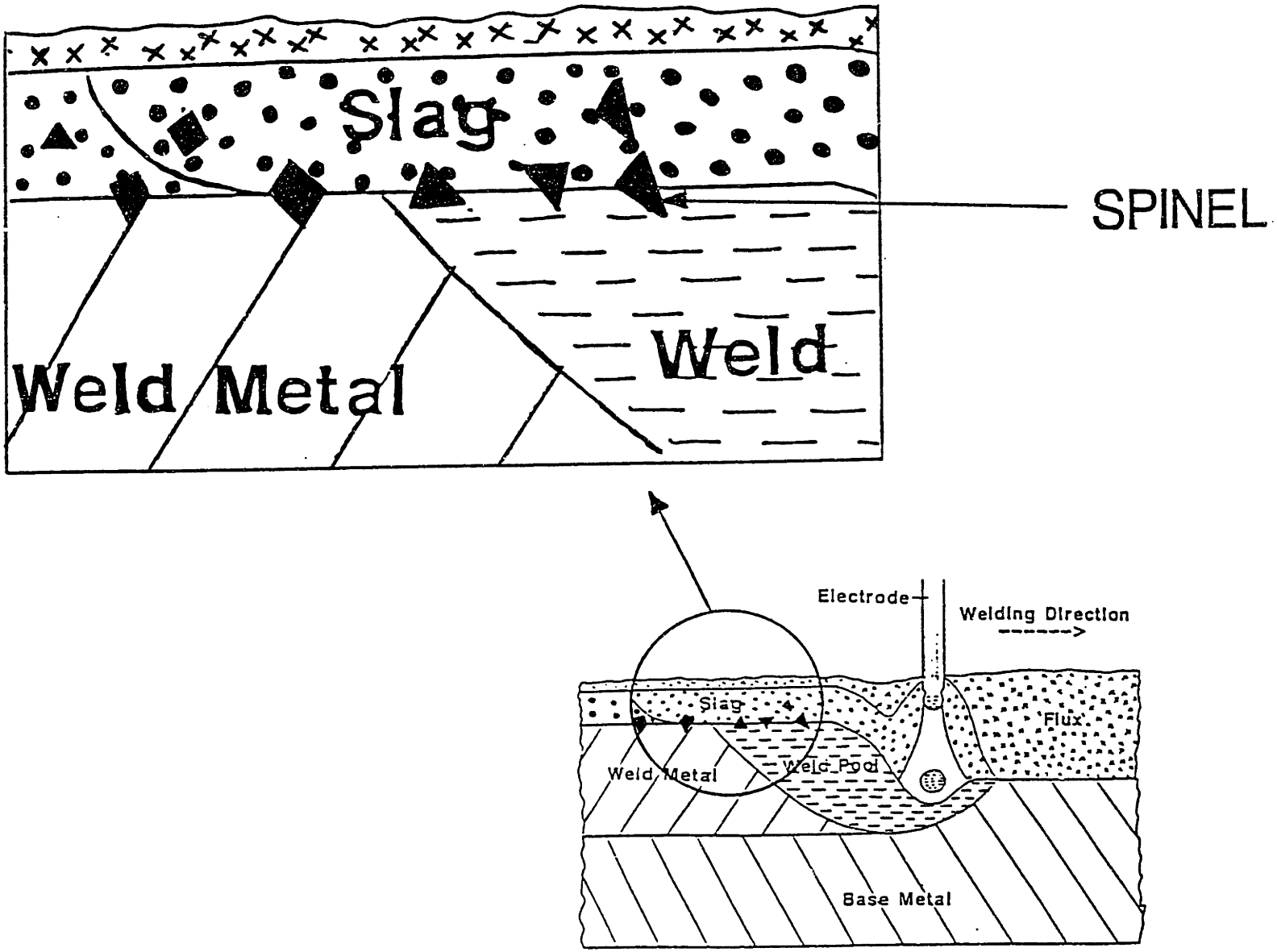

Schematic of Submerged Arc Welding Process

Figure 13(a) shows, two regions A and B with region A that is slag-free and region B with an adherent film of oxide on weld metal AX-HY-Cr8. Figure 13(b) shows region A to have embedded chromium spinels as indicated by SEM and confirmed by x-ray diffraction of slag from this sample and shown in Table 7. Figures 14-18 show x-ray elemental mappings of chromium and chromium spinels embedded in the weld metal surface of various samples. In figure 14(a), a thin film of oxide can be seen covering an underlying layer of chromium spinels. Figures 19(a) and (b) for samples 309-MS-80 and AX-HY-Cr8 show scallop interfaces containing chromium suboxide particles (CrO) and spinels ($MgOAlCrO_3$) as determined by x-ray diffraction and as shown in Table 6. Another observation made in the course of this investigation was that the flux chemistry can prevent chromium spinels from forming even when stainless steel electrodes (26.27 wt.%Cr) are used to deposit a weld on either a thoroughly descaled base metal (sample 309-HY-20) or a heavily scaled base metal (sample 309-HYS-20). The presence of these spinel and suboxide phases at the slag-metal boundary degraded slag detachability by providing a rough interface into which the solidifying slag matrix was attached. Since chromium suboxide is not an equilibrium phase at low temperatures, but it probably is at high temperatures, its formation is believed to be due to the reduction of chromic oxide in the highly reducing atmosphere of the welding arc. The chromite (chromium spinel) with a melting temperature greater than 1660^{0}C and the chromic oxide with a melting temperature of 2250^{0}C (Appendix 4) must have precipitated out of the molten slag and stuck in the solidifying weld metal thus providing anchors onto which the molten slag solidifies and mechanically interlocks. This mechanism is similar to the slag attachment mechanism described by Kohno (23).

Examination of the structures and interfaces of slag samples AX-HY-20, 309-HY-20, and AX-IN-20 showed slag microstructures divorced of any second phases and chromium spinels in particular as shown in figures 20 and 21. This suggests that the observed degrees of slag detachability was not due to chemical effects. A comparison of the ease of slag detachability from stainless steel welds deposited on descaled HY80 base metal with Linde 20, Linde 60, Lincoln 880 and Lincoln 761 fluxes showed that slags from Linde 20 flux were more easily detachable as shown in Table 8. Chai and Eagar (27) in their study of slag-metal reactions in binary CaF_2-Metal oxide fluxes have shown that the stability of metal oxides during welding decreases in the following order:

(1) CaO

(2) K_2O

(3) Na_2O and TiO_2

(4) Al_2O_3

(5) MgO

(6) SiO_2 and MnO

In order to form spinels of chromium at the slag-metal interface and in the slag, it is thus necessary to have dissolved oxygen in the metal. The principal oxides to consider in this oxidation-reduction reaction are: silica, manganese oxide, alumina, magnesium oxide and iron oxide in the fluxes as they are the most reactive metal oxides. As shown in Table 8, Linde 20 flux even though is the most reactive of all the fluxes, due to its high silica content, it does not form chromium spinels. The reason for this observation may be that the slag is too viscous to permit the nucleation of chromium spinels out of the slag. Another factor that may be responsible

for the easier slag detachability with Linde 20 flux is the characteristic gas evolution when welding with this flux; an action which will disturb the slag-metal interactions. Pock marks due to evolution of gases have been observed on the weld metal deposits from the flux.

(B) EFFECT OF TITANIUM OXIDE

The effect of titanium oxide in the presence of a lime flux (Linde 80) and a flux with little or no lime (Linde 60) on slag detachability were investigated. Several investigators (15,22·23) have also observed the detrimental effect of titanium and its oxide on slag detachability as discussed in the introduction to this chapter. However, in this study the detrimental effect was found to be a result of the formation of $CaTiO_3$ precipitates (perovskites) at the slag-metal interface as represented by the reaction equation :

$$(CaO) + (TiO_2) = (CaTiO_3) \qquad (10)$$

Figures 22 and 23 show macrographs comparing the weld metal surfaces of samples made with the same welding electrode and base metal but different fluxes. Macrograph (b) shows adherent slag produced by titanium oxide. Figures 24 and 25 show scanning electron micrographs and x-ray elemental mappings of Fe, Ca and Ti on the weld metal surface of sample 36-MS-Ti8 (made with flux Ti80) with adherent slag. Closer examinations of the slag-free regions of weld metal samples 36-MS-Ti8 and 36-MS-Ti6 show embedded perovskite particles as indicated by ESCA and SEM analyses of their surfaces and confirmed by XRD of their corresponding slags. Table 9 and figures 26-35 show the results of these analyses. Comparing the ESCA spectra of the weld sample with those of the control sample, the former

spectra are broader. This broadness is an indication of more than one chemical state of the element in question. The peak position of the adventitious carbon was used to correct for surface charge effects. This was done by subtracting the amount of shift of the peak, compared to its standard position of 284.6 eV, from the peak positions of the elements of interest. For instance, the peak position of the adventitious carbon in figure 30 is 285.2 eV which implies that a shift of 0.60 eV should be subtracted from the peak position of titanium (459.2 eV) in figure 32 giving a value of 458.6 eV. The possible compounds of titanium in the sample analyzed and its binding energy (ref. 28) in these compounds are: TiC, TiO (454-455 eV), TiN (455-456 eV), TiO_2, and $CaTiO_3$ (458-459 eV). A comparison of these values with that obtained (458.6 eV) clearly eliminates TiC, TiO and TiN as possible compounds leaving only $CaTiO_3$ and TiO_2. Figure 34 also shows that the oxygen is in more than one chemical state and all these results indicate the presence of perovskites on the weld metal surface as well. This observation conforms with that of Kohno et al.(23). Their explanation that perovskite is precipitated at a high temperature (1990^{0}C) and "locks" into the solidifying weld metal appears reasonable. This attachment mechanism is similar to that previously explained for chromium spinels.

(C) EFFECT OF CALCIUM FLUORIDE

During the course of the investigation, it was found that calcium fluoride may have a detrimental effect on detachability depending on the base metal used. For instance, on using Lincoln 880 flux to weld on a descaled HY-80 base metal with AX-90 wire (sample AX-HY-880) and on a descaled Inconel 600 base metal (sample AX-IN-880), it was observed that slag sample AX-HY-880 had easier detachability (2.5) than sample AX-IN-880 (6.0). The weld metal surface of sample AX-IN-880 was also observed to have a tightly adherent scale. X-ray diffraction analyses on slag samples AX-IN-880 and AX-IN-0091 (with detachability value of 6.0) showed AX-IN-880 to contain fluorite, spinels, zirconia dendrites and chromic oxide (Table 10) and AX-IN-0091 to contain cuspidine, $Ca_4F_2SiO_7$, as shown in Table 11. Calcium fluoride has been reported to act as a dilutant of the reactive metal oxides thereby reducing weld metal oxygen contamination (27). Small sample pieces of some welds sectioned, and cleaned of any adherent slag were analyzed for oxygen using vacuum fusion. The results of this analysis are shown in Table (12). From this table one can see that sample 36-MS-60 made from Linde 60 flux (35.28 wt.%MnO and 43.11 wt.%SiO_2) has the highest weld metal oxygen level of 0.0717 wt.%. Alloying of Linde 60 flux with 20 wt.%CaF_2 gave weld metal oxygen levels of 0.036 wt.% and 0.039 wt.% for samples 36-MS-CF6 and 36-IN-CF6 respectively for the same welding conditions. This indicates the diluting effect of calcium fluoride on the reactive oxides of the flux. Silica and manganese oxides were reported to be the most unstable and calcium oxide the most stable. Thus, in slag sample AX-IN-0091 the calcium fluoride acts in diluting the silica of the flux and may, on solidification, give a non-equilibrium phase (cuspidine)

which then attaches to the weld metal surface. It may be prudent to add calcium fluoride to a flux composition as a dilutant in order to minimize the weld metal oxygen content, but one must realize the possible danger of impairing the detachability of the slag layer due to the formation of cuspidine.

Figure 36 compares electron micrographs of microstructures of slag samples AX-HY-880 and AX-IN-880. In addition to fluorite dendrites (arrowed) in sample AX-IN-880, the volume fraction of the spinels is also higher in sample AX-IN-880 (4.175%) than in sample AX-HY-880 (0.725%). Thus, it was necessary to separate the effects of chromium on detachability of slag from that of calcium fluoride. In order to do this, flux CF60 (Linde 60 flux alloyed with 20 wt.% calcium fluoride) was used to deposit a weld on mild steel base metal with Linde 36 electrode (sample 36-MS-CF6). The slag detachability was observed to be poor (3.0) as adherent slag remained in the HAZ of the weld metal. To see if there is any cummulative effect of chromium and calcium fluoride on detachability, the same flux (CF60) was then used to weld on Inconel 600 base metal (sample 36-IN-CF6) and slag detachability was observed to be poorer (5.0) than for sample 36-MS-CF6 as shown in figure 37. This shows that calcium fluoride may have a detrimental effect on slag detachability and that the very poor degree of slag detachability observed for samples 36-IN-CF6 and AX-IN-880 are due to the cummulative effects of calcium fluoride and chromium. One other possible way CaF_2 may have a detrimental effect on detachability is through the reduction of slag viscosity and lowering of the melting point of the slag. In reducing the slag viscosity (or increasing slag fluidity), the molten slag will spread more readily than when the viscosity was high. This

effect is manifested in the slag being adherent to geometric defects as obtainable along the fusion line of the weld metal. A closer examination of the fusion line of weld metal sample 36-MS-CF6, revealed manganese particles (probably MnO) as shown in figures 38 and 39. The almost spherical shape of these particles suggests that there was poor wetting between the particles, the weld metal and the HAZ. The particles then provide a standoff distance, from the weld metal, for the solidifying slag and this may explain why there was little or no adherent slag on the weld metal surface. There was no evidence to suggest that the particles in region C of figure 37 may be responsible for the slag adherence since the HAZ is solid when the slag is still molten. However, it is believed that in the case of slag adherence to the weld metal fusion line, the bonding mechanism is mechanical as adherent slags were found in sharp corners of the weld metal.

(D). EFFECT OF BASE METAL COMPOSITION AND SURFACE CONDITION

The effect of base metal composition on slag detachability is evident from the previous discussion of the effects of chromium on slag detachability. When changing from steel to a nickel-based alloy (Inconel 600), all other conditions being the same, the detachability worsened significantly as shown in Table 4 and figure 40. Compare for example, samples AX-HY-880 (2.5) with AX-IN-880 (6.0); AX-HY-20 (1.0) with AX-IN-20 (3.0) and AX-HY-60 (1.0) with AX-IN-60 (4.0). This effect of the base metal composition on detachability, shown graphically in figure 41, could either be chemical or physical or both. It is chemical when the composition greatly affects the type and amount of intermediate phases that are formed at the slag-metal interface. An example of this effect was discussed under

the effects of chromium on slag detachability. It is physical when the composition affects the physical properties of the resulting weld metal; for instance, the coefficient of thermal expansion, and consequently affects the detachability of the slag layer. This latter effect will be discussed in chapter three.

The surface condition of the base metal was also found to affect the degree of slag detachability. Figure 42 shows the appearance of the weld metal surfaces after welding on both descaled and heavily scaled base metals under the same welding conditions. Adherent slag can be seen on the weld metal surface made on the scaled base metal whereas a cleaner weld metal surface was obtained with the descaled base metal. Poorer detachability was obtained with the scaled base metal than with the descaled base metal (Table 4) as shown in figure 43. The observed deterioration was partly due to the chemical bond formed when the molten slag dissolved the oxide scale on the base metal to form a glass. Also the scale, composed of iron oxide, raises the oxygen potential of the system and promotes reactions between chromium in the metal and silica in the flux. This led to the higher concentration of chromium oxide in the spinels of slag sample 309-HYS-880 and the increased deterioration in the detachability of the slag. Figure 44 shows the two regions of the slag sample AX-HYS-60. The dull region (B) is close to the top surface of the slag while the bright region (A) is the glassy region formed by the oxide dissolution in the molten slag. The cummulative effects of chromium and the formation of chemical bonding produced slags from scaled base metals which were the most difficult to detach of all samples tested. From the above discussion, it becomes obvious that the surface condition of the base metal and the base metal composition are

important factors that affect the detachability of welding slags.

(E) BASICITY OF WELDING FLUX

Welding fluxes are classified into acidic, basic and neutral types by a basicity index (BI) defined in the sixth volum f the Metal's Handbook and modified as:

$$BI = \frac{CaF_2 + MgO + K_2O + Na_2O + 0.5(MnO + FeO)}{SiO_2 + 0.5(Al_2O_3 + TiO_2 + ZrO_2 + Cr_2O_3 + P_2O_5)} \qquad (11)$$

where the oxide compositions are in weight percents.

A flux is acidic if BI < 1.0, basic if BI > 1.5 and neutral for 1.0<BI<1.5. Acidic fluxes are expected to provide easily detachable slags while basic fluxes give difficult slags to detach. In addition to the above functional use of the basicity index, some researchers (3) have used the index to indicate which flux compositions will provide easy slag detachability. The basicity indices of the fluxes used have been calculated using equation (11) and shown in Table 13. A comparison of this table and Table 4 shows that a given flux classified as acidic may or may not give easily detachable slag depending on the welding electrode and base metal used. For instance, Linde 60 and Linde 80 fluxes classified as acidic have degrees of slag detachability varying from a scale of one to seven. Even when detachabilities of equivalent samples of basic (Lincoln 880) and acidic (Linde 60 or Linde 80) fluxes are compared in Table 4, there is no general trend that can be deduced. This again shows the importance of considering

the chemical compositions of not only the flux but also those of the welding electrode and the base metal in the total understanding of the mechanisms controlling slag-metal bonding.

4. CONCLUSIONS

From the results of this study, several conclusions regarding the chemical factors affecting the detachability can be drawn:

* The detrimental effects of chromium and its oxide on slag detachability are mainly through the formation of high melting point (>1600 ^{0}C) chromium spinels, and suboxides that embed in the solidifying weld metal. The resultant irregular interface interlocks with the solidifying slag.

* Titanium oxide's detrimental effect is similar in mechanism to that of chromium except that high melting point (>1900^{0}C) perovskites are formed.

* The detrimental effect of calcium fluoride on detachability of slag may be due to the formation of cuspidine resulting from interaction with the silica in the flux. This cuspidine phase will only form in fluxes of high silica activity. This high melting point non-equilibrium phase then attached to the weld metal.

* Base metal chemical composition affects slag detachability by influencing the physical and chemical properties of the resultant weld metal and slag and hence the type of intermediate phases formed. For instance, a base metal containing chromium will lose some chromium to the slag in the form of oxide and spinel as it will be selectively oxidized in preference to iron. It has been shown in this study that chromium spinels are detrimental to slag detachability and the presence of iron oxide increases the quantity of spinel which forms.

* The surface condition of the base metal was shown to be an important factor in slag detachability due to its effect on the oxidizing potential of the flux and the amount of the oxidizable element lost from the weld metal to the slag. The dissolution of any oxide scale or rust by the molten slag can lead to a chemical bond causing poor detachability of slag.

* The basicity index can not be used a priori to determine which flux compositions will give a readily detachable slag without considering other related factors such as the chemical compostions of the electrode and base metal.

CHAPTER THREE

PHYSICAL FACTORS AFFECTING DETACHABILITY OF SLAGS

Abstract

A two-dimensional thermal model of the slag-weld metal system indicates that the differential thermal contraction and the softening temperature of the slag will affect the distribution of the residual stresses in the slag. In addition, the effects of differential thermal contraction of the slag-metal system and the softening temperature of slag on detachability were investigated experimentally. It was found that in the absence of microfissures and second phases in the slag, higher effective differential thermal contraction per unit length correlated with easier slag detachability. There was no correlation between the ease of slag detachability and the differential coefficient of thermal expansion of the slag-metal system. The rate of cooling of the slag-metal system was also found to affect slag detachability. The higher the cooling rate the more difficult it was to detach the slag. The thickness of the flux layer may be an important factor affecting detachability when cooling rate effects become significant.

In the absence of a chemical bond between the slag and the weld metal, the weaker physical bond becomes important. Thus, the physical properties of the slag, weld metal and the base plate will affect the detachability of the slag. Much has been done on the effects of coefficient of thermal expansion, viscosity and surface tension on slag detachability. However, there has been difficulty correlating the data since chemical interactions were not removed completely and measurement of bulk physical properties does not always reflect conditions at the interface.

The coefficient of thermal expansion or contraction has been found to be important in glass manufacturing. In ceramic-metal seals in bifocal lenses, it is necessary that the coefficients of thermal expansion of both materials be as close as possible. Thus, one may expect that in order to promote slag detachment the coefficient of thermal expansion of the slag should be significantly different from that of the weld metal. Many investigators (2, 29-31) have studied the effects of the coefficient of expansion on the slag detachability. Vornovtskii et. al. (29) observed a correlation between the coefficient of thermal expansion of slag and the ease of slag detachability. He concluded that electrodes containing calcium carbonate and calcium fluoride gave slags with coefficient of thermal expansion (α_s) lower or higher than the coefficient of thermal expansion of the metal (α_m). The higher this coefficient, the easier the detachability he reported. Vornovtskii's conclusion is not clear in the light of the following. Is it being suggested that easier slag removal is achieved when α_s approaches α_m, or if α_s is greater than α_m the slag is more easily

detached. Or when α_s is much greater than α_m? To avoid the apparent confusion in this conclusion, it will be more important to consider the differential thermal contraction of the slag-metal system and not the absolute values of the coefficient of thermal expansion of either the slag or the weld metal. For instance, even if one has a slag with a theoretical coefficient of thermal contraction that is significantly different from that of the weld metal, in practice, polymorphic transformations may occur in either the metal or the slag during cooling depending on the cooling rate. This transformation can be accompanied by a volume expansion of the metal or a contraction of the slag which will reduce the net thermal contraction that could have been achieved in its absence. A volume contraction in the metal accompanying such a transformation will be beneficial to slag detachability as this will increase the differential contraction. It becomes obvious from above that the effect of thermal expansion on slag detachability is closely related to the cooling rate of the slag-metal system. This illustrates further the importantance of considering only the quantity of differential thermal contraction between the slag and the weld metal as opposed to the absolute values of coefficients of thermal expansion or contraction.

2. EXPERIMENTAL PROCEDURES

(A) DILATOMETRY

Recognizing the significant effect of thermal coefficients of expansion of slag and weld metal on slag detachability, measurements of this variable were done using an Orton Recording dilatometer. Figure 45 depicts the head assembly while figure 46 shows the flow diagram for the instrument. The

dilatometer is designed to plot percent linear thermal expansion or contraction as a function of temperature. It can accept a specimen of up to two inches in length and 3/4 inch in diameter and can provide a controlled cooling rate. The dilatometer uses a platinum-platinum 10% rhodium thermocouple for control purposes and for sensing the specimen temperature. The furnace uses a silicon carbide heating element to provide a uniform heating zone along the entire length of the sample. The dilatometer is also equipped with a linear variable displacement transducer (LVDT); an electromechanical transducer that produces an electrical output proportional to the displacement of a separate movable core. The instrument uses both fused silica and alumina sample tubes and provides an automatic correction factor for the sample tube expansion and machine errors.

An argon atmosphere was used in the furnace to minimize the oxidation of the specimens and hence to reduce measurement errors. The argon gas flow rate was 0.2 ft^3/hr under an 8 psi pressure. The exit tube to the atmosphere was connected to a beaker of water to provide a back pressure to the flow of the argon gas and to inhibit back effusion of air. The thermocouple was placed at the top middle of the specimen. The specimens were prepared approximately one inch in length and sectioned with two flat ends and a flat base. This practice was necessary to minimize the rotation of the specimen during expansion and contraction periods.

The dilatometer was programmed to heat the specimen from room temperature to $1300^{\circ}C$ through various temperature segments at different heating rates, as shown in figure 47, and then cool it from $1300^{\circ}C$ to room temperature at $3^{\circ}/min$. The program was then stored as P-S in the program

controller: P being the program position, and S the segment number. A constant force of 4 ozs. was applied on the push rod throughout experimentation. Prior to running the program, the LVDT was initialized as each new specimen was loaded. This was necessary to account for the differences in the original length of the specimens. The thermal expansion and contraction of the specimens were recorded on an X-Y chart recorder as a function of temperature. These charts were then used as input data to a computer program written to calculate an integrated amount of contraction of slag and weld metal and their integrated differential contraction from the softening point to $30^{\circ}C$. Appendix 5 contains the program used.

(B) TWO-DIMENSIONAL FINITE ELEMENT ANALYSIS (FEA)

The need to know the temperature and stress distributions in the welding process required theoretical modelling of the system. To accomplish these tasks, ADINAT and ADINA (32) finite element codes were used. The temperature output from ADINAT was used in ADINA to calculate the residual stresses. For the transient temperature calculations, the model assumed that molten weld metal was deposited instantaneously on a preheated base plate which was covered with flux. Account was made for phase transformations in the weld metal. Table 14 shows the phase transformation data for Fe-0.2C alloy (33) used in the analysis. The governing equations, and the initial and boundary conditions for the heat transfer analysis are given below using the thermal properties as a function of temperature.

$$k\nabla T + \dot{q} = \rho C_p \partial T/\partial t \qquad (12)$$

with initial conditions as shown in figure 48.

Boundary conditions:

$$k_z \partial T/\partial z|_{z_1} = 90.71 \text{ W/mm}^2 \quad (13)$$

$$k_\chi \partial T/\partial \chi|_i = h_i(T)(T_e - T) \quad (14)$$

$$k_\chi \partial T/\partial \chi|_i = \sigma \epsilon F(T_e^4 - T^4) \quad (15)$$

where $\dot{q}$ is the internal heat generated, i denotes the surfaces for convection and radiation. In figure 49, Z_1 is the plane of application where a heat flux of 90.71 W/mm^2 was applied; this value was calculated by the method given in appendix 5. Due to symmetry considerations, only half of the slag-metal system was analyzed. The heat transfer coefficient, $h_i(T)$, was calculated as a function of temperature and geometry of the system. That is, whether the heated surface is horizontally facing upwards or downwards or whether it is vertical as in reference 28. Figure 50 shows the discretized domain of the analyzed system, comprised of 291 nodal points and 130 8-node rectangular elements.

Due to the non-availability of physical and mechanical properties for the slag and flux, the thermal properties (heat capacity, density, thermal conductivity etc.) for a soda-lime-silica glass were substituted as given in reference 34. Values for the coefficient of thermal expansion were taken from the experimental results on each slag-metal system. The physical and mechanical properties used for the slag are shown in Tables 15-17. The physical and mechanical properties for the base metal were taken from reference 35 and are shown in Tables 18 and 19. The properties for the flux were estimated from those of the slag using the relationships given below. These relationships were deduced from equivalent property values for silica and quartz noted in reference 36. The flux being a loose powder, its

properties were taken to be equivalent to those of silica sand and the slag (fused flux) was assigned the properties of quartz, i.e.

$$k_{slag} = 10 * k_{flux} \quad (16)$$

$$E_{slag} = 4.5 * E_{flux} \quad (17)$$

$$\alpha_{slag} = 23.3 * \alpha_{flux} \quad (18)$$

where k is thermal conductivity, E is modulus of elasticity, and α is the coefficient of thermal expansion.

The thermal stress analysis was then performed using the ADINA code with temperature output from ADINAT as input. A thermo-elastic, nonlinear analysis model under a plane strain condition was invoked for this purpose. Figure 51 shows the displacement constraints on the system. The softening points of the slag were incorporated in the analysis by inputing $\alpha_s = 0$ for $T > T_s$ to the stress program. A sensitivity analysis was then performed to determine the effects of softening point, differential thermal contraction of slag and weld metal, and slag thickness on the residual stress levels. The softening point of the slag was chosen as the reference temperature: the temperature at which the residual stress is zero. This is justified by the fact that after the weld metal has solidified, the still molten slag can relieve any built up stresses. However, it would be more accurate to use the glass transition temperature as the reference temperature, if it were available.

(C) COOLING RATE

A study of the effect of cooling rate on the detachability of slag was performed by welding on preheated base plate, base plate placed on a water-cooled copper block and in water-cooled copper troughs. This study is qualitative since no measurement of the cooling rate was performed. Artificial base metals were made from the welding electrodes by splicing six-inch lengths and binding them together with pieces of the same electrode. The bundled electrode was then laid in the groove of the water-cooled copper hearth (37).

(D) MEASUREMENT OF TEMPERATURE

The temperature fields encountered during welding operations are important to the magnitude of the residual stresses in the weld and slag system and consequently the weld metal properties and the detachability of slag. There are two major ways to determine these temperature fields: contact (use of thermocouple) and non-contact (the use of infrared radiometer) methods.

A model 600 Inframetrics with an 8-14 μm spectral response was used. The model uses a mercury-cadmium-telluride detector operating at 77k for high thermal sensivity and spectral resolution. The sensitivity of the instrument is $0.05^{o}C$ on a $30^{o}C$ target with a maximum error of $2^{o}C$ on the temperature readout. The instrument uses a rotating thermal reference which is looked at sixty times per second for calibration purposes. The calibration is then updated every half second. Even though the longwave

region (8-14 μm) is characterized by minimal losses of infrared energy due to atmospheric absorption, measurements used in a comparative study were performed within minutes of each other on the same day. Because of the nature of the measurement, the base metals used were ground clean and smooth and the detector's angle of view of the object was maintained constant. Linde 36 wire and Lincoln 880 flux were used to deposit welds on HY80 base metal. A video cassette recorder (VCR) attached to the Inframetrics scanner was used to record the observed images for post-processing. The welding parameters and procedure used are as described in Table 1 and chapter two. The data collection was begun shortly after the contact tip of the welder head and the flux hopper were out of view of the detector. The objective of this temperature measurement was to compare the temperature profiles in a slag without an insulating flux layer with those in a slag covered with an insulating flux layer during cool down period of a welding thermal cycle.

The first measurement was made on a slag system (A) that had its flux layer taken off by tilting the base plate and the still red-hot slag exposed to the atmosphere. The second slag system (B) had its insulating flux layer for the entire period of measurement. The recorded images are then processed by thermaGRAM software run on an IBM PC-XT and displayed on an RGB monitor. All VCR settings (e.g. background temperature, emmitance etc) are encoded with the image and authomatically factored into the temperature analysis. An emmisivity of 0.85 was assumed for both the flux and slag layers while the detector distance from the object was 0.58 meters.

3. RESULTS AND DISCUSSION

The results of this chapter will be discussed under separate headings even though these headings are interrelated.

(A) EXPERIMENTAL RESULTS

(i) Integrated Differential Thermal Contraction

The results of the measurements on thermal expansion (contraction) as a function of temperature are typified in figure 52 for two base metals and a typical slag system with a high softening temperature. The slope of these curves give the coefficients of thermal expansion. This figure indicates that using the raw data of coefficient of thermal expansion of the base metal and slag, HY80 base metal should provide slags that will be more difficult to detach than corresponding slags from the mild steel base metal. However, this deduction contradicts the experimental observation that HY80 base metal provided slags that were the easiest to detach of the base metals used in this study. This points out the error of judgement that can result from the use of the absolute values of the coefficients of thermal expansion of the slag and base metal to determine which slag-metal combination will provide easy or difficult detachability.

It will be more insightful to study the effects of the quantity of differential thermal contraction, obtainable in a given thermal cycle, on detachability. Hence, the dilatometric measurements as typified in figure 52 were used to calculate the integrated thermal contractions of the slag,

the metal as functions of temperature and the mean integrated differential thermal contraction per unit length from the softening temperature of the slag to room temperature (Table 20) by means of a computer program (Appendix 5). To interprete or correlate results of Table 20 with detachabilty of the slag (Table 4), caution has to be exercised for the following reasons. At first glance, there appears to be no obvious correlation between these two tables. However, an examination of the slag microstructure provides a clue to the lack of general correlation between differential thermal contraction per unit length and detachability of the slag. Slag samples with microcracks gave very high values of differential thermal contraction per unit length (Table 21). This table also shows the lack of a correlation between slag detachability and differential thermal contraction per unit length and shown in figure 53. During expansion of such a slag sample, the heat input is initially used to fill the microcracks in the slag matrix before a uniform expansion of the sample is achieved. Thus, this will lead to a small apparent expansion (contraction) of the slag sample and hence a high differential contraction. Figures 54-57 show electron micrographs of slag samples with microcrack-free structures while figures 58-59 show those with cracked microstructures. Table 22 compares the degree of slag detachability with differential thermal contraction per unit length for the latter. On examining only slag samples that have microcrack-free structures, it was found that the higher the differential thermal contraction per unit length the easier the detachability of slag as shown in Table 22 and figure 60. One should also note the absence of second phases (due to slag-metal reactions) in these slag samples. Figures 61 and 62 show the plots of percent integrated thermal contraction as a function of temperature for two of these slag-metal systems with good (1.0) and poor

(3.5) slag detachabilities. In figure 61, where the slag was easier to detach, the effective differential thermal contraction at $30^{0}C$ is about 0.0045 mm/mm compared with the slag of figure 62 that is more difficult to detach having a value of 0.003 mm/mm. Thus, the observed trend in degree of slag detachability can be attributed to the effective differential thermal contraction per unit length in the slag-metal systems.

As mentioned earlier in the previous chapter, the chemistry of the base metal will affect the detachability of slag both physically and chemically. The chemical effects have been explained. Figures 63 and 64 show plots of percent integrated thermal contraction as a function of temperature for two slag-metal systems using the same flux and electrode but different base metals. In these figures, no difference is clearly observable in the contraction characteristics despite the significant difference in the detachabilities of the two slag-metal systems. This result indicates that there must be another factor beside the thermal contraction that affects detachability. In fact, the results of figure 64 are those of sample AX-IN-0091 in which cuspidine was found to contribute to the poor detachability. Figure 41 shows that the detachability of slag is worse with mild steel base metal than with HY80 base metal. This difference in detachability has to do with the difference in metallurgical structure of the base metals. HY80 is a quenched and tempered martensitic steel whereas mild steel is a low-carbon steel with finer microstructure. During cooling cycle of the slag-metal system, the martensitic steel will generate a higher mechanical strain at the slag-metal interface due to the high volume change associated with martensitic transformation. Hence, for the same conditions the slags from welds deposited on HY80 base metal may be more easily

detached than those from welds deposited on mild steel base metal.

(ii) Measured Temperature

A direct comparison of the actual temperature measurements with those of the thermomechanical model at equivalent times is not feasible for the following reasons. By the very nature of the measurement technique, there is a lag between the time when the slag and the weld metal are molten and the time when the data collection can be started. This time lag will cause an inherent difference in the temperature values measured and calculated by the model since the model assumed initially molten weld metal and slag. However, the trends predicted in the temperature distribution should follow what is observed experimentally. Hence a comparative study of the temperature distribution was performed on two slag systems A and B. Slag system A had no insulating flux cover while slag B had a flux cover as described previously. The temperature of the flux layer in B is what is measured and for the first one and a half minute, the flux was still heating up before it starts to cool down. The temperature values for the equivalent cooling periods of slag systems A and B are then compared and reported in Table 23. In this table the temperature was measured at identical positions of both slag systems. The temperature values were measured to be higher in the slag with an insulating flux cover than in the slag without this flux layer after equal times have elapsed. The net effect of this result is a higher temperature gradient in slag A as shown in figure 65 and possibly higher residual stress which may have a significant effect on the detachability of the slag.

(iii) Softening Temperature

The softening temperatures of the welding slags were determined from the dilatometric measurements as the temperature at which the slag starts to creep. The results of this determination are shown in Table 24. This table shows that the softening temperature is a function only of the welding flux and when compared with the degrees of slag detachability in Table 4, no general correlation can be drawn between slag detachability and softening temperature of the slag. Again this shows that softening temperature has little or no effect on the detachability of slag.

(iv) Cooling Rate

The effect of cooling rate on slag detachability has been studied only qualitatively. Table 25 shows the detachability of slags from welds deposited in a water-cooled copper trough. The slags from these welds were observed to adhere much more strongly than their counterparts shown in the same table. For instance, slag sample AX-AXC-880 from Table 25 had a detachability rating of 7 compared to its counterpart AX-HY-880 with a rating of 2.5. This effect of cooling rate can be related to macrostresses, microstresses and polymorphic transformations in the base metal, in the weld metal and in the slag during cooling. At a high cooling rate, stresses are generated in the first solidified slag layer and it will crack up unless the rest of the molten slag can accomodate the microstrain generated by redistributtion. But at a low cooling rate, polymorphic transformations may have time to occur and the expansion due to this transformation will generate mechanical strain which will also affect the detachability. Thus,

it appears that high cooling rate will minimize the quantity of microstrain from polymorphic transformation but maximize thermal strains unless the slag can redistribute the generated thermal strains. For this scenario the slag may thus be more difficult to detach. This result implies that a very viscous slag cooled rather rapidly may be more difficult to detach than a fluid slag cooled rather slowly. A viscometry determination may be necessary to explain fully the effect of cooling rate on detachability.

(B) THERMOMECHANICAL MODEL

The temperature profile as a function of time through the thickness of the slag-metal system was calculated and the results were used to calculate the thermal stresses in the system. Due to the lower thermal conductivity of the slag/flux layers and the high viscosity of the molten slag as compared with the molten weld metal, heat transfer through the slag/flux layers will be rate limiting. Thus, it will be interesting to know the position and magnitude of the thermal gradient with time. This thermal gradient will affect the magnitude of the residual stress which will affect the detachability of the slag. A sensitivity analysis was performed on the effects of softening temperature and differential thermal contraction per unit length of the slag-metal system on the magnitude of the residual stresses in the slag.

(i) Thickness of slag

The effect of the thickness of slag or flux on the gradient of the temperature profile and magnitude of the peak temperature as a function of

time is shown in figures 66 and 67. Figure 67 shows that the temperature gradient in the slag becomes steeper when the thickness of the slag is reduced in half. This reduction will consequently lead to a higher residual stress level in the slag which can affect the ease of slag detachability since it will affect its contraction characteristics.

(ii) Differential thermal contraction and softening temperature

Figures 68 and 69 show plots of effective residual stress at the slag-metal interface as a function of time for two slag samples of the same softening temperature ($950^{0}C$) but different differential thermal contractions. Figure 68 shows that a sample with differential thermal contraction per unit length of $24*10^{-4}$ mm/mm has a higher thermal stress than a sample with a differential thermal contraction per unit length of $20*10^{-4}$ mm/mm (see figure 69). The implication of this result is that a slag system with a higher differential thermal contraction per unit length will be easier to detach than one with a lower differential thermal contraction per unit length all other conditions held constant. Figures 70 and 71, however, show the effect of softening temperature of the slag system on the effective residual stress at the slag-metal interface. In these figures, the differential thermal contractions are equal while the softening temperatures differ by $300^{0}C$. Despite this large difference, there was very little change in the residual stresses. In fact the higher softening temperature slag had a lower residual stress level. This latter result suggests that for all other conditions being equal, the slag system with the lower softening temperature may be more easily detached. Also the results show that the differential thermal contraction will influence the

detachability of slag much more than the softening temperature of the slag based on the calculated residual stresses.

(iii) Temperature distribution

The temperature fields in a slag metal system with and without an insulating flux cover were simulated and the results displayed in figures 72 and 73. For the same elasped time, figure 72 shows a slag layer without flux cover to have a less steep temperature gradient than a slag layer with flux cover as shown in figure 73. However, it is interesting to note from these figures the progressive march of the hump in the temperature profile into the flux region with time. Hence, it will be important to know both the magnitude of this peak and its position during cooling as it could make the difference between an easily detachable slag and one that is difficult to detach due to the consequent magnitude of the residual stresses.

4. CONCLUSIONS

From the results of this study, several conclusions regarding the physical properties affecting the detachability can be drawn:

* The effect of differential thermal contraction of slag and weld metal on detachability can be understood when the structure of the slag is included in the analysis. This is necessary in order to exclude slags that have cracked microstructures which might distort the measured values of the differential thermal contraction per unit length.

* For slags that have microcrack-free structures, it was found that the higher the differential thermal contraction per unit length of the slag-metal system, the easier the detachability of the slag.

* The softening temperature of the slag is a function only of the welding flux and has little or no effect on the detachability.

* The insulating effect of the unfused welding flux tends to keep a higher temperature gradient in the slag layer than in the case when the slag had no insulating flux cover. This effect can be viewed also in terms of the thickness of the welding flux used. The thicker the flux layer the, the higher will be the temperature gradient in the slag. This difference in the temperature gradients will affect the magnitude of the thermal residual stresses in the slag and may affect the detachability.

* For any given flux compositon, the higher the cooling rate of the slag-metal system the more difficult it will be to detach the slag.

CHAPTER FOUR

SUMMARY OF CONCLUSIONS

The principal objective of this thesis has been to identify the main factors affecting the detachability of slags from welds in flux-shielded welding processes and to provide a fundamental understanding of the bonding mechanism between the slag and the weld metal. This knowledge can then, hopefully, be used to improve development of welding fluxes. Several conclusions can be drawn from this work. The factors affecting detachability can be classified into two broad categories:

(A) CHEMICAL EFFECTS & (B) PHYSICAL EFFECTS

When present, the chemical effects will dominate the physical effects providing slags of very poor detachabilities.

(A) CHEMICAL EFFECTS

1). CHROMIUM SPINEL

The detrimental effects of chromium in metal form and oxide form on slag detachability are mainly through the formation of high melting point (>1600 ^{o}C) chromium spinels ($FeCr_2O_4$) and suboxides that embed in the solidifying weld metal. The resultant irregular interface interlocks with the solidifying slag causing poor slag detachability. Hence, prevention of the formation of this type of spinel may improve detachability. This can be achieved by adjusting the reactive oxide composition of the flux such that it has a moderately high viscosity or the concentrations of the

spinel-forming oxides are moderately low. For instance, Linde 20 flux that was observed to provide slags with the easiest detachability from stainless steel welds and spinel-free slags, has the highest viscosity (based on the silica content) and is moderately low in magnesium oxide and alumina. The basic structure of the spinel is AB_2O_4 or that of $MgAl_2O_4$. As shown in appendix 4, the spinel compound will most likely form at a 50:50 mixture of magnesium oxide and alumina because it has the least free-energy of formation at 1750°C. Chromium spinels were formed in the slags from Lincoln 880 flux because it has high concentrations of MgO and Al_2O_3 (in about equal amounts) which combine with the oxidized chromium to form $MgAlCrO_4$ spinel. It was shown in this work that these spinels become richer in chromium as the welding electrode is changed to a stainless steel electrode and/or the oxidizing potential of the flux is raised via the use of a scaled base plate. Consequently, the detachability of slag worsened. Hence, it will be important to prevent the formation of $MgAl_2O_4$ spinel if chromium must be alloyed to the weld metal by adjusting the compositions of MgO and Al_2O_3 in the flux.

2). TITANIUM OXIDE IN FLUX

Titanium oxide's detrimental effect is similar in mechanism to that of chromium except that high melting point (>1900°C) perovskites are formed which mechanically interlock the slag with the weld metal.

3). CUSPIDINE

As was shown in this work and by previous researchers, calcium fluoride

can minimize the oxygen content of the weld metal by diluting the reactive metal oxides in the flux. However, a copious addition of calcium fluoride to a high silica activity flux may prove detrimental to slag detachability. The interaction of calcium fluoride with silica in the flux may result in the formation of cuspidine which was found to be detrimental to detachability. Calcium fluoride is an important flux constituent because of its role in lowering the viscosity and the melting temperature of the slag and, as reported in the literature, it also minimizes the oxygen content of the weld metal. So, calcium fluoride will still remain an important constituent of the flux composition despite its deleterious effect on detachability. However, this effect can be avoided if calcium fluoride is added to a basic flux rather than a flux with a high silica activity to prevent the possible formation of cuspidine. This actually explains why large amounts of calcium fluoride are not added to acidic fluxes.

4). BASE METAL CHEMICAL COMPOSITION

The chemical composition of the base metal was found to affect the detachability of slags. Changing from a quenched and tempered martensitic steel (HY80) to a nickel-based alloy, detachability worsened by almost a factor of three for equivalent welding conditions. Base metal chemical composition affects slag detachability by influencing the physical and chemical properties of the resultant weld metal and slag and hence the type of intermediate phases formed. For instance, a base metal containing chromium will lose some chromium to the slag in the form of oxide and spinel as it will be selectively oxidized in preference to iron. It has been shown in this study that chromium spinels are detrimental to slag detachability.

Hence, the effect of the base metal chemical composition on detachability can be minimized by following the same guidelines discussed under chromium spinels for a suitable base metal, electrode and flux combination that will provide easy detachability. By this practice, flux can then be tailored to specific new steels.

5). IRON OXIDE & OXIDIZING POTENTIAL OF FLUX

The surface condition of the base metal was shown to be an important factor in slag detachability due to its effect on the oxidizing potential of the flux and the amount of the oxidizable element lost from the weld metal to the slag. The dissolution of any oxide scale or rust by the molten slag can lead to a chemical bond causing poor detachability of slag. A comparison of the detachability of slag from several welds deposited with similar fluxes on thoroughly descaled base metal and scaled base metal, showed the detachability of slags from welds deposited on the scaled base metal to be the poorest. This deterioration was also shown to be due to the increased amount of chromium spinels formed. In the light of the finding on the effect of chromium spinels on detachability and the dissolution of the oxide scale by the molten slag, it will be prudent to thoroughly descale the base metal before a weld is deposited; especially if chromium is to be alloyed with the weld metal.

6). BASICITY INDEX OF FLUX

The basicity index can not be used a priori to determine which flux compositions will give a readily detachable slag without considering other

related factors such as the chemical compostion of the electrode, and base metal and the welding conditions. It has been shown that a flux classified as acidic by this index provided slags with both easy and poor detachability depending on the welding conditions and the materials used. This result also indicates that one can not and should not base formulation of a new flux composition that will provide slags with easy detachability on the basicity index.

(B) PHYSICAL EFFECTS

In the absence of a chemical effect, the important factors to consider affecting detachability are physical effects as summarized below.

1). COEFFICIENT OF THERMAL EXPANSION OF SLAG & METAL.

When a weld is deposited on a base metal, the weld metal can be safely assumed to possess the same coefficient of thermal expansion as the base metal because of the fusion between them. This will be especially true in a groove weld. However, the use of the absolute values of these coefficients to determine which base metal and flux combination will provide a slag with easy detachability has been shown in this work to lead to an erroneous judgement. A more important indicator was found to be the effective differential thermal contraction of the slag-metal system. From the chemistry of the flux and base metal, and predetermined continuous-cooling-transformation curves, one can estimate the net thermal contraction expected in a given cooling cycle.

2). MICROSTRUCTURE OF THE SLAG

The effect of the differential thermal contraction of slag and weld metal on detachability can be understood when the structure of the slag is included in the analysis. This is necessary in order to exclude slags that may have cracked-microstructures which might distort the measured values of the effective differential thermal contraction per unit length. For slags that have microcrack-free structures, it was found that the higher the differential thermal contraction per unit length of the slag-metal system, the easier the detachability of the slag. The microfissuring of the slag is tied closely to the cooling rate of the slag-metal system, and the physiochemical properties of the slag and weld metal. Most of the slags with second phases like spinels, had microcracked-structures while the glassy slags were microcrack-free.

3). THICKNESS OF THE WELDING FLUX

The insulating effect of the unfused welding flux tends to keep a higher temperature gradient in the slag layer than in the case when the slag had no insulating flux cover. This effect can be viewed also in terms of the thickness of the welding flux used. The thicker the flux layer, the higher will be the temperature gradient in the slag. This difference in the temperature gradients will affect the magnitude of the thermal residual stresses in the slag and may affect the detachability especially when cooling rate effects are significant. Hence, it will be advisable that only enough flux to just submerge the arc should be used during welding. This practice will not only minimize the thermal residual stresses in the slag

but will also minimize the production cost due to a lesser flux consumption.

4). COOLING RATE OF THE SLAG-METAL SYSTEM

The effect of cooling rate on slag detachability will depend on a number of factors such as viscosity of the slag, base metal composition, thermal properties of the base metal and slag and the welding parameters. A base metal that undergoes polymorphic transformation under normal cooling rates, can have this transformation suppressed under a high cooling rate. This will thus reduce or eliminate mechanical strains that would have otherwise been generated thus affecting the detachability. The viscosity of the slag can be such as to minimize the increased thermal strains due to a higher cooling rate by redistribution. It was found in this study that the higher the cooling rate of the slag-metal system the more difficult it was to detach the slag. The cooling rate can be controlled through the welding parameters: current, voltage and travel speed and by either preheating or chilling of the base metal. Once a link between the cooling rate and the viscosity of slag can be established and a quantitative appraisal of the effect of cooling rate on detachability is performed, then new flux compositions can be developed that under a controlling physical effect, will produce slags of easy detachability.

In closing, it must be mentioned that the factors identified above are not the only factors that can affect slag detachability. Nevertheless, these factors are very important to any fabricator or flux manufacturer that must be concerned about slag adherence to the weld metal surface. This work has confirmed the mechanisms of slag-to-metal bonding suggested by some

previous investigators. It has also corrected the notions of some others on this mechanism, and more importantly provided explanations (supported by data) of some experimental observations that were previously not understood. As can be seen from this summary, the factors are very much interrelated and a distinct isolation of the factors is almost impossible. However, the results of this work show that there exists a systematic relationship between the factors such that, if a scientific approach is followed in the process of flux manufacturing, the development time of a new flux composition can be reduced drastically.

CHAPTER FIVE

RECOMMENDATIONS FOR FUTURE WORK

As noted in the chapter on summary of conclusions, there are many more factors to be investigated that can affect the detachability of slag. Also, the interrelationships of these factors makes the study even more challenging. Nickel-based alloys are widely used in the nuclear reactor industry which makes the study of slag detachability in submerged arc welding of these alloys very desirable. Inconel 600 base metal provided slags with the worst detachabilities showing that the base metal composition is an important factor to consider. However, Inconel 600 is a nickel-based alloy, HY80 base metal, and AX-90 wire also contain nickel. In this work we have not isolated any contributing effects of nickel to detachability. It will be interesting to investigate any possible effects of nickel by either alloying the flux with nickel oxide or welding on a mild steel base metal covered with a nickel foil.

Some detachability problems have been experienced in the welding industry when using C-Mn-Mo electrodes. It was found that C-Mn-Mo electrodes improved detachability with a flux that otherwise provided adherent slag when C-Mn electrodes were used. Molybdenum is not expected to oxidize out of the molten weld pool but it is well known to affect the transformation of the weld metal. Thus, it is very likely that Mo shifts the γ-α transformation temperature thereby affecting the differential thermal contraction of the slag-metal system. This work has shown how the differential thermal contraction can affect the detachability. Therefore,

an investigation is needed into the mechanics of molybdenum effects on detachability.

The effects of cooling rate on detachability has been studied only qualitatively and as noted earlier, it will be necessary to study this effect quantitatively and also relate it to the viscosity of the slag. The joint design of the parts to be welded will influence the cooling rate of the slag-metal system and may significantly affect detachability. This shape factor effect needs to be investigated fully considering the increasing importance of Narrow Gap Submerged Arc Welding process. The thermomechanical model used in calculating the temperature and thermal stresses in the slag-metal system can be improved upon. We have accounted for phase transformations in the weld metal only and neglecting any possible transformations in the slag. This assumption obviously reduces the actual heat content of the system; an inclusion of which will predict higher temperatures. Also in calculating the residual stresses, we have used the perfectly elastic model which may not be the case due to possible plasticity at the slag-metal interface. The effect of other variables such as viscosity, heat input, cooling rate and base metal thermal properties still need to be investigated in the model. The continuation of the study of the model is recommended because of its importance in providing a theoretical understanding of the factors that can affect not only the detachability of slag but also the weld metal properties.

Finally, it is recommended that a factorial experimental study be performed on the factors identified in this work in order to understand better their relative importance and their interactions. A controlled

addition of some of the alloying elements found to be detrimental to detachability has not been done in this work. As noted in the introductory chapter, the objective was to identify the major factors affecting detachability and to provide an understanding of the mechanisms of the slag-to-metal bonding. However, it would be necessary to carry out the experimental study mentioned above since some of these elements are desirable for improved weld metal properties. Then, it will be possible to establish a threshold beyond which the alloying element will start to have a deleterious or beneficial effect on detachability.

LIST OF REFERENCES

(1). Chai, C.S. "Slag-Metal Reactions During Flux Shielded Arc Welding" M.I.T. Ph.D. Thesis, 1980.

(2). Davis, M.L.E., and Bailey, N., "Have We The Right Ideas About Fluxes" Proc. International Conference on Trends In Steels and Consumables for Welding. The Welding Institute London, Nov. 1978 p. 231.

(3). Patchett, B.M., and Renwick, B.G., Welding Journal vol. 55 1976 p. 69s.

(4). Podgaetskii, V.V., "Mechanical Retention of the Slag on the Weld in Automatic Welding" Avt. Svarka 1950, No. 6.

(5). Yakobashvili, S.B., "Effects of Cr and V on Inter-phase Surface Tension Between Liquid Steel & Flux" Avt. Svarka, 1962, No. 8.

(6). Rabkin, D.M., et. al., "Ease of Removal of the Slag Crust in Automatic SAW" Avt. Svarka, 1950, No. 3.

(7). Rabkin, D.M., et. al., "Adhesion of the Slag Crust to the Surface of the Weld Metal when welding by SA Process" Autogennoe delo, 1951, No. 6.

(8). Hazlett, T.H., "Coating Ingredients Influence on Surface Tension, Arc Stability, and Bead Shape" Welding Journal, 36(1), 18s-22s, 1957.

(9). Yakobashvili, S.B., "The Inter-Phase Tension of Welding Fluxes and Its Effect on the Ease With Which the Slag Crust is Removed." Avt. Svarka, 1962, No. 9.

(10). Yakobashvili, S.B., and Frumin, I.I., "Investigation of Inter-Phase Tension at the Slag Metal Boundary and of the Surface Tension of Welding Slags" Automatic Welding 1961, No. 10.

(11). Vaisberger, A., "Physical Methods in Organic Chemistry" IIL, Moscow, 1950.

(12). Shono, S.A., "Research into the Surface Properties of the Slags formed during the deposition of Wear-Resistant Metal" Avt. Svarka, 1976, No. 8 p. 24-25.

(13). Vernovtskii, I.N., et. al., "A Method of Quantitative Appraisal of the Removability of Slags" Svar. Proiz., 1957, No. 2 p. 67

(14). Pokhodnya, I.K., et al., Avt. Svarka, 1976, No. 6, p. 1-4.

(15). Pokhodnya, I.K., et al., "The Mechanism of the Bond between the Slag Crust and the Weld Surface" Avt. Svarka, 1974 No. 5.

(16). Wittung, L., Paper 35, Proc. International Conference on Trends in Steels and Consumables for Welding The Welding Institute London, Nov. 1978.

(17). Naka, M., et al., "Technical Note", Trans. JWRI

(18). Naka, M., et al., Trans. JWRI, 11(1982) No. 1, p. 133

(19). Cole, S.S. Jr., et al., "Metal-to-Ceramic Seal Technology Study" Final Report ASTIA AD 248535, Oct. 1960

(20). Klomp, J.T., Ceramic Bulletin, vol. 59, No. 8, 1980

(21). Klomp, J.T., and Vrugt, P.J., in "Surfaces and Interfaces in Ceramic and Ceramic-Metal Systems" Materials Science Research vol. 14, p. 97 ed. J. Pask and A. Evans.

(22). Bobrikov, Yu. V., et al., "Controlling the Ease of Slag Removal from Metal deposited with a Strip electrode." Avt. Svarka, 1983, No. 5

(23). Kohno, R., et al., Welding Journal, vol. 61 Dec. 1982, p. 373s

(24). Okuda, N., and Kumagai, M., "Summary of lecture at meeting of the Japan Welding Society," Oct. '82- Apr. '83; issued Sept. '84

(25). Mitra, U., "Slag-Metal Reactions During SAW of Low Alloy and Stainless Steels." M.I.T. S.M. Thesis, 1982

(26). Riboud, P.V. and Lucas, L.D., "Mass Transfer in Iron & Steelmaking" Canadian Metallurgical Quarterly vol. 20, No. 2 1981

(27). Chai, C.S., and Eagar, T.W., "Slag-Metal Reactions in Binary CaF_2-Metal Oxide Welding Fluxes." Welding Journa, vol. 61 July, 1982, p. 229-s.

(28). Physical Electronics Handbook of X-ray Photoelectron Spectroscopy.

(29). Vornovtskii, et al., "Thermal Expansion of Slags from Certain Welding Electrodes" Avt. Svarka, 1977 No. 7, p. 49

(30). Lazarev, B.I., et al., Svar. Proiz., 1979, No. 5, p. 25

(31). Ukebe, et al., "Development of NSA Process" Kawasaki Steel Technical Report No. 5, May 1982.

(32). ADINA ENGINEERING, "Reports AE81-1 and AE81-2": ADINAT & ADINA Users Manuals.

(33). Kubaschewski, O., "Metallurgical Thermochemistry" p. 372 Pergamon Press Publishers.

(34). Babcock, C.L., "Silicate-Glass Technology Methods" p. 198, J. Wiley Publishers.

(35). Papazoglou, M.I.T. Ocean Engineering, Ph. D. Thesis, 1981.

(36). Van Vlack, L., "Elements of Materials Science" p. 419, 2nd. edition. Addison-Wesley Publishers.

(37). Mitra, U., "Kinetics of Slag-Metal Reactions During SAW of Steels" M.I.T. Sc. D. Thesis 1984.

(38). Levin, E.M., et. al., "Phase Diagrams for Ceramists", 1964, The American Ceramic Society Inc. Publishers.

(39). Kingery, W.D., et. al., "Introduction to Ceramics", 2nd. Ed. p. 133, J. Wiley Publishers.

TABLE 1: WELDING PARAMETERS

VOLTAGE	32-33 volts
CURRENT	300 amperes
TRAVEL SPEED	5.93 mm/s
PREHEAT TEMPERATURE	Room temperature
ELECTRODE STICKOUT	19 mm
ELECTRODE DIAMETER	2.38 mm
POLARITY	DCEP

BASE METAL THICKNESSES:

HY80 and 1010 steel : 12.5 mm

Inconel 600 : 19.05 mm

Table 2 Composition of Base Metals and Welding Electrodes (wt.%) *

		C	Si	Mn	P	S	Cr	Ni	Mo	V	Al	Ti	Fe	Thickness Diameter(mm)
Base Metal	HY-80	0.16	0.22	0.26	0.012	0.011	1.35	2.17	0.23	0.004	0.011	0.002	bal.	12.5
	Mild Steel	0.12	0.13	0.45	0.025	0.037	0.10	0.11	0.02	---	0.011	---	bal.	12.5
	Inconel 600	0.018	0.26	0.45	0.018	.005	15.9	bal.	0.29	0.06	0.23	0.32	8.0	19.05
Electrodes	AX-90	0.05	0.46	1.31	0.016	0.007	0.066	1.93	0.41	0.058	0.003	0.003	bal.	2.38
	Ld 36	0.14	0.03	2.00	0.017	0.024	---	---	---	---	---	---	bal.	2.38
	Ld 40	0.15	0.03	2.00	0.017	0.024	---	---	0.53	---	---	---	bal.	2.38
	309 L	0.014	0.44	1.43	---	0.009	26.27	12.36	0.06	---	---	---	bal.	2.38

* Analysis performed by Arnold Greene Testing Laboratories using ICAP spectrometer.

Table 3: Composition of Welding Fluxes (wt.%)*

	MgO	CaO	CaF_2	SiO_2	Al_2O_3	FeO	TiO_2	MnO	K_2O	Na_2O	P_2O_5	ZrO_2	Cr_2O_3
Lnc 880	24.21	2.10	20.80	16.59	22.73	1.21	0.07	0.19	0.07	2.07	0.25	6.62	-
Lnc 761	20.76	-	7.83	42.47	2.05	3.11	1.46	19.58	0.22	2.14	0.22	-	-
Ld 20	9.10	22.12	6.52	55.72	3.08	0.41	0.32	0.60	0.12	0.17	0.14	-	-
Ld 60	-	-	6.30	43.11	3.83	2.59	0.27	35.28	0.70	0.16	0.27	-	-
Ld 0091	0.60	28.61	19.25	31.30	3.67	0.28	4.11	0.17	0.10	4.62	0.14	-	-
Ld 80	11.86	16.84	8.69	37.16	14.56	0.94	0.55	6.99	0.12	0.12	0.13	-	-
Cr80	7.86	11.81	6.49	31.90	15.10	1.93	0.55	4.48	-	-	-	-	19.69
Ti80	9.40	14.73	6.83	29.93	11.69	1.56	19.65	5.05	-	-	-	-	0.33
Ti60	-	-	5.51	34.93	3.74	3.12	19.71	31.25	0.20	-	0.11	-	-
CF60	-	-	21.52	35.94	3.36	1.04	0.29	28.96	0.38	0.21	0.17	-	0.20

* Analysis performed at the University of Toronto, Canada using X-ray fluorescence and Neutron activation methods.

TABLE 4:

Degree of Slag Detachability

FLUX ↓ / B.M. ** → / WIRE →	HY-80				MILD STEEL				INCONEL 600			
	AX-90	LD 36	LD 40	309L	AX-90	LD 36	LD 40	309L	AX-90	LD 36	LD 40	309L
Lnc 880	2.5 / 7.5	2.5	-	5.5 / 9.0	5.0	5.0	5.0	-	6.0	-	6.5	-
Lnc 761	1.0	1.0	-	6.5	1.0	1.0	-	6.0	-	-	-	-
LD 20	1.0	1.0	-	3.5 / 8.5	1.0	2.0	-	-	3.0	-	5.0	-
LD 60	1.0 / 7.0	3.0	-	5.0	5.0	1.0	-	-	4.0	-	-	-
LD 0091	1.0 / 7.5	2.0	-	5.0	-	5.0	-	3.0	6.0	-	-	-
LD 80	3.0	1.0	-	7.0	1.0	1.0	1.0	7.0	-	-	3.0	-
Cr80	8.0	-	-	-	-	-	-	-	-	-	-	-
Ti80	3.0	-	-	-	-	4.0	-	-	-	-	-	-
Ti60	-	-	-	-	-	5.0	-	-	-	-	-	-
CF60	-	-	-	-	-	3.0	-	-	-	5.0	-	-

* In boxes with two #s, the bottom # is for scaled base metal condition.
** B.M. = Base metal.

TABLE 5:

Degree of Slag Detachability *
(Chromium effects only)

FLUX ↓ / WIRE → \ B.M. ** →	HY-80				MILD STEEL				INCONEL 600			
	AX-90	LD 36	LD 40	309L	AX-90	LD 36	LD 40	309L	AX-90	LD 36	LD 40	309L
Lnc 880	7.5		-	5.5 / 9.0				-	6.0	-	6.5	-
Lnc 761			-	6.5				6.0	-	-	-	-
LD 20			-	3.5 / 8.5					3.0	-	5.0	-
LD 60	7.0		-	5.0					4.0	-	-	-
LD 0091	7.5		-	5.0				3.0	6.0	-	-	-
LD 80	3.0		-	7.0				7.0	-	-	3.0	-
Cr80	8.0	-	-	-	-	-	-	-	-	-	-	-
Ti80		-	-	-	-		-	-	-	-	-	-
Ti60	-	-	-	-	-		-	-	-	-	-	-
CF60	-	-	-	-	-		-	-	-	5.0	-	-

* In boxes with two #s, the bottom # is for scaled base metal condition.
** B.M. = Base metal.

TABLE 6: Identification of phases in slag sample 309-MS-80 using X-ray diffraction analysis.

TWO-THETA (DEG.)	d-SPACING (Å)	IDENTIFIED PHASES			
		File No. 8-254	File No. 23-1221	File No.	File No.
14.4	6.1456				
29.8	2.995	2.82	2.90		
35.2	2.547	2.59	2.48		
44.2	2.047	2.04	2.05		
CHEMICAL FORMULA		CrO	$MgAlCrO_4$		

TABLE 7 : Identification of phases in slag sample AX-HY-Cr8 by x-ray diffraction analysis.

TWO-THETA (DEG.)	d-SPACING (Å)	IDENTIFIED PHASES		
		File No. 24-511	File No.	File No.
45.6	2.954	2.944		
53.2	2.557	2.551		
54.6	2.496	2.478		
89.2	1.6304	1.629		
98.9	1.5067	1.502		
103.6	1.4568	1.467		
		$FeO.Cr_2O_3$		

TABLE 8: Comparison of detachability of slags from stainless steel welds* using different fluxes of varying amounts of reactive oxide compositions.

FLUX	REACTIVE OXIDE COMPOSITION (wt. %)					SLAG DETACHABILITY
	SiO_2	MgO	Al_2O_3	MnO	FeO	
Linde 20	55.72	9.10	3.08	0.60	0.41	3.5
Lincoln 880	16.59	24.21	22.73	0.19	1.21	5.5
Lincoln 761	42.47	20.76	2.05	19.58	3.11	6.5
Linde 60	43.11	-	3.83	35.28	2.59	5.0

* Welds were made with 309 L (26.27 wt.% Cr) electrodes on a descaled HY80 base metal.

TABLE 9: Identification of phases in slag sample 36-MS-Ti8 using X-ray diffraction analysis.

TWO-THETA (DEG.)	d-SPACING (Å)	IDENTIFIED PHASES			
		File No. 22-153	File No. 15-742	File No.	File No.
28.2	3.16				
31.1	2.873		2.865		
32.9	2.72	2.72			
33.1	2.704	2.701			
34.9	2.569	2.56	2.562		
37.0	2.427	2.428	2.44		
38.6	2.33	2.31	2.34		
40.0	2.25		2.25		
42.6	2.12	2.121	2.092		
44.4	2.039	2.04			
52.2	1.75	1.752			
56.2	1.635		1.65		
61.6	1.50		1.53		
63.0	1.47		1.46		
65.2	1.43		1.43		
66.2	1.41		1.41		
CHEMICAL FORMULA		$CaTiO_3$	$Mg_3Al_2(SiO_4)_3$		

TABLE 10: Identification of phases in slag sample AX-IN-880 using X-ray diffraction analysis.

TWO-THETA (DEG.)	d-SPACING (Å)	IDENTIFIED PHASES			
		File No. 24-1165	File No. 4-864	File No. 21-1152	File No. 6-532
19.1	4.643			4.66	
28.3	3.1508	3.162	3.153		
30.4	2.9377				2.95
31.3	2.8553			2.858	
35.2	2.5474	2.54			
35.5	2.527				2.52
36.8	2.44			2.437	
43.0	2.102				2.09
44.8	2.021	2.019		2.02	
47.1	1.9278		1.931		
50.7	1.799	1.8026			
55.8	1.646	1.65	1.647	1.65	
57.1	1.6117	1.6095			
57.5	1.6014	1.5911			
59.4	1.5546	1.545		1.555	
60.3	1.5336	1.539			
62.5	1.4847	1.495			
65.2	1.4297			1.4289	
CHEMICAL FORMULA		ZrO_2	CaF_2	$MgAl_2O_4$	Cr_2O_3

TABLE 11: PHASE IDENTIFICATION IN SAMPLE AX-IN-0091 USING X-RAY DIFFRACTION.

TWO-THETA (DEG.)	d-SPACING (A)	IDENTIFIED PHASES			
		File No. 13-410	File No	File No.	File No.
21.2	4.1872				
27.4	3.2522	3.259			
29.3	3.0455	3.06			
30.6	2.9190	2.90			
31.2	2.8643	2.873			
33.2	2.6961				
35.3	2.5404	2.57			
36.7	2.4466	2.45			
39.2	2.2962	2.289			
44.2	2.0473	2.047			
44.9	2.0170	2.018			
45.6	1.9876	1.994			
48.4	1.8790	1.883			
50.1	1.8192	1.821			
53.1	1.7232	1.73			
58.8	1.5691	1.658			
CHEMICAL FORMULA $Ca_4F_2Si_2O_7$					

TABLE 12: Weld Metal Oxygen Content (wt. %) *

SAMPLE	wt. % OXYGEN
36-MS-60	0.0717
36-MS-CF6	0.036
36-IN-CF6	0.039
AX-HY-0091	0.032
AX-IN-0091	0.035
AX-HY-880	0.026
AX-IN-880	0.042

* Analysis performed using inert gas fusion technique.

TABLE 13: Basicity indices of welding fluxes used.

FLUX	INDEX
Lincoln 880	1.59
Lincoln 761	0.95
Linde 20	0.67
Linde 60	0.58
Linde 80	0.93
Linde 0091	1.38
Cr80	0.59
Ti80	0.75
Ti60	0.49
CF60	0.98

Table 14: Weld Metal Phase Transformation Data Used in FEM Analysis (Ref 30)

Transformation	Transition Temperature (^{o}C)	Enthalpy of Transition, J/mm^3
$\alpha - \gamma$	870	0.128
$\gamma - \delta$	1430	0.122
$\delta - L$	1525	2.119

Table 15 : Mechanical Properties for AX-HY-20 and AX-HY-880 slags (Ref 31)

T	20	500	700	900	1200	1400
E	68.9	68.9	68.9	68.9	68.9	68.9
ν	0.22	0.22	0.22	0.22	0.22	0.22

T = Temperature (^{o}C)

E = Young's Modulus ($MPa*10^{-3}$)

ν = Poisson's Ratio

Table 16 : Physical Properties for Slag AX-HY-20 (Ref 31)

T	20	500	600	645	950	1400
$k*10^{6}$	2.092	3.082	4.15	5.02	10.88	78.24
C_p	1.023	1.023	1.101	1.128	1.206	1.366
$\rho*10^{-3}$	2.474	2.452	2.44	2.438	2.398	2.335
$\alpha*10^{6}$	---	5.16	1.0	0	0	0

T = Temperature (^{o}C)
k = Thermal conductivity ($W/m^{o}C$)
C_p = Specific heat ($KJ/Kg^{o}C$)
α = Coefficient of thermal expansion ($m/m^{o}C$)
ρ = Density, (Kg/mm^{3})

Table 17: Physical Properties for slag AX-HY-880 (Ref 31)

T	20	500	600	700	950	1400
$k*10^{6}$	2.092	3.08	4.15	5.02	10.88	78.24
C_p	1.023	1.023	1.101	1.128	1.206	1.366
$\rho*10^{-3}$	2.474	2.452	2.44	2.438	2.398	2.335
$\alpha*10^{6}$	---	10.0	8.2	7.3	0	0

T = Temperature (^{o}C)
k = Thermal conductivity ($W/m^{o}C$)
C_p = Specific heat ($KJ/Kg^{o}C$)
α = Coefficient of thermal expansion ($m/m^{o}C$)
ρ = Density, (Kg/mm^{3})

Table 18 : Mechanical Properties for HY-130 (Ref 32)

T	20	500	700	900	1200	1400
E	206	167	56.5	25.5	9.6	0.4
ν	0.3	0.353	0.374	0.396	0.429	0.451

T = Temperature (^{o}C)

E = Young's Modulus ($MPa*10^{-3}$)

ν = Poisson's Ratio

Table 19: Physical Properties for HY-130 (Ref 32)

T	20	500	700	900	1200	1400
$k*10^{6}$	35.1	34.6	28.5	26.6	28.4	29.6
C_p	0.427	0.665	0.481	0.653	0.653	0.653
$\rho*10^{-3}$	7.86	7.69	7.62	7.604	7.604	7.604
$\alpha*10^{6}$	---	14.27	14.94	12.42	13.14	13.50

T = Temperature (^{o}C)
k = Thermal conductivity ($W/m^{o}C$)
C_p = Specific heat ($KJ/Kg^{o}C$)
α = Coefficient of thermal expansion ($m/m^{o}C$)
ρ = Density, (Kg/mm^{3})

TABLE 20: Integrated Mean Differential Thermal Contraction per unit length for various slag-metal systems studied from T_s to 30°C. +

FLUX \ B.M.** → / WIRE →	HY-80				MILD STEEL				INCONEL 600			
	AX-90	LD 36	LD 40	309L	AX-90	LD 36	LD 40	309L	AX-90	LD 36	LD 40	309L
LC 880	20	24		14	12	23					34	
LC 761	35					20						
LD 20	24			2.4 1.3					2.8			
LD 60	21 2.1	23			1.7	38						
LD 0091	3.2					1.9			30			
LD 80	24					31						

+ T_s is softening point of slag.

** B.M. = Base metal.

TABLE 21: Slag detachability vs. differential thermal contraction per unit length for slags with microcracks.

SAMPLE	DIFFERENTIAL THERMAL CONTRACTION PER UNIT LENGTH. (mm/mm * 10^4)	SLAG DETACHABILITY
36-MS-880	12	5.0
309-HY-880	14	5.5
AX-HY-880	20	2.5
AX-HY-80	24	3.0
40-IN-880	34	6.5

TABLE 22: Slag detachability vs. differential thermal contraction per unit length for slags without microcracks.

SAMPLE	DIFFERENTIAL THERMAL CONTRACTION PER UNIT LENGTH. (mm/mm * 10^4)	SLAG DETACHABILITY
36-MS-60	38	1.0
AX-HY-761	35	1.0
AX-HY-20	24	1.0
AX-HY-60	21	1.0
AX-IN-20	2.8	3.0
309-HY-20	2.4	3.5
36-MS-0091	1.9	5.0
AX-MS-60	1.7	5.0

TABLE 23: Measured temperature values in samples A & B* during the cooling cycle.

TIME (s)	TEMPERATURE (^{o}C)	
	A	B
95	152.7	260.4
100	148.8	254.4
105	144.2	251.9
110	136.1	248.5
115	127.3	242.1
120	120.1	239.5

* A has no insulating flux cover
B shows the temperature of the flux cover .

+ Time is measured from the time when the arc is switched off and the flux hopper is removed.

TABLE 24: Softening Temperatures of slags T_s (^oC) *

FLUX \ B.M.** → / WIRE →	HY-80				MILD STEEL				INCONEL 600			
	AX-90	LD 36	LD 40	309L	AX-90	LD 36	LD 40	309L	AX-90	LD 36	LD 40	309L
LC 880	950	948		970	950	960					970	
LC 761	1016					995						
LD 20	645			660 670					658			
LD 60	966 950	950			958	960						
LD 0091	950 960					930			949			
LD 80	648					637 637						

* Determined from dilatometer measurement as the temperature where the slag starts to creep.

** B.M. refers to base metal.

TABLE 25: Detachability of slags from welds showing the effect of cooling rate.

SAMPLE *		DETACHABILITY	
A	B	A	B
AX-AXC-880	AX-HY-880	8.0	2.5
AX-AXC-60	AX-HY-60	7.0	1.0
AX-AXC-0091	AX-HY-0091	6.0	1.0

* A: Base metal is AX-90 wire laid in grooves of a water-cooled copper block.

B: Base metal is unpreheated, descaled HY80.

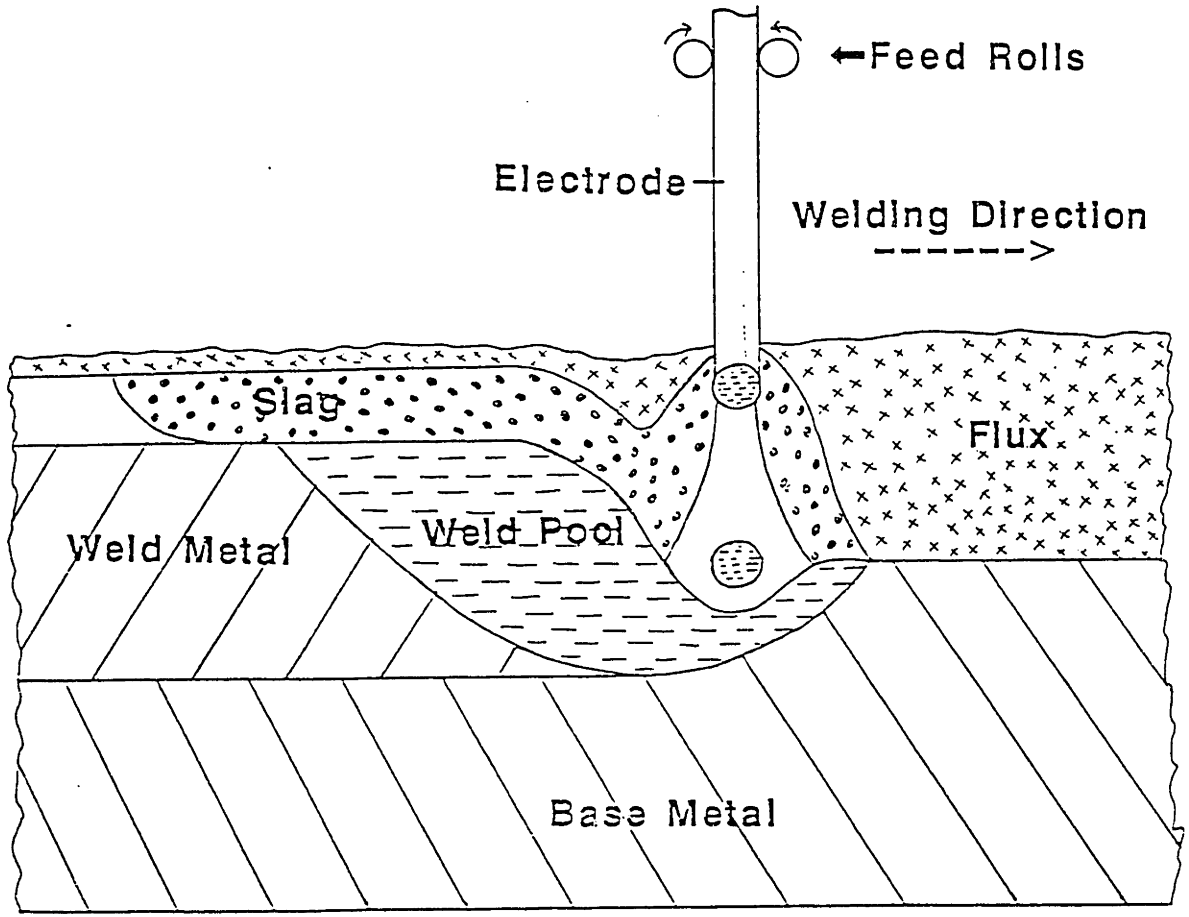

FIGURE 1: Schematic of Submerged Arc Welding Process

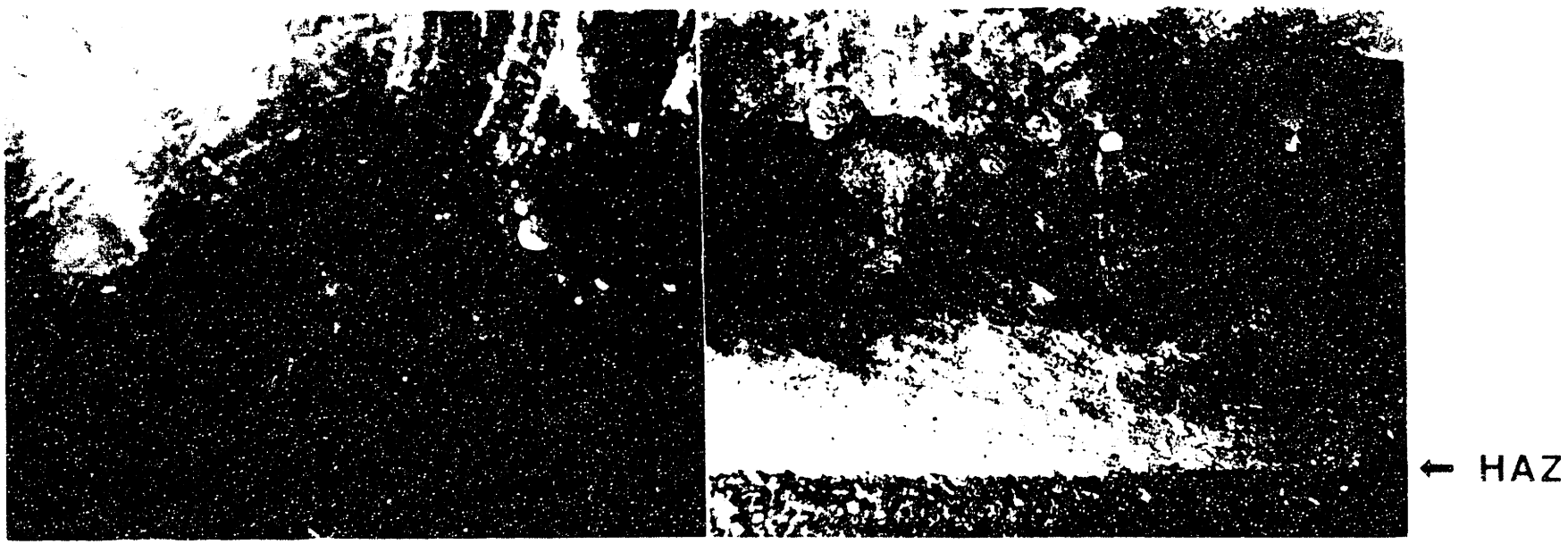

(a) AX-HY-20 x9.6 (b) 309-HY-20 x9.6

FIG. 2 Macrographs comparing surface appearances of weld metal samples of same base metal and flux but different electrodes. Notice in (b) adherent slag in the HAZ.

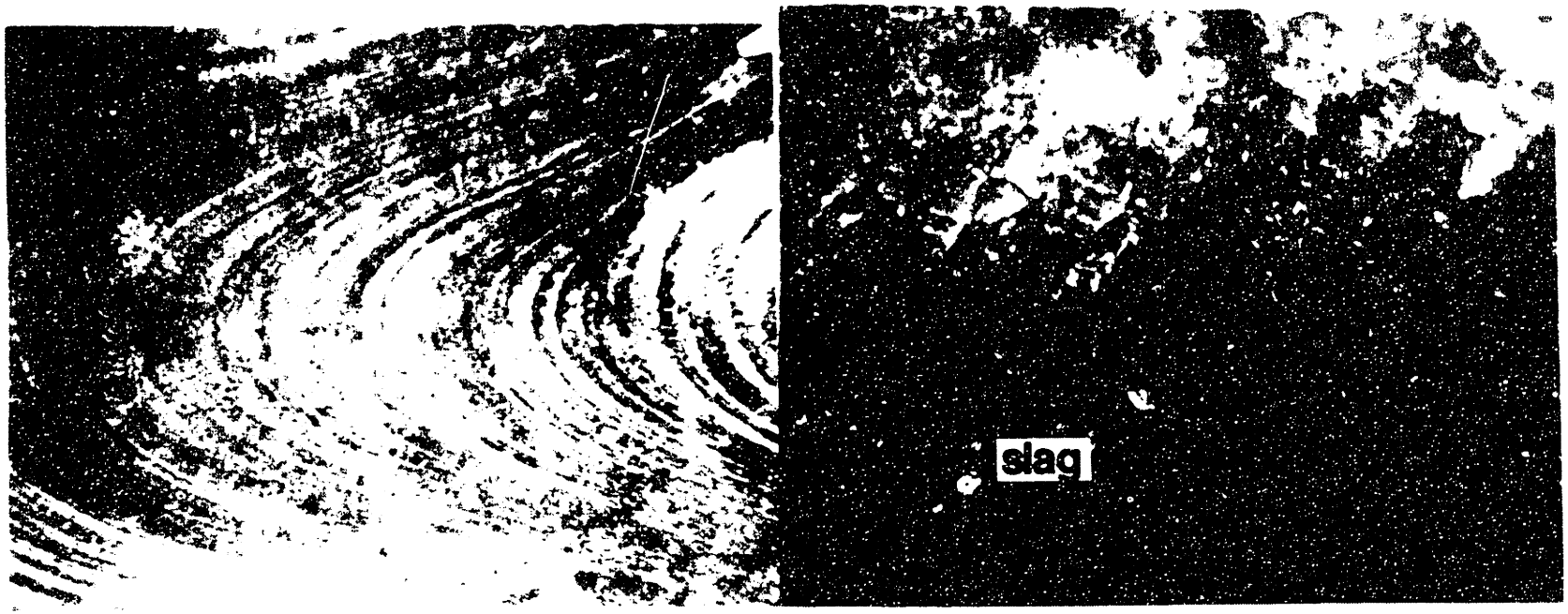

(a) AX-HY-80 x8 (b) AX-HY-CR x8

FIG. 3 Macrographs comparing surface appearances of weld samples of same electrode and base metal but different fluxes. Adherent slag is shown in (b).

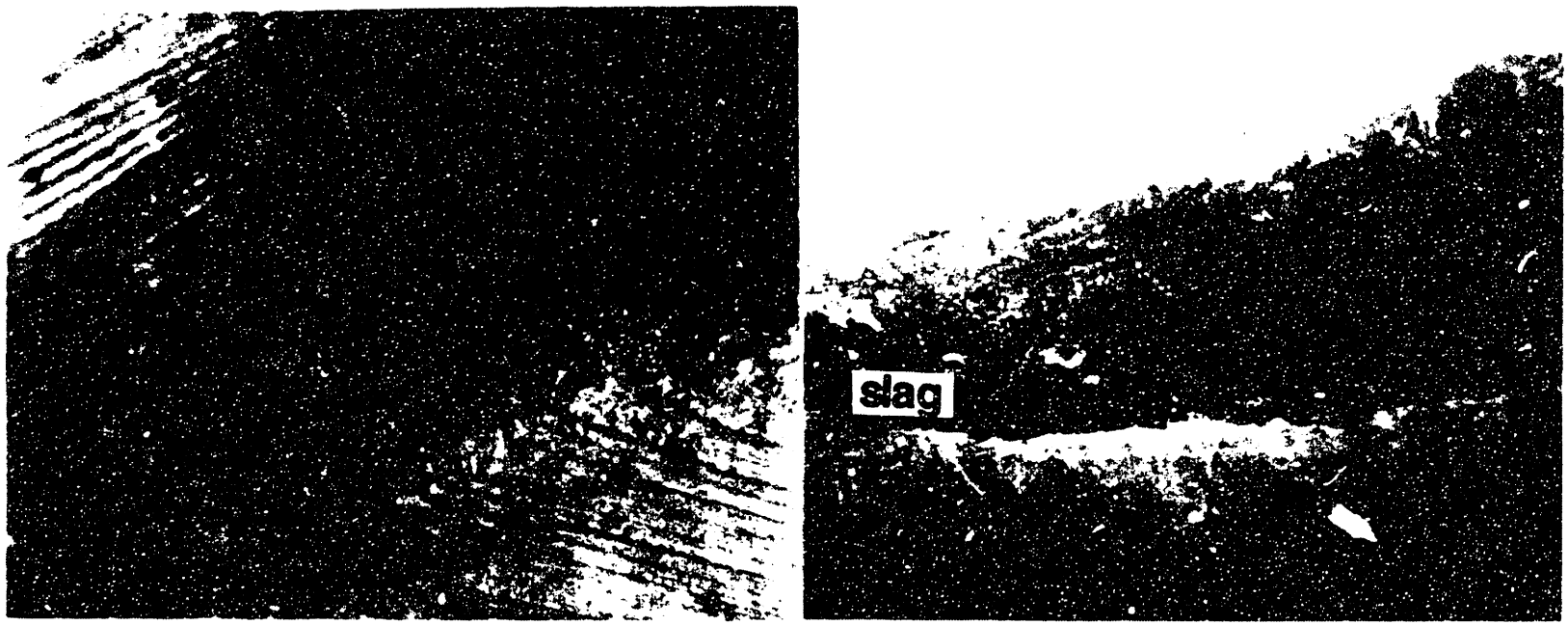

(a) AX-HY-60 x8 (b) 309-HY-60 x8

FIG. 4 **Macrographs comparing surface appearances of weld metal samples of same base metal and flux but different electrodes. Adherent slag is shown in (b).**

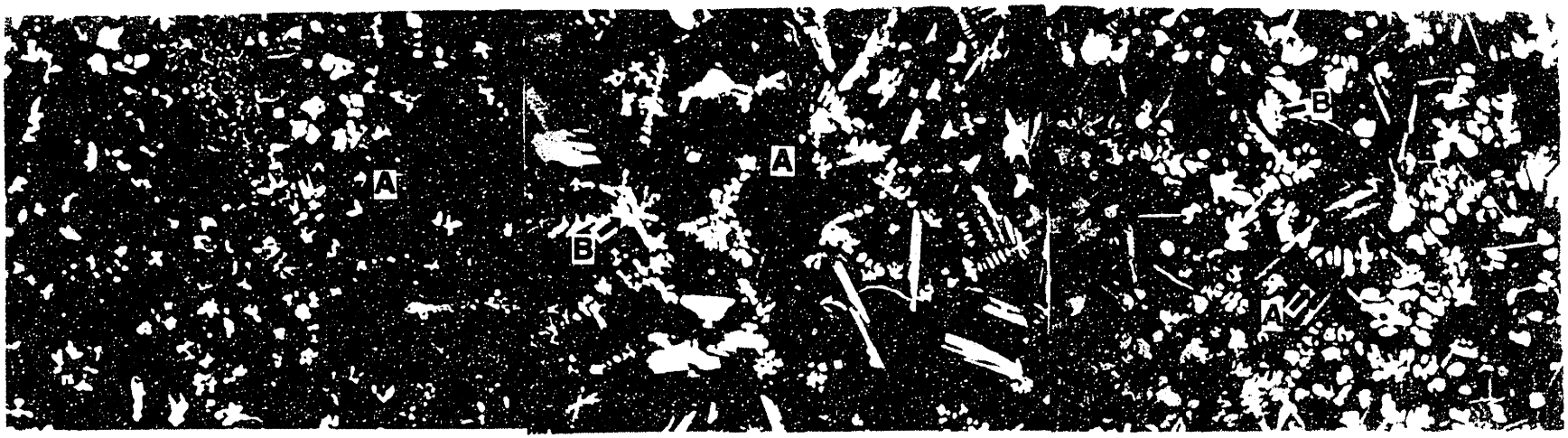

(a) 309-HY-880 x800 (b) AX-HYS-880 x800 (c) 309-HYS-880 x800

FIG. 5 Electron micrographs showing slag structures and increasing Chromium content of spinels (white center region).

A: Spinel B: Zirconia dendrite

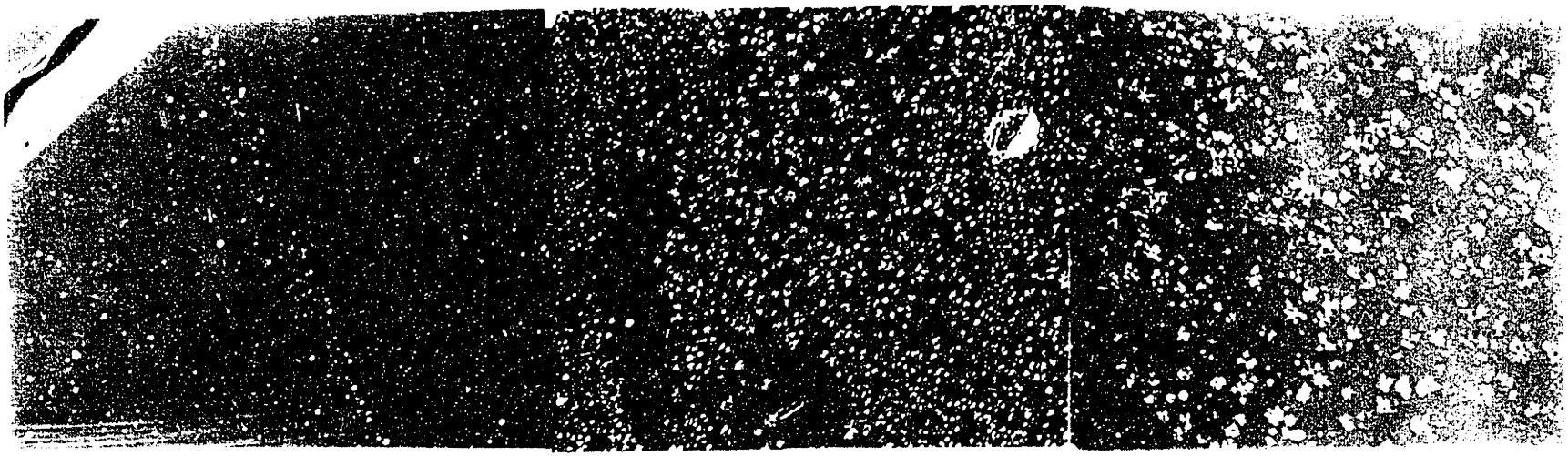

(a) AX-HY-60 x400 (b) 309-HY-60 x400 (c) AX-IN-60 x80

FIG. 6 Electron micrographs showing the effect of Chromium on the slag microstructures. In (b) and (c), Cr-spinels are shown in addition to the metallic precipitates of (a).

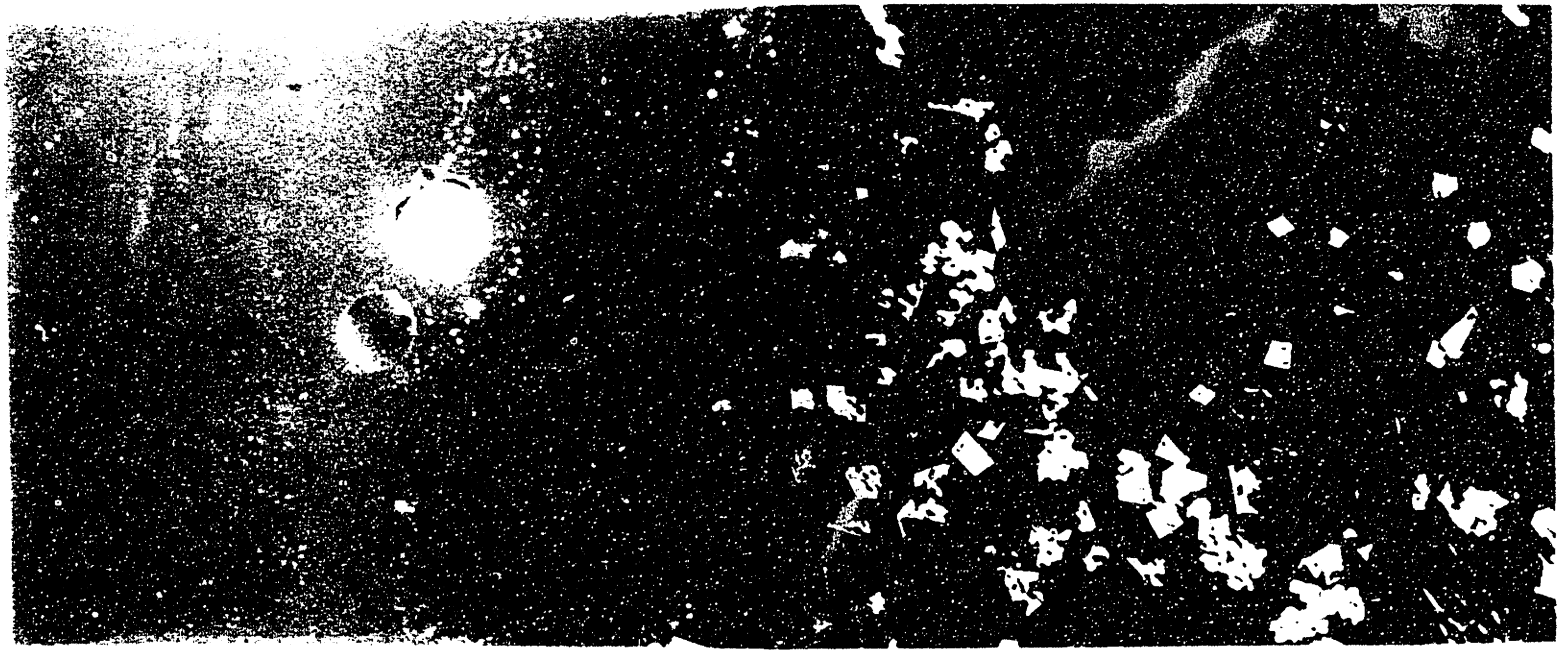

(a) AX-HY-80 x400 (b) AX-HY-CR x400

FIG. 7 Electron micrographs showing the effect of Chromium on slag microstructures. In (b) Cr-spinels are shown; whereas (a) shows metallic precipitates only.

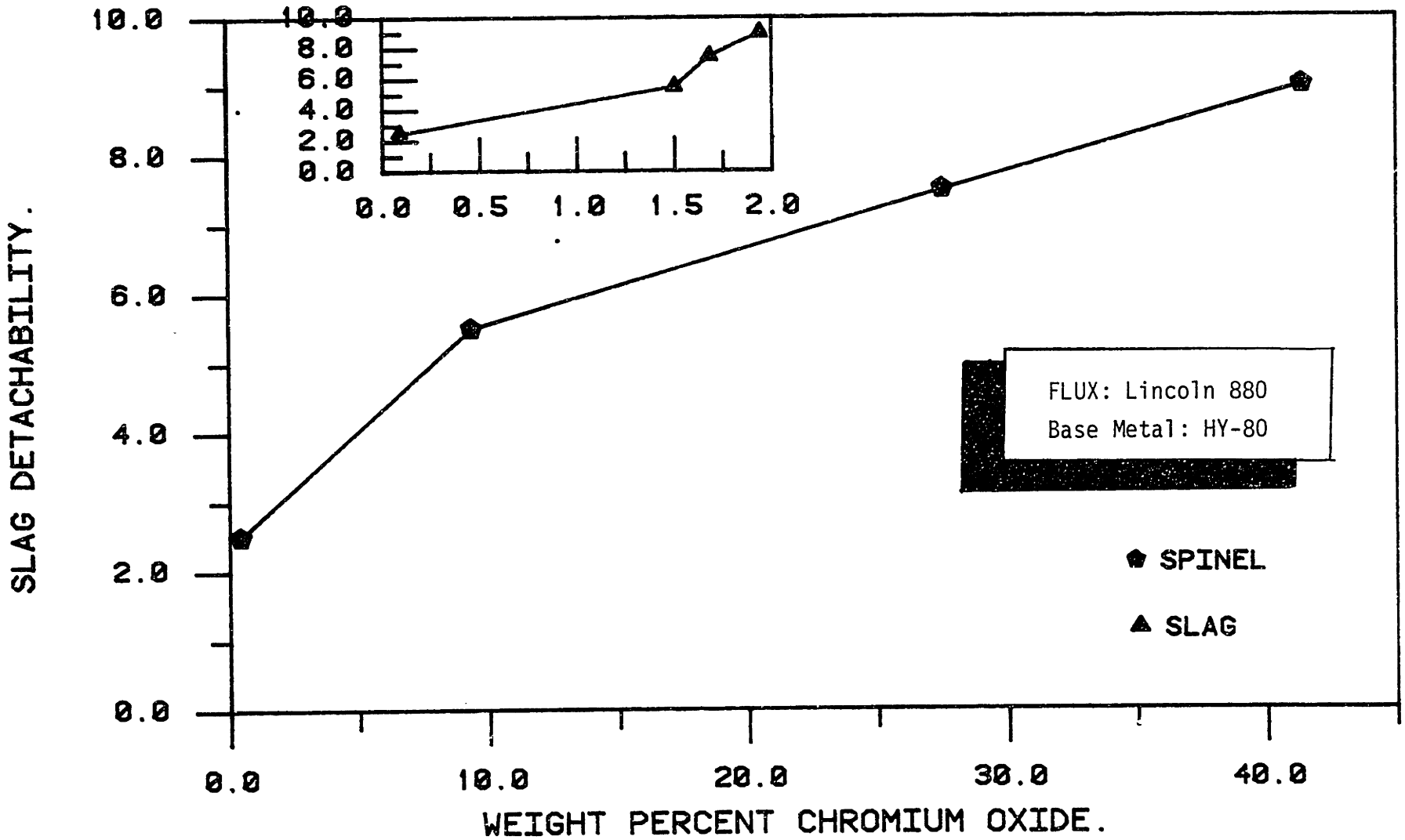

FIGURE 8: Shows the effect of chromium oxide content of slag & spinel on detachability.

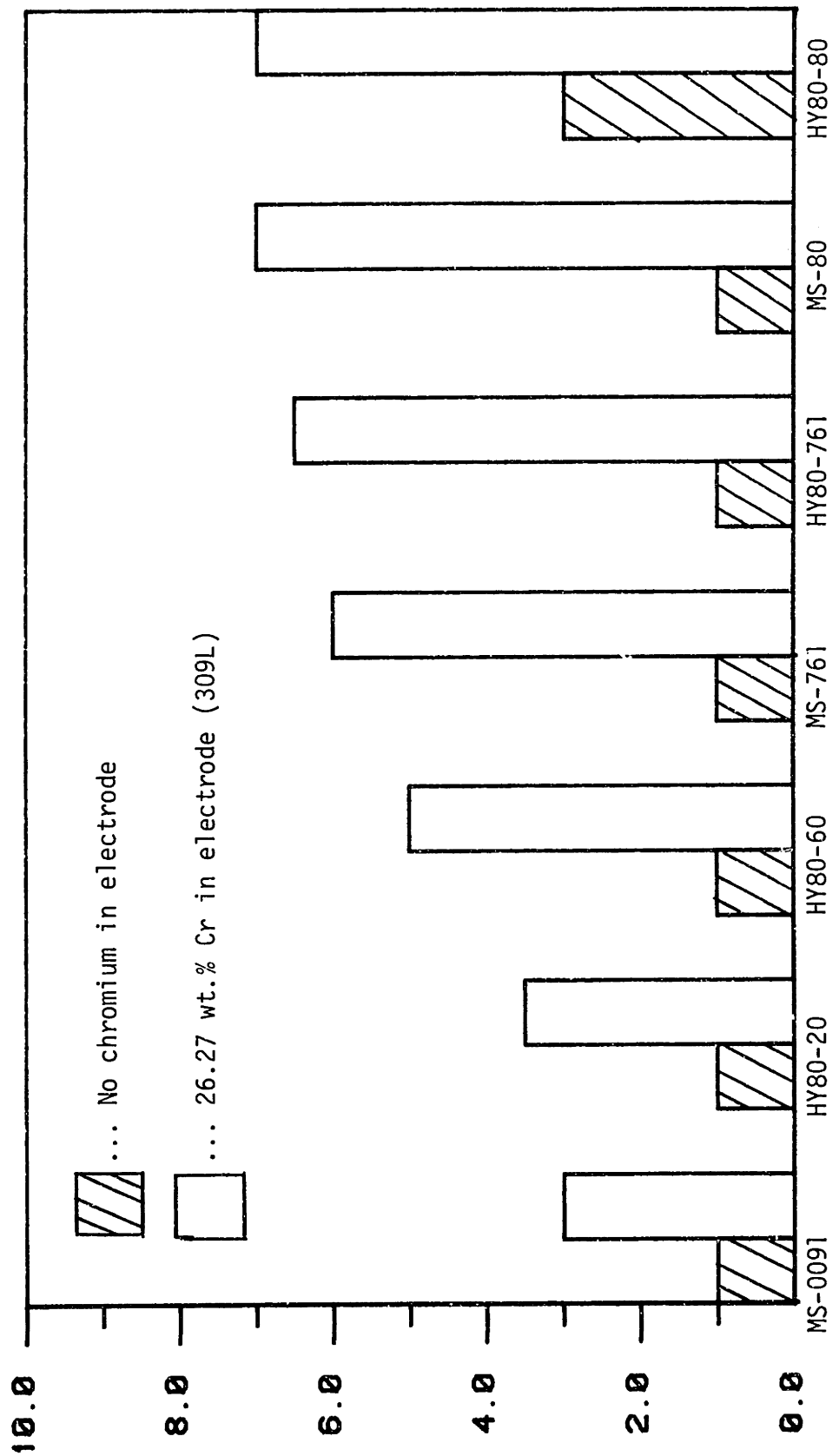

FIGURE 9: Shows the effect of chromium in electrode on detachability of slags from welds deposited on the same base metal with the same flux.

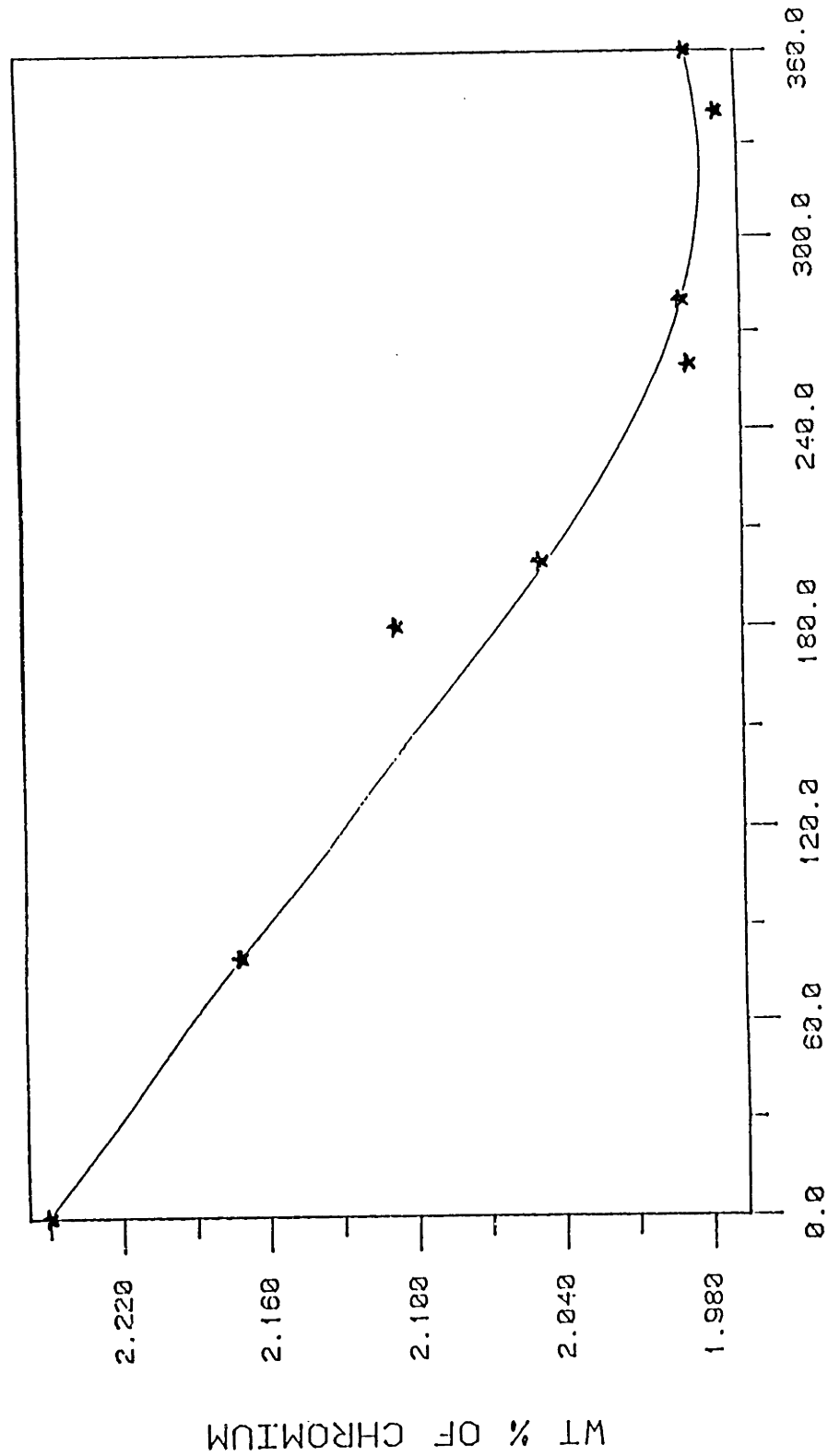

FIG. 10 Diffusion profile of Chromium in weld of sample AX-HY-Cr8; showing higher Cr at the interface than in the bulk.

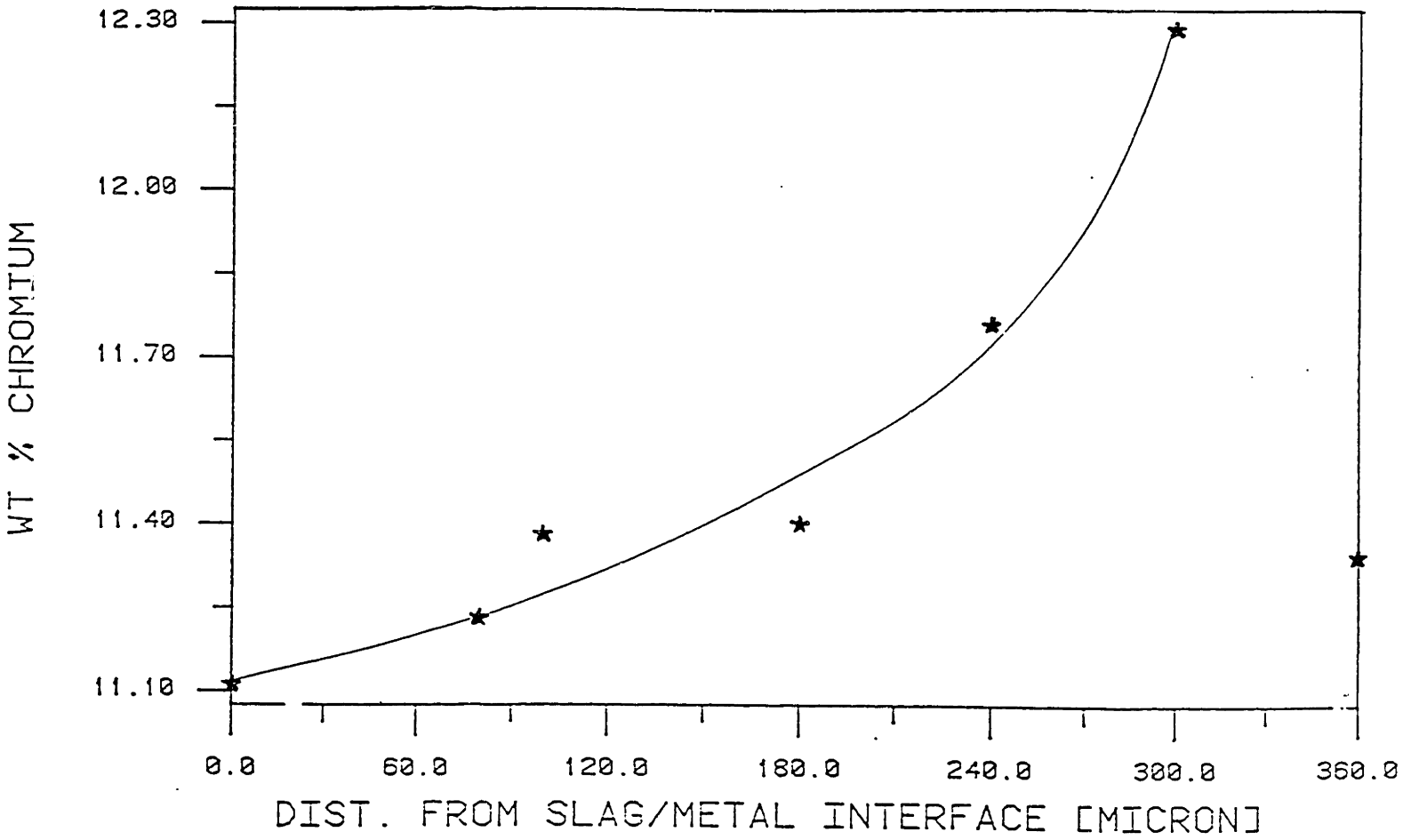

FIG. 11 Diffusion profile of Chromium in weld 309-HY-60; showing lower Cr at the interface than in the bulk.

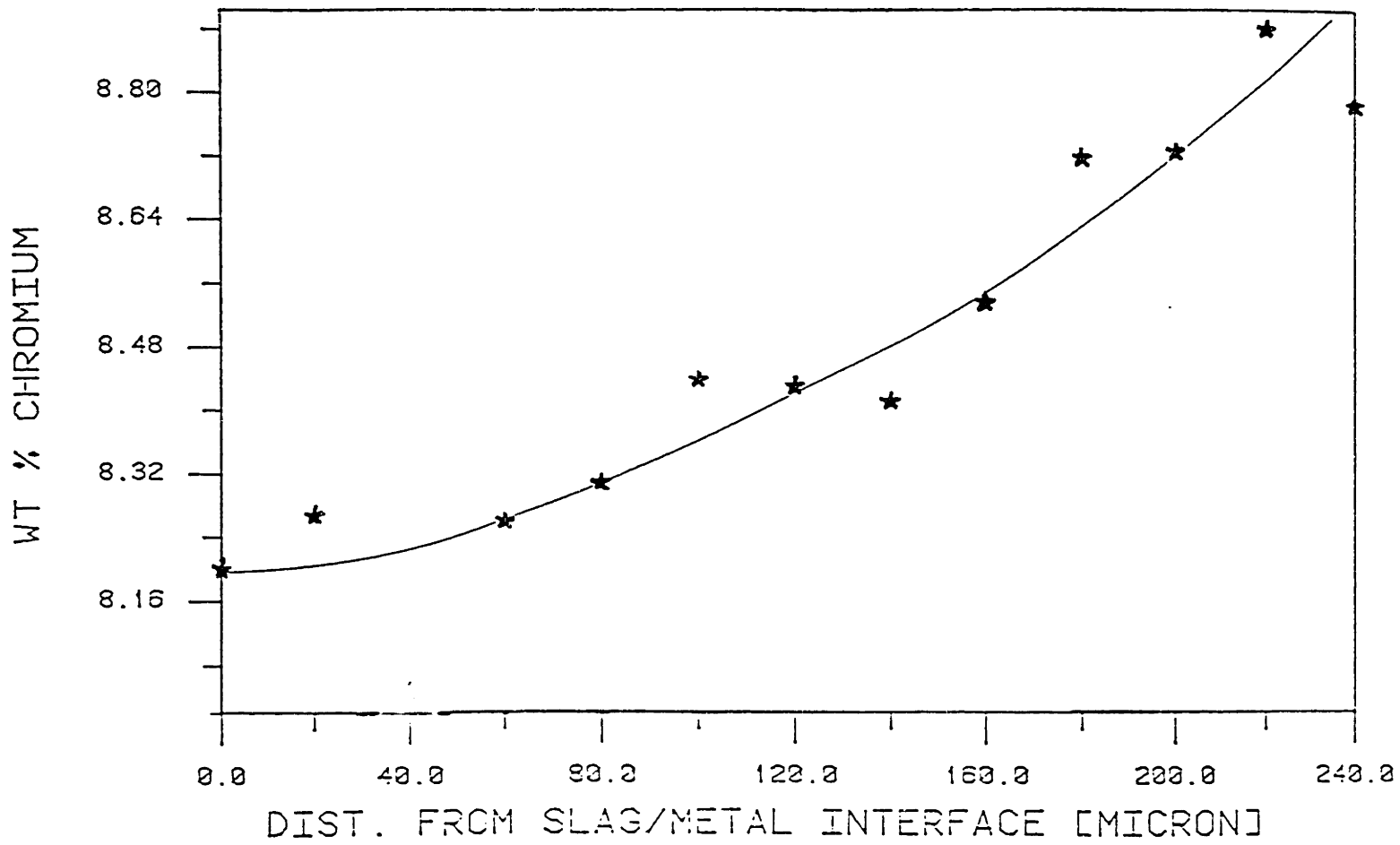

FIG. 12 Diffusion profile of Chromium in weld AX-IN-60; showing lower Cr at the interface than in the bulk.

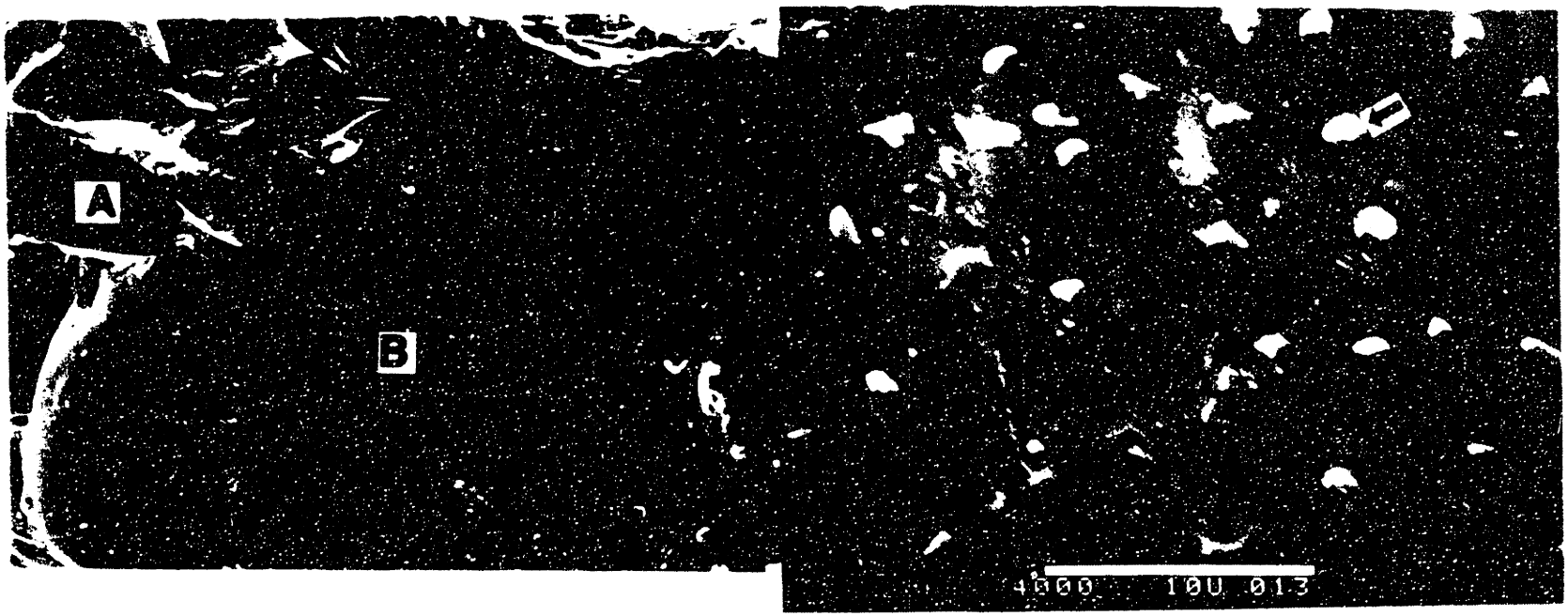

(a) x70 (b)

FIG. 13 **Weld metal surface of sample AX-HY-Cr8 shows (a) adherent slag film and (b) Cr-particles (arrowed) in region**

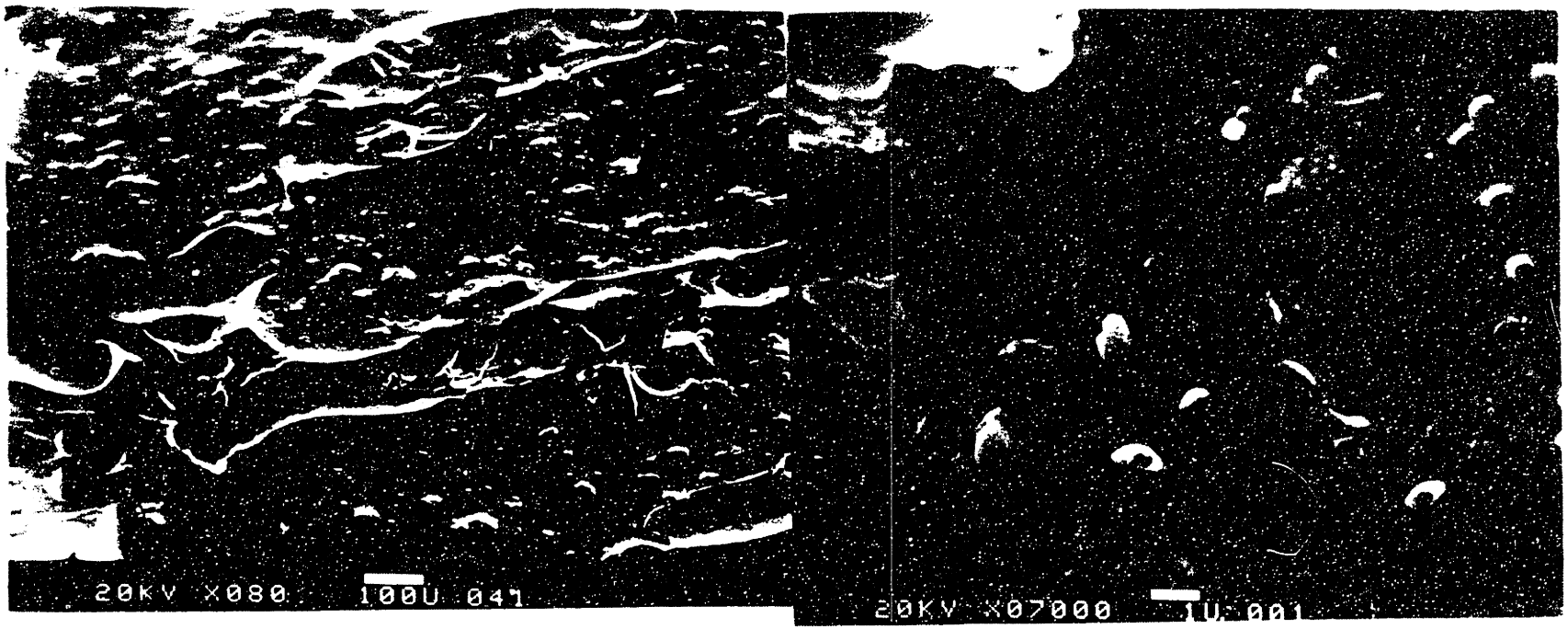

(a) AX-HYS-60

(b) 309-HY-0091

FIG. 14 Scanning electron micrographs showing chomium spinels embedded in weld metal surfaces.

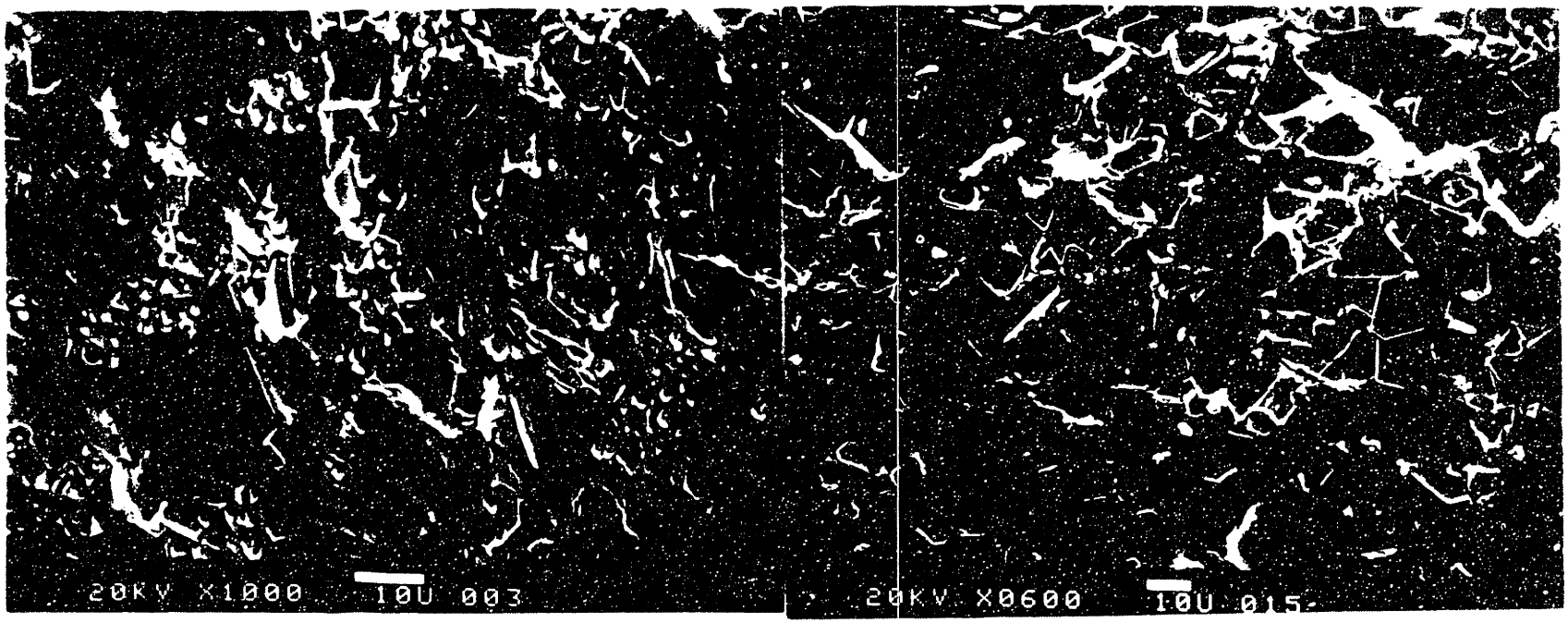

(a) 309-HYS-880 (WELD)

(b) 309-HYS-880 (SLAG)

FIG. 15 Shows electron micrographs of weld metal and slag surfaces with chromium spinels revealed.

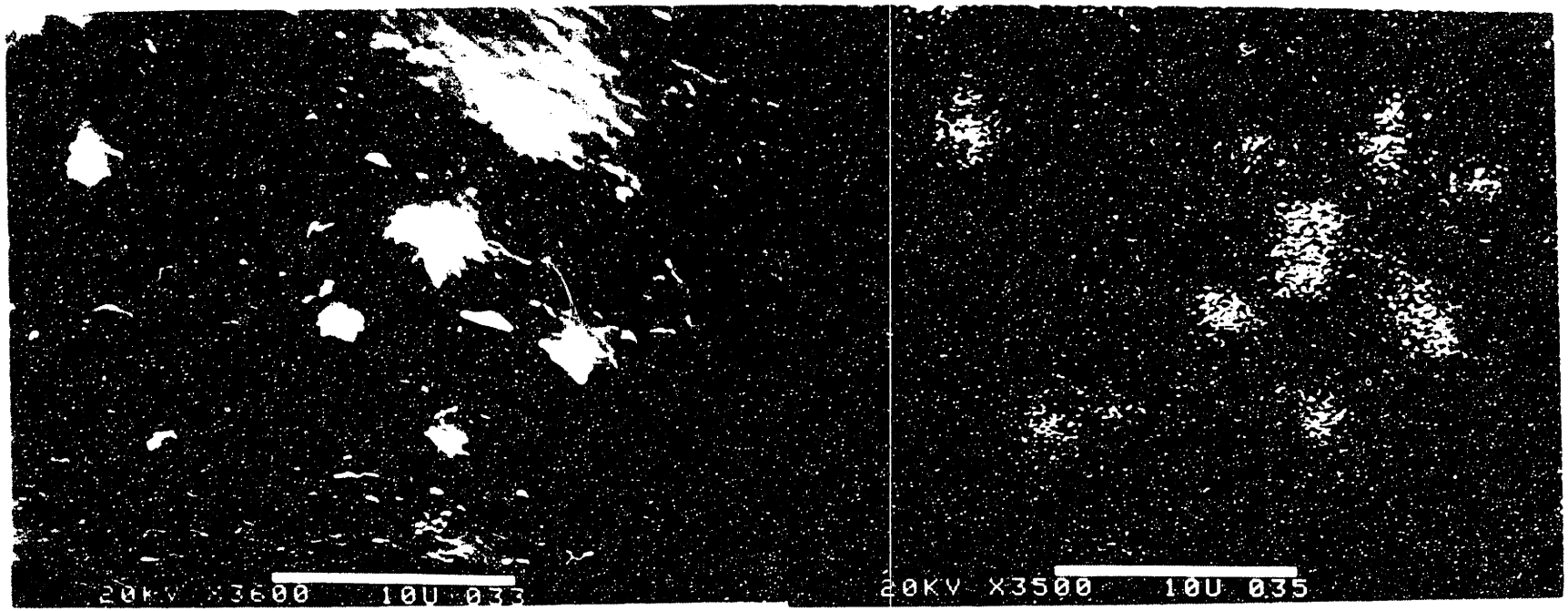

(a) AX-HYS-60 (b) Cr-map of (a).

FIG. 16 Shows chromium spinels embedded in the weld metal in (a).

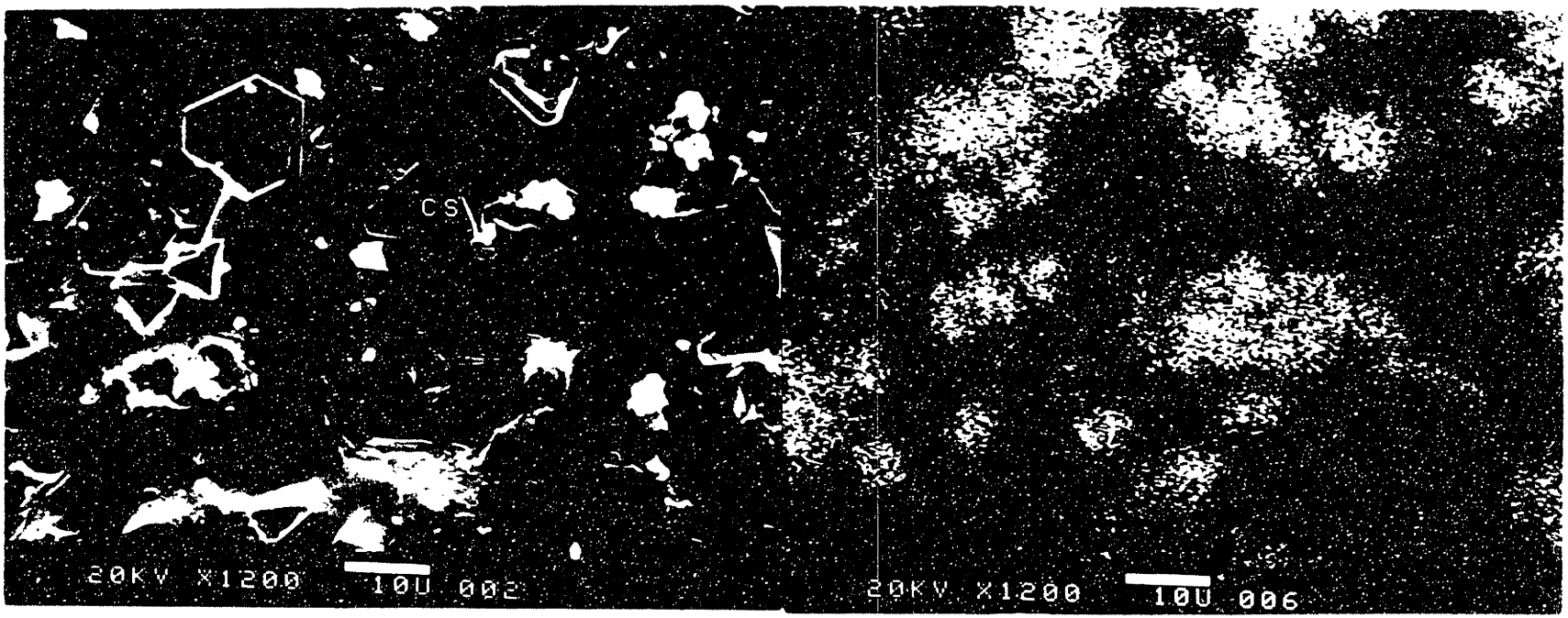

(a) 309-HYS-880 (SLAG) (b) Cr-map of (a).

FIG. 17 Shows chromium spinels on the slag interface.

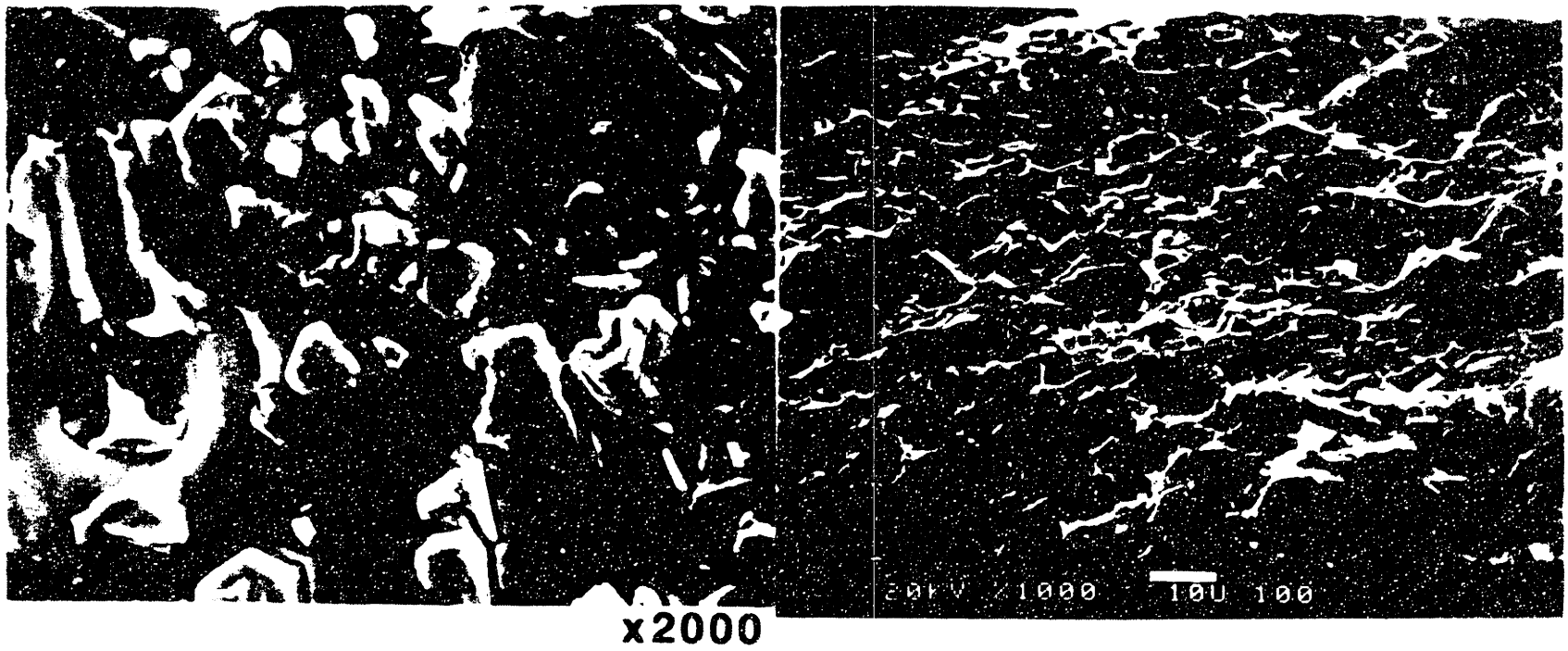

(a) AX-HYS-880 (WELD) (b) AX-HYS-880 (SLAG)

FIG. 18 Scanning electron micrographs showing spinels.

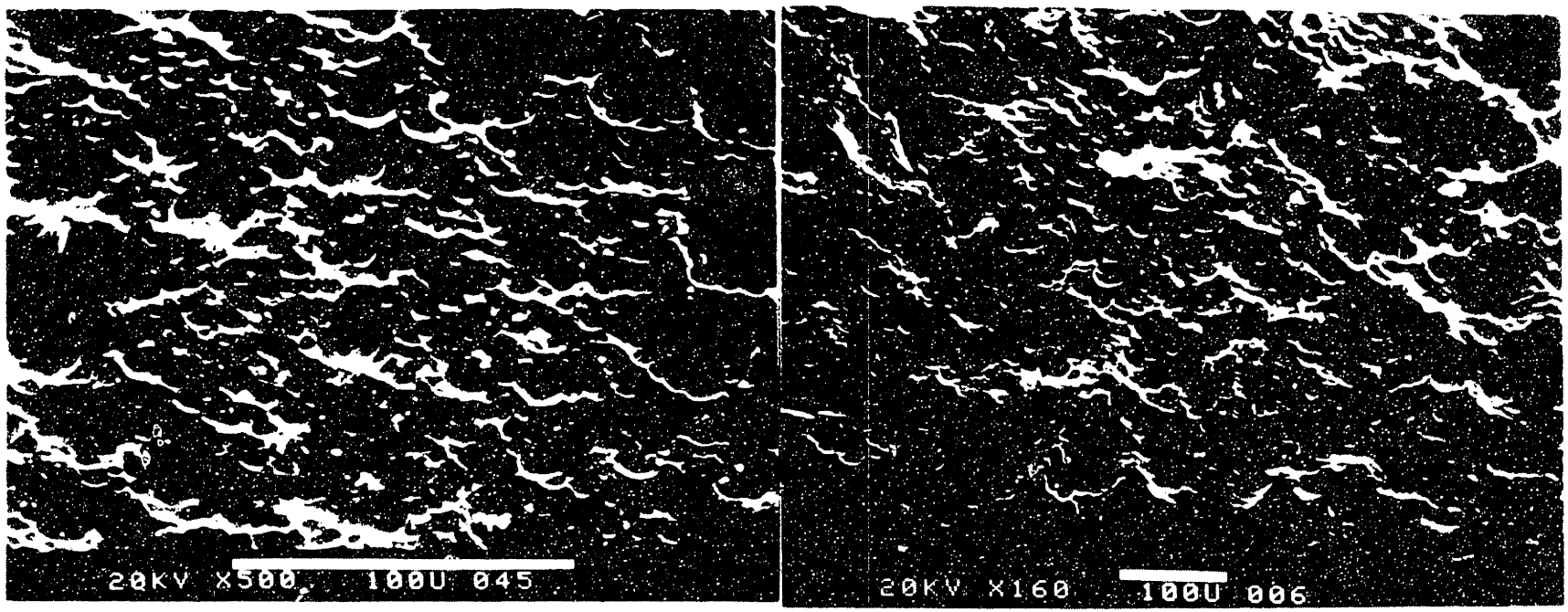

(a) AX-HY-Cr 8

(b) 309-MS-80

FIG. 19 Shows scallop-type interfaces of slags.

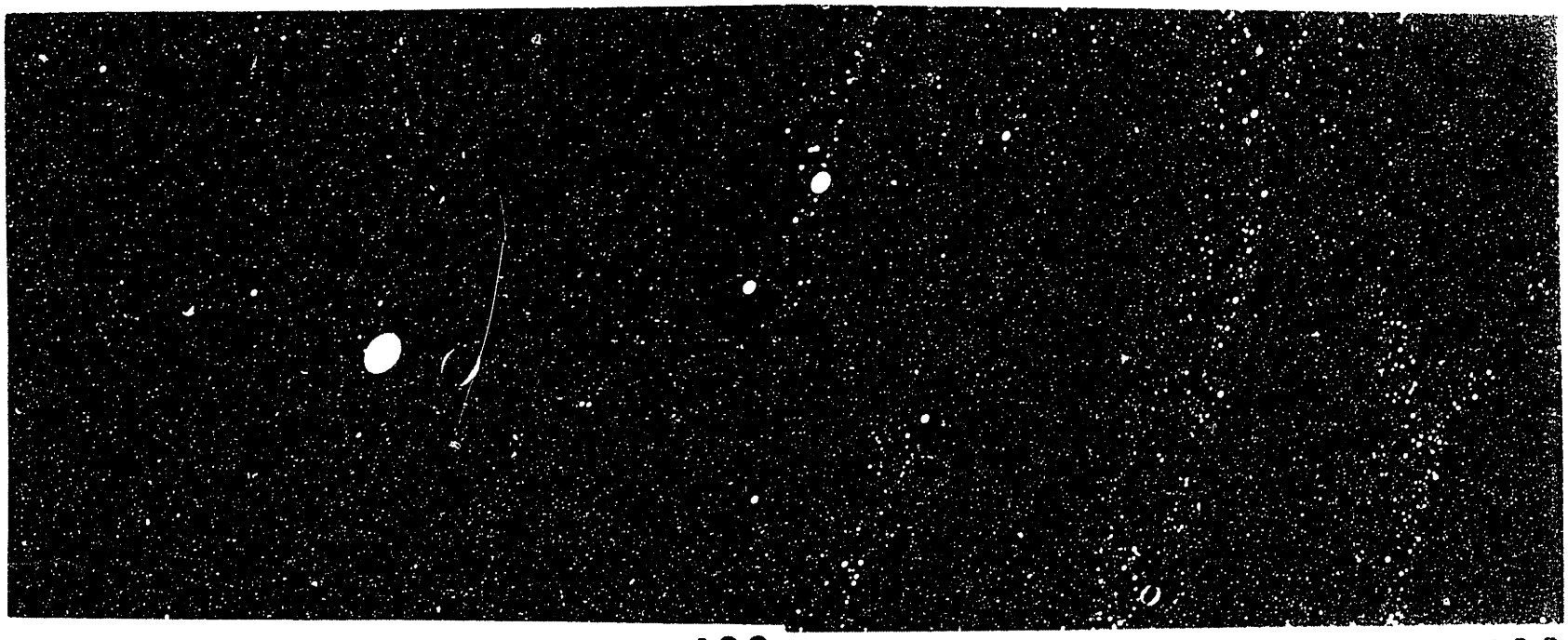

x400 x400

(a) AX-HY-20 (b) 309-HY-20

FIG. 20 Shows spinel-free structure of slags despite welding with stainless steel electrode.

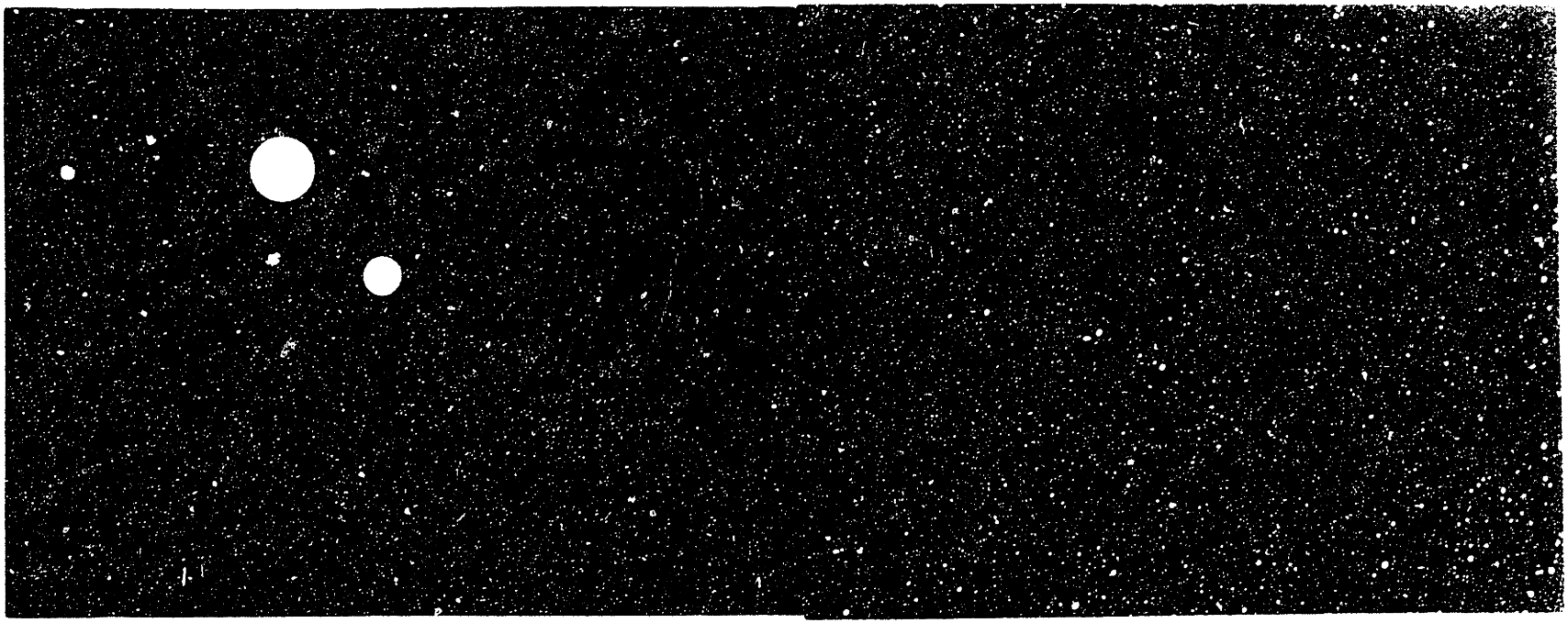

x100 x400

(a) 309-HYS-20 (b) AX-IN-20

FIG. 21 Shows spinel-free structure of slags.

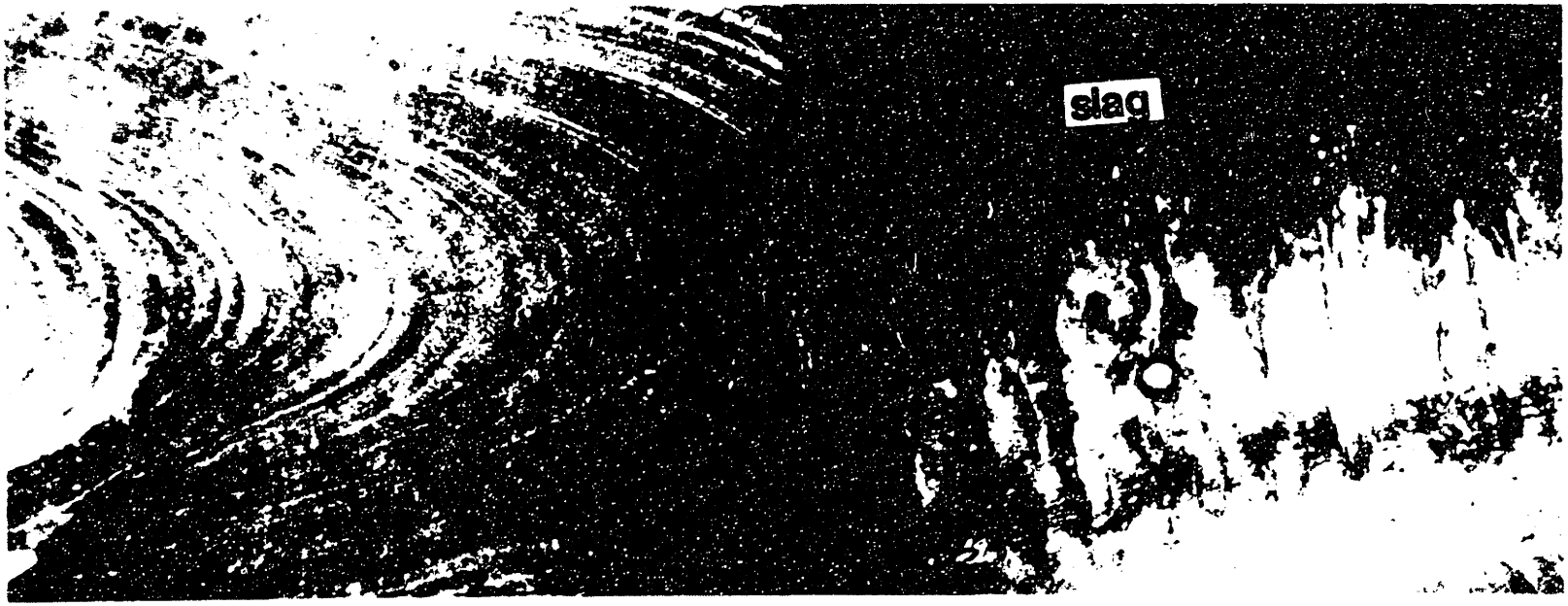

(a) AX-HY-80 x8 (b) AX-HY-Ti8 x8

FIG. 22 Macrographs comparing surface appearances of weld samples of same electrode and base metal but different fluxes. Adherent slag is shown in (b).

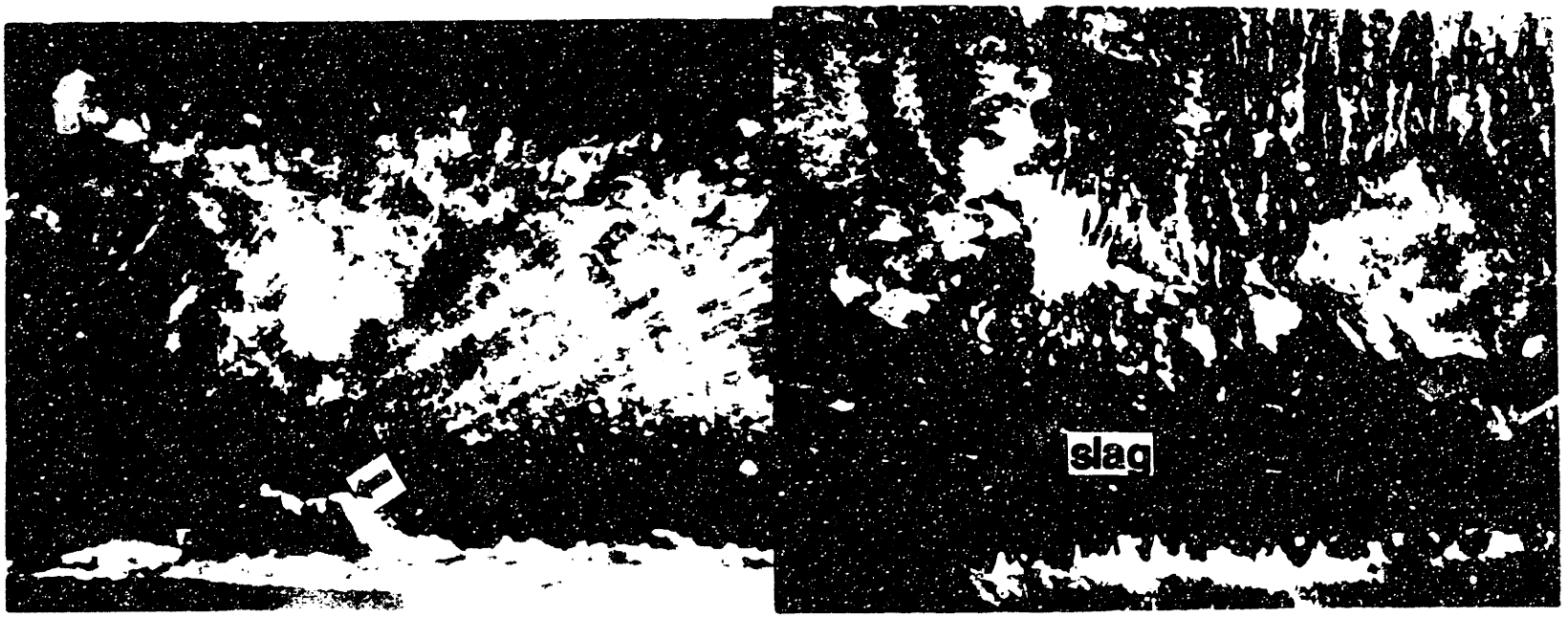

(a) 36-MS-60 x8

(b) 36-MS-Ti6 x8

FIG. 23 Macrographs comparing surface appearances of weld samples of same electrode and base metal but different fluxes. Adherent slag is arrowed in (a) and shown in (b).

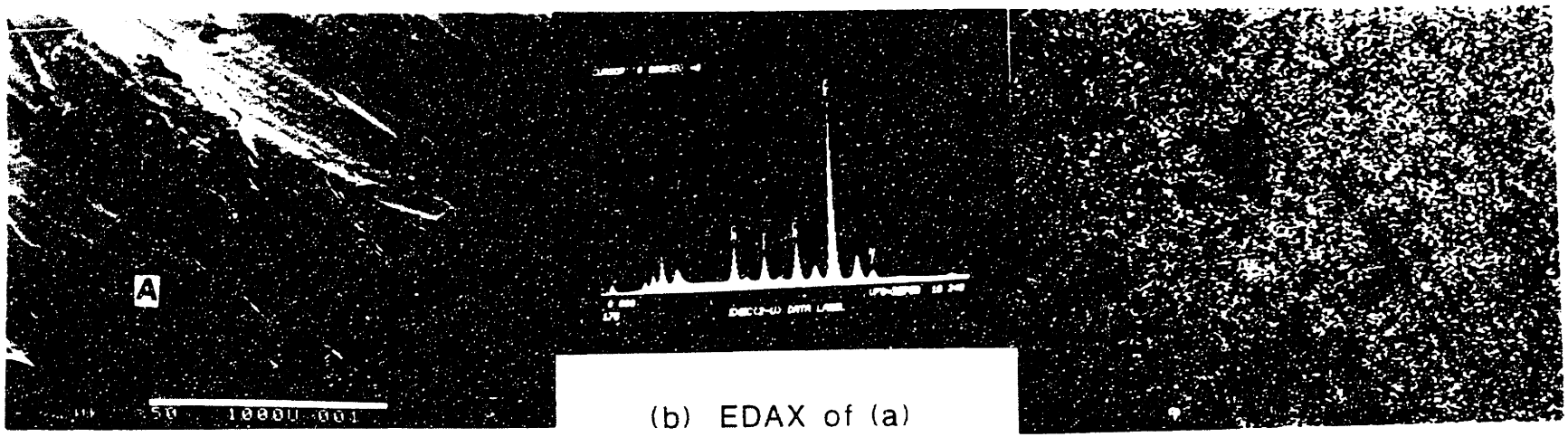

FIG. 24 Scanning Electron micrographs of sample **36-MS-Ti8** showing adherent slag on the weld metal surface

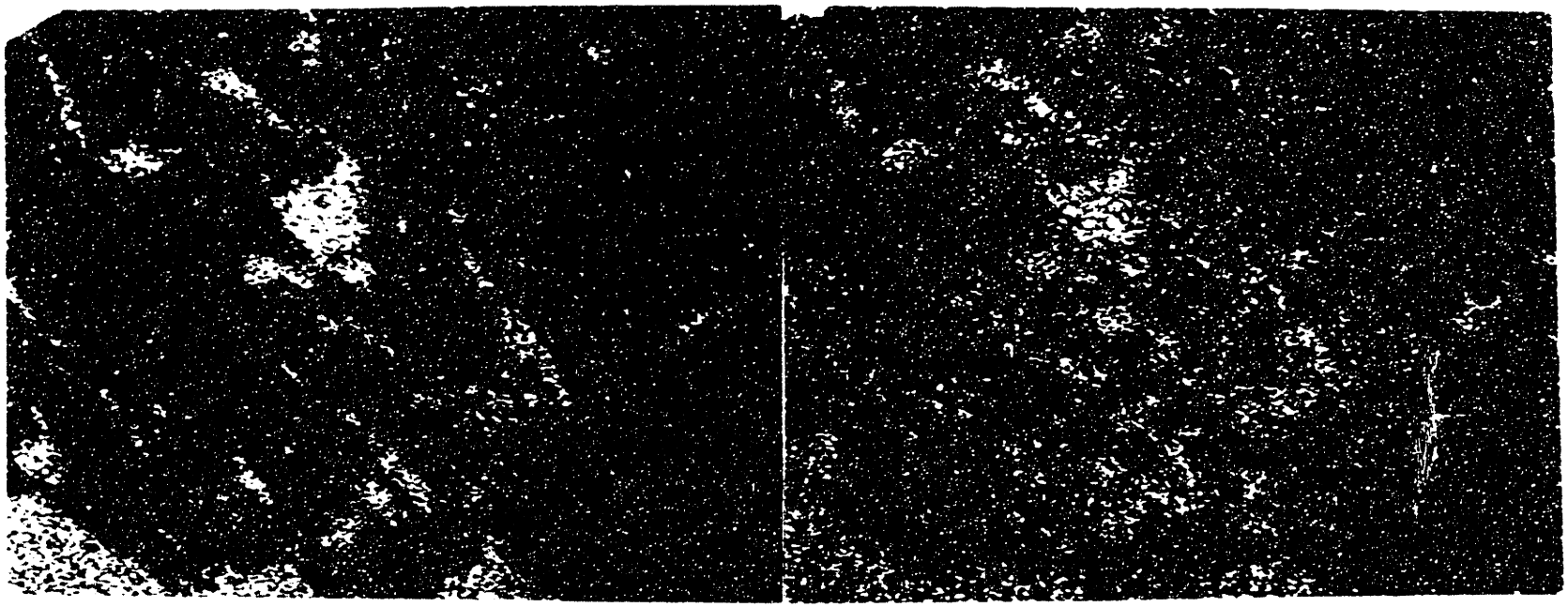

(a) Ca-map (b) Ti-map

FIG. 25 X-ray element mapping of FIG. 24(a).

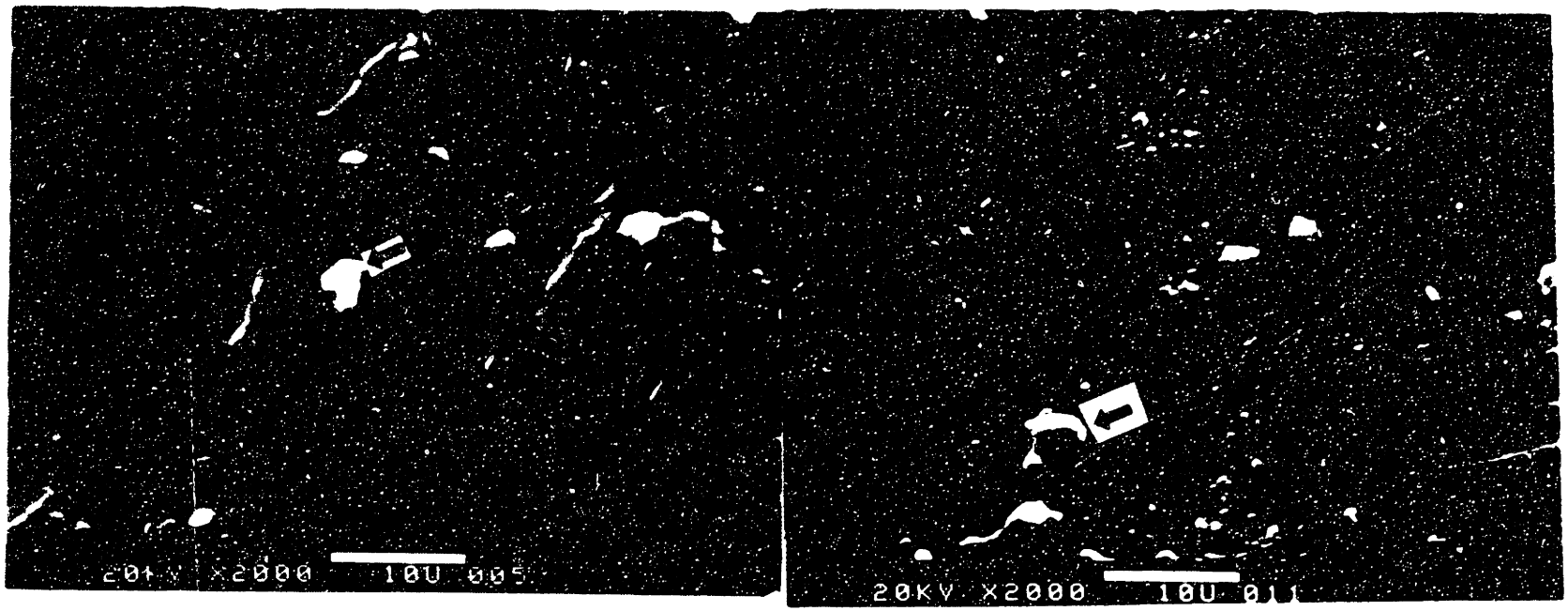

(a) 36-MS-Ti8 (b) 36-MS-Ti6

FIG. 26 Perovskite particles are shown (arrowed) embedded in the weld metal surfaces.

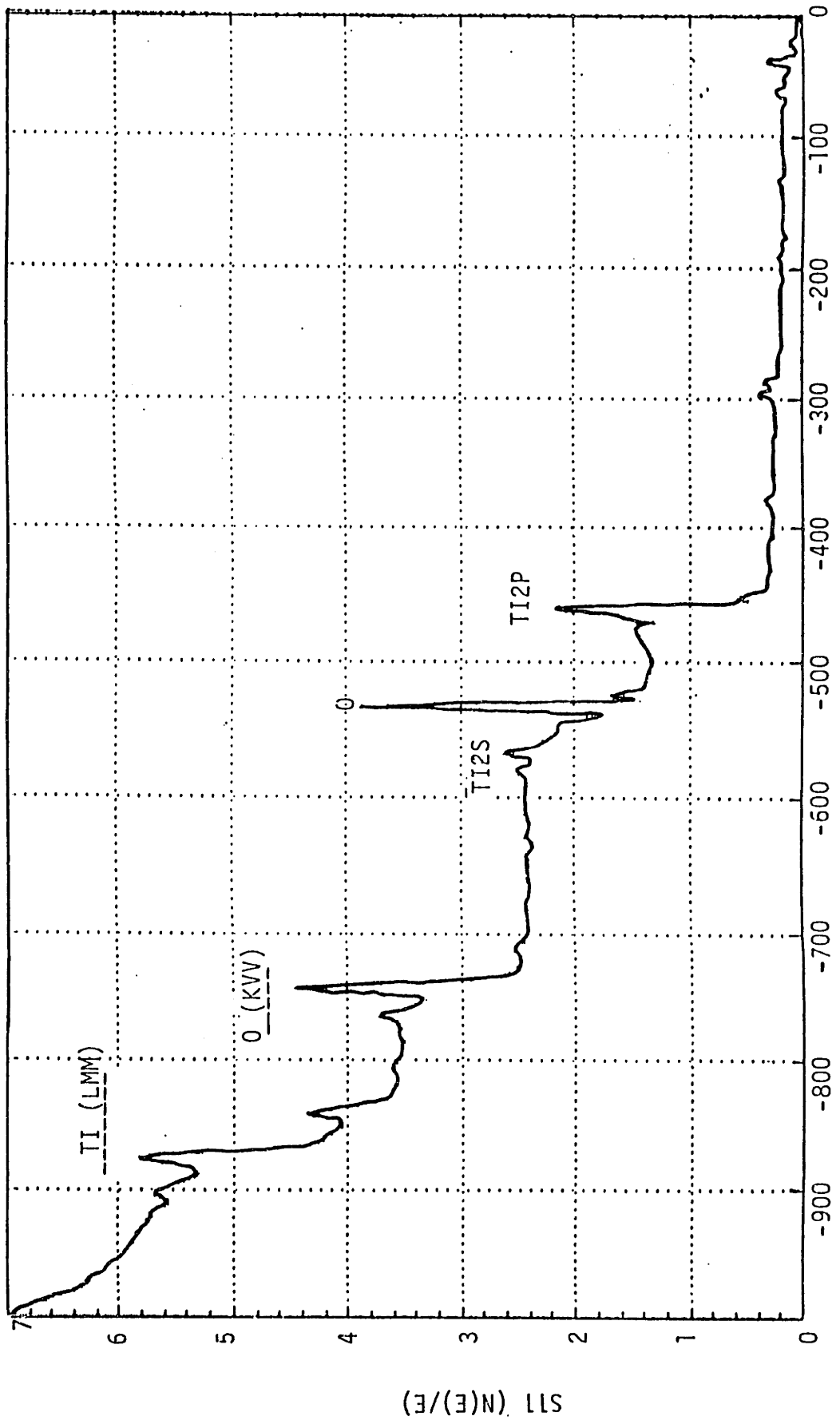

Figure 27: ESCA survey spectra in half-inch diameter control sample of titanium dioxide.

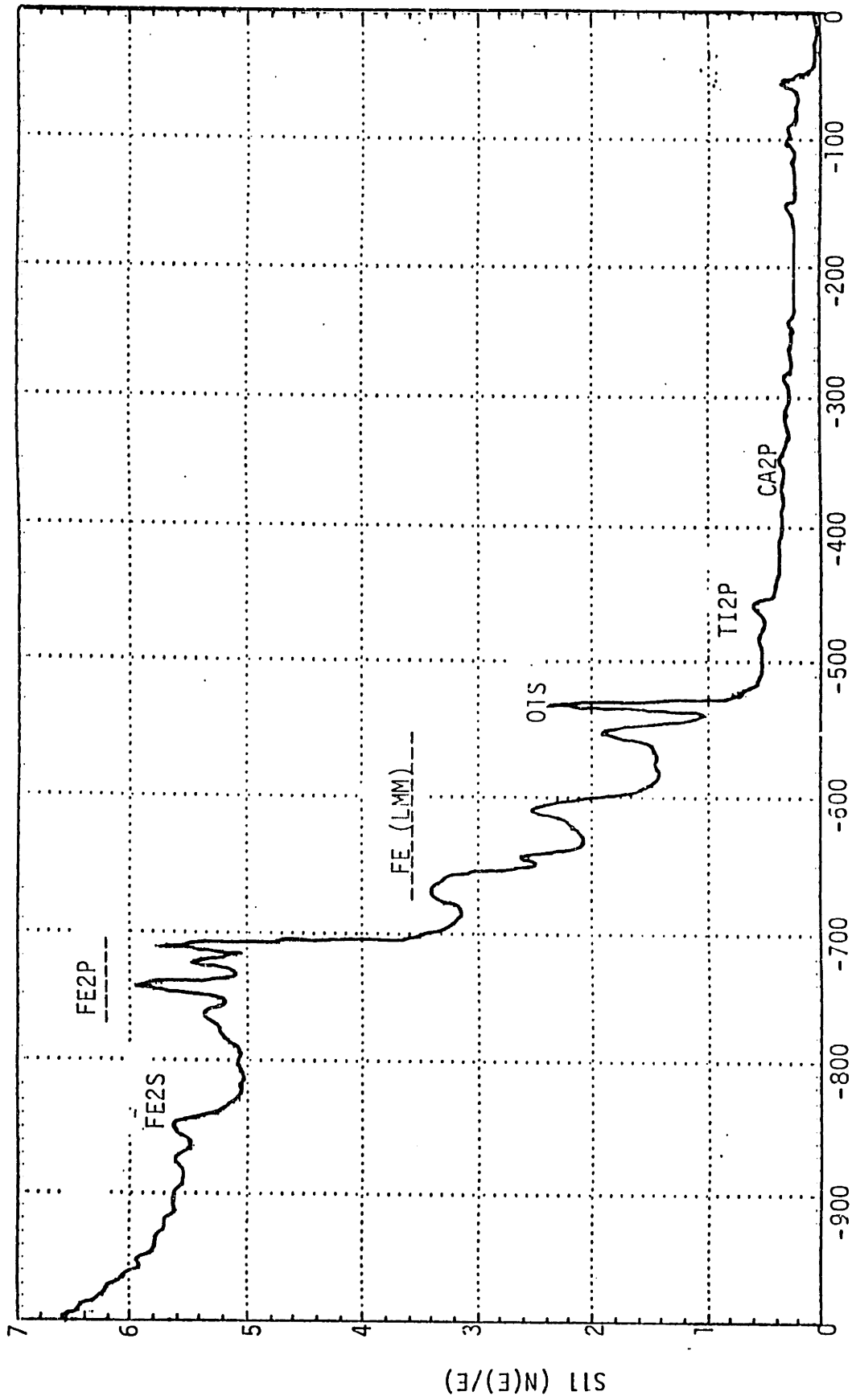

Figure 28: ESCA spectral survey of slag sample 36-MS-Ti8

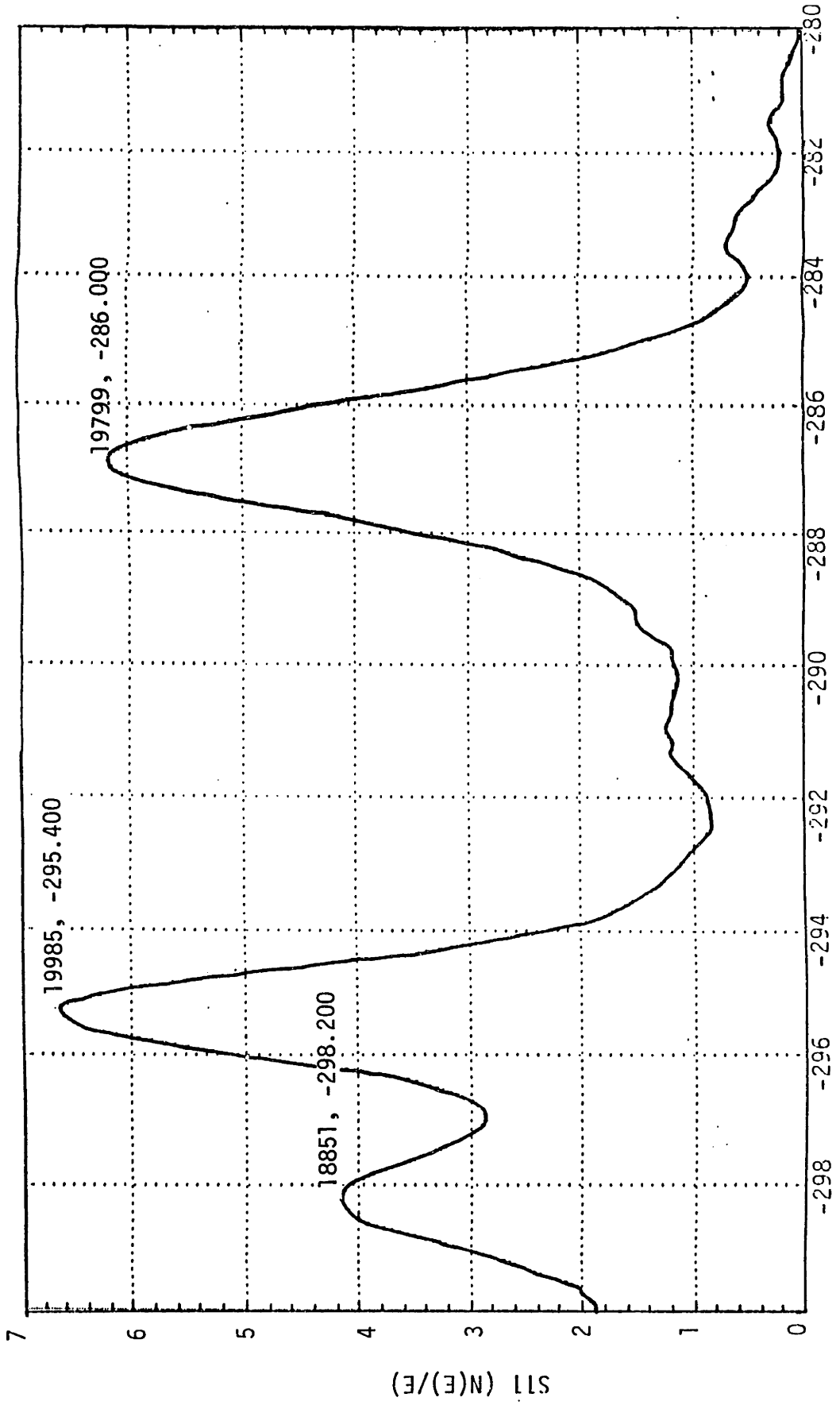

Figure 29: Shows ESCA multiplex spectra for carbon in the titanium dioxide control sample.

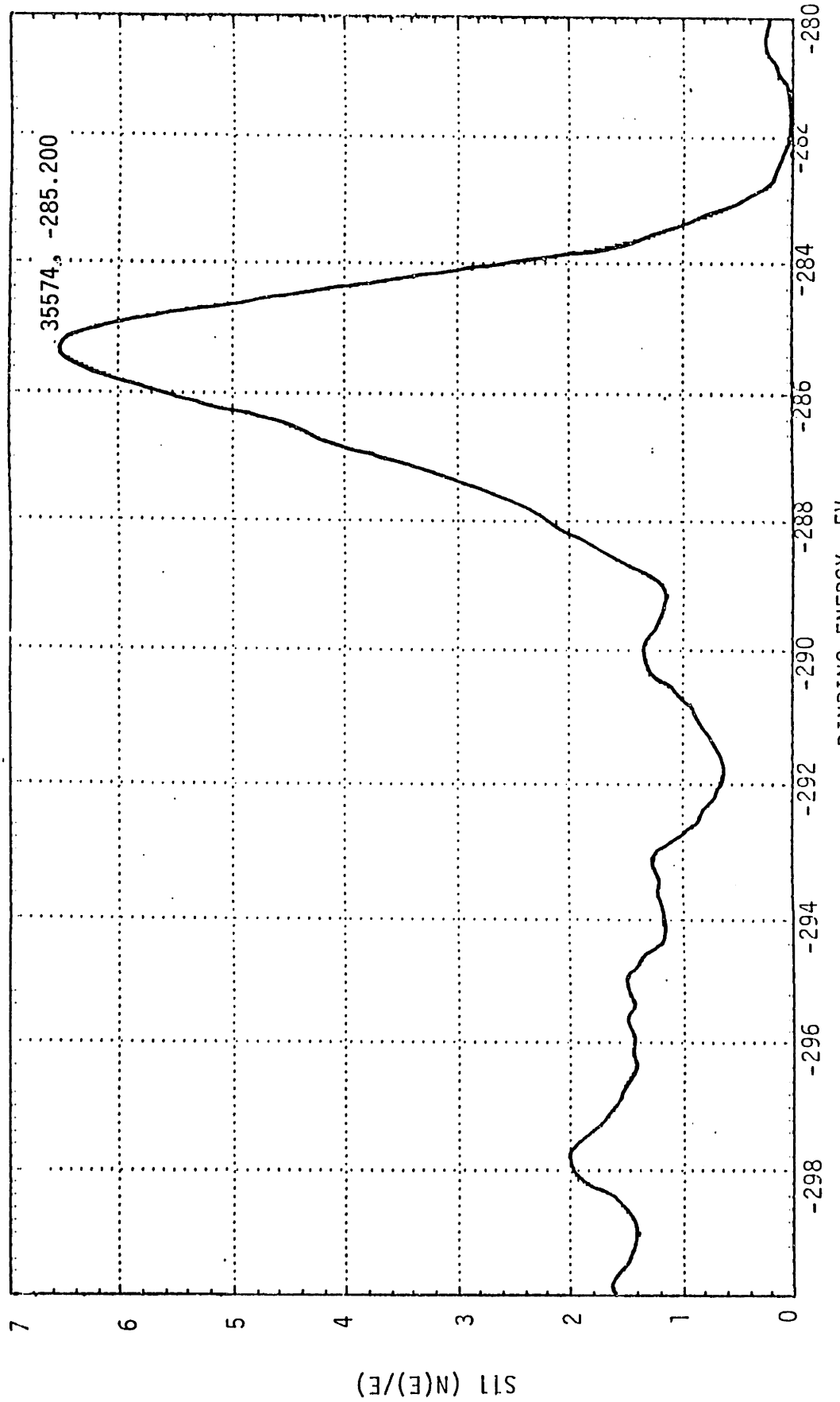

Figure 30: Shows ESCA multiplex spectrum of carbon in slag sample 36-MS-Ti8.

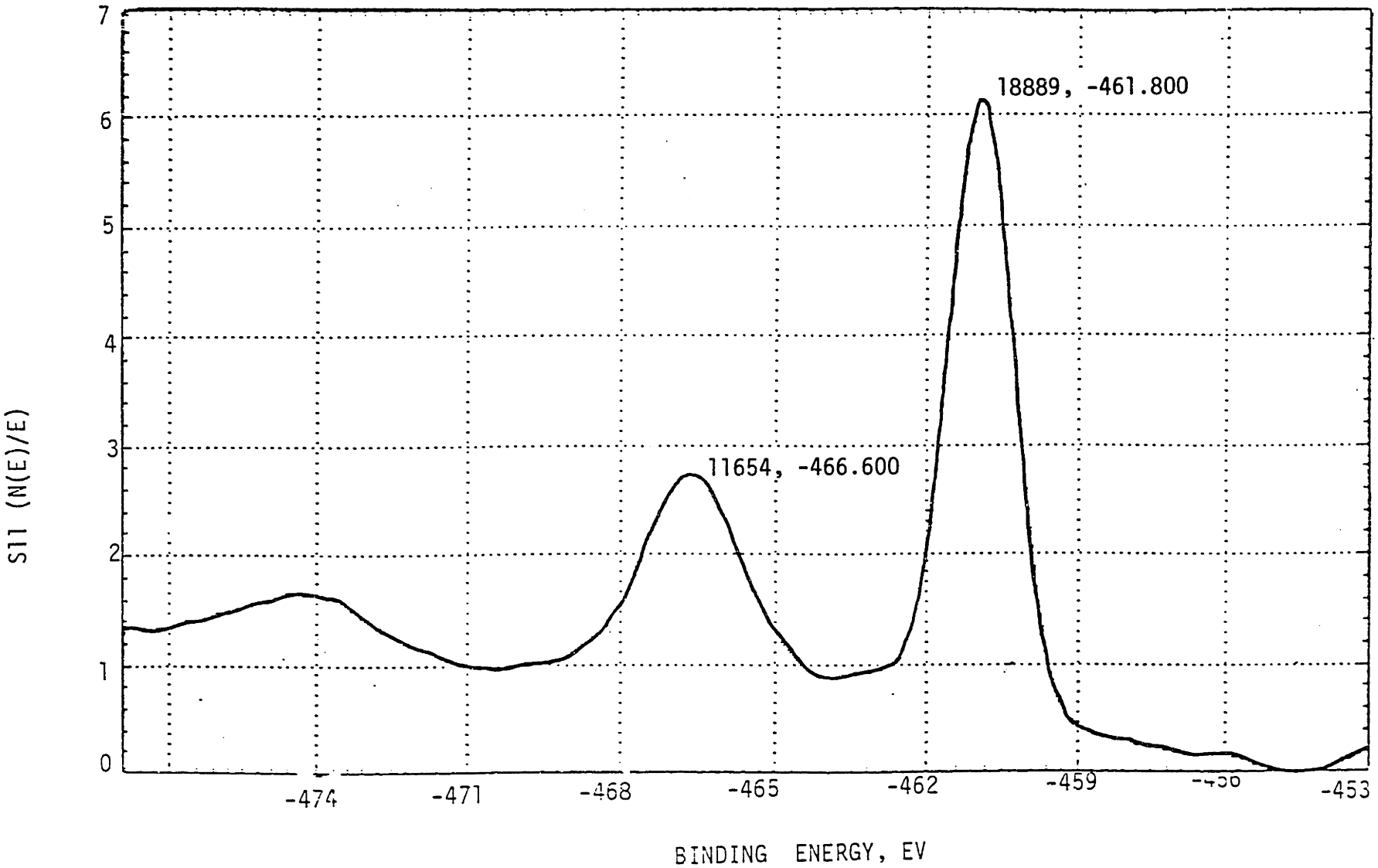

Figure 31: Shows ESCA multiplex spectra of titanium in the control sample of titanium dioxide.

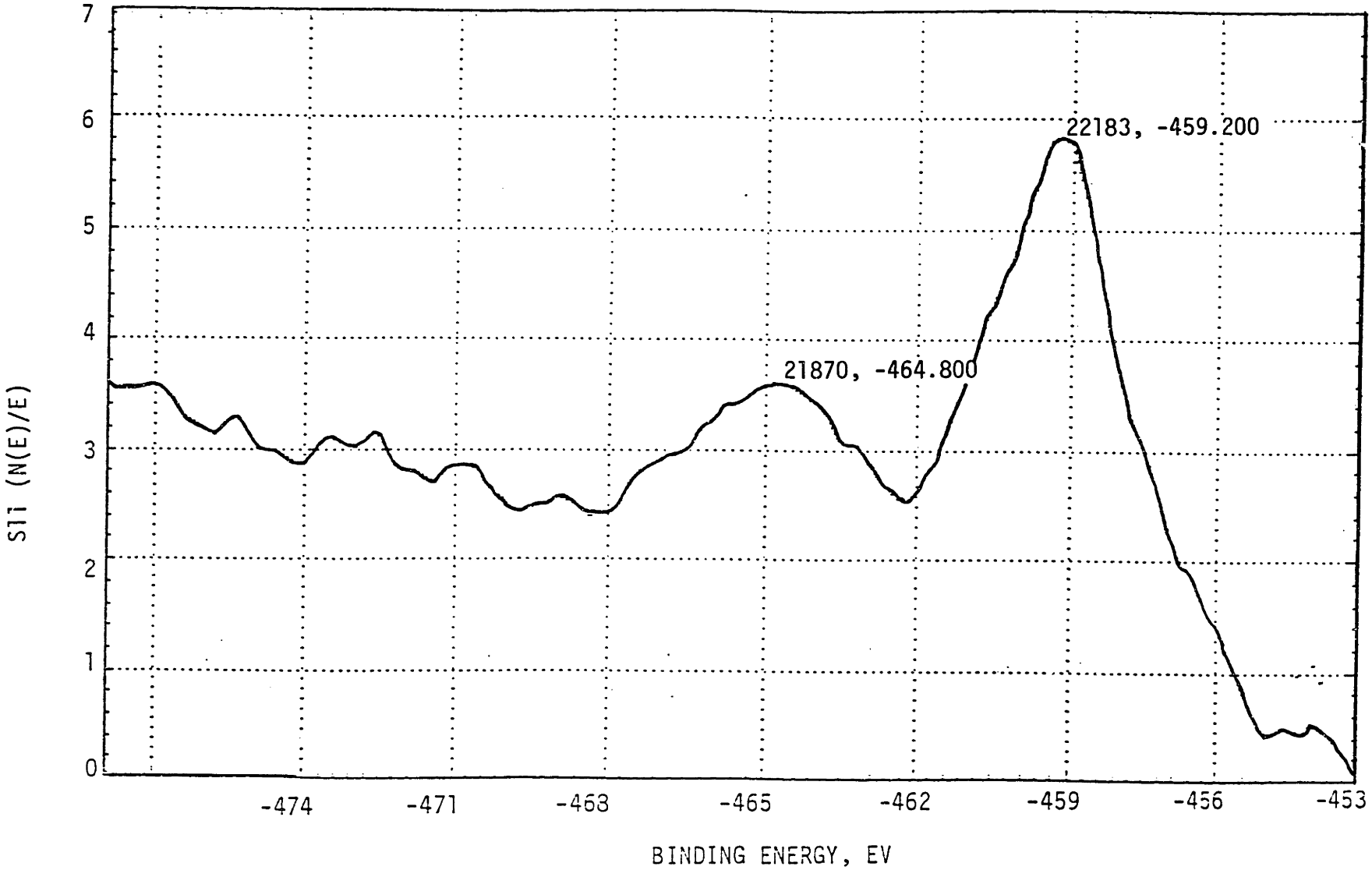

Figure 32: Shows ESCA multiplex spectra of titanium in the slag sample 36-MS-Ti8.

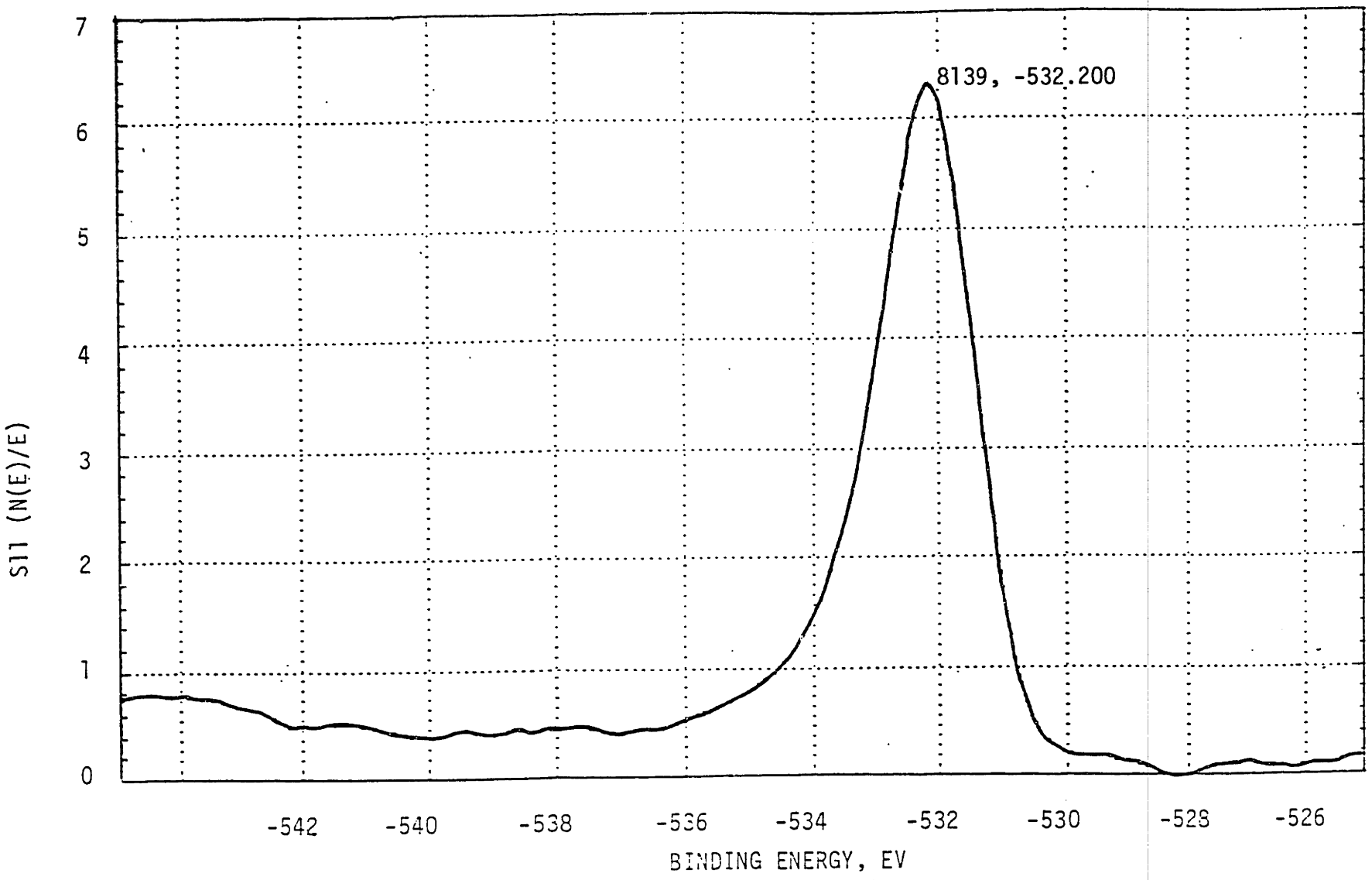

Figure 33: Shows ESCA multiplex spectra of oxygen in the control sample.

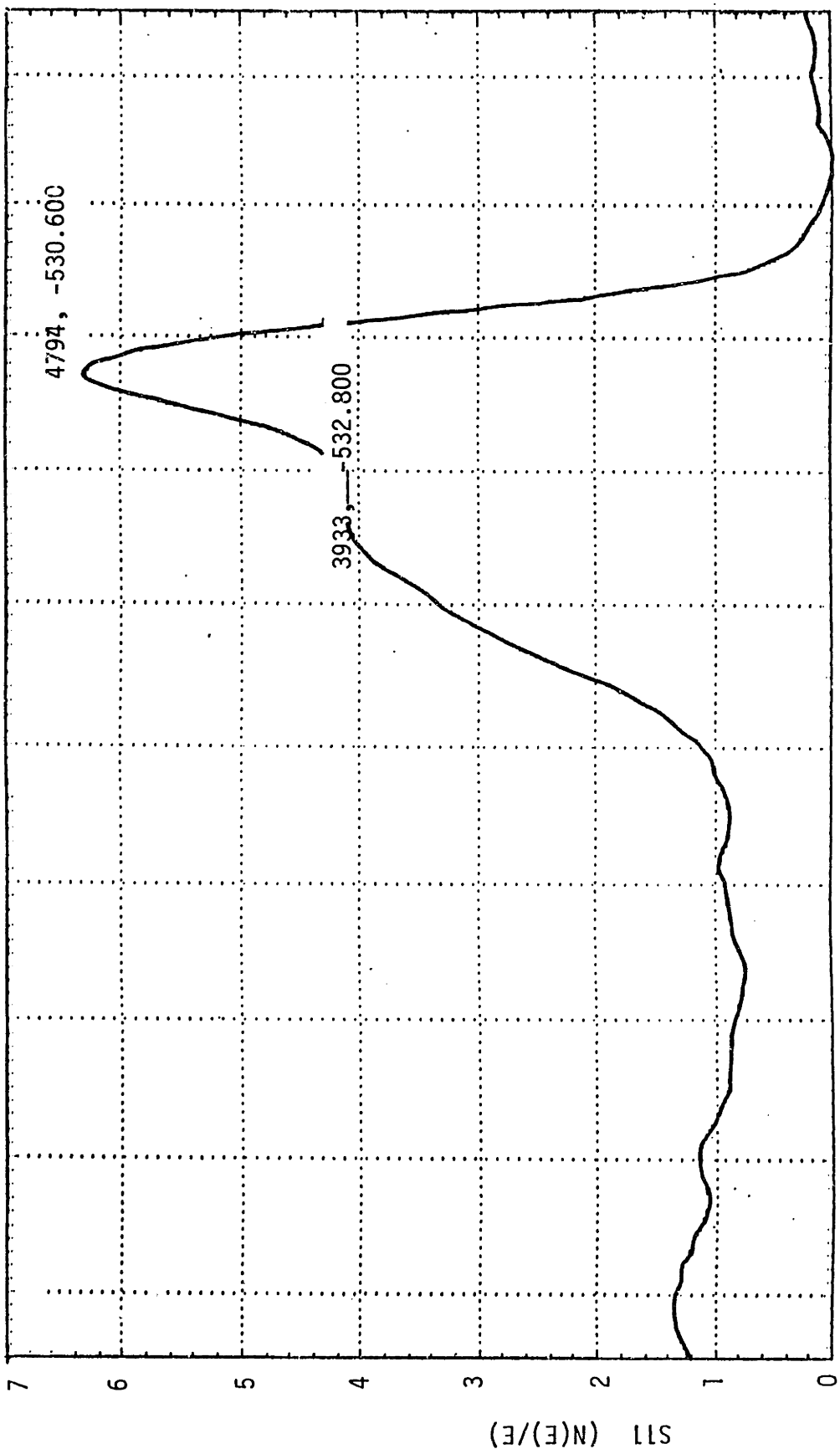

Figure 34: Shows ESCA multiplex spectra of oxygen in slag sample 36-MS-Ti8.

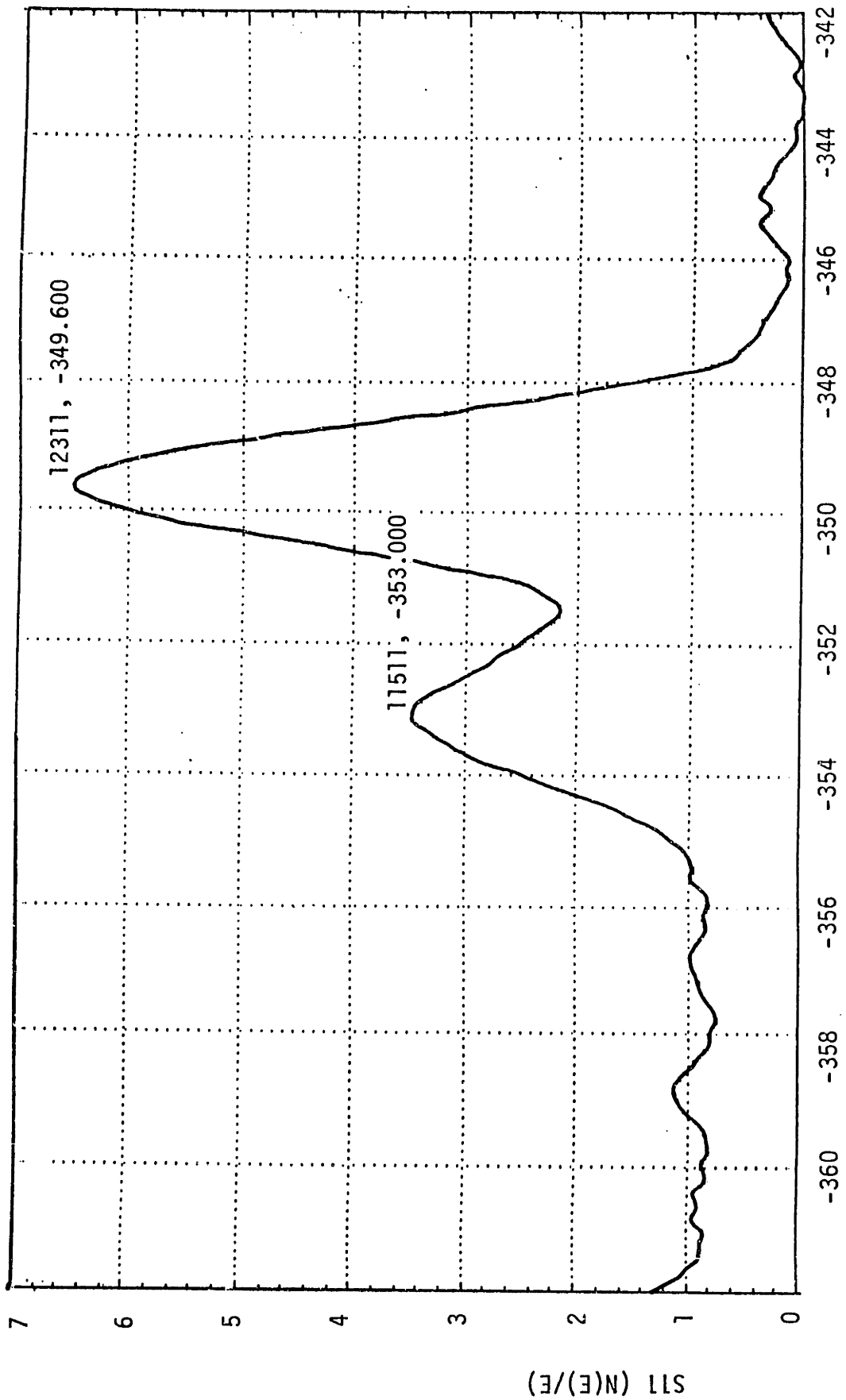

Figure 35: Shows E SCA multiplex spectra of calcium in slag sample 36-MS-Ti8.

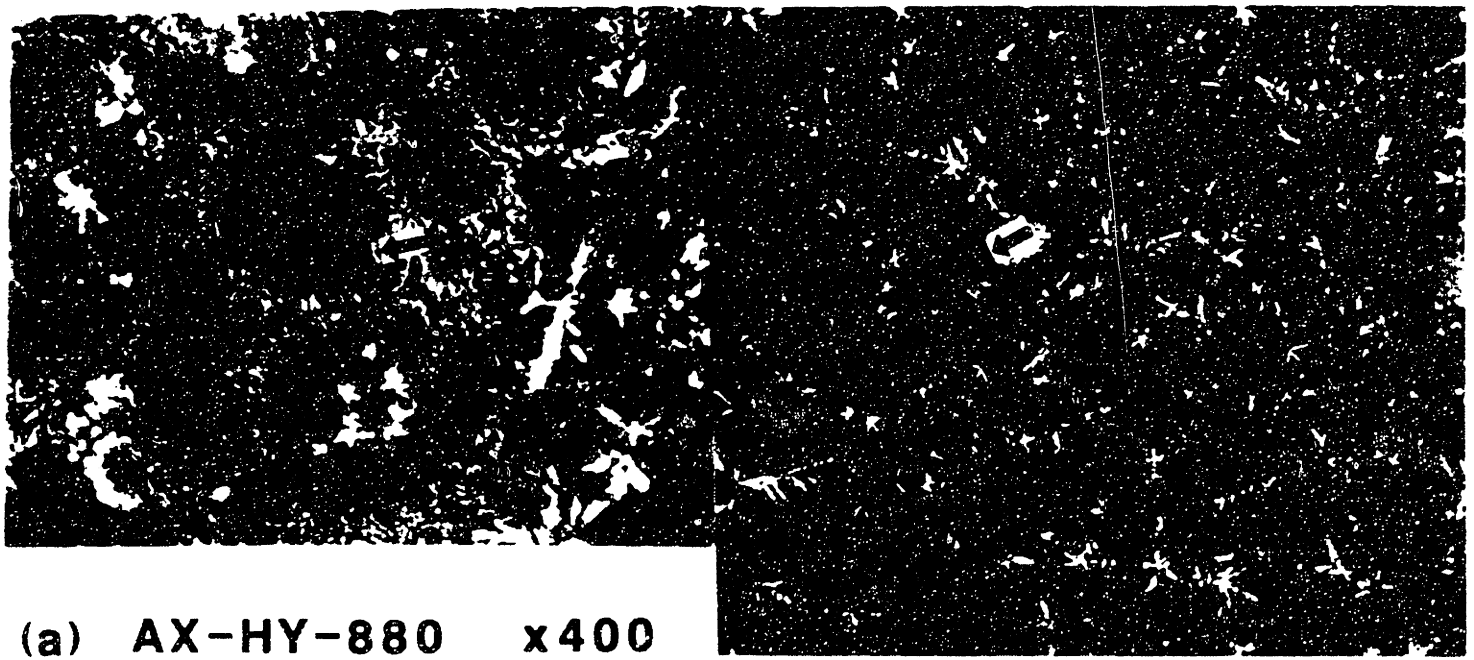

(a) AX-HY-880 x400

(b) AX-IN-880 x400

FIG. 36 Electron micrographs showing slag microstructures and fluorite dendrites in (a) and (b) (arrowed).

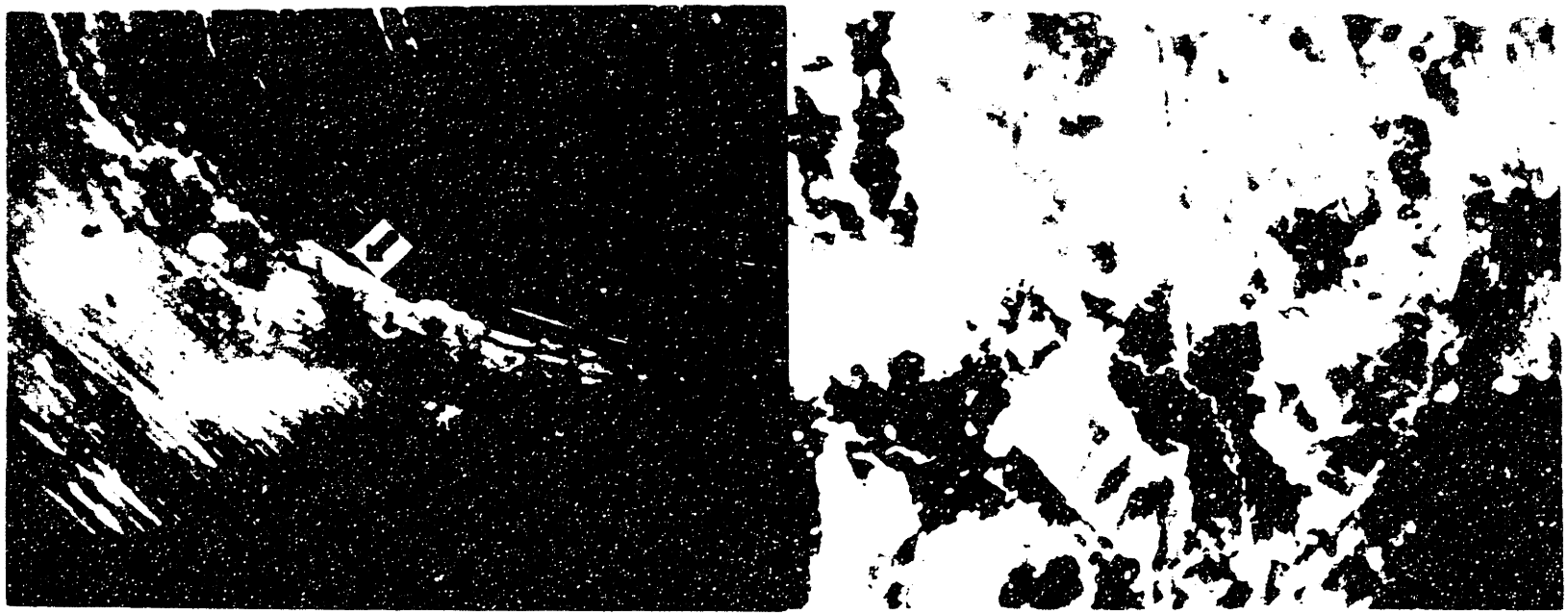

(a) 36-MS-CF6 x8

(b) 36-IN-CF6 x8

FIG. 37 Macrographs comparing surface appearances of weld samples of same electrode and flux but different base metal. Adherent slag is arrowed in (a) and shown in (b)

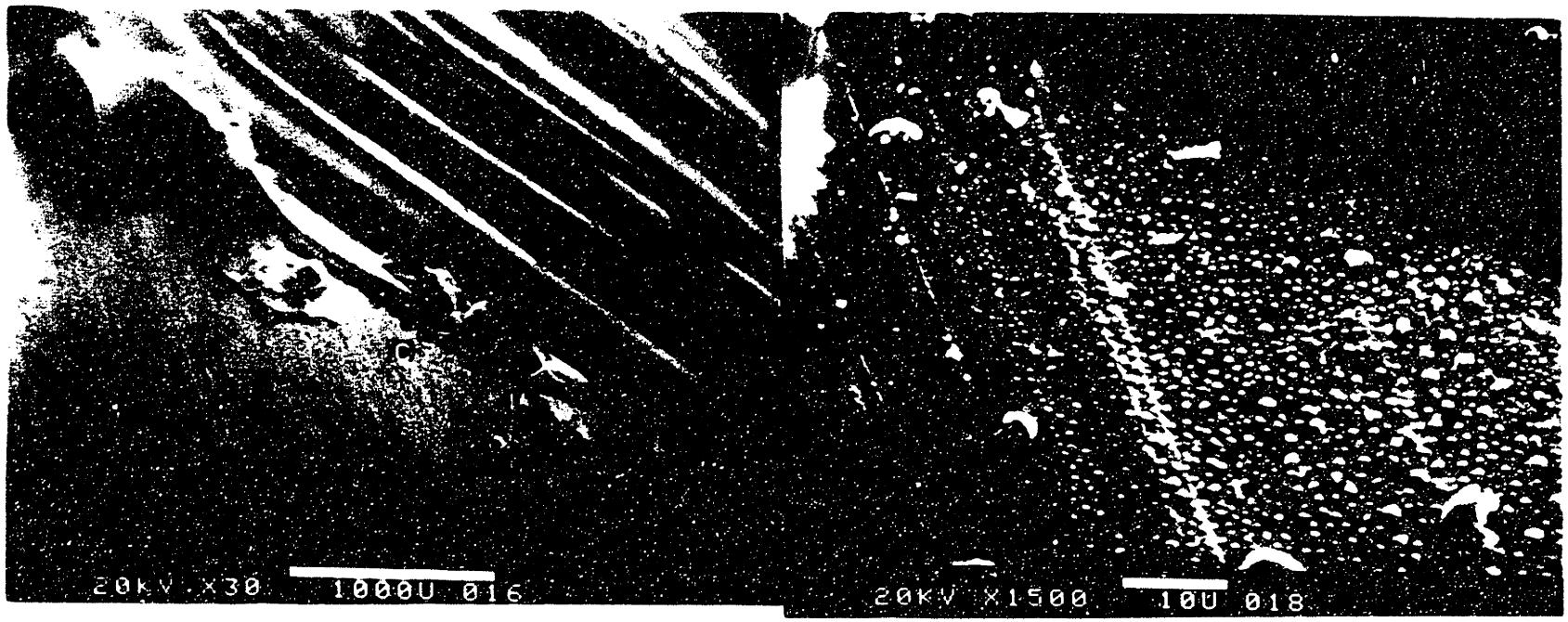

(a) 36-MS-CF6

(b) Region C of (a).

FIG. 38 Shows adherent slag in the HAZ (a) and MnO particles (b).

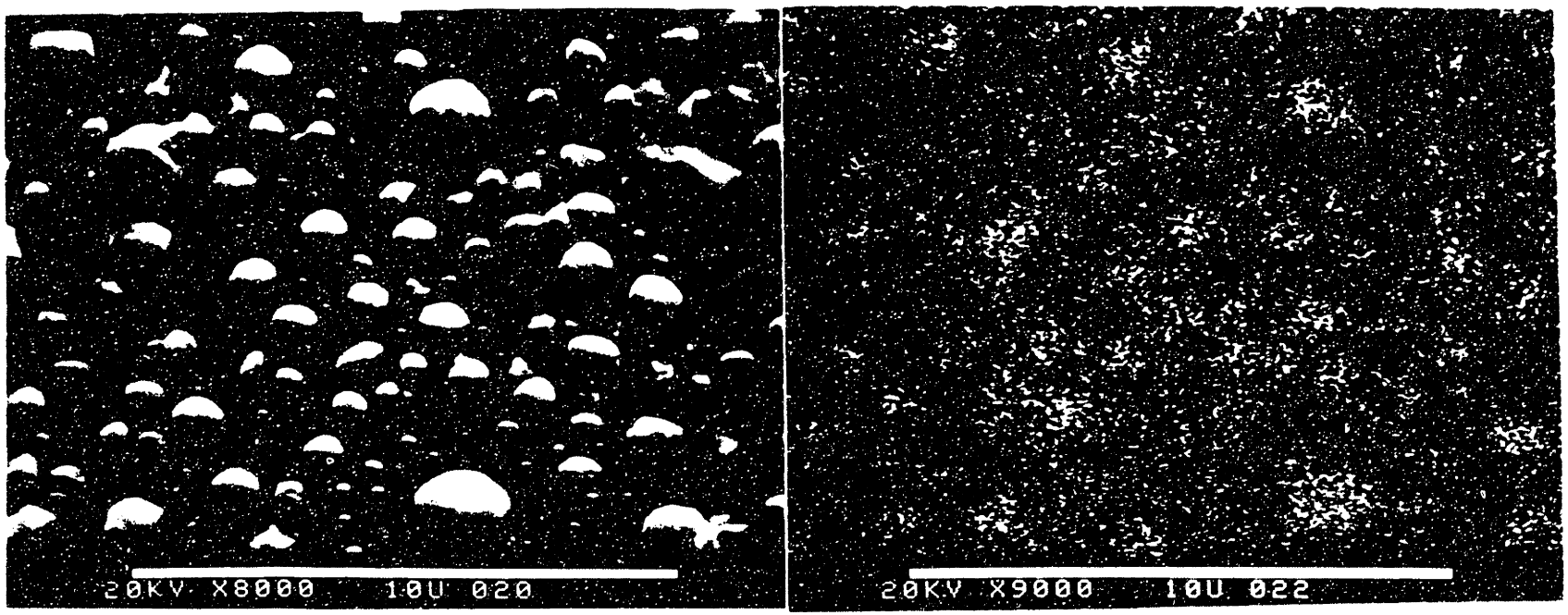

(a) 36-MS-CF6

(b) Mn-map of (a)

FIG. 39 Shows particles in region C to contain manganese.

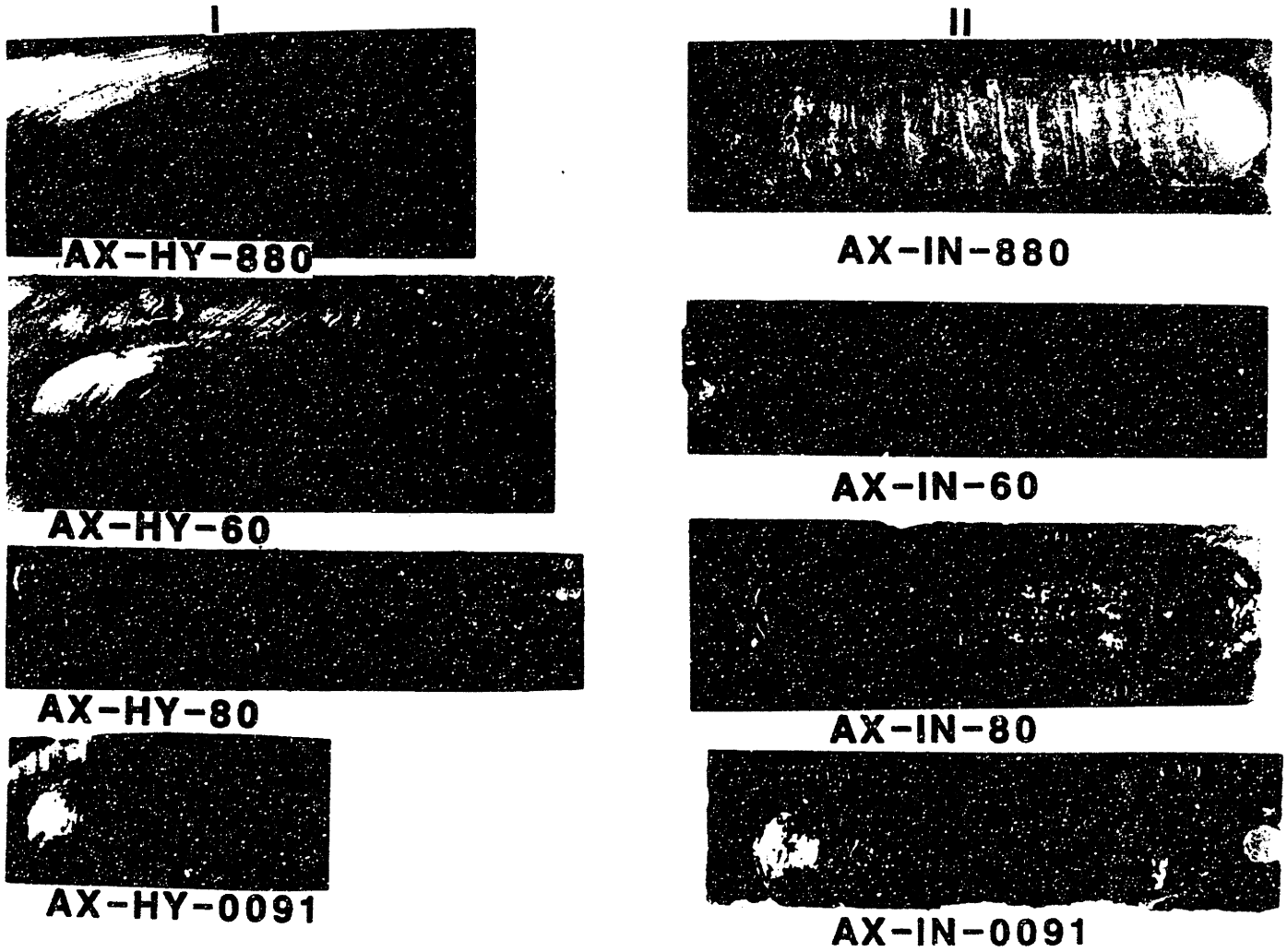

FIG. 40 Macrographs comparing surface appearance of weld samples of same electrode and flux but different base metals (I vs II).

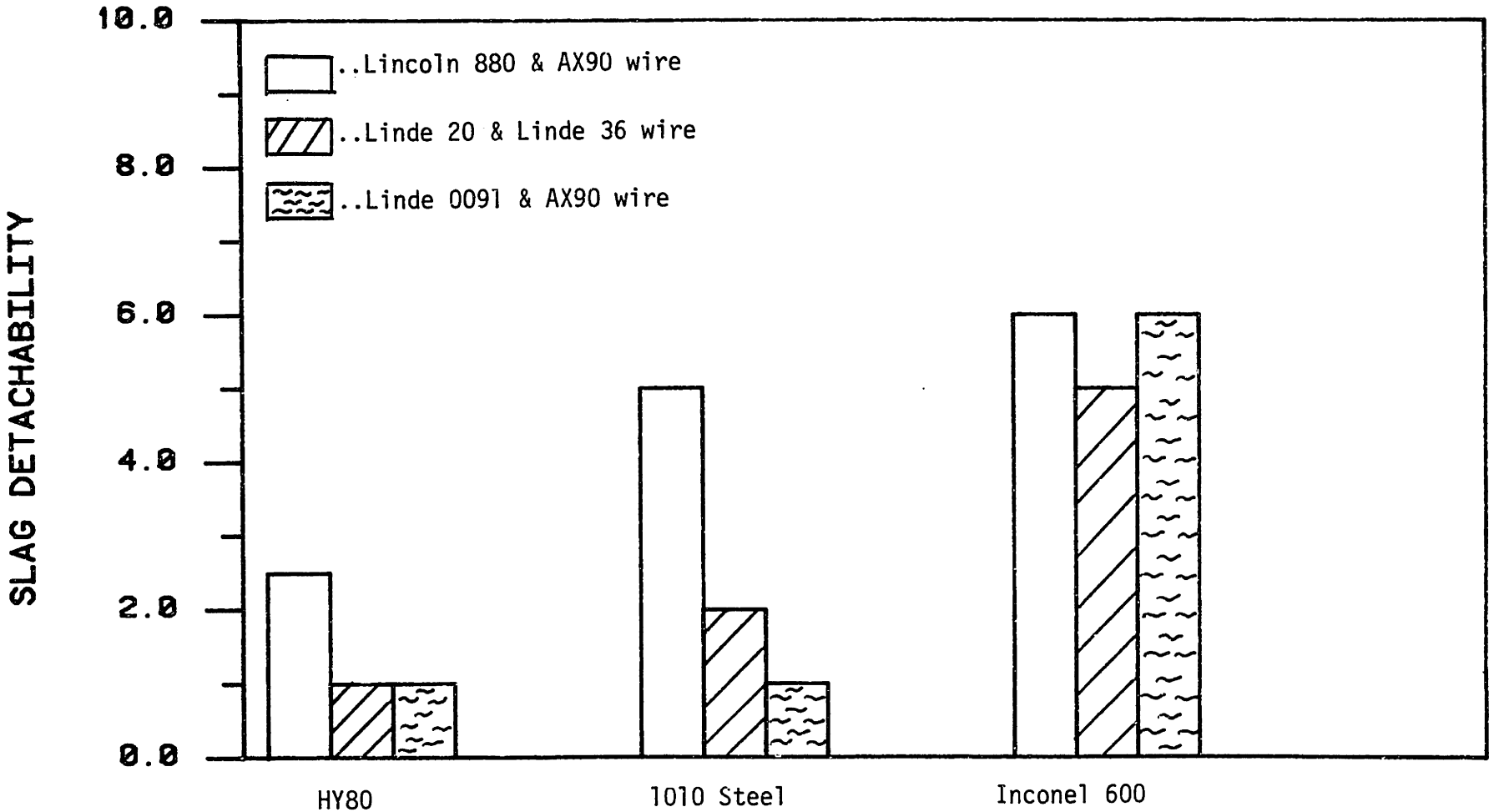

FIGURE 41: Shows the effect of base metal chemistry on slag detachability for various flux-electrode combinations.

(a) AX-HY-60 x8 (b) AX-HYS-60 x8

FIG. 42 Macrographs showing the effect of surface condition of base metal on slag detachability. (a) Descaled base metal (b) Heavily scaled base metal showing adherent slag (dark areas).

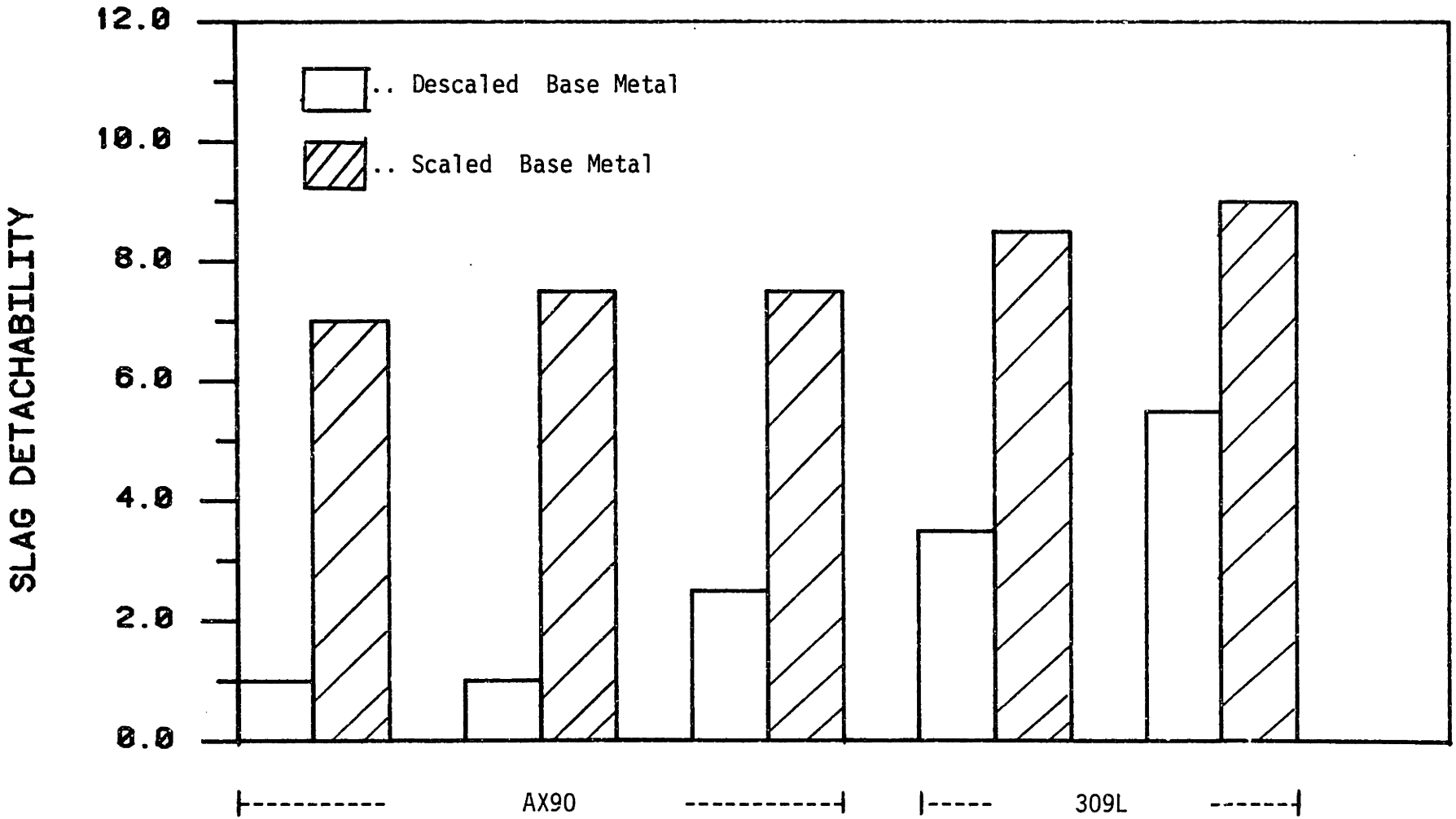

FIGURE 43: Shows the effect of base metal's surface condition on detachability for electrodes AX90 and 309L. Scaled base metal condition is detrimental to detachability.

(a) AX-HYS-60 (b) AX-HYS-60 (Glassy Region)

FIG.44 SEM micrographs showing glassy region (A) where the molten slag had contacted the scaled base metal. Region B is the top of the slag layer.

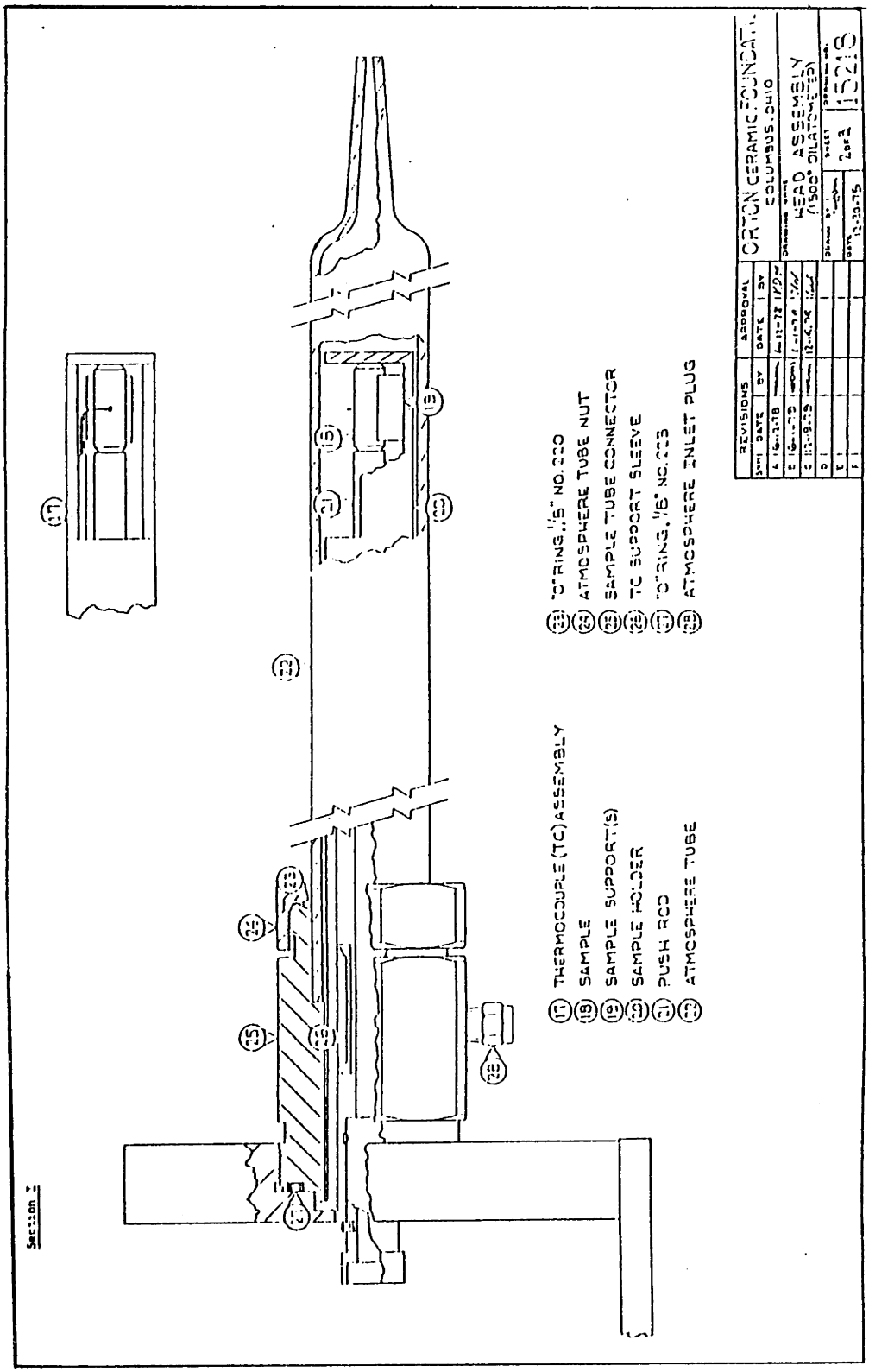

Figure 45 shows a diagram of the head assembly of the dilatometer.

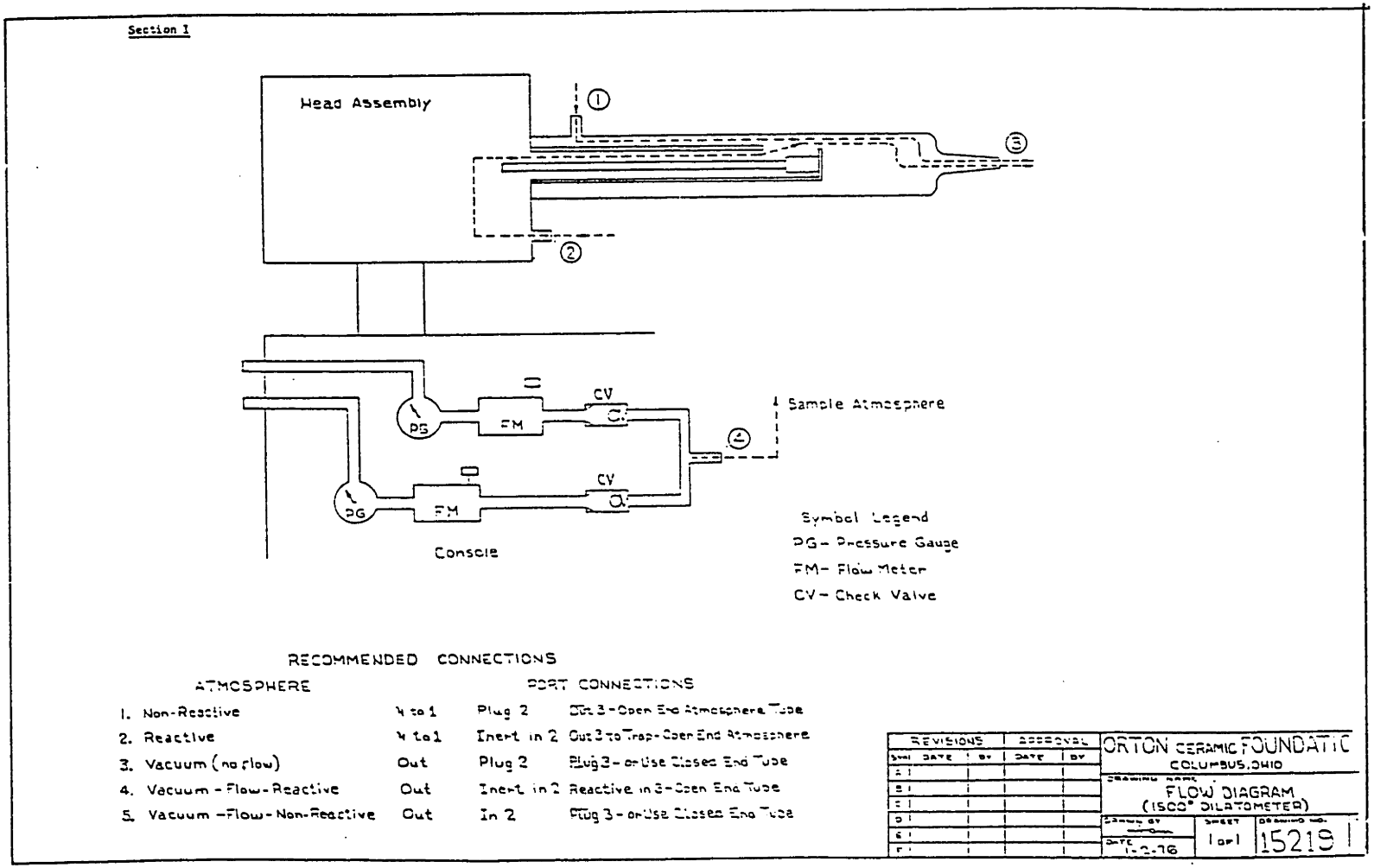

Figure 46: Shows the flow diagram of the atmosphere through the dilatometer.

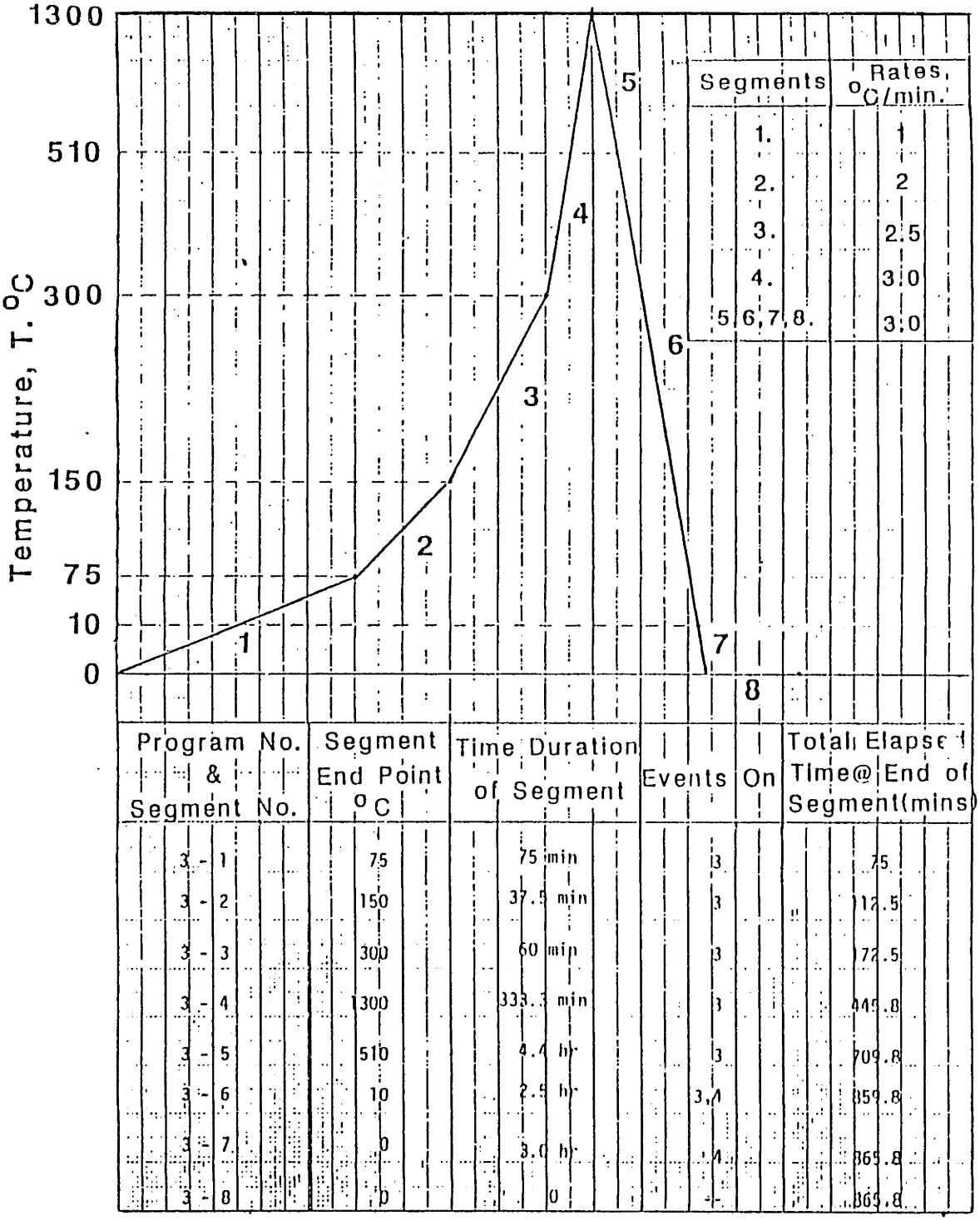

Program No. & Segment No.	Segment End Point °C	Time Duration of Segment	Events On	Total Elapsed Time@ End of Segment(mins)
3 - 1	75	75 min	3	75
3 - 2	150	37.5 min	3	112.5
3 - 3	300	60 min	3	172.5
3 - 4	1300	333.3 min	3	445.8
3 - 5	510	4.4 hr	3	709.8
3 - 6	10	2.5 hr	3,4	859.8
3 - 7	0	3.0 hr	4	865.8
3 - 8	0	0	-	865.8

Figure 47: Programmed run for the dilatometer experiments.

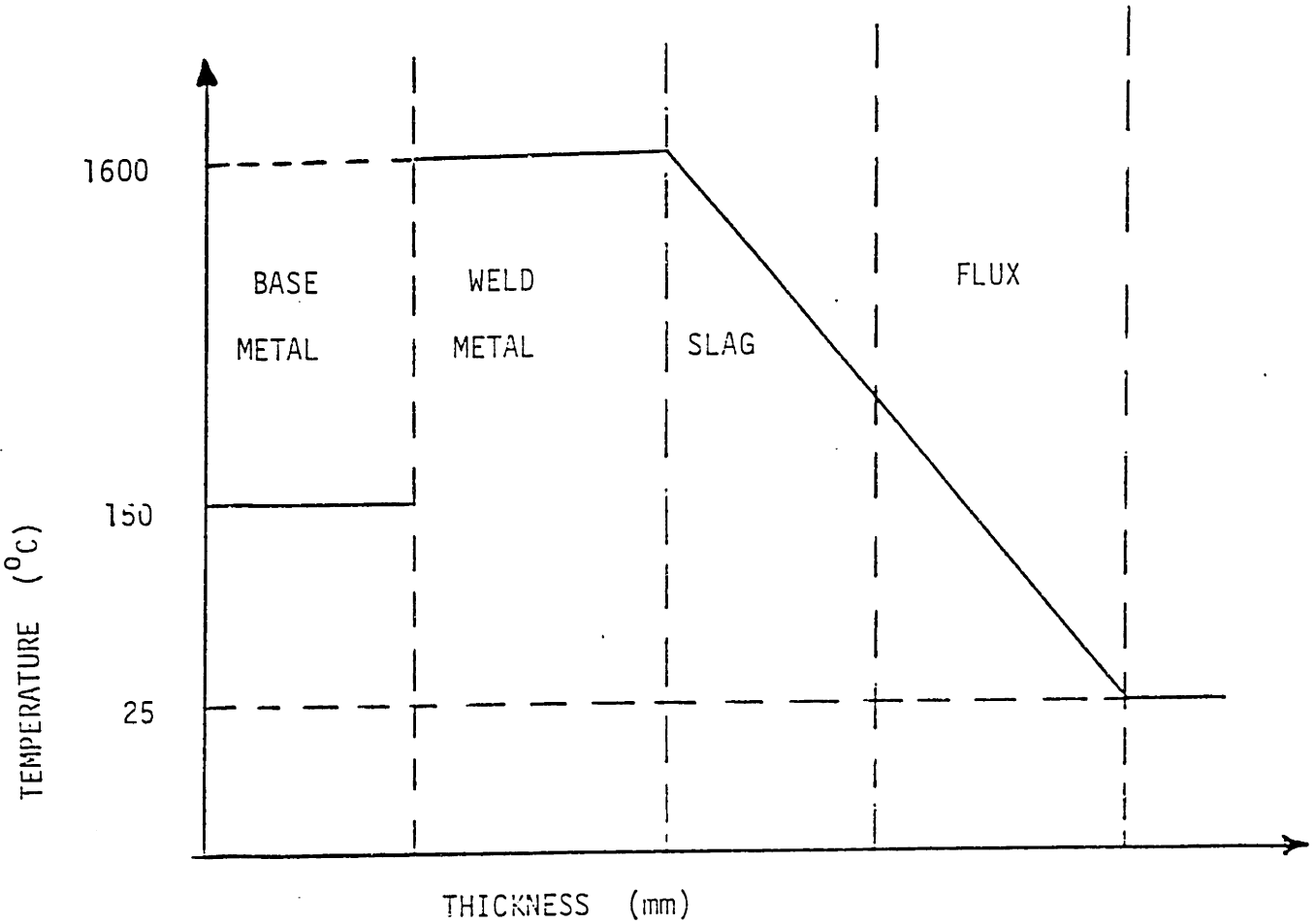

Figure 48: Shows initial temperature distribution imposed in the finite element analysis.

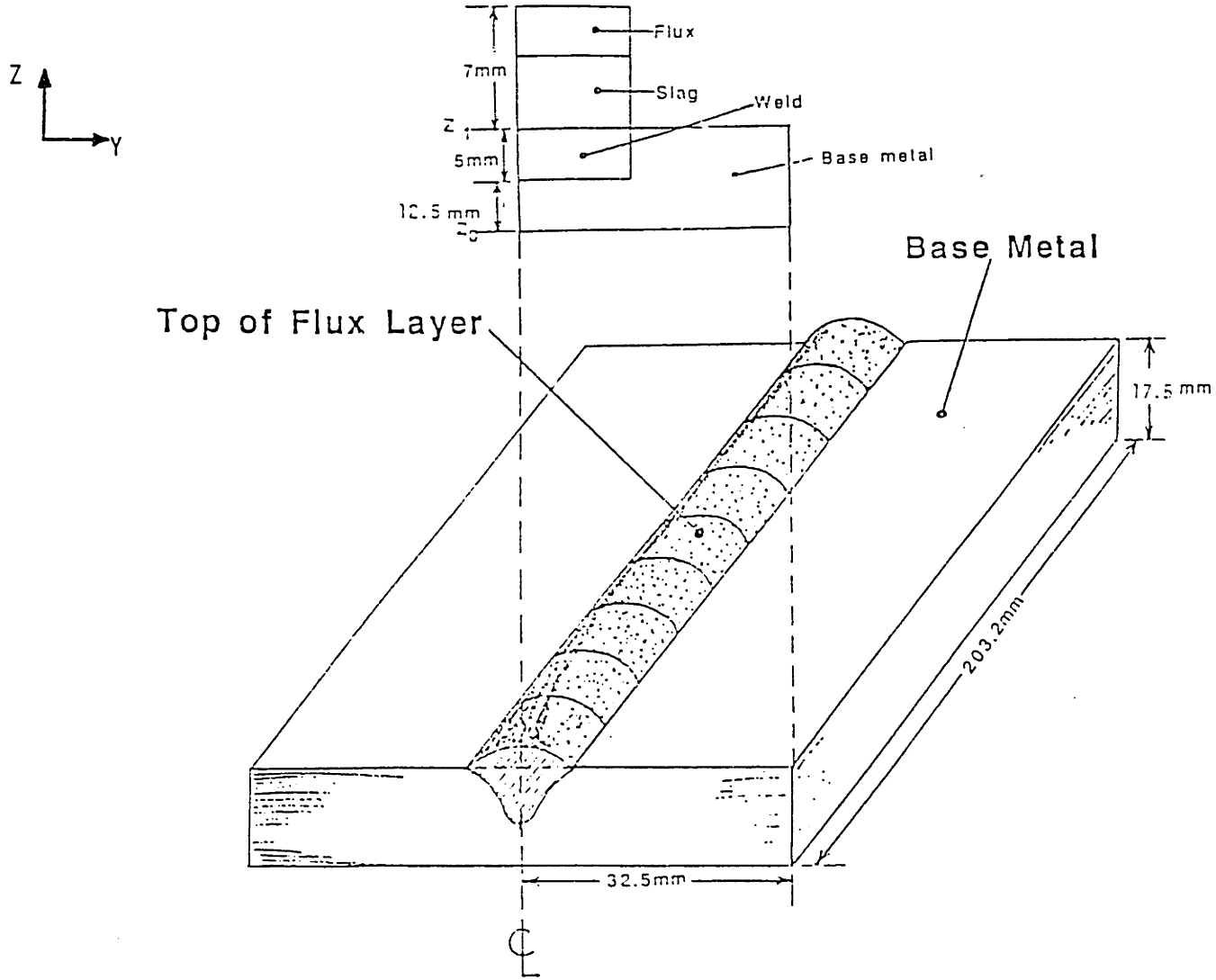

Figure 49: Shows the region chosen for the finite element analysis.

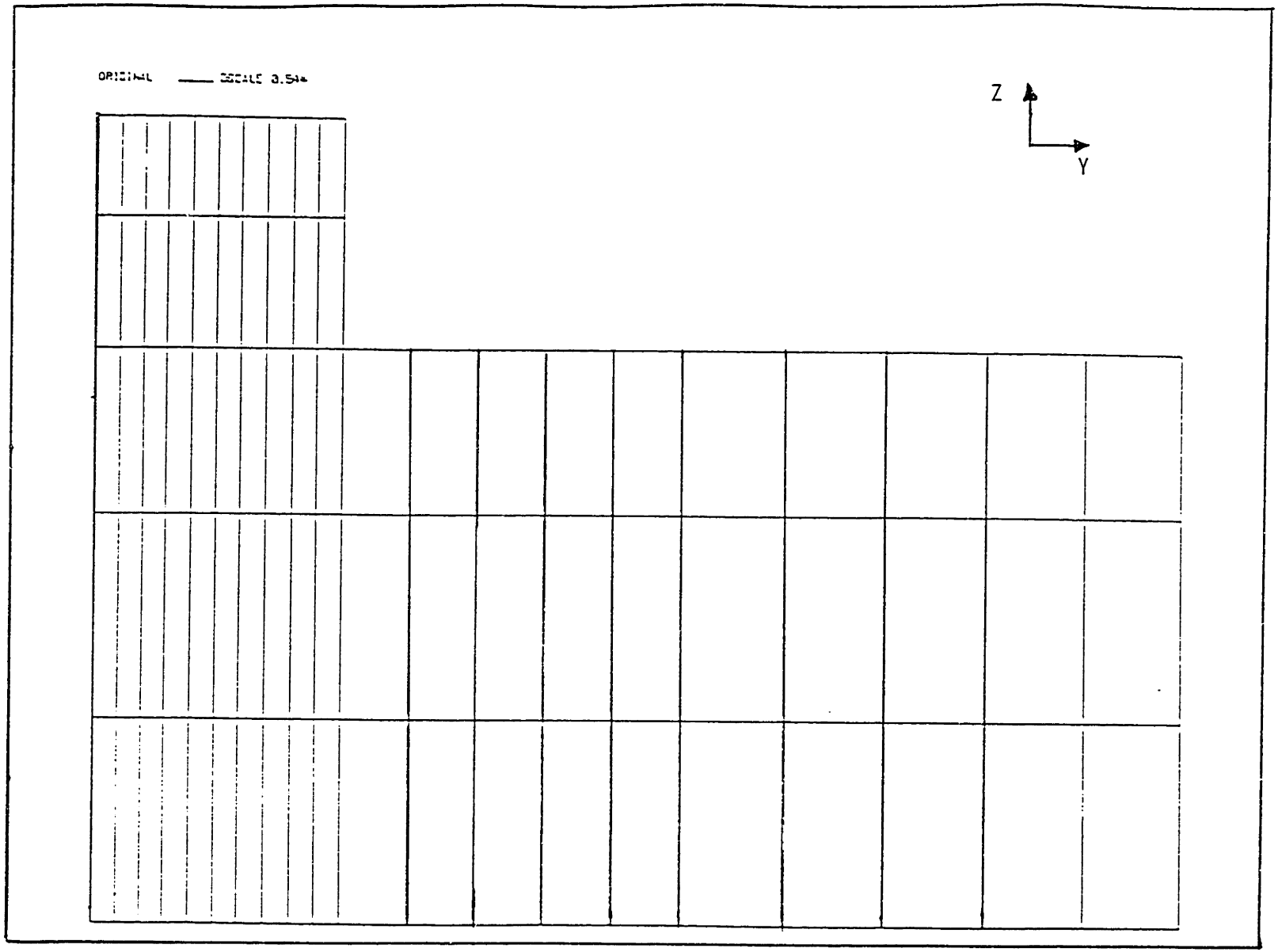

Figure 50: Shows mesh used in the finite element analysis.

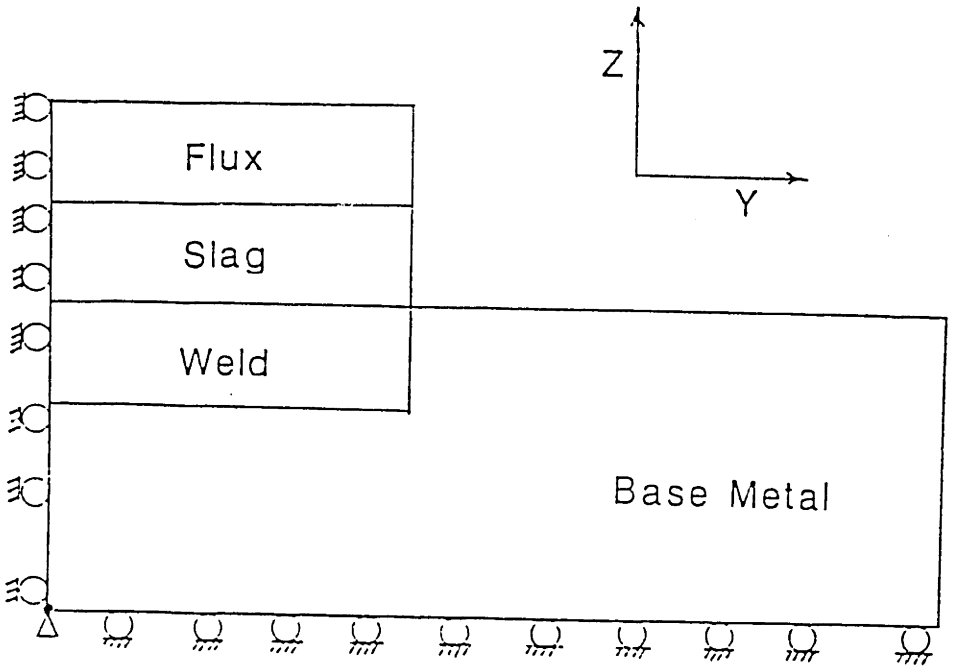

FIGURE 51: Shows the displacement constraints on the system for stress(σ) analysis.

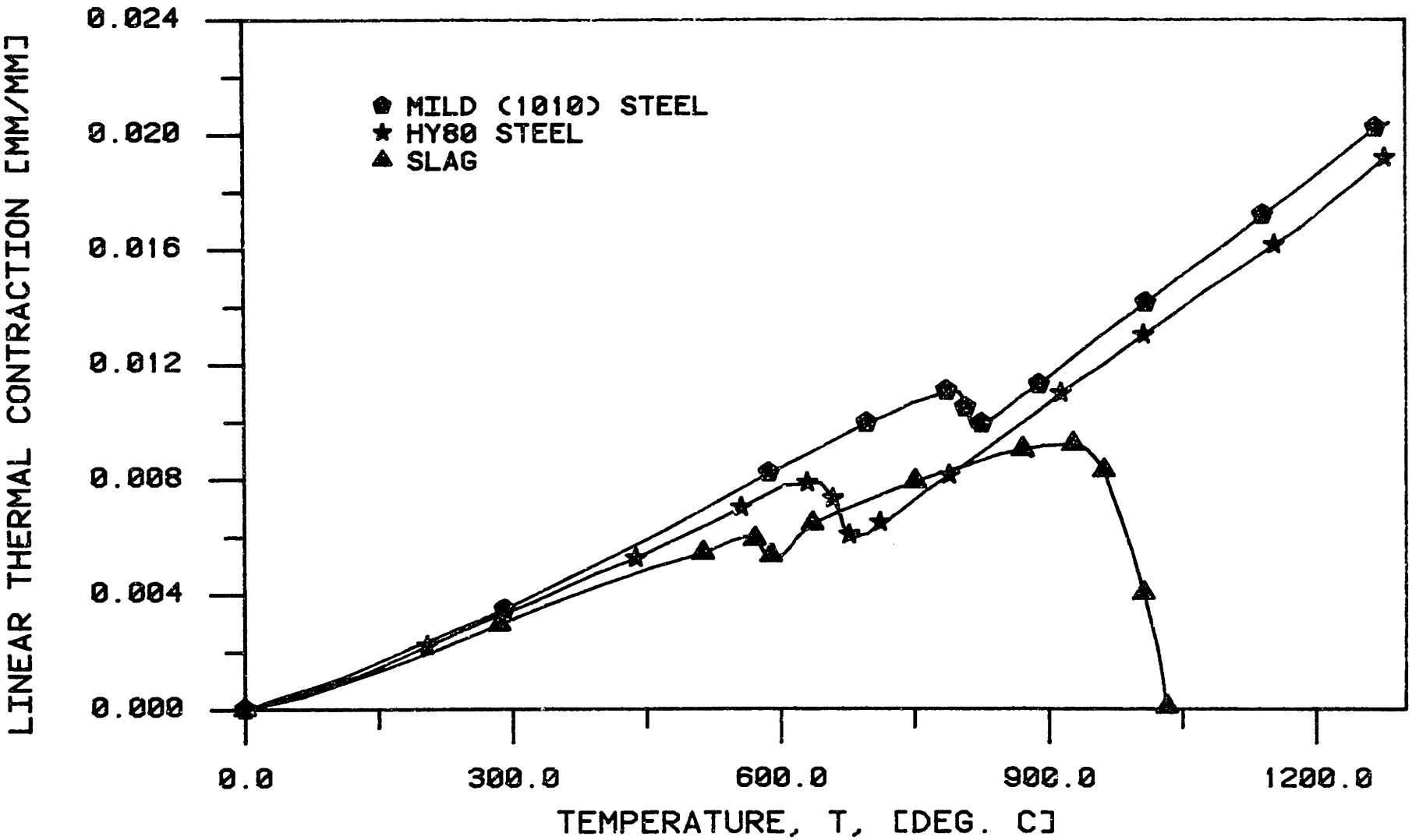

FIGURE 52: Shows linear thermal contraction per unit length for two base metals and a slag as a function of temperature. Based on this figure, HY80 base metal should provide slags easier to detach than with the mild steel base metal.

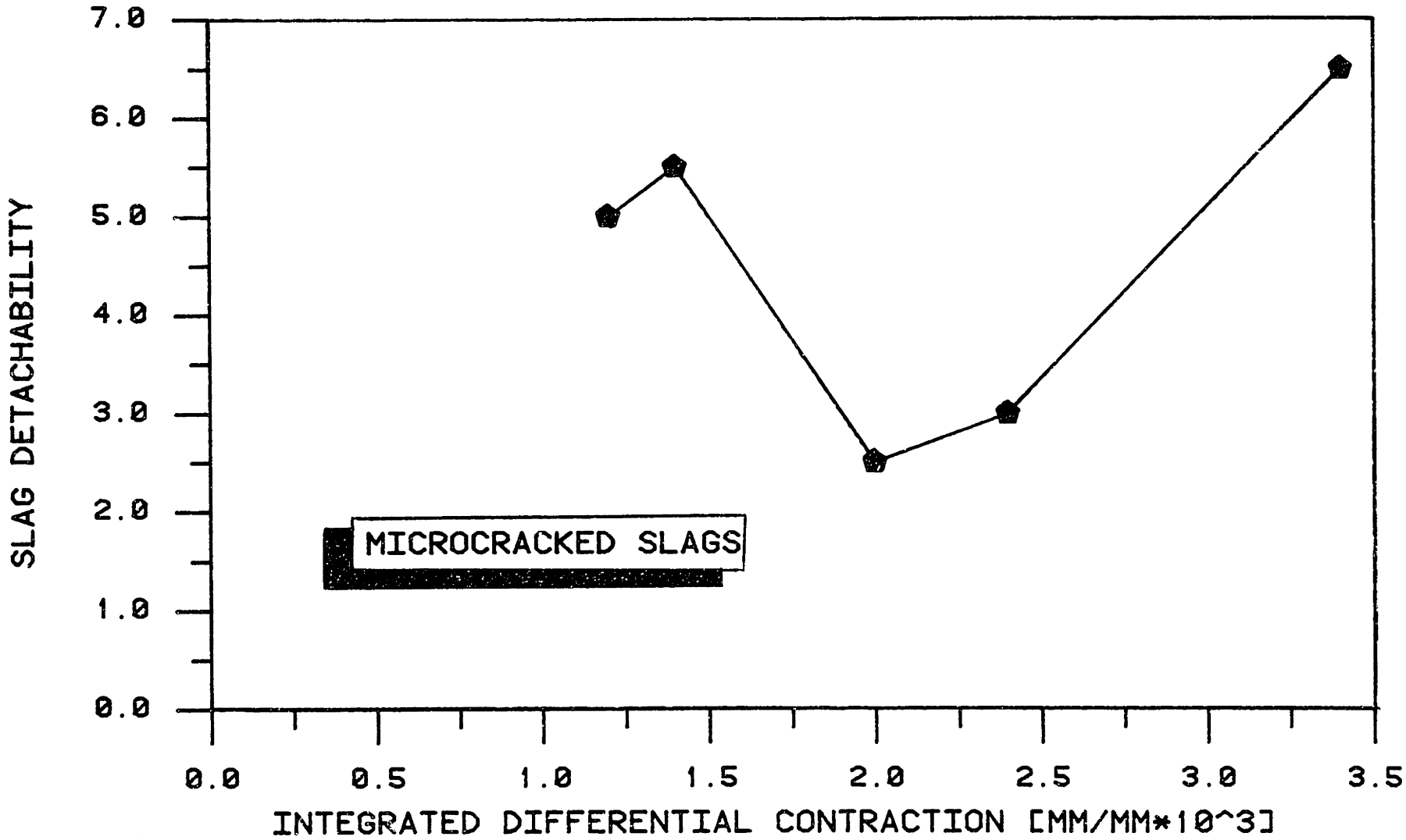

FIGURE 53: Shows the effect of cracks in the microstructure of slag on integrated differential thermal contraction per unit length as typified in a lack of correlation with slag detachability.

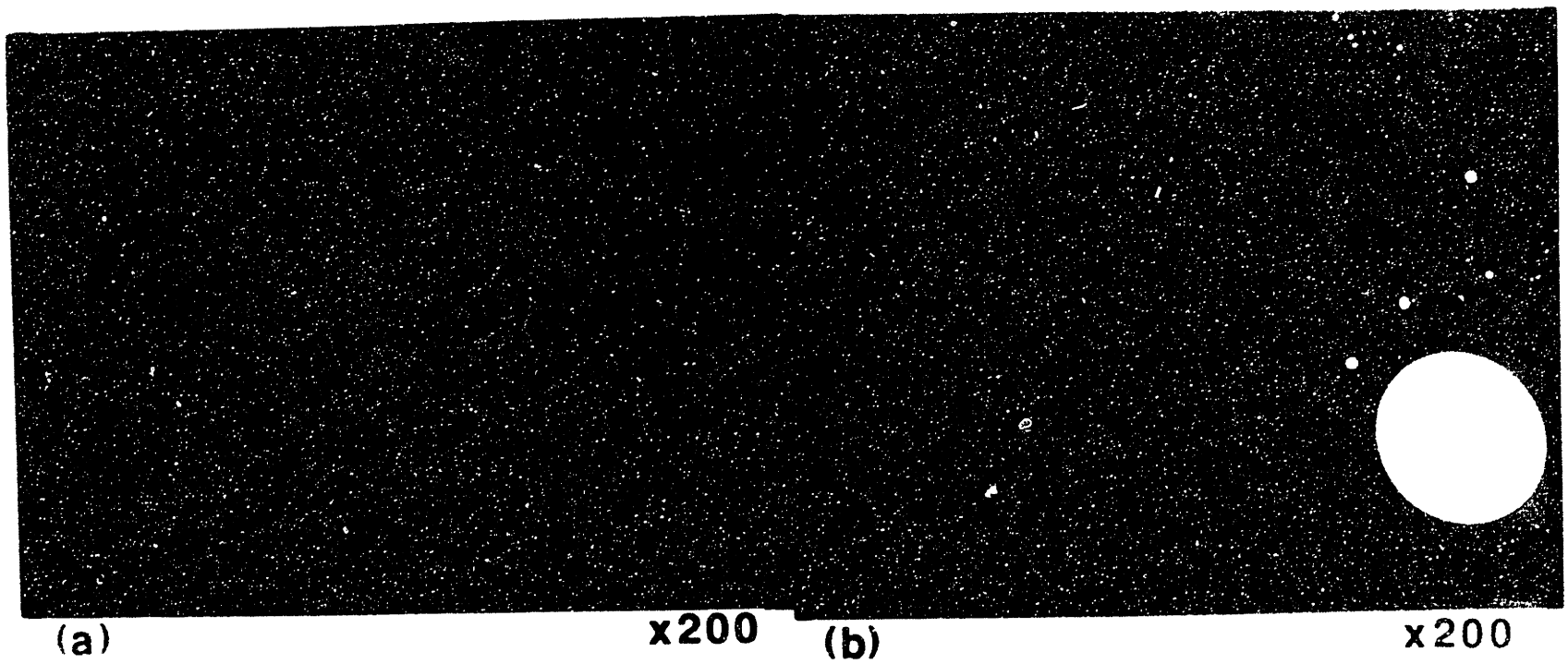

Figure 54: Shows microcrack-free and glassy slag structures.
(a) AX-HY-20 (b) AX-IN-20

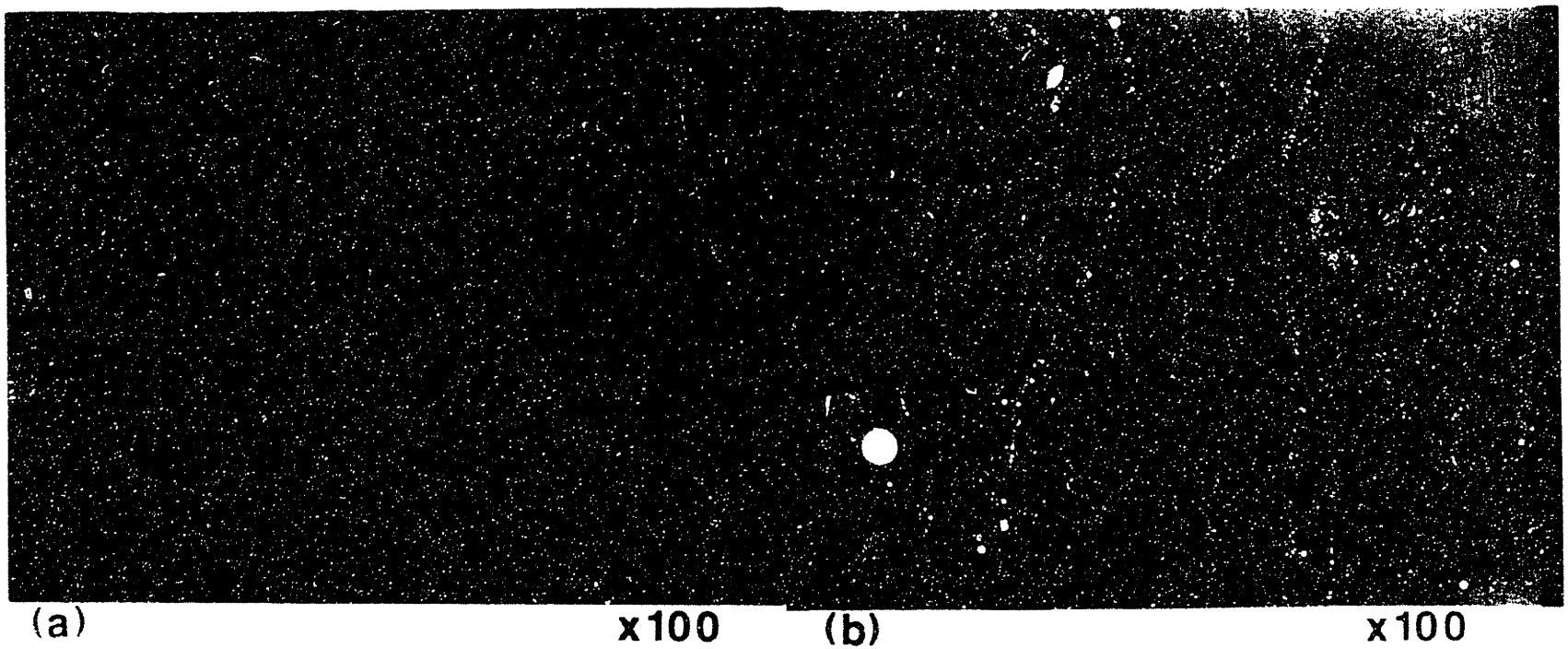

Figure 55: Shows microcrack-free and glassy slag structures.
(a) 36-MS-0091 (b) 36-MS-60

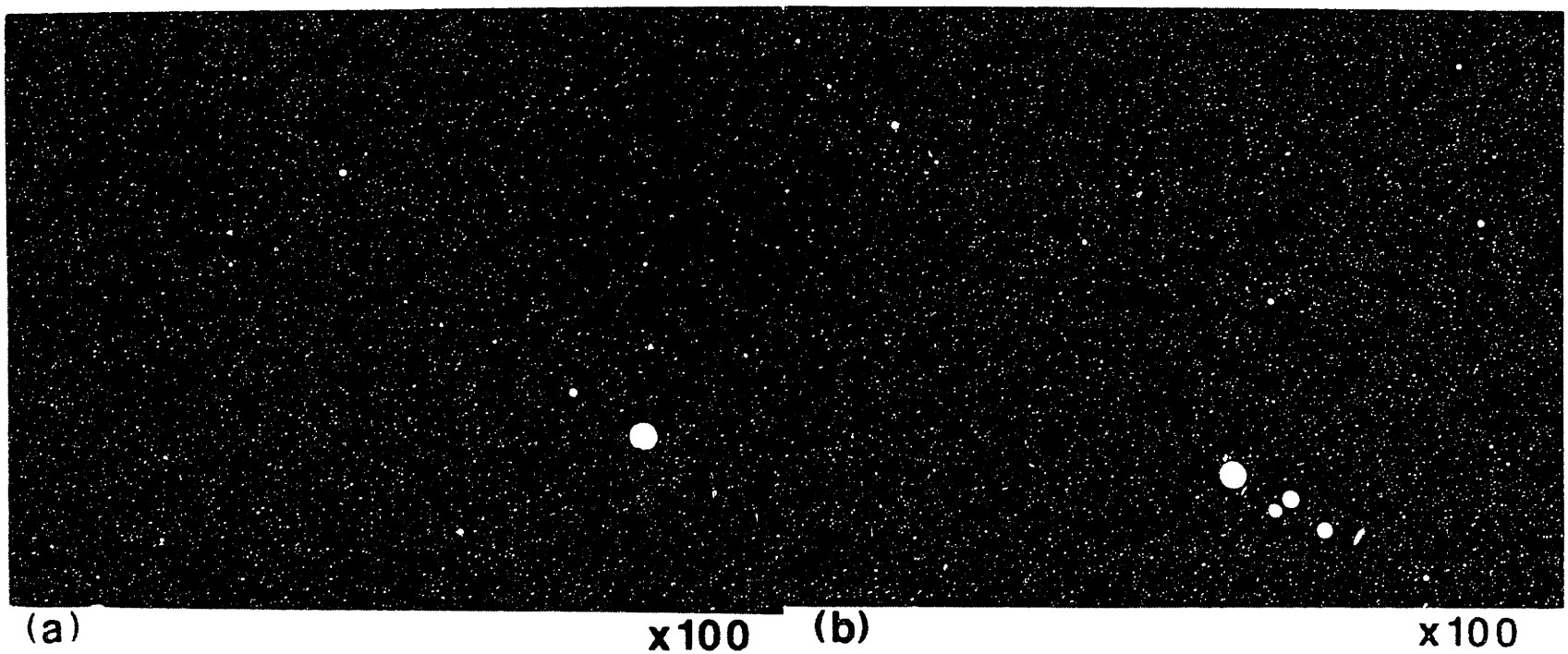

Figure 56: Shows microcrack-free and glassy slag structures.
(a) AX-HY-60 (b) AX-MS-60

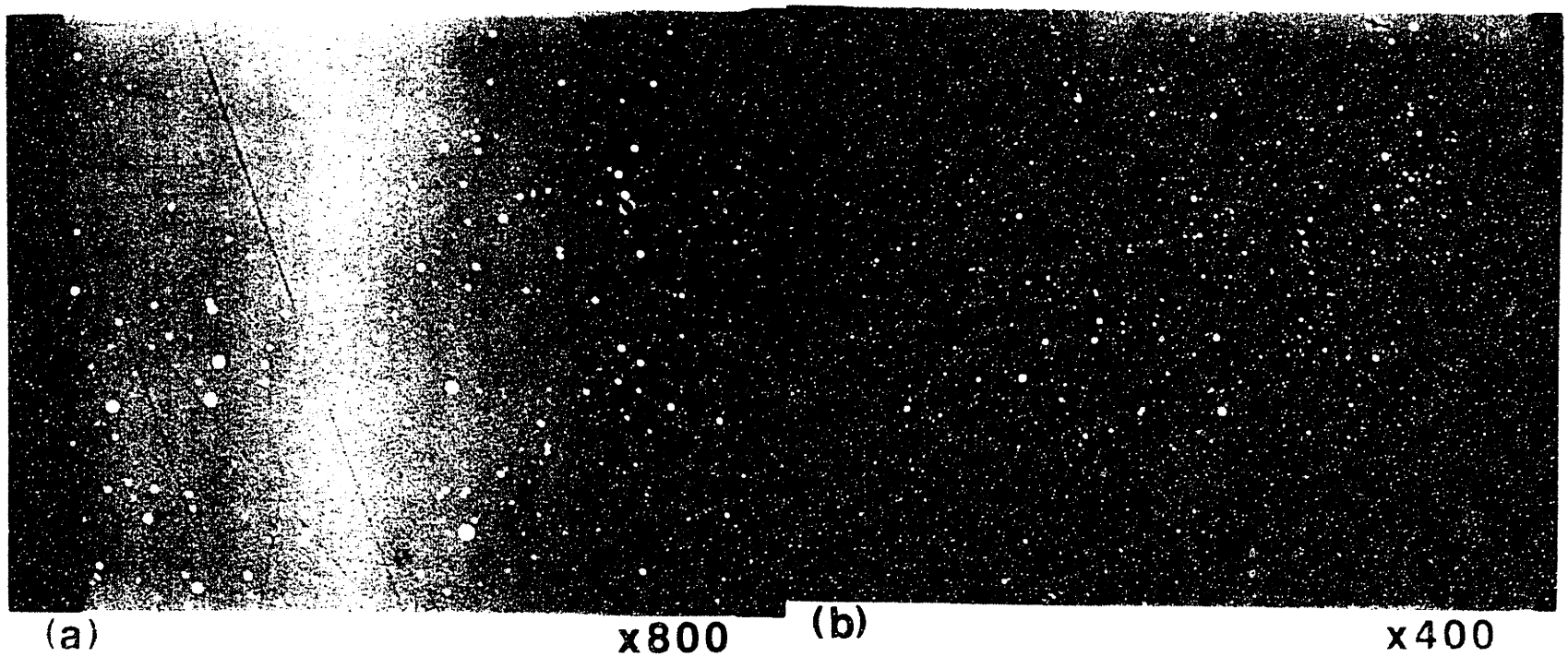

Figure 57: Shows microcrack-free and glassy slag structures.
(a) 309-HY-20 (b) AX-HY-761

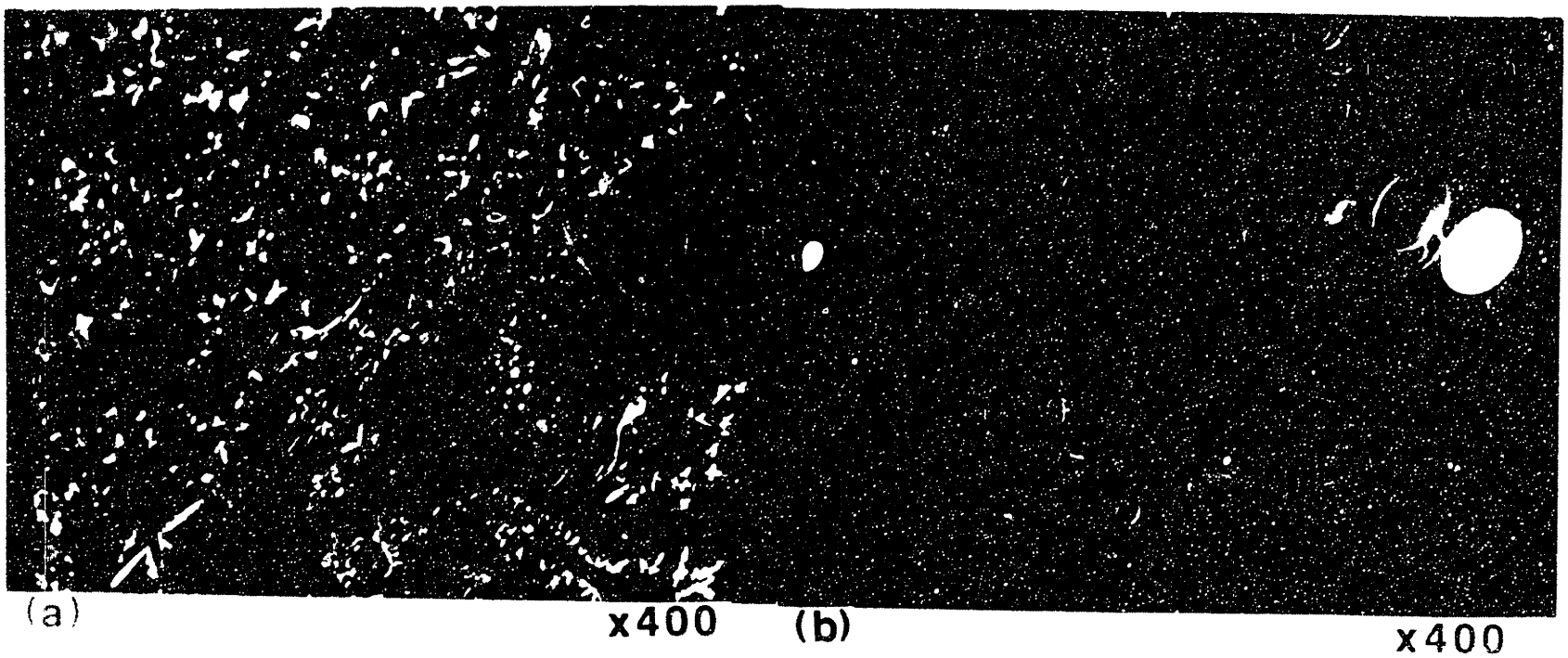

Figure 58: Shows slag structures with cracked matrix.
(a) 36-MS-880 (b) AX-HY-80

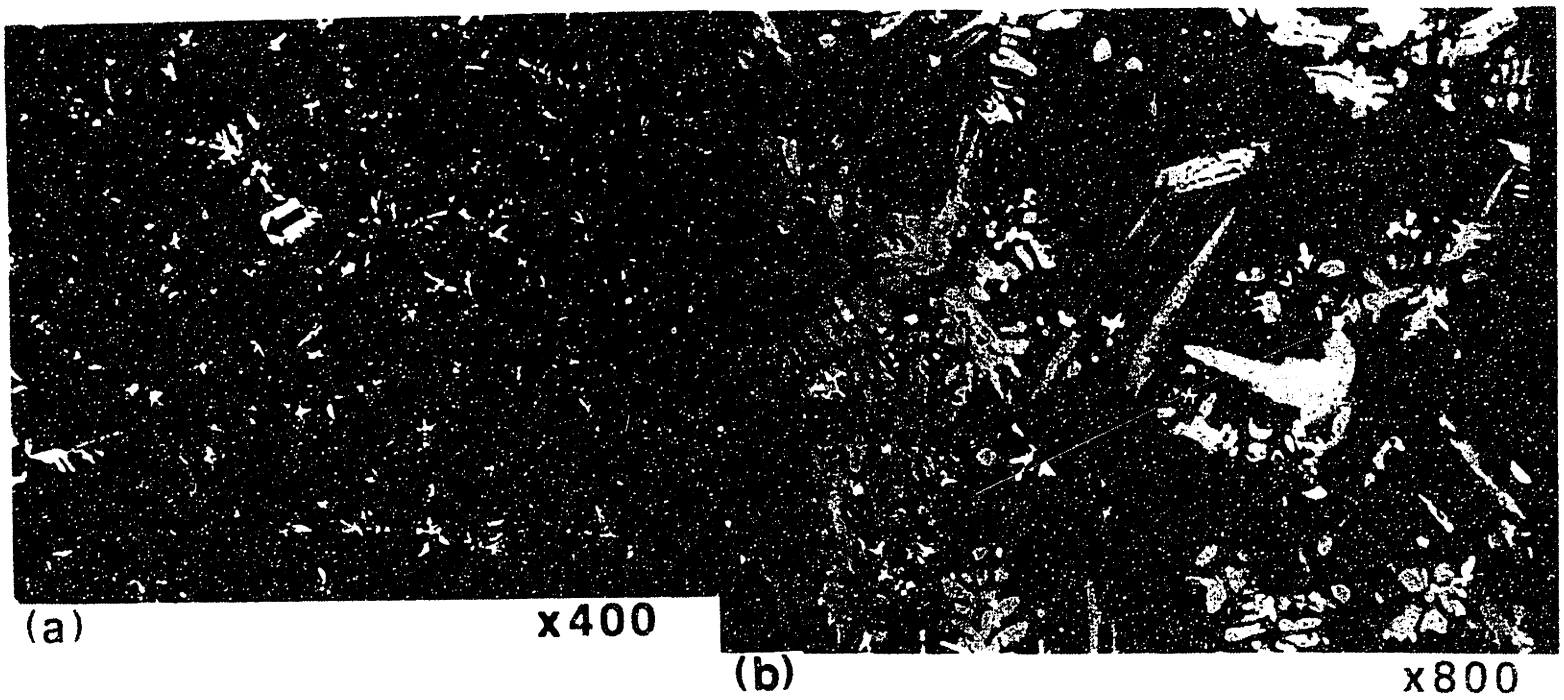

Figure 59: Shows slag structures with cracked matrix and phases.
(a) 40-IN-880 (b) 309-HY-880

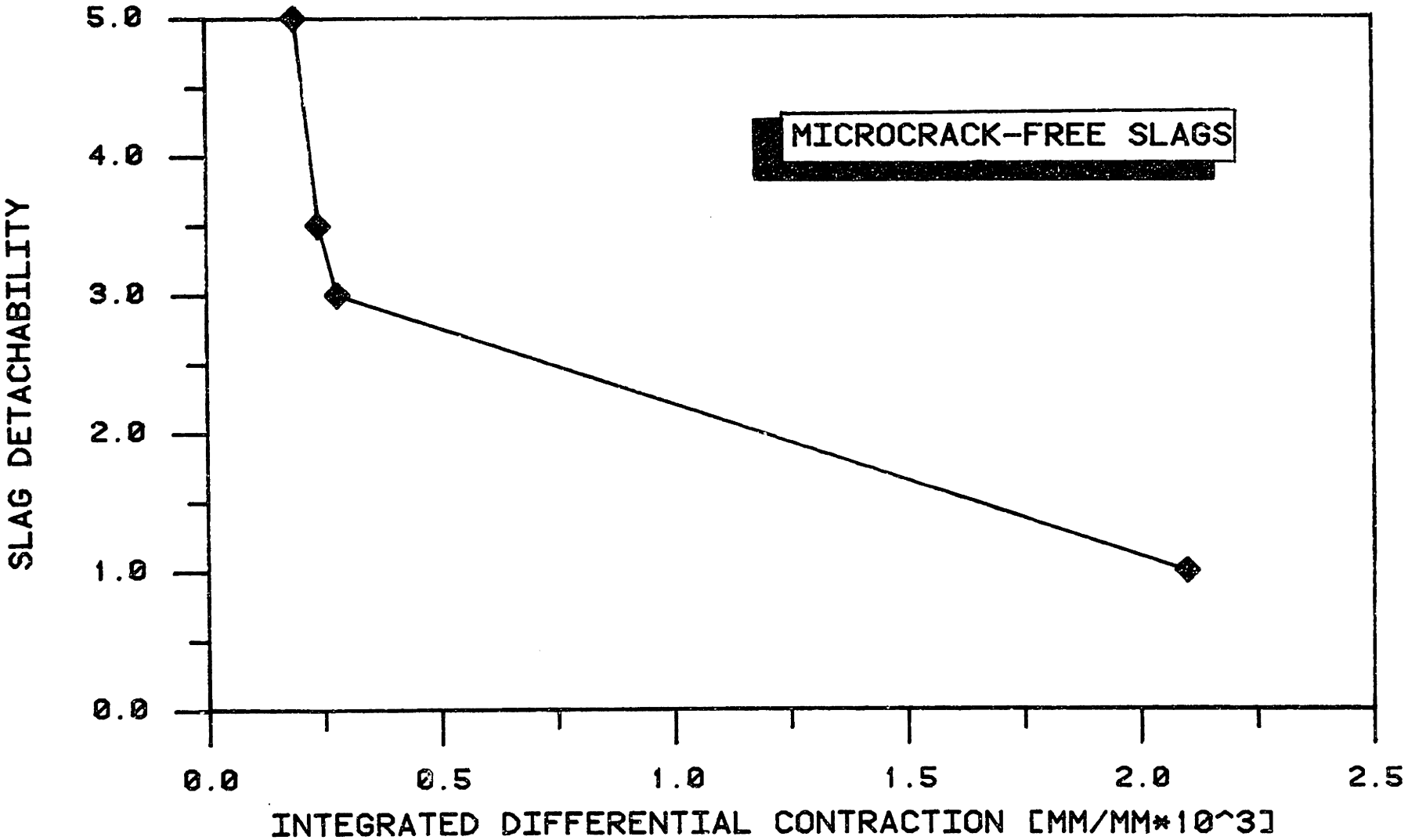

FIGURE 60: Shows an improvement in slag detachability as the integrated differential thermal contraction per unit length increases for slags without cracked microstructures.

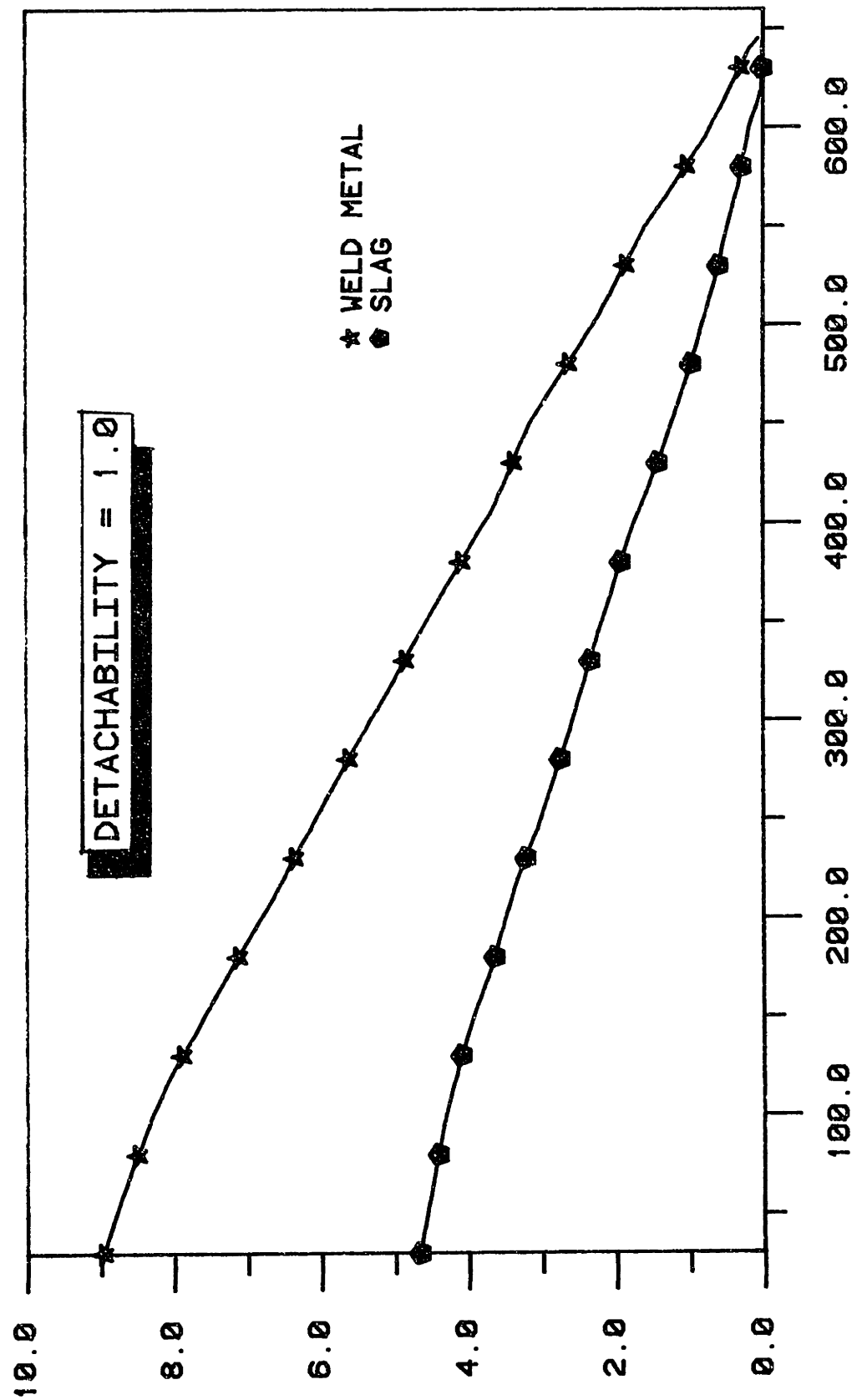

FIGURE 61: Shows integrated contraction per unit length of slag & weld metal from the softening temperature of slag to 30^{o}C for sample AX-HY-20.

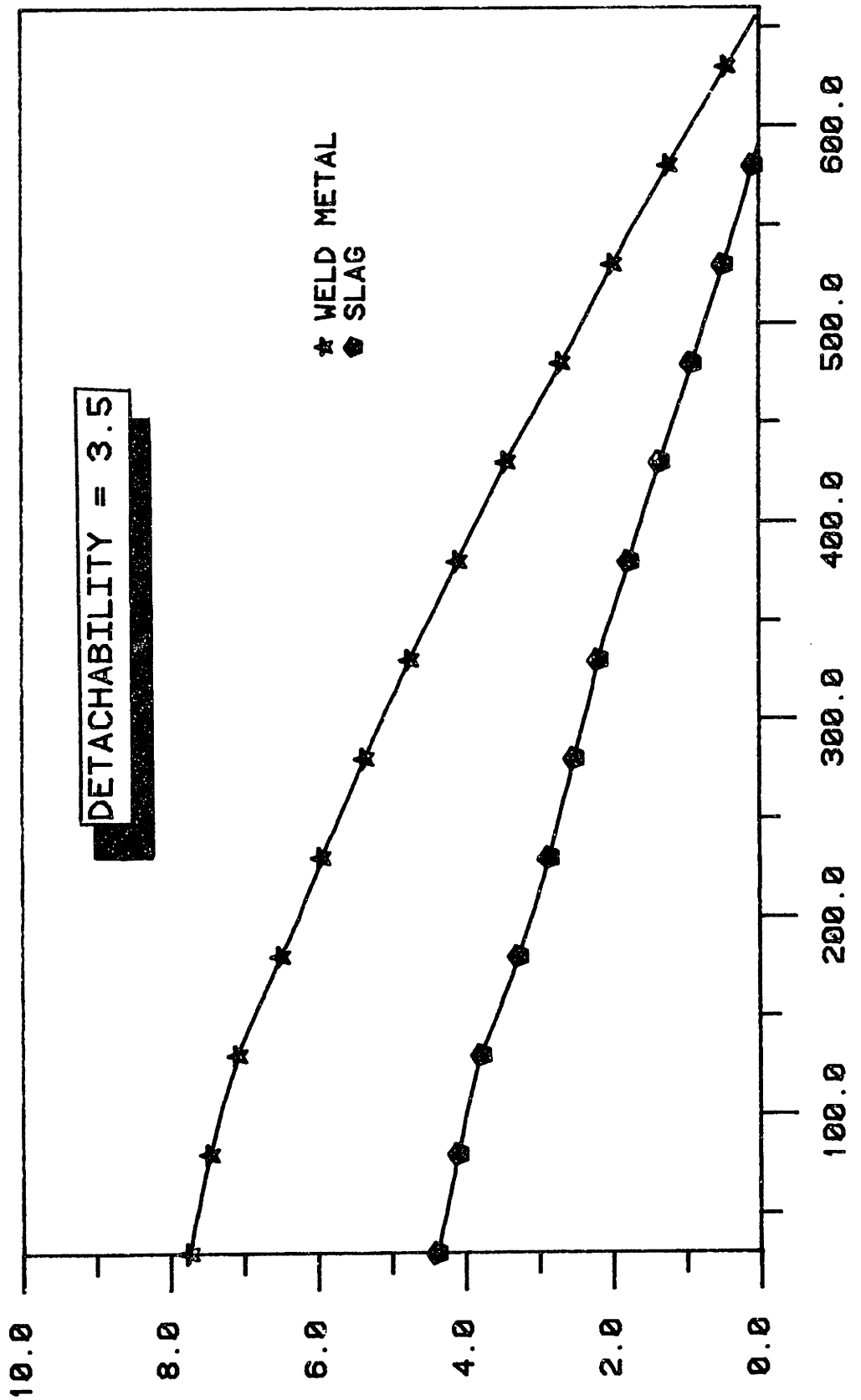

FIGURE 62: Shows integrated contraction per unit length of slag & weld metal from the softening temperature of slag to 30°C for sample 309-HY-20.

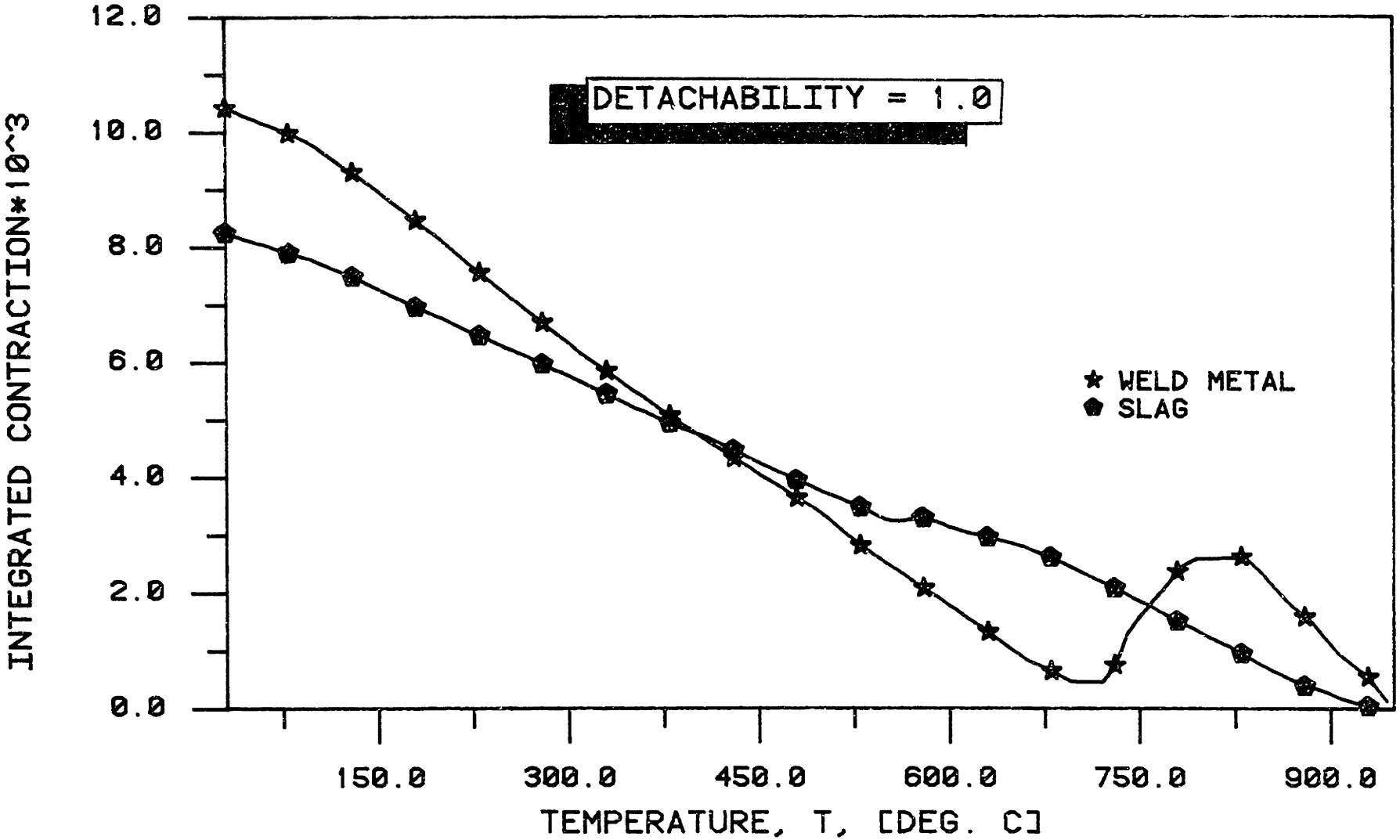

FIGURE 63: Shows integrated contraction per unit length of weld metal & slag from the softening temperature of slag to 30^{o}C for sample AX-HY-0091.

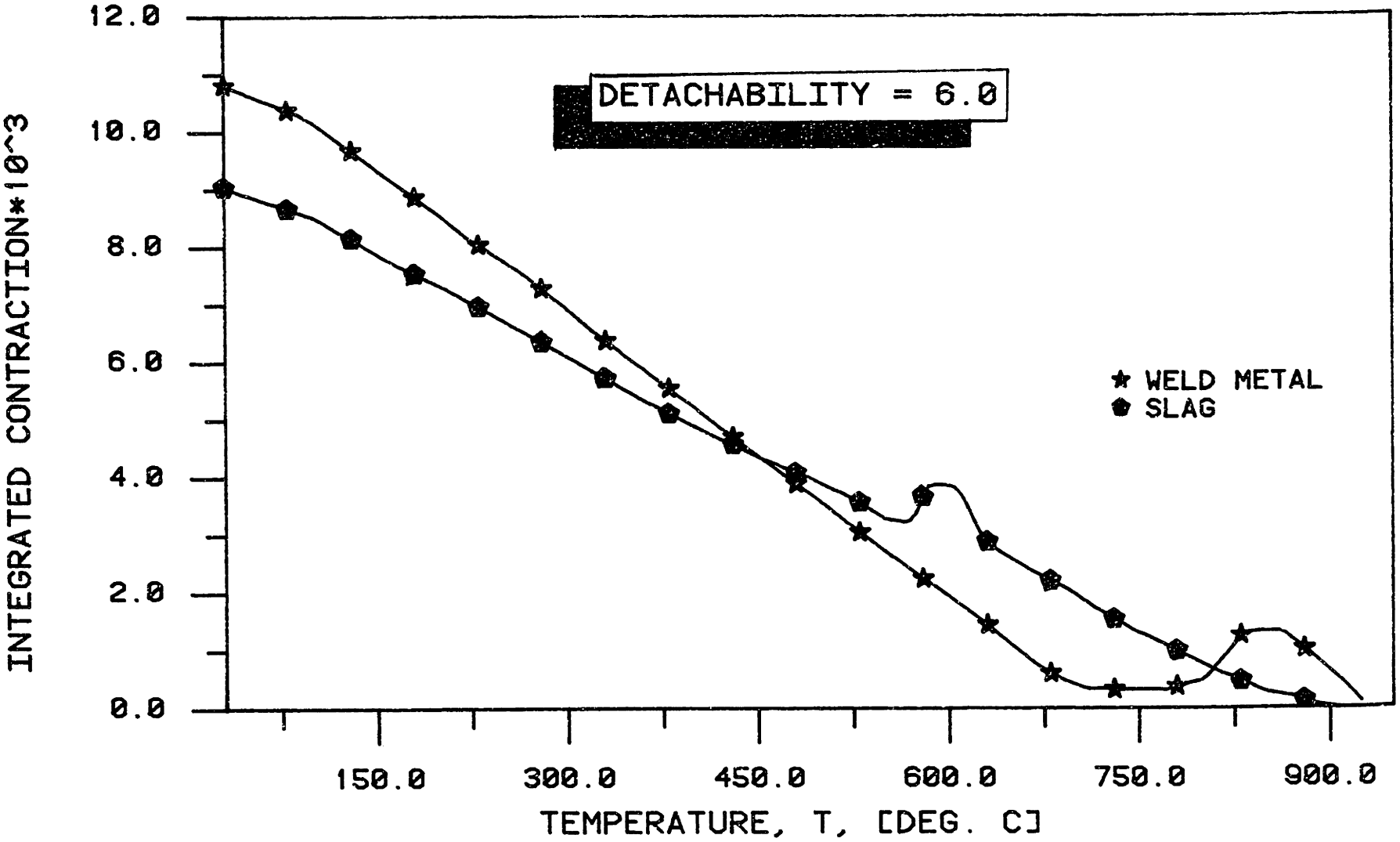

FIGURE 64: Shows integrated contraction per unit length of slag & weld metal from the softening temperature of slag to 30^{o}C for sample AX-IN-0091.

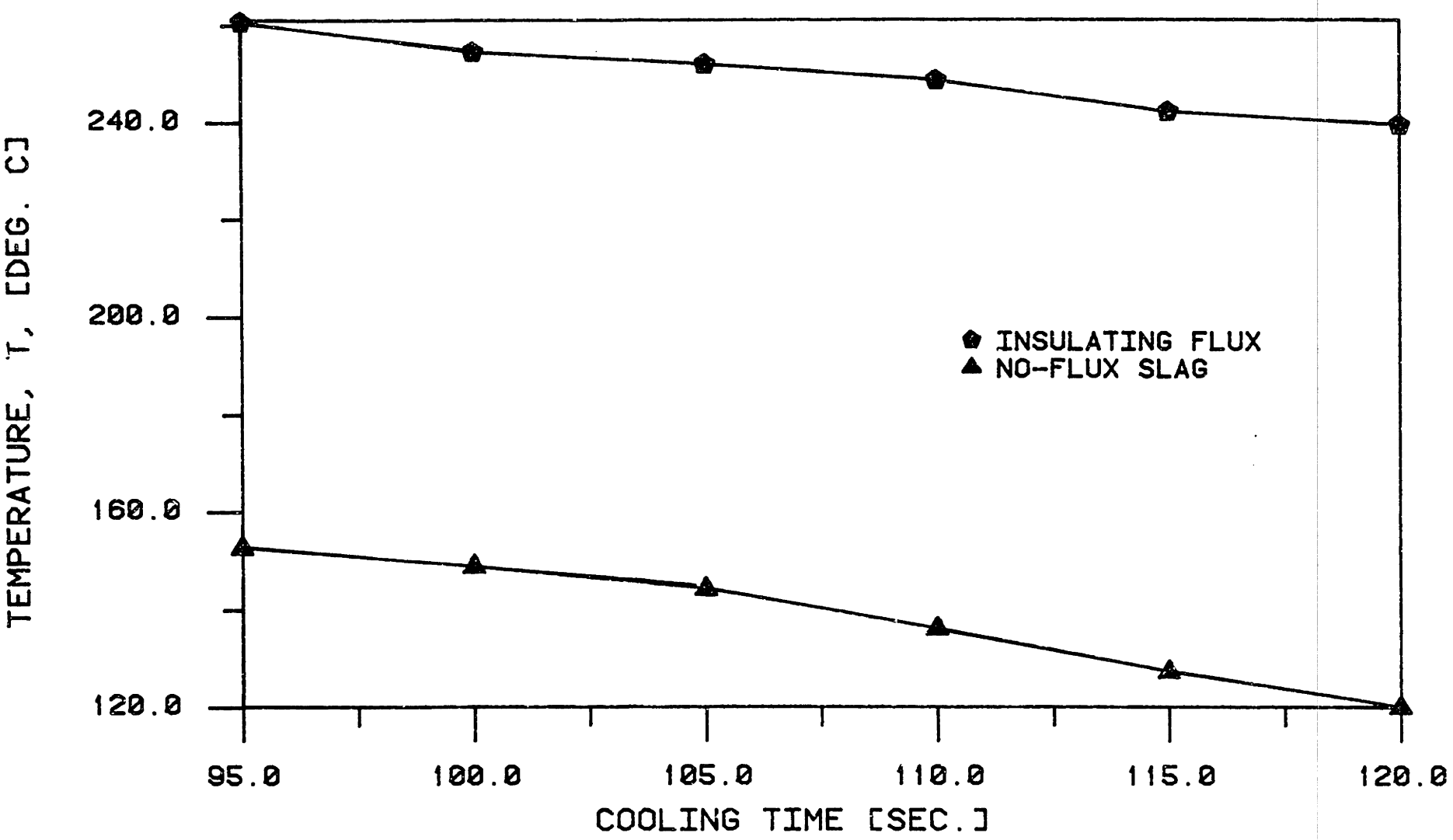

FIGURE 65: Shows the effect of an insulating flux cover on the temperature distributions in the slag layer.

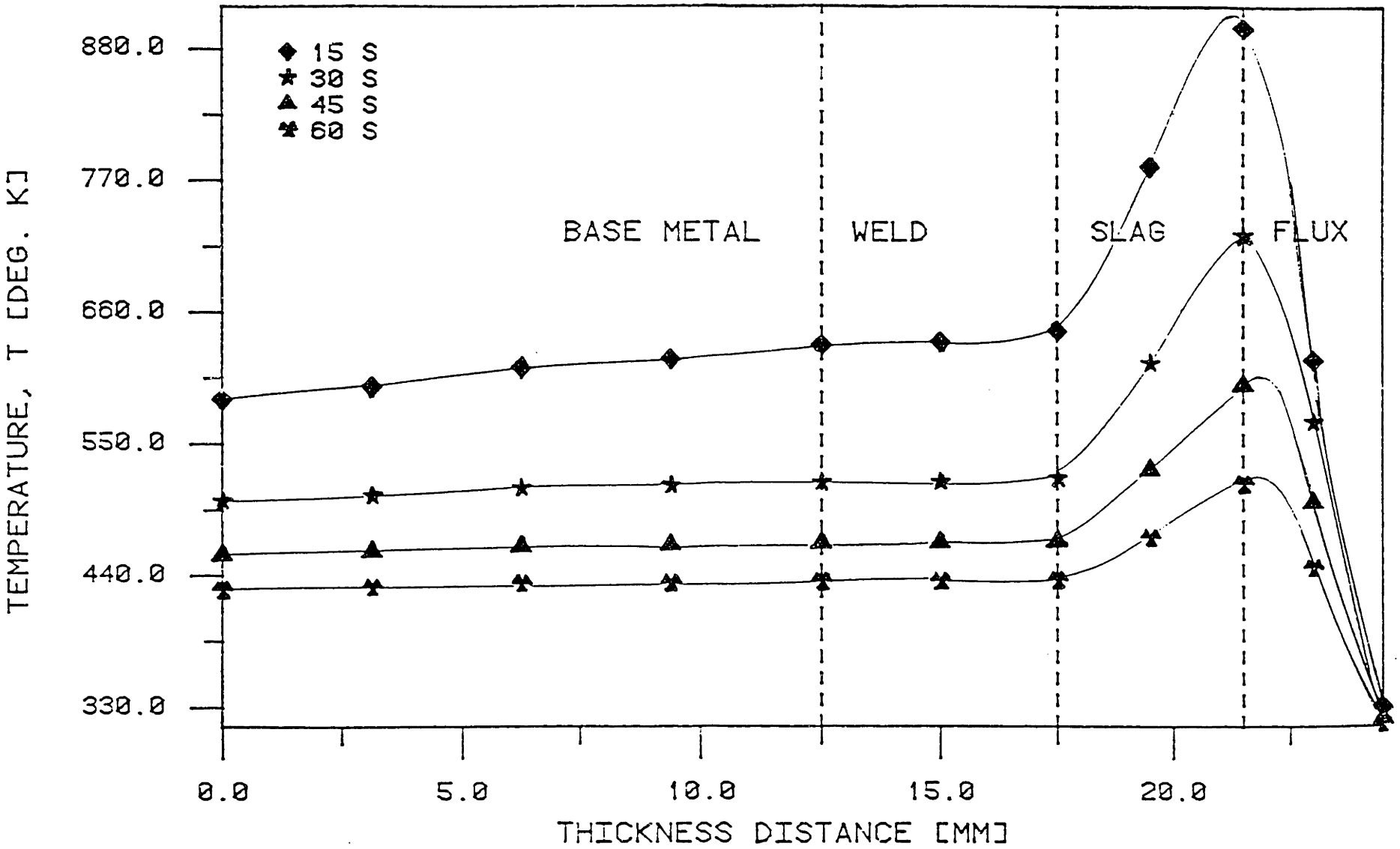

Figure 66: Shows the effect of thickness of slag on the temperature distribution in the slag-metal system.

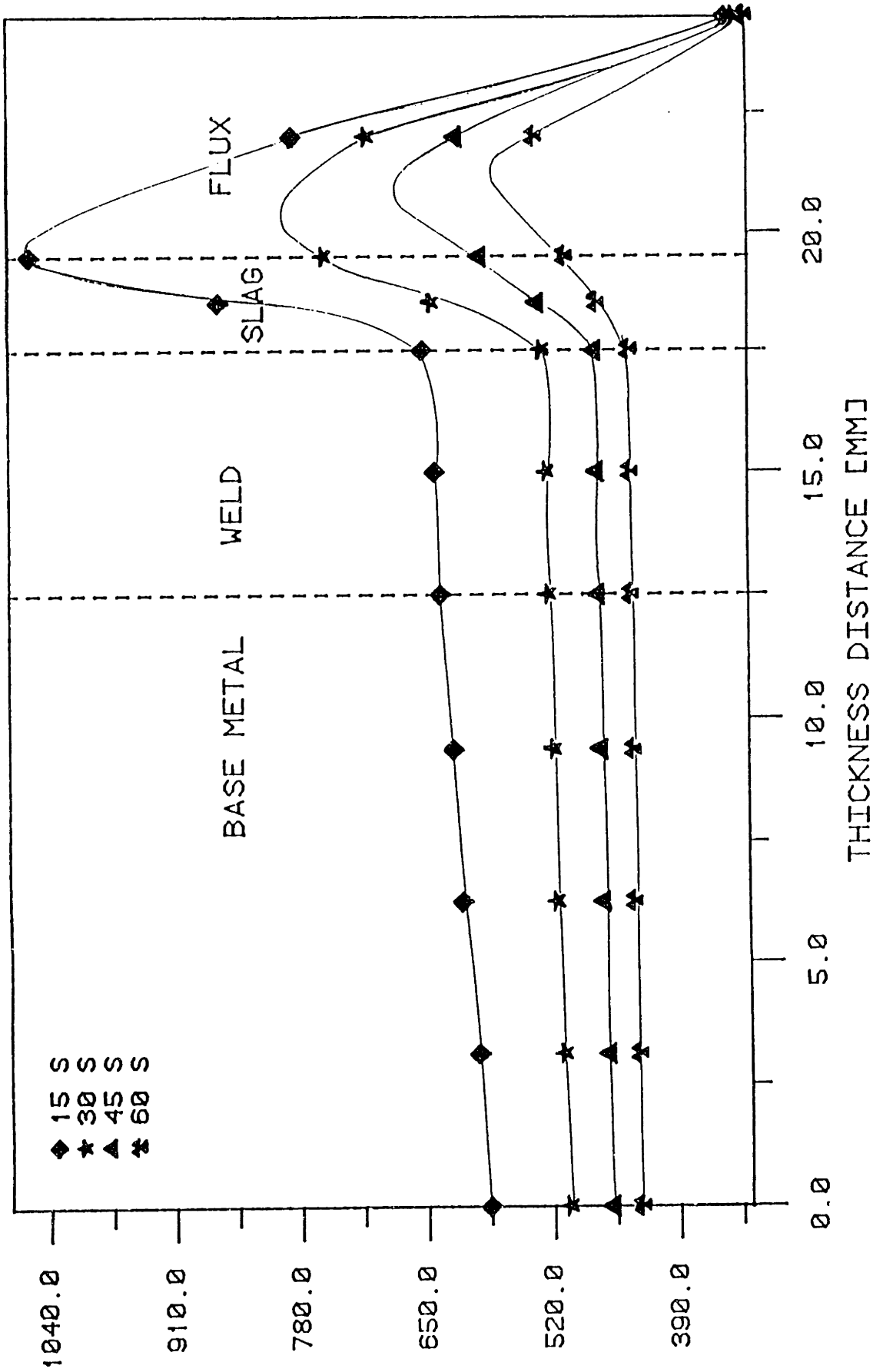

Figure 67: Shows the effect of thickness of slag on the temperature distribution in the slag-metal system.

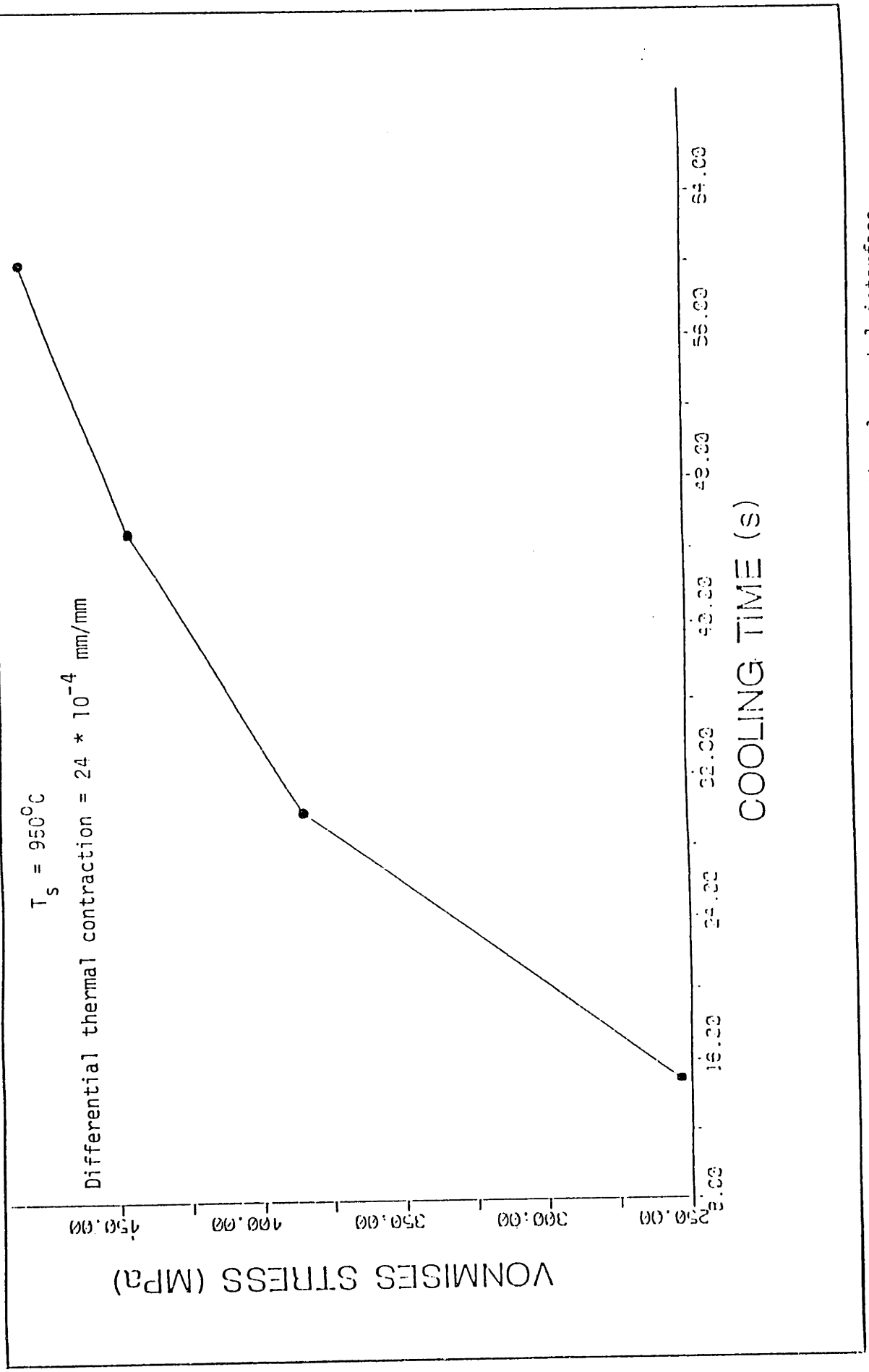

Figure 68: Transient effective residual stress at the slag-metal interface calculated by the finite element methods.

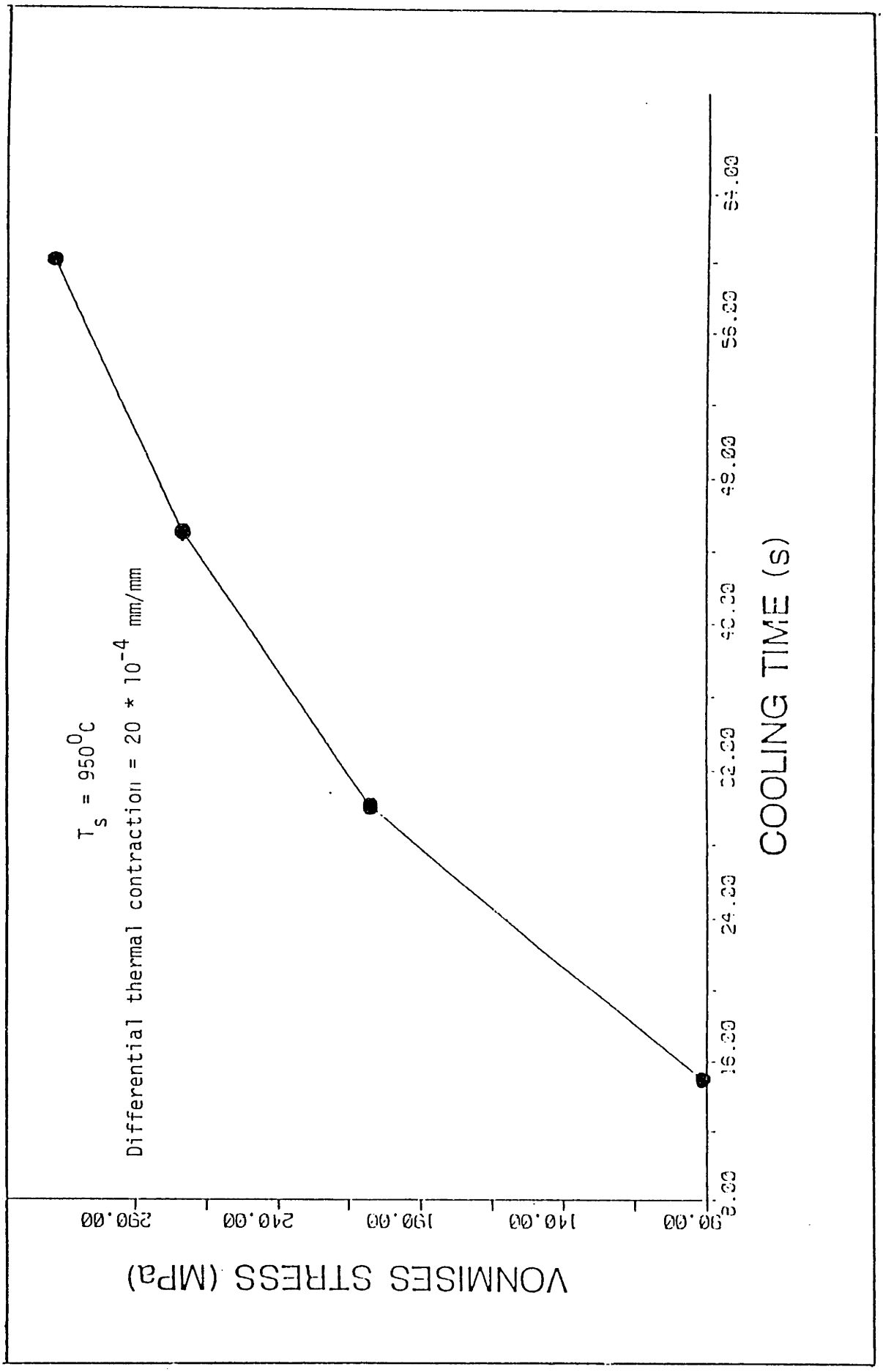

Figure 69: Transient effective residual stress at the slag-metal interface calculated by the finite element methods.

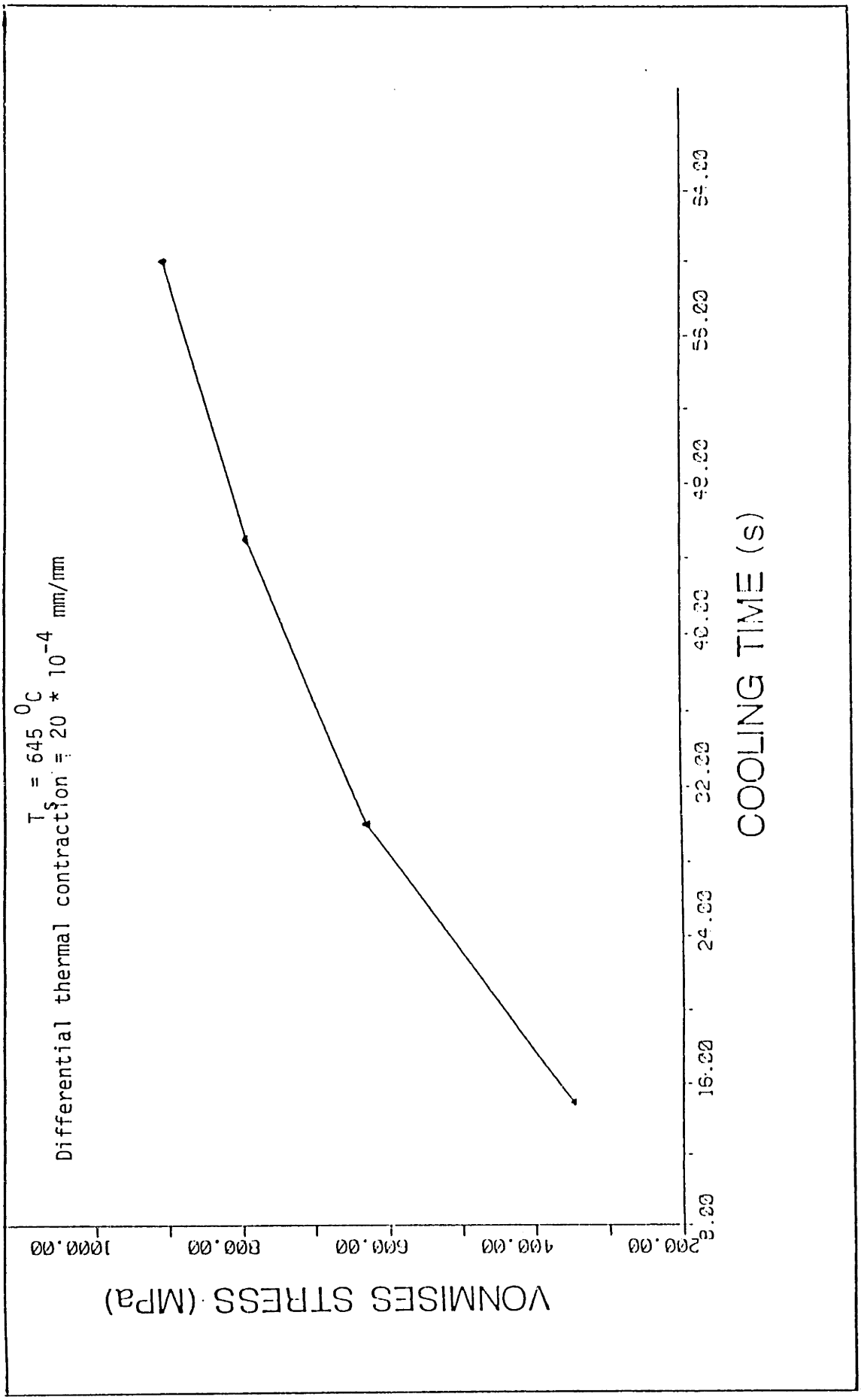

Figure 70: Transient effective residual stress at the slag-metal interface calculated by finite element methods.

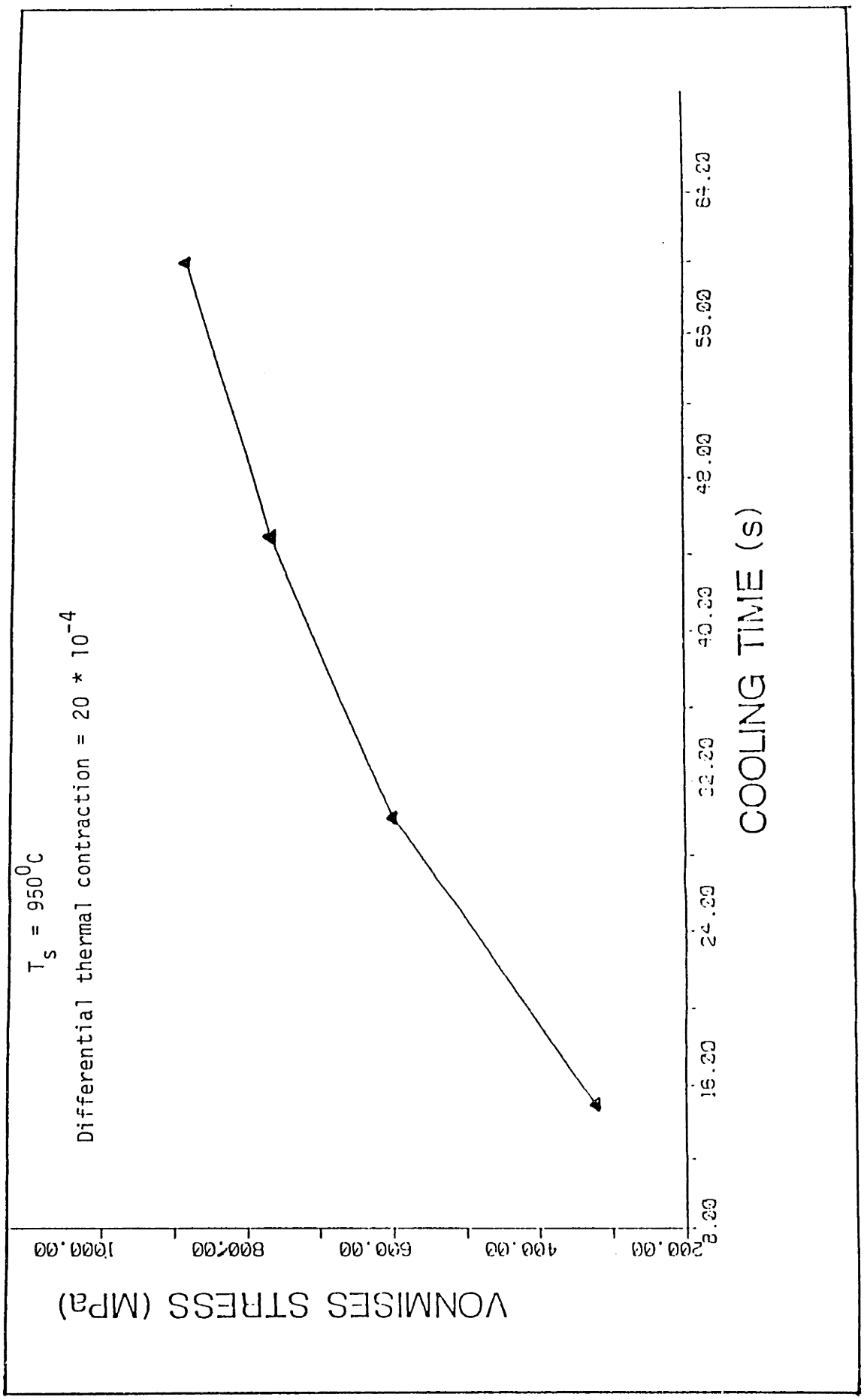

Figure 71: Transcient effective residual stress at the slag-metal interface calculated by finite element methods.

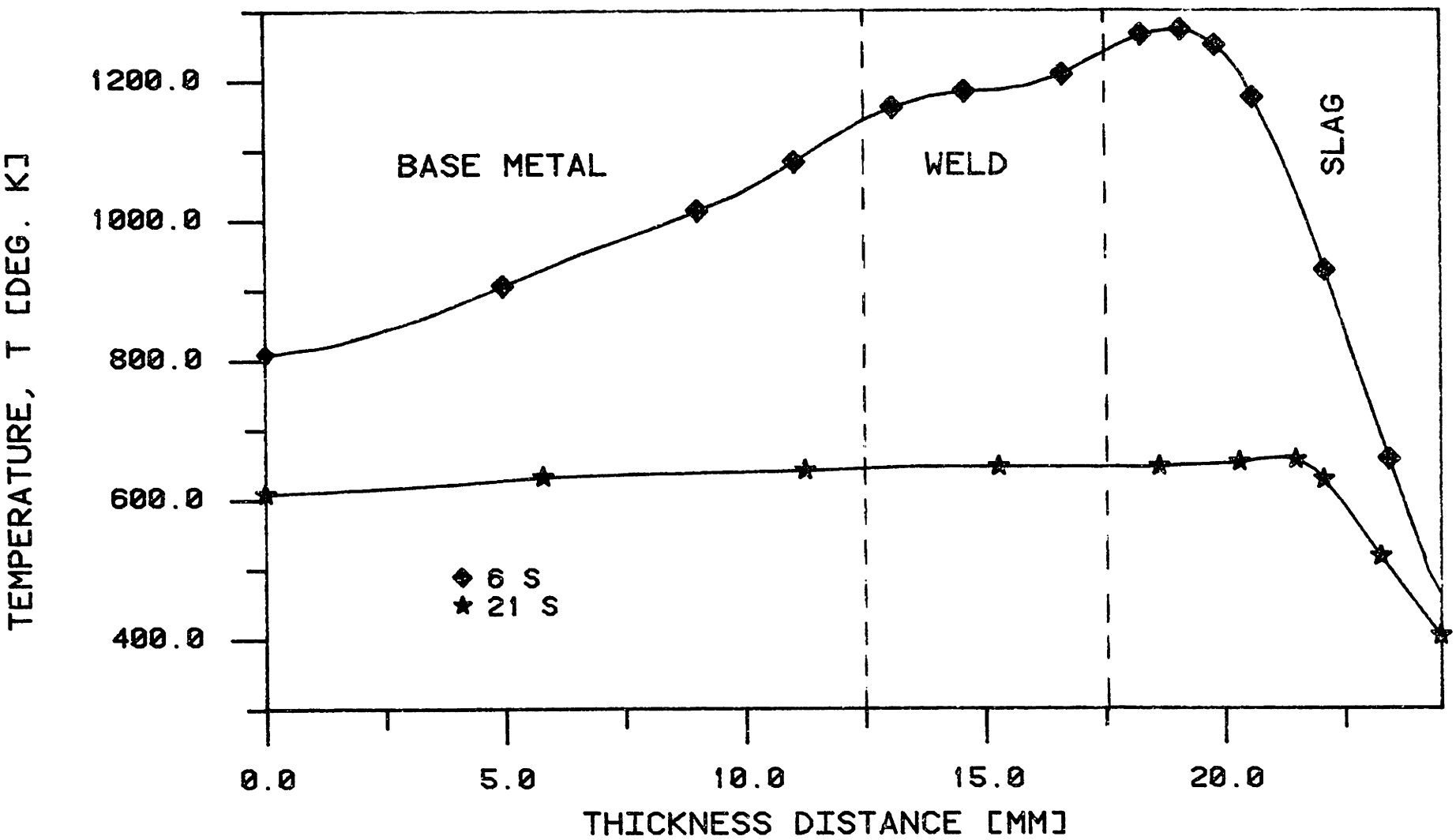

FIGURE 72: Shows temperature fields in a slag-metal system without an insulating flux cover. Notice the progression of the peak temperature with time into the slag layer.

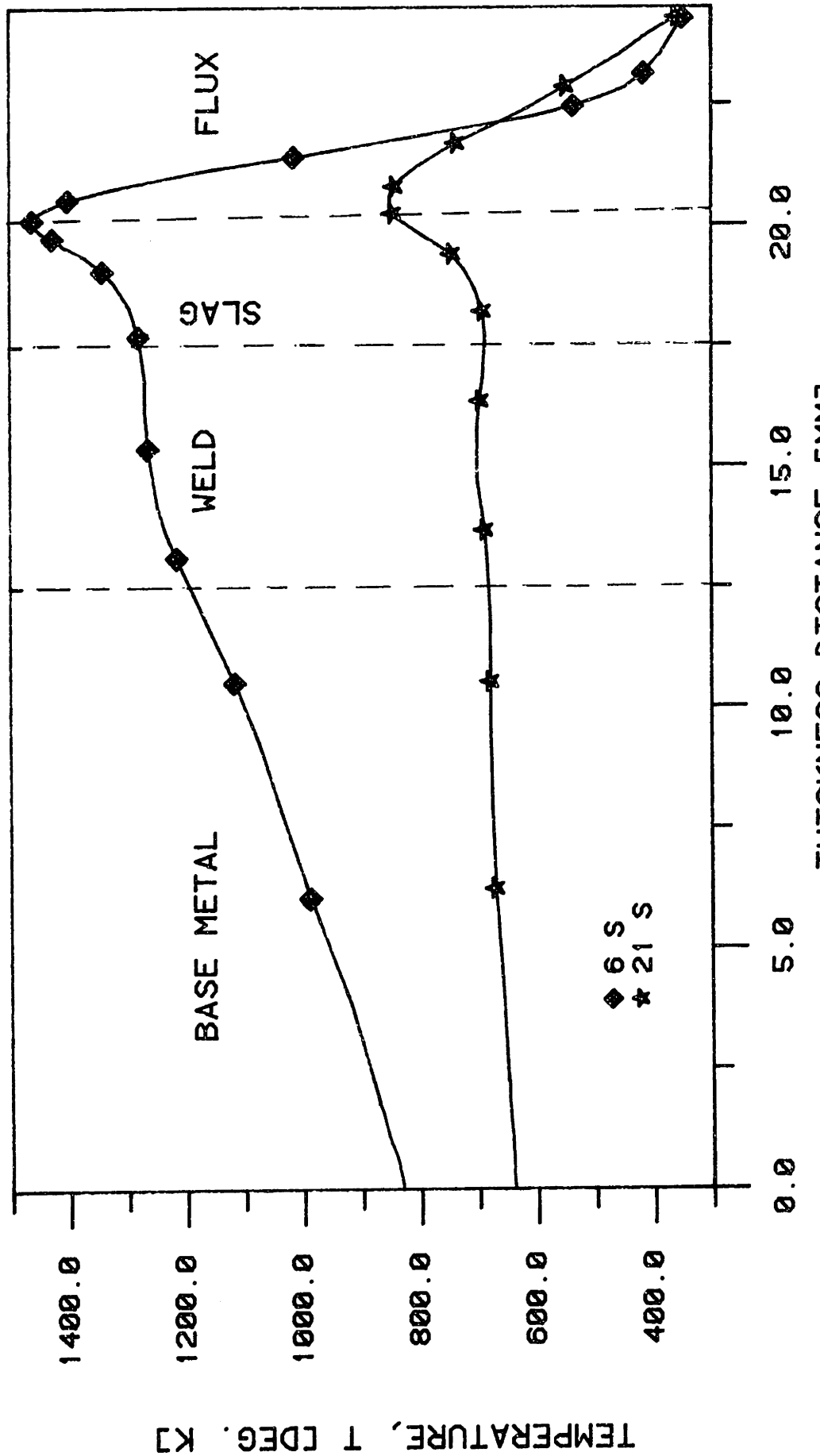

FIGURE 73: Shows temperature fields in a slag-metal system with an insulating flux cover. Notice the steep temperature gradient in the slag layer due to the flux cover.

APPENDIX 1

This appendix shows the scheme used to assess the degree of slag detachability for the welding fluxes used in this study. The scheme is simple and fairly reproducible.

ASSESSMENT OF*

SLAG DETACHABILITY

1. ...SLAG CAME OFF CLEAN AT THE TIPPING OF THE BASE METAL.

2. ...SLAG CAME OFF AT THE TIPPING OF THE BASE METAL BUT LEFT ADHERENT FLAKES IN THE HAZ OF THE WELD METAL.

3. ...AS IN (2) ABOVE BUT WITH ADHERENT FLAKES IN THE HAZ AND ON THE WELD METAL.

4. ...AS IN (3) ABOVE BUT WITH MANY FLAKES

5. ...SLAG CAME OFF IN A SINGLE LUMP AFTER 1 OR 2 BLOWS ON THE BACK OF THE BASE METAL.

6. ...SLAG CAME OFF IN SEVERAL LUMPS AFTER 1 OR 2 BLOWS ON THE BACK OF THE BASE METAL.

7. ...SLAG CAME OFF IN FRAGMENTS AFTER BEING CHISELLED AT ITS SIDES.

8. ...AS IN (7) ABOVE BUT WITH ADHERENT SLAG IN THE HAZ.

9. ...AS IN (7) ABOVE BUT WITH ADHERENT SLAG IN THE HAZ AND ON THE WELD METAL.

10. ...UNDETACHABLE SLAG.

* Assessment is cummulative. For instance, ranking 7 included all operations from 1 to 7.

APPENDIX 2

The X-ray diffraction conditions used are shown below. The choice of two different characteristic radiations was based on the chemical compositions of the slag and the need to minimize background fluorescence that might mask weak diffraction peaks.

DIFFRACTION CONDITIONS

CrKα Radiation

λ = 2.28962 A^0

Filter : Vanadium

Divergence slit : 3^0

CuKα Radiation

λ = 1.5405 A^0

Filter : Nickel

Divergence slit : 1^0

Tube Voltage : 35 KV

Current : 15 mA

Scale range : 5000

Time constant : 1 s

2θ rate : 2^0/min.

APPENDIX 3

The chemical compositions of the slag and weld metal as determined by neutron activation and x-ray fluorescence techniques are shown in this appendix.

Composition of Weld metal samples (wt.%) *

	C	Si	Mn	P	S	Cr	Ni	Mo	V	Al	Ti	Fe
AX-HY-880	.12	.37	.67	.016	.003	.99	2.52	.40	—	—	—	bal
AX-MS-880	.092	.21	.52	.026	.024	.11	.33	.09	—	.032	—	bal
309 -HY-20	.080	.87	.46	.012	.009	10.2	7.0	.22	.02	.036	—	bal
AX-IN-0091	.025	.38	.72	.017	.005	15.4	60.	.34	.05	.11	.18	30.
AX-IN-60	.062	.46	.80	.015	.005	12.0	50.	.38	.04	.034	.08	40.
40-IN-880	.087	.32	.73	.018	.005	15.0	55.	.30	.05	.13	.19	25.
40-IN-80	.068	.39	.99	.019	.005	15.5	60.	.30	.05	.13	.20	22.
40-IN-20	.058	.76	.66	.018	.006	9.2	50.	.35	.04	.012	.02	35.
36-MS-761	.095	.47	1.34	.025	.029	.099	.097	.02	—	.01	—	bal
36-MS-0091	.095	.19	.77	.018	.023	.10	.09	.03	—	—	—	bal

* Analysis performed by Arnold Greene Testing Laboratories using ICAP spectrometer.

Composition of Weld metal samples (wt.%).*

	C	Si	Mn	P	S	Cr	Ni	Mo	V	Al	Ti	Fe
36-MS-60	.079	.40	1.15	.020	.026	.06	.09	.02	—	—	—	bal
36-MS-20	.077	.56	.48	.021	.030	.12	.24	.02	—	—	—	bal
40-MS-80	.10	.32	.84	.015	.034	.09	.09	.17	—	—	—	bal
36-MS-80	.10	.17	.50	.023	.030	.10	.11	.04	—	—	—	bal
AX-MS-761	.081	.60	1.42	.022	.023	.10	.80	.17	—	—	—	bal
AX-HY-761	.091	.82	1.71	.010	.004	.74	2.20	.25	—	—	—	bal
AX-MS-0091	.090	.27	.54	.015	.021	.09	.84	.17	.01	—	—	bal
AX-HY-0091	.10	.45	.59	.013	.004	.93	2.52	.38	.01	—	—	bal
AX-MS-60	.071	.62	1.33	.021	.020	.10	1.19	.26	—	—	—	bal
309 -HYS-20	.031	.47	.20	.013	.009	11.0	8.7	.18	.03	.040	.01	bal

* Analysis performed by Arnold Greene Testing Laboratories using ICAP spectrometer.

Composition of Weld metal samples (wt.%).*

	C	Si	Mn	P	S	Cr	Ni	Mo	V	Al	Ti	Fe
AX-HY-0091	.060	.07	.10	.016	.007	.40	3.44	.49	—	—	—	bal
309 -HY-880	.12	.40	.33	.023	.005	1.69	2.65	.33	—	.030	—	bal
36-HY-60	.14	.33	.66	.025	.008	1.80	.22	.41	.01	.083	—	bal
309 -HYS-880	.076	.55	1.21	.022	.006	.73	1.43	.19	—	.038	—	bal
AX-HY-80	.11	.50	.73	.015	.004	1.22	2.58	.35	—	.015	—	bal
AX-HY-60	.091	.56	1.18	.025	.005	.86	2.51	.38	—	—	—	bal
AX-HYS-60	.062	.14	.28	.023	.005	.47	3.19	.43	—	—	—	bal
AX-HY-CR	.13	.30	.34	.016	.005	1.62	2.55	.30	—	.019	—	bal

* Analysis performed by Arnold Greene Testing Laboratories using ICAP spectrometer.

Composition of Welding Slags (wt.%) *

	MgO	CaO	CaF_2	SiO_2	Al_2O_3	FeO	TiO_2	MnO	K_2O	Na_2O	P_2O_5	ZrO_2	Cr_2O_3
AX-HY-60	0.10	-	6.89	41.80	3.73	5.72	0.29	33.85	0.68	0.14	0.27	-	0.40
AX-HYS-60	-	-	6.58	39.65	3.75	12.43	0.40	34.89	0.70	0.14	0.33	-	0.97
AX-HY-20	8.56	20.79	6.77	52.09	3.05	3.42	0.30	1.81	0.13	-	0.16	-	0.20
AX-HY-0091	0.47	24.50	20.49	30.32	3.55	1.14	3.71	2.37	0.11	3.50	0.16	-	0.05
AX-HY-80	11.54	16.68	8.69	35.72	14.20	2.60	0.55	6.78	0.10	0.10	0.16	-	0.18
AX-HY-880	25.40	1.33	19.57	17.11	21.16	2.03	0.14	0.89	-	1.24	0.26	9.35	0.09
36-MS-0091	0.61	26.22	18.94	31.27	3.58	1.44	4.02	0.63	0.10	3.97	0.16	-	0.02
AX-MS-761	19.49	-	3.97	40.46	1.84	6.28	1.43	18.09	0.25	2.22	0.20	-	0.06
AX-IN-20	8.48	20.54	6.77	49.77	3.52	3.09	0.66	1.52	0.12	0.13	0.16	-	2.42
AX-IN-0091	0.80	24.34	20.51	32.21	3.78	1.57	4.13	0.55	-	3.59	0.16	-	0.72
AX-HY-Cr	7.85	11.63	5.59	35.71	9.71	6.19	0.40	5.54	0.14	3.19	0.16	-	12.38
AX-IN-880	24.80	1.12	21.19	17.20	20.69	2.61	0.14	0.99	-	1.86	0.16	8.97	3.01

* Analysis performed at the University of Toronto, Canada using X-ray fluorescence and Neutron activation methods.

Composition of Welding Slags (wt.%)*

	MgO	CaO	CaF_2	SiO_2	Al_2O_3	FeO	TiO_2	MnO	K_2O	Na_2O	P_2O_5	ZrO_2	Cr_2O_3
AX-IN-60	0.50	-	6.89	40.65	3.75	6.23	0.32	33.91	0.54	0.16	0.27	-	3.20
AX-HYS-880	18.62	1.93	14.61	13.80	17.03	21.09	0.14	1.93	-	1.15	0.23	5.52	1.68
AX-HY-Ti8	9.35	14.00	7.14	28.47	11.78	2.03	16.31	4.85	0.12	0.20	0.18	-	0.16
AX-MS-80	11.35	16.61	8.69	34.98	14.08	3.45	0.71	6.91	-	0.30	-	-	-
309-HY-880	21.04	1.41	20.09	18.99	20.34	1.54	0.42	5.43	0.10	1.58	0.17	7.01	1.50
309-HYS-880	16.34	1.31	18.56	12.16	13.54	30.36	0.18	1.68	-	1.12	0.23	3.48	1.94
309-HY-20	7.69	18.34	6.83	47.28	2.78	5.08	0.33	1.68	0.10	0.34	0.18	-	1.15
309-HYS-20	8.77	21.74	5.90	51.05	2.90	2.63	0.30	1.74	0.12	-	0.16	-	2.68
309-HY-60	-	-	7.20	39.70	3.71	3.28	0.31	32.53	0.68	-	0.25	-	5.82
309-HY-761	19.71	-	4.23	38.78	1.81	6.41	1.51	17.62	0.25	2.22	0.20	-	5.61
309-HY-0091	1.00	22.30	25.81	29.73	3.86	0.78	4.36	0.84	-	4.45	-	-	1.43
309-HY-80	11.36	15.73	8.85	34.73	14.09	1.49	0.56	6.59	-	-	-	-	2.24

* Analysis performed at the University of Toronto, Canada using X-ray fluorescence and Neutron activation methods.

Composition of Welding Slags (wt.%)*

	MgO	CaO	CaF_2	SiO_2	Al_2O_3	FeO	TiO_2	MnO	K_2O	Na_2O	P_2O_5	ZrO_2	Cr_2O_3
309-MS-761	21.35	-	4.06	41.04	1.93	2.82	1.66	18.18	0.28	2.64	-	-	4.59
309-MS-0091	0.64	28.63	19.25	30.48	3.42	0.64	4.74	0.94	-	4.5	-	-	1.56
309-MS-80	11.39	13.07	10.95	34.27	14.10	1.29	0.57	6.68	-	0.30	-	-	2.98
36-HY-761	20.01	-	4.07	41.16	1.84	4.90	1.46	18.33	0.27	2.16	0.20	-	0.17
36-MS-Ti6	-	-	6.51	40.21	2.15	1.48	18.92	34.97	0.71	0.21	0.23	-	-
36-MS-CF6	-	-	21.59	36.39	3.74	1.81	0.29	29.55	0.36	0.15	0.15	-	0.17
36-MS-880	21.56	2.1	21.81	14.13	19.41	6.20	0.28	1.26	-	1.35	0.36	9.44	-
36-HY-0091	0.48	28.71	20.49	29.94	3.34	1.53	4.58	0.69	-	4.27	-	-	-
36-MS-60	-	-	8.31	43.16	3.70	2.45	0.26	34.91	-	0.14	0.21	-	-
36-MS-80	11.41	16.61	7.76	34.85	14.26	3.10	0.53	6.92	0.14	-	0.18	-	0.04
36-MS-Ti8	9.37	15.85	6.83	28.90	11.29	1.90	16.45	5.10	0.13	0.52	0.15	-	0.90
36-IN-CF6	0.16	-	21.55	36.44	3.83	1.80	0.61	29.06	0.33	0.18	0.17	-	1.24

* Analysis performed at the University of Toronto, Canada using X-ray fluorescence and Neutron activation methods.

APPENDIX 4

The equilibrium ternary phase diagrams in this appendix are taken from references 38 and 39. They show the melting temperatures of the primary phases and their solidification paths.

(Ref. 38)

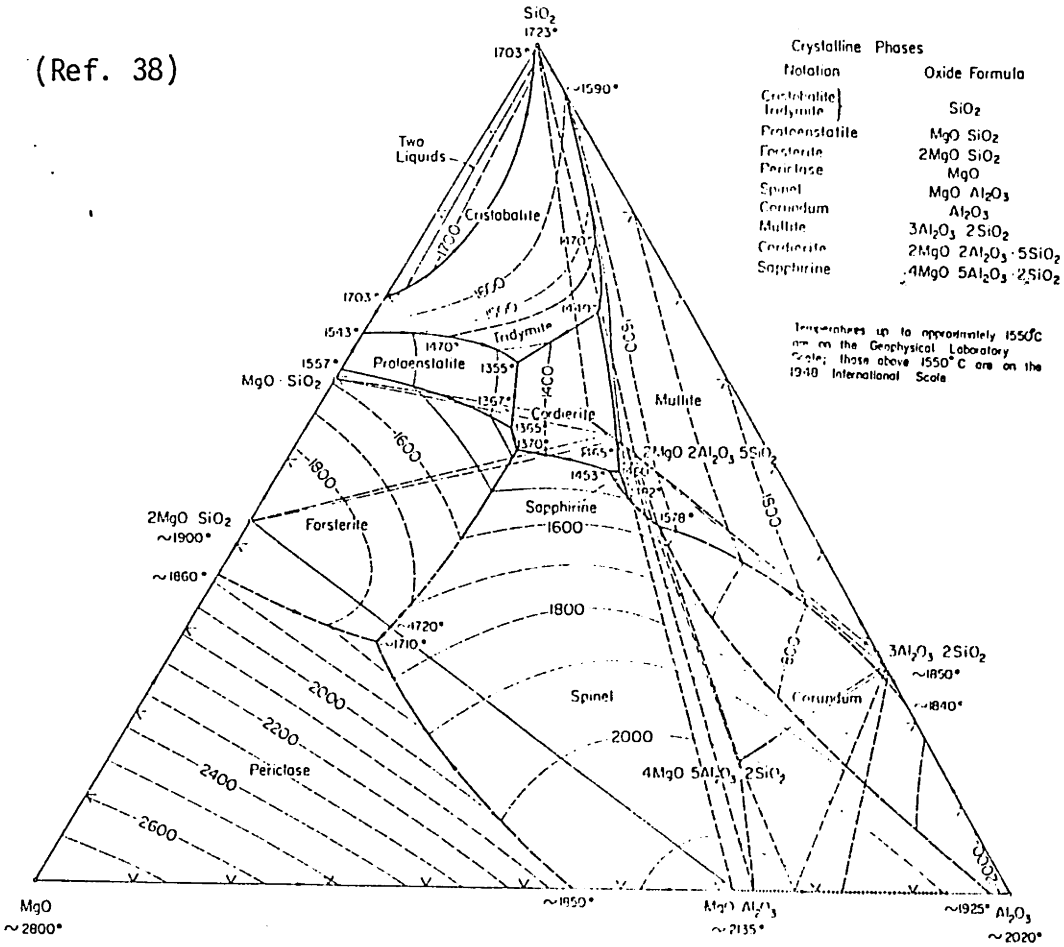

FIG. 712.—System MgO-Al_2O_3-SiO_2; composite.

E. F. Osborn and Arnulf Muan, revised and redrawn "Phase Equilibrium Diagrams of Oxide Systems," Plate 3, published by the American Ceramic Society and the Edward Orton, Jr., Ceramic Foundation, 1960.

CaO–SiO_2–TiO_2

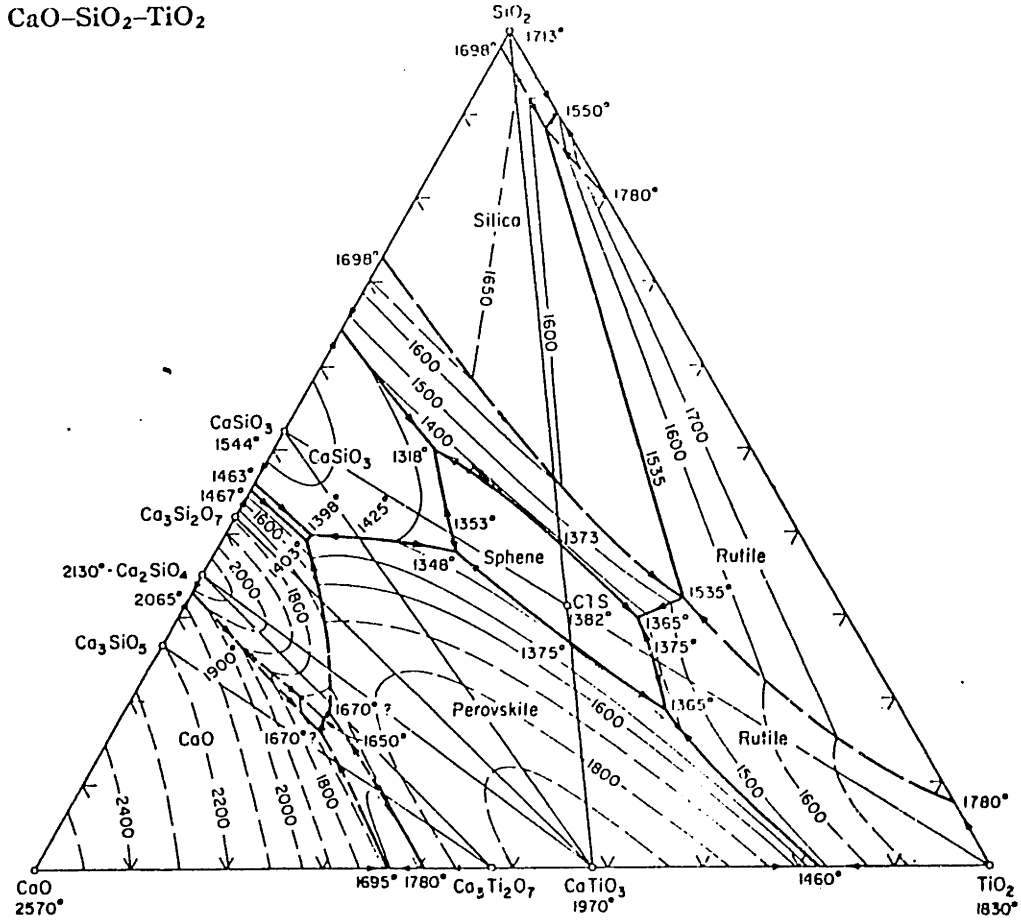

FIG. 660.—System CaO-SiO_2-TiO_2.

——two liquid boundary.

Fe_3O_4–Cr_2O_3–SiO_2

(Ref. 38)

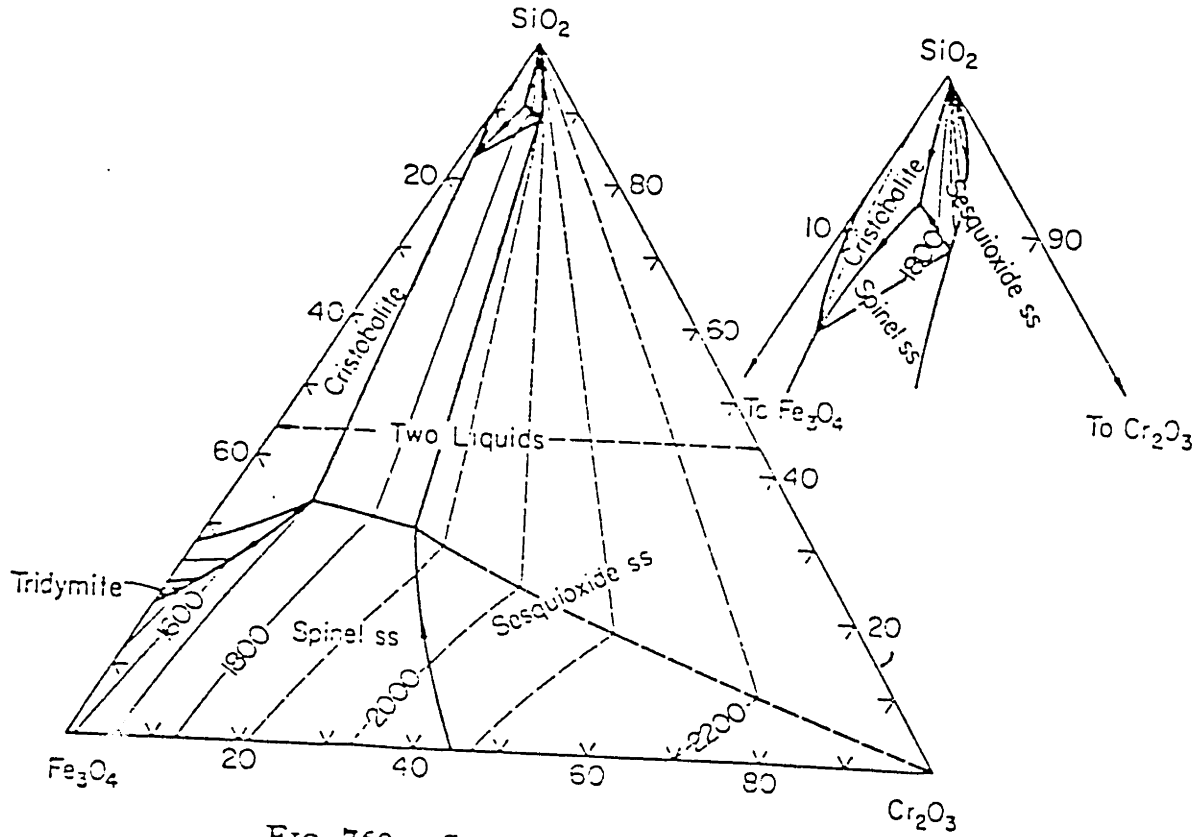

FIG. 760.—System Fe_3O_4–Cr_2O_3–SiO_2 in air.

Arnulf Muan and Shigeyuki Sōmiya, *J. Am. Ceram. Soc.*, 43 [10] 533 (1960).

These diagrams taken from reference 39 show that at a 50:50 mixture of MgO and Al_2O_3, the stable compound is the spinel because it has the lowest free energy of formation.

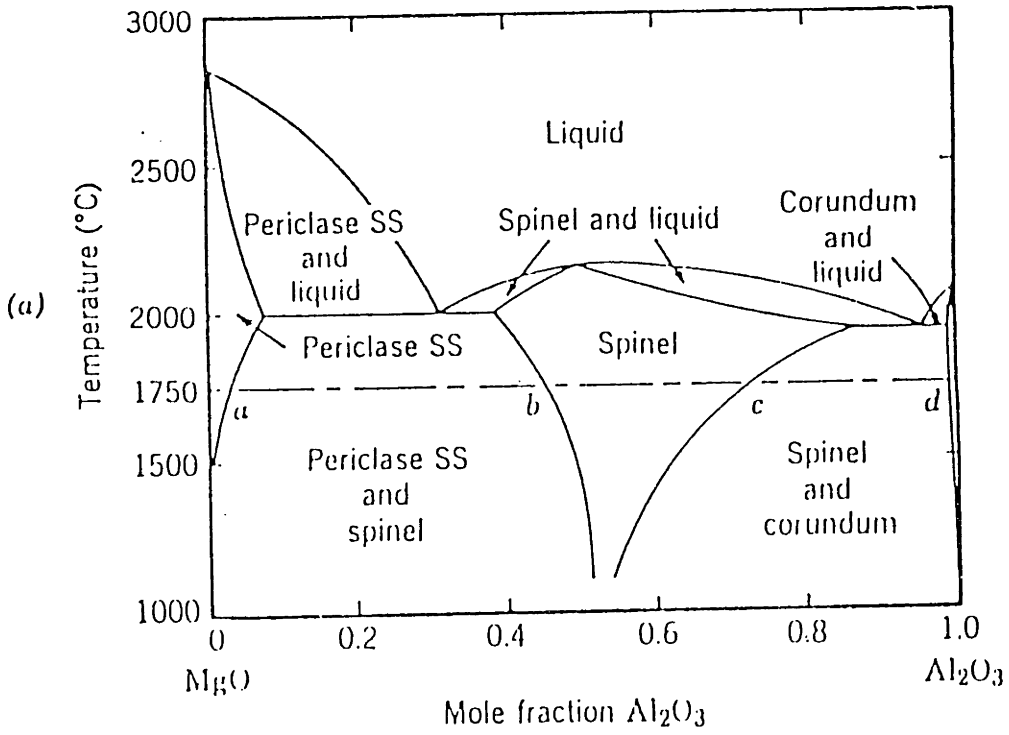

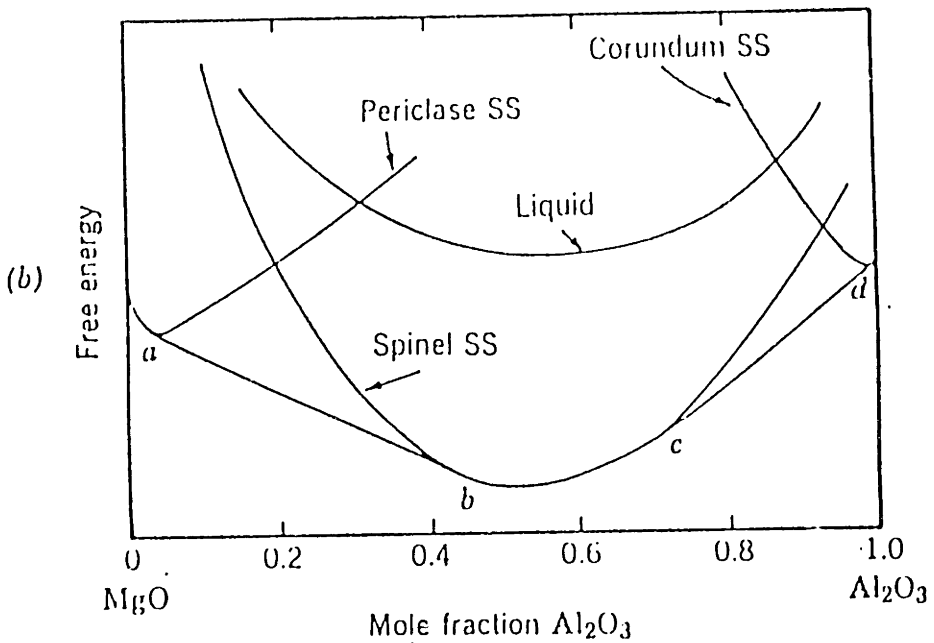

(*a*) Phase diagram of the $MgO–Al_2O_3$ system. (*b*) Schematic representations of free-energy–composition diagram of $MgO–Al_2O_3$ for $T = 1750°C$.

```
      C*************************************************************
      C
      C                  APPENDIX  5
      C
      C     THIS PROGRAM USES DATA FROM THE EXPANSION
      C     CURVES OF SLAG AND WELD METAL TO CALCULATE
      C     THE MEAN INTEGRATED DIFFERENTIAL THERMAL
      C     CONTRACTION, THE INTEGRATED DIFFERENTIAL
      C     THERMAL CONTRACTIONS AS FUNCTIONS OF TEMPERATURE
      C     FOR ANY GIVEN SLAG-METAL SYSTEM.
      C
      C*************************************************************
      C
0001        PROGRAM DIFCON
      C
      C*************************************************************
      C     THIS SEGMENT TAKES DATA FROM DIGITIZED
      C     EXPANSION CURVES (DELTA L/L VS. DISTANCE) AND
      C     CONVERTS DATA TO DELTA L/L VS. TEMPERATURE
      C     USING A CALIBRATED DISTANCE-TEMPERATURE FILE:
      C     RELAXT. (I.E. RELATE X AND T). THIS IS NECESSARY
      C     BECAUSE THE TEMPERATURE AXIS OF THE RECORDING
      C     CHART IS NON-LINEAR WITH DISTANCE.
      C*************************************************************
      C
0002        REAL XSLG(60), YSLG(60)
0003        REAL XMET(60), YMET(60)
0004        REAL XDAT(20), TDAT(20)
      C
      C*************************************************************
      C     BYTE DECLARATION IS FOR ARRAYS AND VARIABLES.
      C     WID IS WELD ID, NWID IS NUMBER OF CHARACTERS
      C     IN WID.
      C*************************************************************
      C
0005        BYTE WID(3), SLGIN(8), METIN(8)
0006        BYTE SLGOUT(11), METOUT(11), DIFOUT(11)
0007        TSTART = 30.0
0008        DELTAT = 5.0
0009        TYPE 1000
0010  1000  FORMAT('$ ENTER WELD I.D.:')
0011        ACCEPT 1001, NWID,WID
0012  1001  FORMAT(Q,3A1)
      C
      C*************************************************************
      C     PREPARATION OF FILE NAMES. THE INPUT FILES
      C     SLGIN AND METIN WILL HAVE EXTENSIONS: .SLG
      C     AND .MET RESPECTIVELY ( i.e. WID.SLG, WID.MET
      C*************************************************************
      C
0013        CALL SCOPY(WID,SLGIN(1),NWID)
0014        CALL SCOPY('.SLG',SLGIN(NWID + 1))
0015        SLGIN(8) = 0
0016        OPEN(UNIT=1,NAME=SLGIN,TYPE='OLD',FORM='FORMATTED')
```

```
FORTRAN IV      V02.5-3

0017          CALL SCOPY(WID,METIN(1),NWID)
0018          CALL SCOPY('.MET',METIN(NWID + 1))
0019          METIN(8) = 0
0020          OPEN(UNIT=2, NAME=METIN,TYPE='OLD',FORM='FORMATTED')
      C
      C*************************************************************
      C       THE OUTPUT FILES WILL HAVE PREFIXES OF
      C       SLGCON. ,METCON. , AND DIFCON. (i.e.
      C       SLGCON.WID
      C       METCON.WID AND DIFCON.WID
      C*************************************************************
      C
0021          CALL SCOPY('SLGCON.',SLGOUT(1))
0022          CALL SCOPY(WID,SLGOUT(8),NWID)
0023          SLGOUT(11) = 0
0024          CALL SCOPY('METCON.',METOUT(1))
0025          CALL SCOPY(WID,METOUT(8),NWID)
0026          METOUT(11) = 0
0027          CALL SCOPY('DIFCON.',DIFOUT(1))
0028          CALL SCOPY(WID,DIFOUT(8),NWID)
0029          DIFOUT(11) = 0
      C
      C*************************************************************
      C       NOW READ IN XDAT AND TDAT VALUES FROM
      C       FILE RELAXT. (i.e. RELATE X AND T)
      C*************************************************************
      C
0030          OPEN (UNIT=3, NAME='RELAXT.', TYPE='OLD',FORM='FORMATTED')
0031          READ (3,*) ITYPE,NDAT,FACTOR,OFFSET
0032          DO 55 I=1,NDAT
0033          READ(3,*) XDAT(I), TDAT(I)
      C       TYPE *, XDAT(I),TDAT(I)
0034       55 CONTINUE
0035          CLOSE(UNIT=3)
      C
      C*************************************************************
      C       READ IN SLAG AND METAL EXPANSIONS AS A FUNCTION
      C       OF DISTANCE FROM FORMATTED X-Y FILES
      C       WITH A HEADER LINE.
      C*************************************************************
      C
0036          READ(1,*) ITYP, NSLG, FACTOR, OFFSET
0037          DO 66 I = 1,NSLG
0038          READ(1,*) XSLG(I), YSLG(I)
      C       TYPE *,XSLG(I),YSLG(I)
0039       66 CONTINUE
0040          READ(2,*) ITYP, NMET,FACTOR, OFFSET
0041          DO 77 I = 1,NMET
0042          READ(2,*) XMET(I), YMET(I)
      C       TYPE *,XMET(I),YMET(I)
0043       77 CONTINUE
0044          CLOSE(UNIT=1)
0045          CLOSE(UNIT=2)
0046          CALL HOOKUP(XDAT,TDAT,NDAT,XSLG(NSLG),TS,1)
```

```
0047          TYPE *,'TS = ',TS
0048          YSFT = YSLG(NSLG)
      C       TYPE *,'XSLG(NSLG) = ',XSLG(NSLG)
0049          CALL HOOKUP(XMET,YMET,NMET,XSLG(NSLG),YMSFT,2)
      C       TYPE *,'YMSFT = ',YMSFT
      C       TYPE *,'YSFT = ',YSFT
0050          SUMDIF = 0.0
      C       AVDALF = 0.0
0051          T = TSTART-DELTAT
0052          NT = (TS - TSTART)/DELTAT + 1
      C
      C*************************************************************
      C       OPEN ALL OUTPUT FILES AND WRITE IN
      C       HEADER LINES.
      C*************************************************************
      C
0053          OPEN(UNIT=1, NAME=SLGOUT, TYPE='NEW')
0054          OPEN(UNIT=2, NAME=METOUT, TYPE='NEW')
0055          OPEN(UNIT=3, NAME=DIFOUT, TYPE='NEW')
0056          WRITE(1,*) 1,NT,0.0,0.0
0057          WRITE(2,*) 1,NT,0.0,0.0
0058          WRITE(3,*) 1,NT,0.0,0.0
      C
      C*************************************************************
      C       THIS SECTION CALCULATES THE EXPANSION VALUES
      C       YS AND YM AT A GIVEN T OR X BY STEP INCREMENT
      C       METHOD (SEE SUBROUTINE HOOKUP).
      C       IT ALSO CALCULATES THE INTEGRATED COEFFS OF
      C       EXPANSION OF SLAG AND METAL, THE DIFFERENTIAL
      C       INTEGRATED COEFF OF EXPANSION AND THE
      C       MEAN DIFFERENTIAL CONTRACTION.
      C       NOTE THAT THESE CALCULATED VALUES HAVE BEEN
      C       INCREASED BY A FACTOR OF 1.0*E06 IN THE CASE OF
      C       THE COEFFICIENTS AND 1.0*E03 IN THE CASE OF
      C       THE CONTRACTIONS FOR ARITHMETIC
      C       TIDYNESS ONLY!
      C*************************************************************
      C
0059          DO 88 IT = 1,NT
0060          T=T+DELTAT
0061          CALL HOOKUP(TDAT,XDAT,NDAT,T,X,3)
0062          CALL HOOKUP(XSLG,YSLG,NSLG,X,YS,4)
0063          CALL HOOKUP(XMET,YMET,NMET,X,YM,5)
0064          DT = (TS - T)
0065          CONTRS = (YSFT - YS)*1.0E3
0066          CONTRM = (YMSFT - YM)*1.0E3
      C       TYPE *, CONTRM,CONTRS
0067          DIFCON = (CONTRM - CONTRS)
      C       TYPE *,'DIFCON =',DIFCON
0068          ALFAS  = CONTRS*1.0E03/DT
0069          ALFAM  = CONTRM*1.0E03/DT
0070          DIFALF = DIFCON*1.0E03/DT
0071          SUMDIF = SUMDIF + DIFCON
      C       AVDALF = AVDALF + DIFALF
```

```
0072          WRITE(1,*) T, CONTRS
0073          WRITE(2,*) T, CONTRM
0074          WRITE(3,*) T, DIFCON
      C       TYPE *,YMSFT,YM,CONTRM,DT,ALFAM
0075       88 CONTINUE
      C
      C*****************************************************************
      C       THE MEAN DIFFERENTIAL CONTRACTION THAT WILL BE
      C       TYPED TO THE SCREEN IS ALSO FACTORED BY
      C                        1.0*E03
      C*****************************************************************
      C
0076          TYPE 2000, ABS(SUMDIF)/NT
0077    2000  FORMAT(1X,'MEAN DIFFERENTIAL CONTRACTION IS ',G9.2)
      C       TYPE 2001, (AVDALF)/NT
      C2001 FORMAT(' MEAN DIFALF IS ',G9.2)
0078          CALL EXIT
0079          END
```

```
      C
      C*****************************************************************
0001        SUBROUTINE HOOKUP(INDARY,DEPARY,NPTS,INDVAL,DEPVAL,IER)
0002        REAL INDARY(1),DEPARY(1),INDVAL
      C
      C*****************************************************************
      C     LOOK UP A VALUE FROM A TABLE
      C
      C     THE INDEPENDENT VALUES ARE IN THE ARRAY INDARY
      C     THE DEPENDENT VALUES ARE IN THE ARRAY DEPARY
      C     THE INDEPENDENT VALUE OF THE DESIRED POINT IS INDVAL
      C     THE DEPENDENT VALUE OF THE DESIRED POINT IS RETURNED
      C        IN DEPVAL
      C     IER IS A NUMBER TO INDICATE THE CALLING POINT IN CASE OF
      C        ERROR
      C*****************************************************************
      C
0003        IF (INDVAL.GE.INDARY(1).AND.INDVAL.LE.INDARY(NPTS)) GOTO 5
0005        TYPE 1000,IER
0006   1000 FORMAT (' ? ARGUMENT OUT OF RANGE FROM POINT',I6)
0007        TYPE 1001,INDVAL,INDARY(1),INDARY(NPTS)
0008   1001 FORMAT (' VALUE :',G9.2,' MINIMUM :',G9.2,' MAXIMUM :',G9.2)
0009        STOP
      C
0010      5 I = 1
0011     10 IF(INDVAL.LT.INDARY(I)) GO TO 20
0013        I = I + 1
0014        GO TO 10
0015     20 DEPVAL = DEPARY(I-1) + (DEPARY(I) - DEPARY(I - 1))*
          1    (INDVAL - INDARY(I - 1))/(INDARY(I) - INDARY(I - 1))
0016        RETURN
0017        END
```

APPENDIX 6

This appendix shows the calculation of the heat flux used in the finite element analysis to calculate the temperature fields in the slag-metal system.

Travel speed, T = 14 ipm = 5.93 mm/s

Current, I = 300 A

Voltage, V = 30 V

Weld metal length = 4 mm

Time of deposit, t = 0.675 s

Arc efficiency for SAW = 95%

So, heat flux H = 300 * 32 * 0.95

= 9.12 KW

Consider a 4 mm radius arc (uniform distribution)

Area, $A = r^2$

$= 50.27\ mm^2$

So, heat flux intensity = 9.12/50.27

$= 181.42\ W/mm^2$

Due to symmetry about centerline of arc, we use only half of the intensity i.e. $90.71\ W/mm^2$.

APPENDIX 7

The figures in this appendix are included to further indicate the effects of integrated differential thermal contraction, base metal chemistry, chromium and the microstructures of slag on slag detachability.

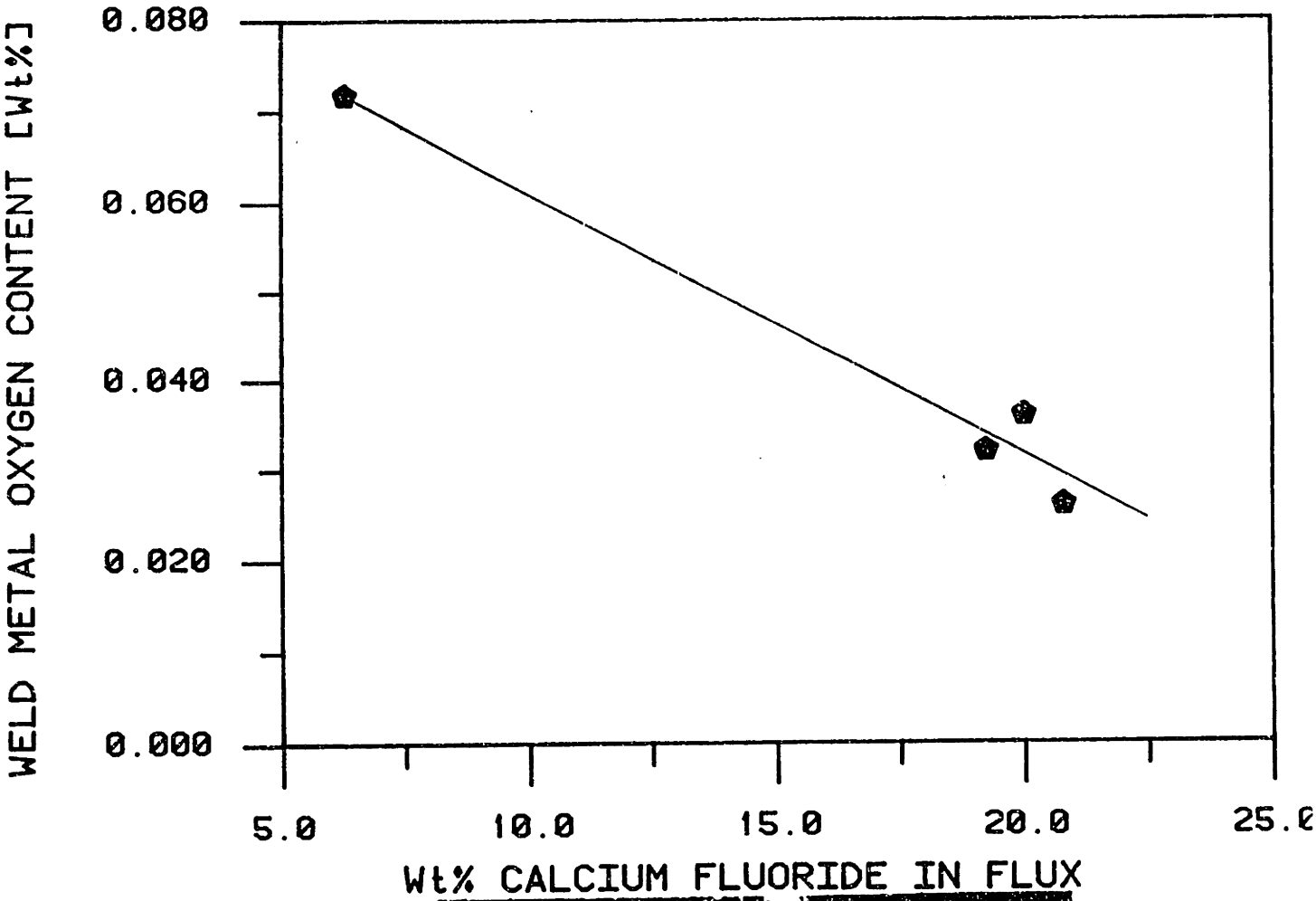

Electron micrograph showing cuspidine in slag structure.
AX-IN-0091 x400

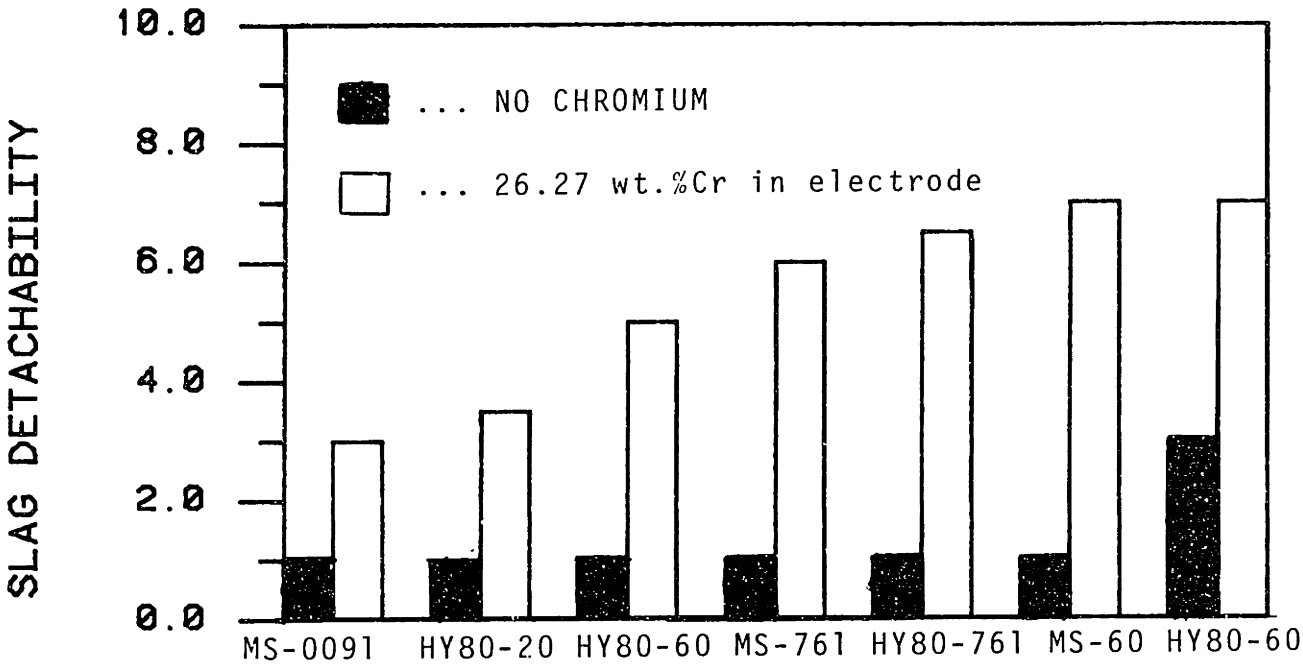

Shows the effect of chromium in electrode on detachability for the same flux and base metal.

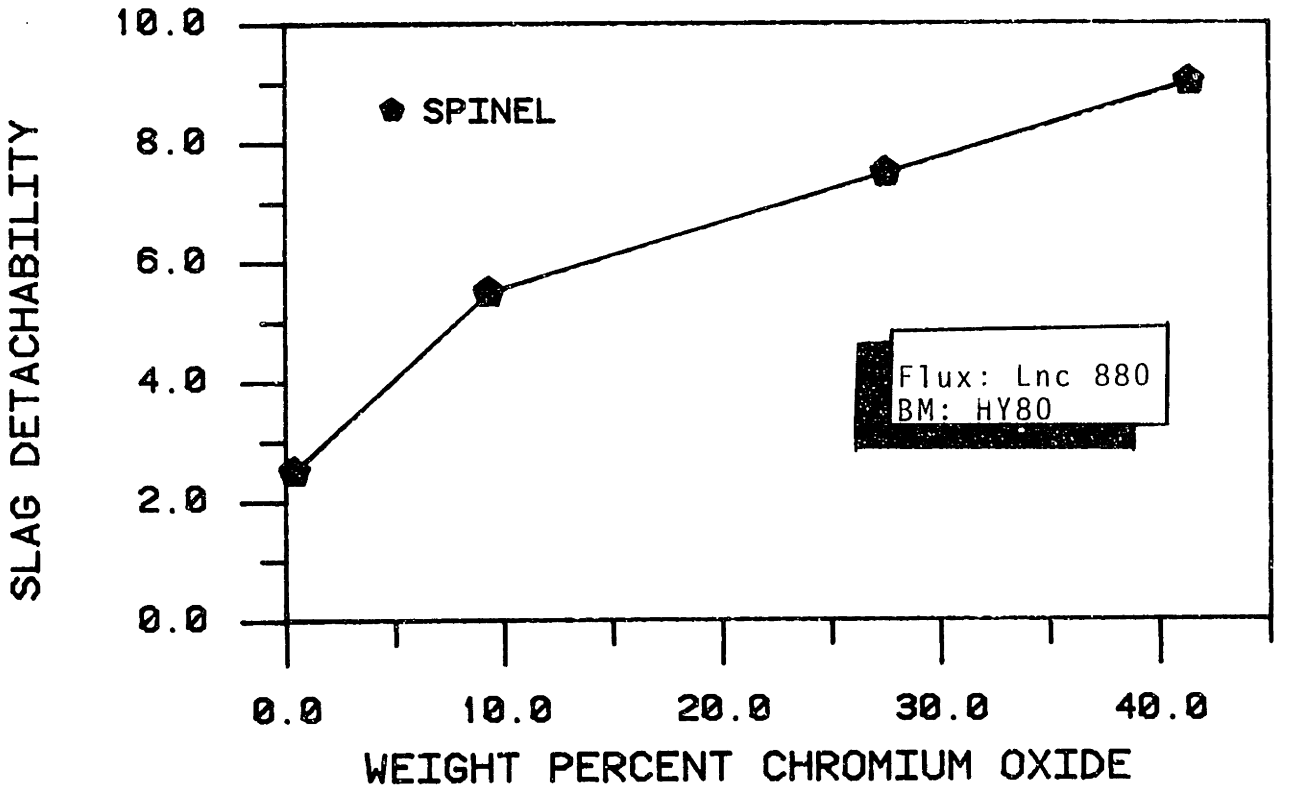

Shows the effect of chromium oxide content of spinels in the slag microstructure on detachability.

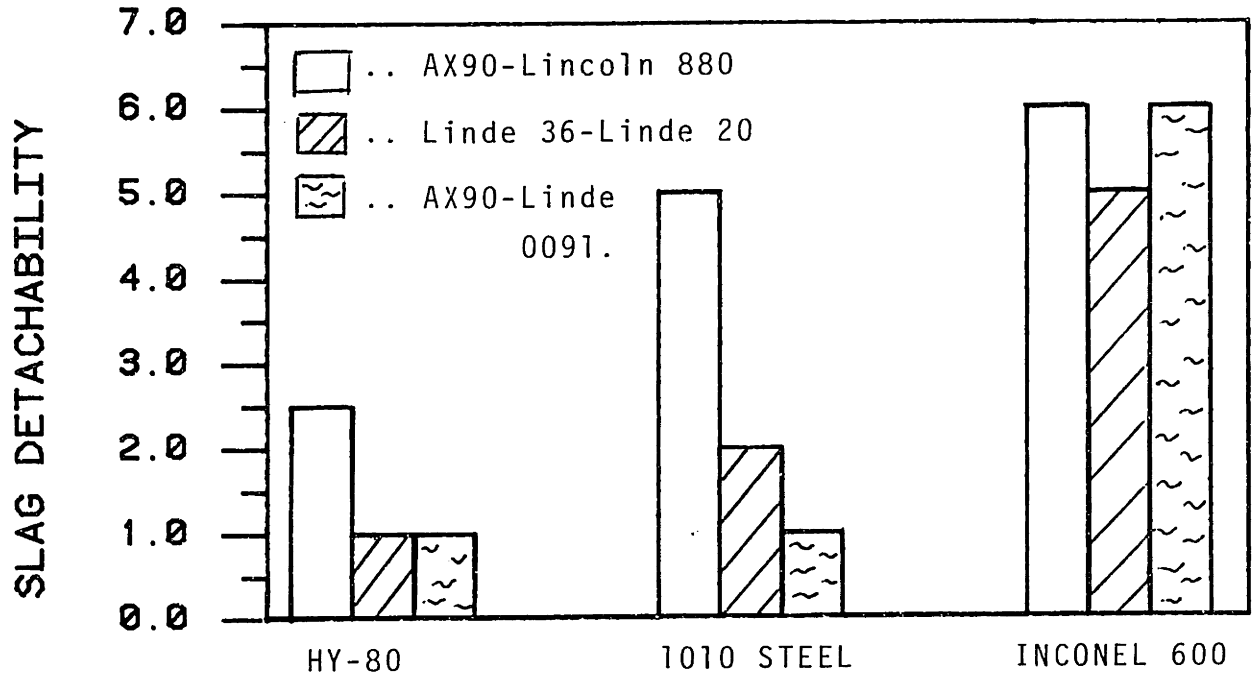

Shows the effect of base metal on detachability.

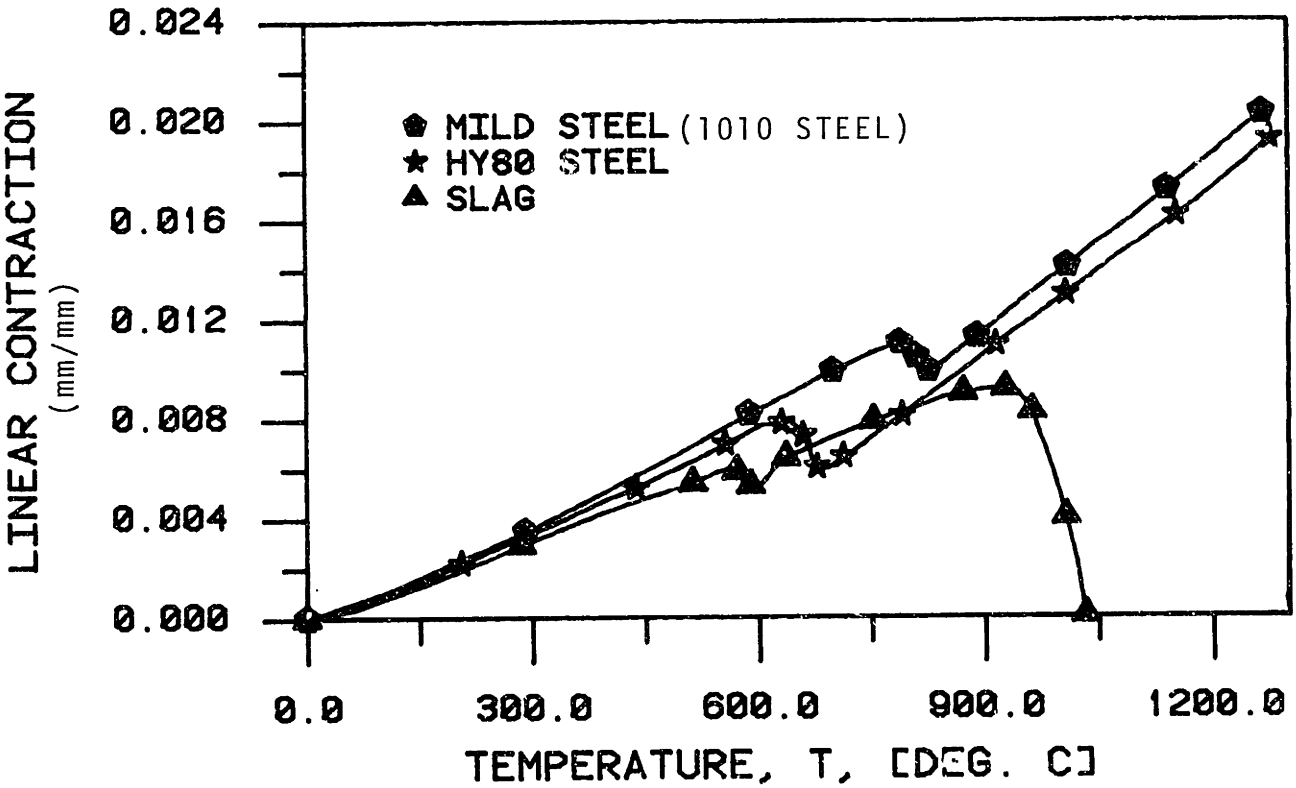

Shows the thermal expansion characteristics of base metals and slag and that mild steel should provide slags that are more easily detachable than HY80. This of course disagrees with the results above.

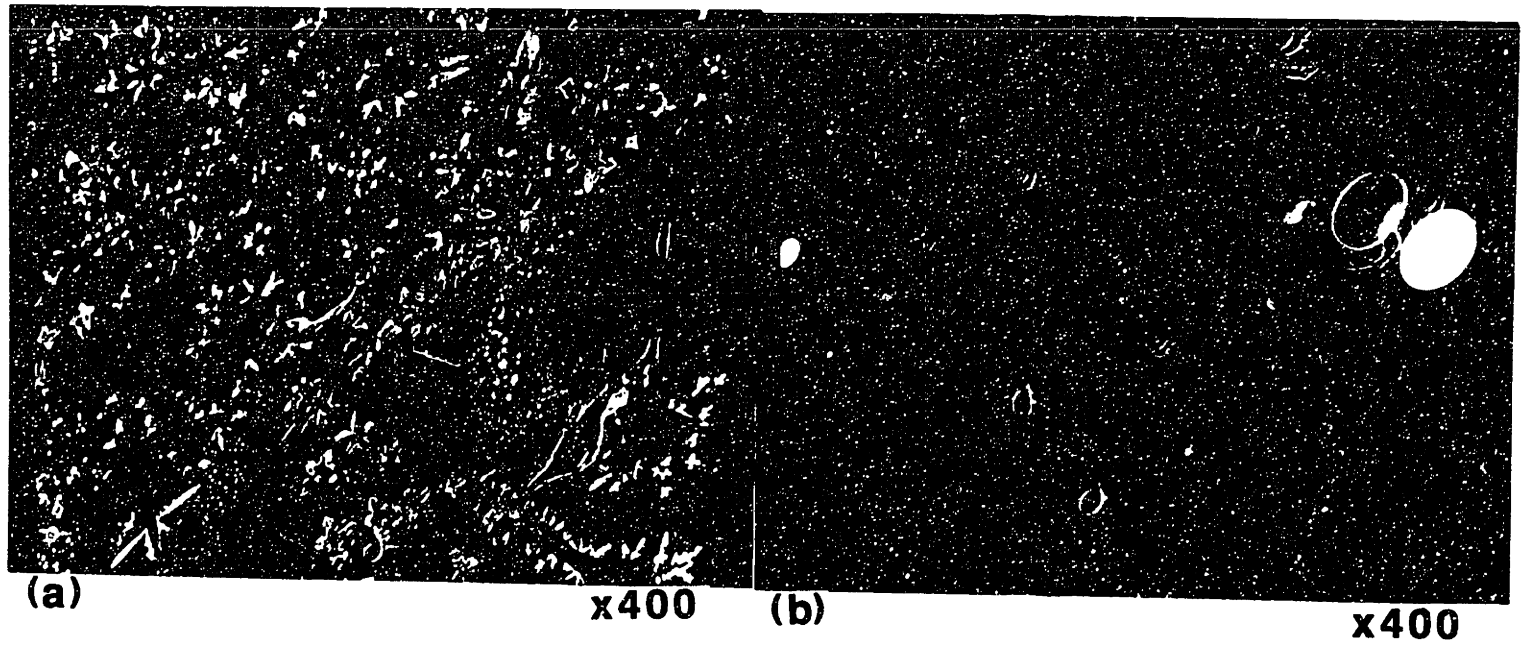
(a)
x400
(b)
x400

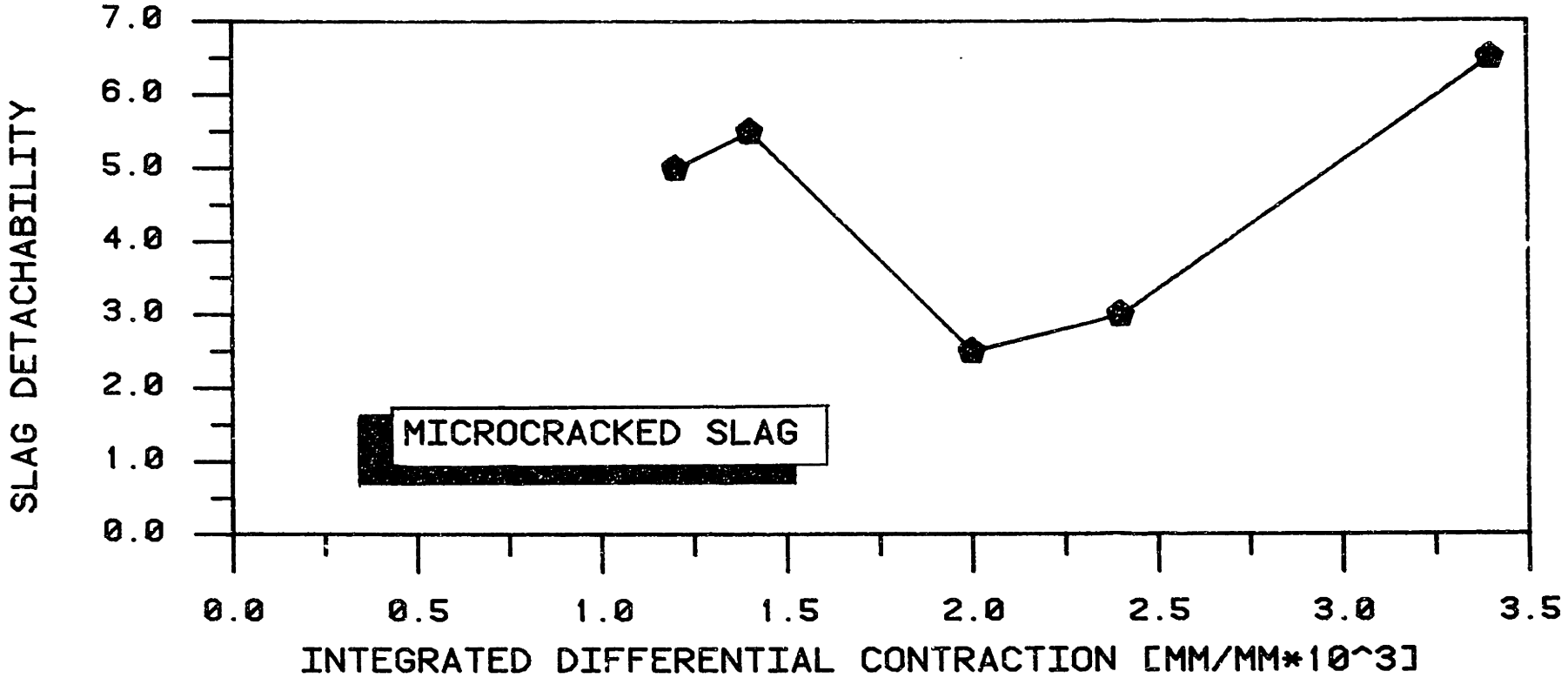
SLAG DETACHABILITY
7.0
6.0
5.0
4.0
3.0
2.0
1.0
0.0
MICROCRACKED SLAG
0.0
0.5
1.0
1.5
2.0
2.5
3.0
3.5
INTEGRATED DIFFERENTIAL CONTRACTION [MM/MM*10^3]

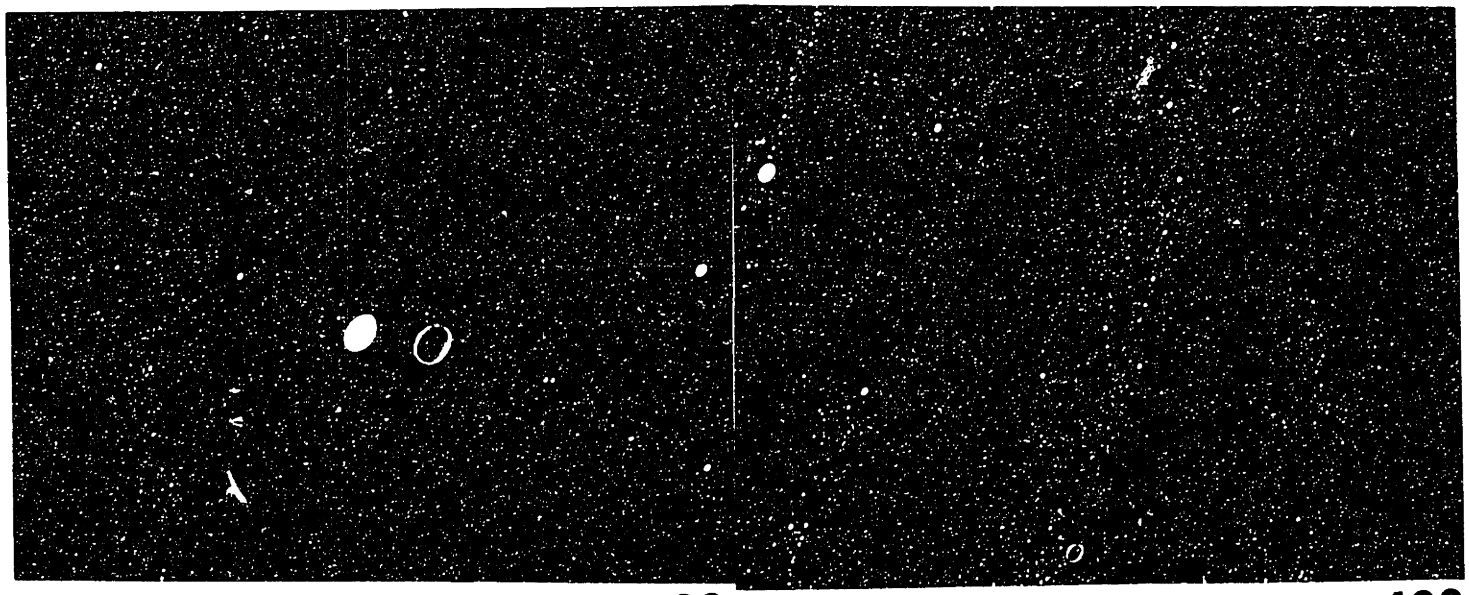

x400 x400

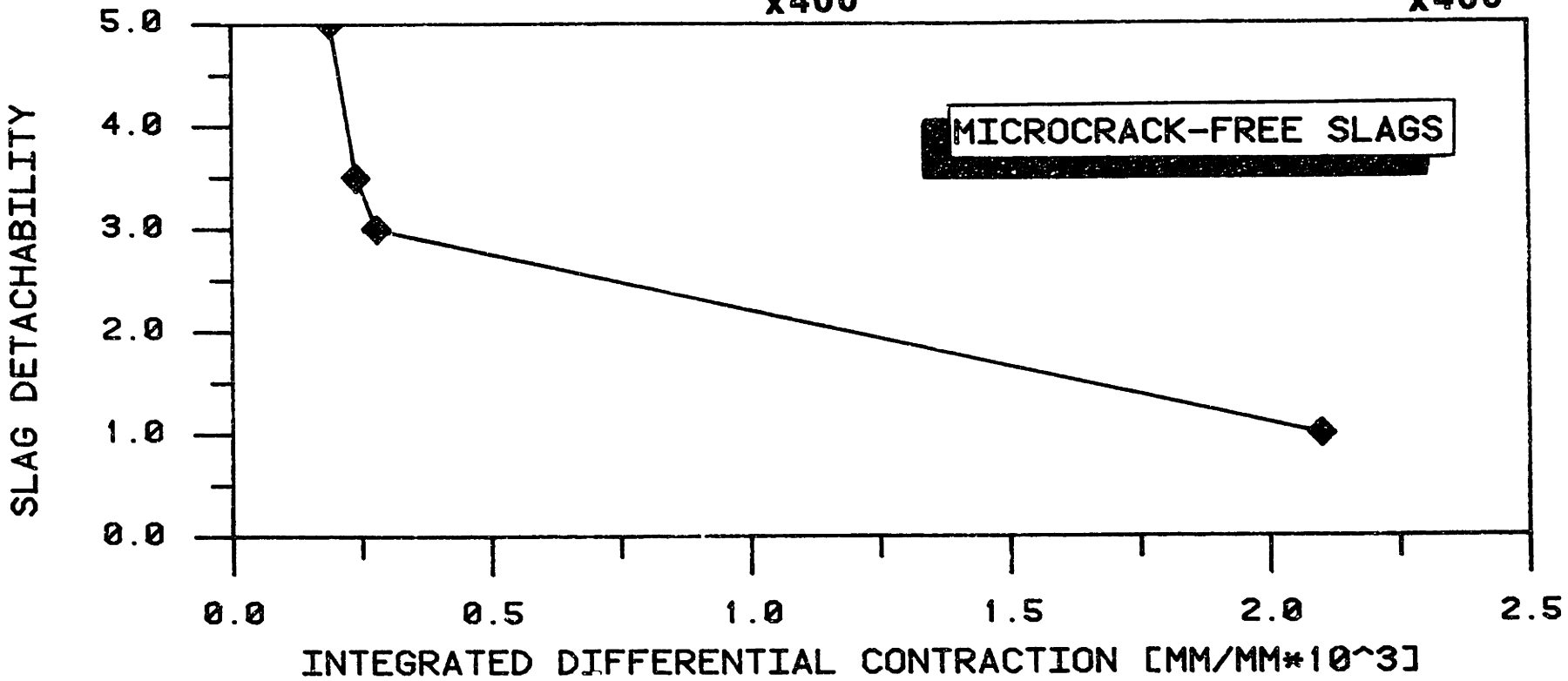
SLAG DETACHABILITY
5.0
4.0
3.0
2.0
1.0
0.0
MICROCRACK-FREE SLAGS
0.0
0.5
1.0
1.5
2.0
2.5
INTEGRATED DIFFERENTIAL CONTRACTION [MM/MM*10^3]

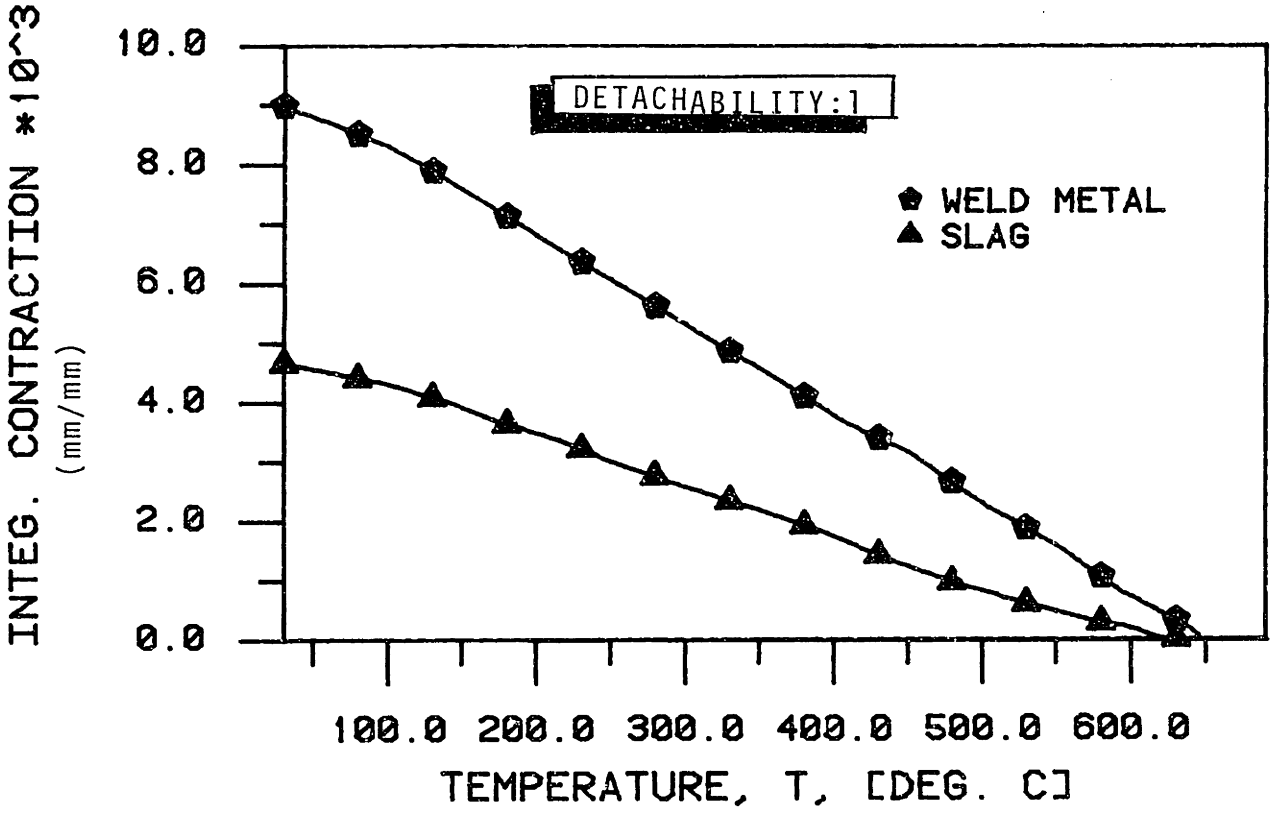

Shows integrated contraction of slag & weld metal from softening point of slag to 30°C; AX-HY-20

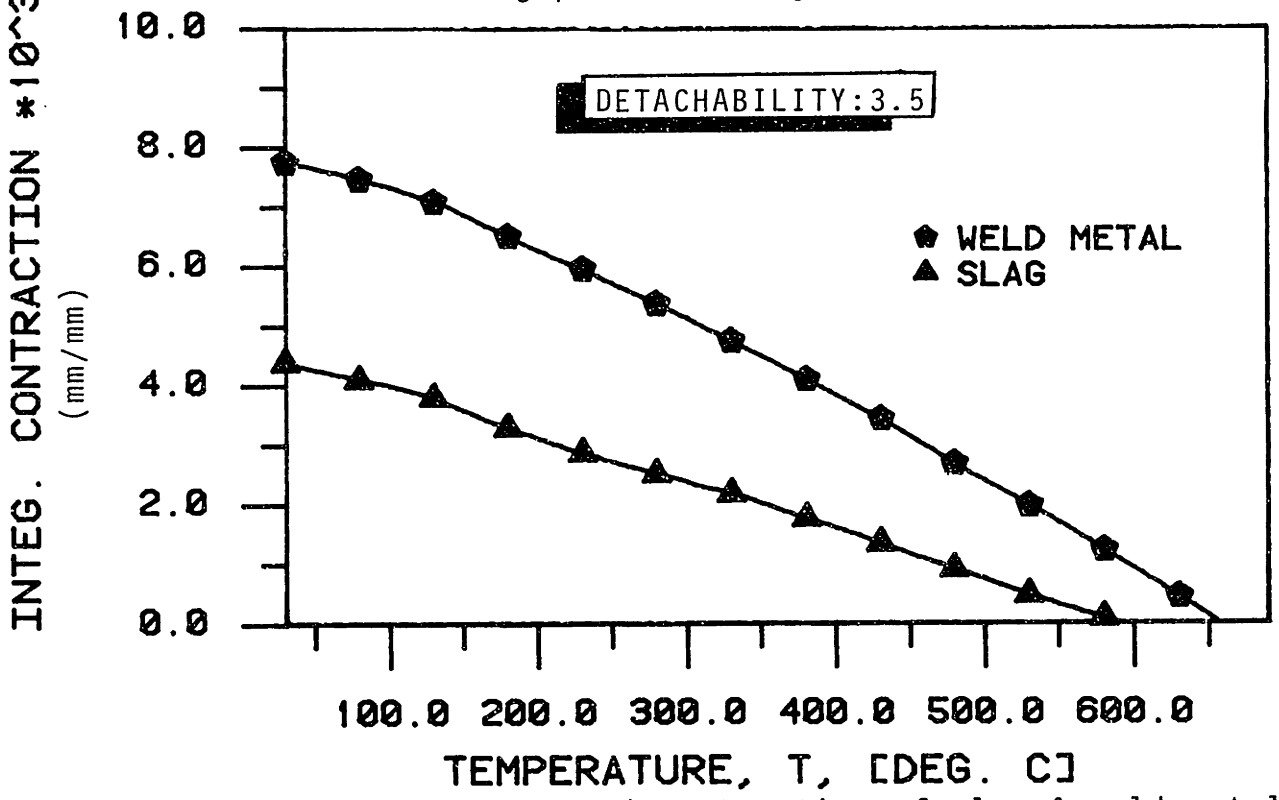

Shows integrated contraction of slag & weld metal from softening point of slag to 30°C; 309-HY-20.

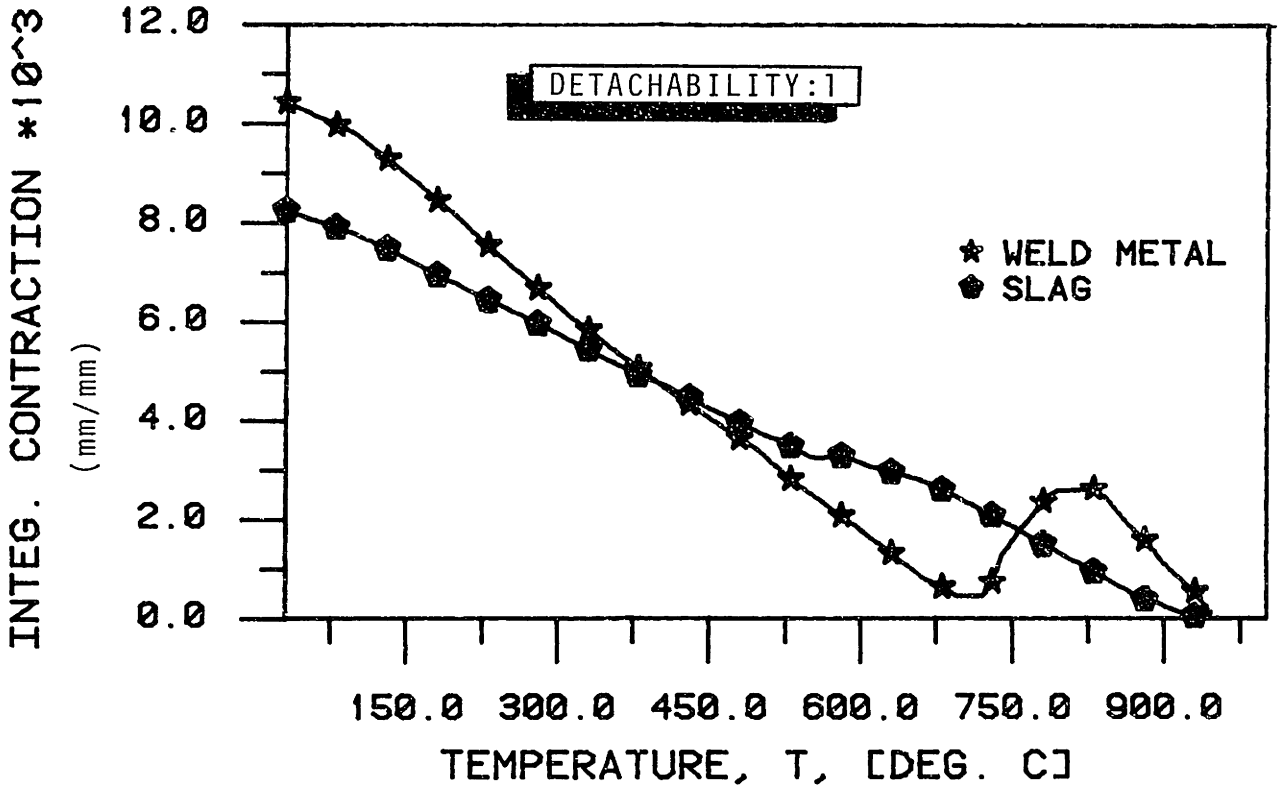

Shows integrated contraction of weld & slag from softening temperature of slag to 30°C;AX-HY-0091

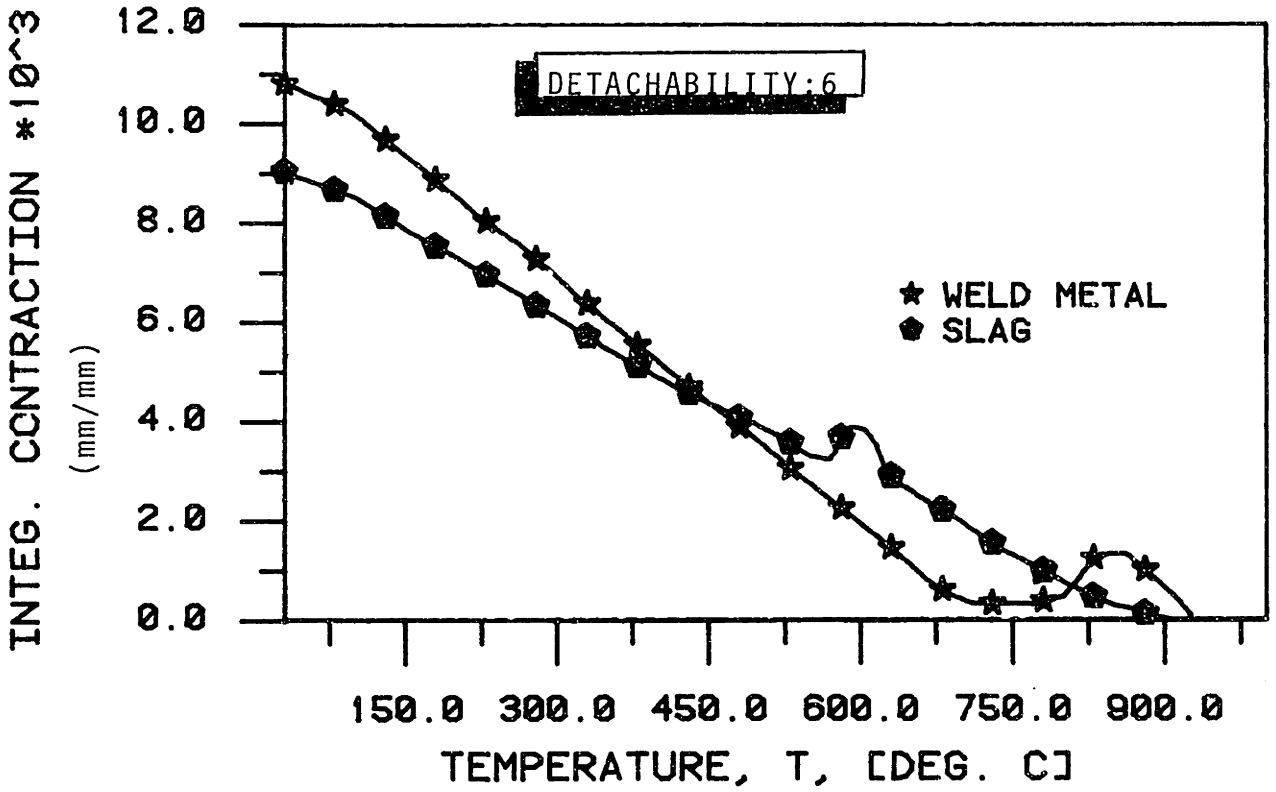

Shows integrated contraction of slag and weld from the softening temperature of slag to 30°C; sample AX-IN-0091